Detrimental Thoracoabdominal Interaction With Lateral Airbag Restraints

Jason John Hallman
Marquette University

DETRIMENTAL THORACOABDOMINAL INTERACTION WITH LATERAL AIRBAG RESTRAINTS

by

Jason John Hallman

A Dissertation submitted to the Faculty of the Graduate School,
Marquette University,
in Partial Fulfillment of the Requirements for
the Degree of Doctor of Philosophy

Milwaukee, Wisconsin

December 2010

ABSTRACT
DETRIMENTAL THORACOABDOMINAL INTERACTION WITH
LATERAL AIRBAG RESTRAINTS

Jason John Hallman

Marquette University, 2010

Side impact motor vehicle crashes pose unique challenges for occupant protection, particularly with regard to torso injury mitigation. The minimal crush distance between the vehicle exterior and the occupant torso has necessitated advanced passive safety technologies in response to tightened regulatory requirements and increased public awareness of safety issues. In particular, lateral airbag restraints (side airbags) have undergone a rapid and unregulated introduction in recent years, with US availability increasing to over 90% of new vehicles in 2010. As with frontal airbag restraints, the propensity for injury to occupants in close proximity to side airbag deployment remains a concern. Test protocols have been proposed to evaluate occupant injury risk from airbag deployment with mechanical occupant surrogates. Yet few studies have attempted to characterize thoracoabdominal responses to close-proximity airbag contact in actual crashes, leaving unaddressed the relevance of test protocols and occupant surrogates currently employed.

To address this issue, the present study sought to identify and characterize injury and biomechanical responses of the thoracoabdominal region to torso-interacting side airbag restraints. A novel biological experimental approach was developed from a multi-body analysis and from an evaluation of documented restraint performance. Biomechanical responses of deflection, deflection rate, the Viscous Criterion, and deformation obliquity with respect to subject anatomy were quantified. Further, tissue-level material response was examined through a comparative finite element analysis of subject-specific loading. Results indicated that traumatic visceral injury specific to the posterolateral region was associated with close-proximity airbag interaction. Deformation response was uniquely oblique with respect to anatomy, necessitating the refinement of existing injury metrics. Biomechanical tolerances were also determined for risk of trauma to posterolateral viscera. These results are useful for the development of mechanical occupant surrogates and reductions to injury risks from close-proximity side airbag loading.

DEDICATION

To God our Father:
"Whatsoever you do, do it from the heart,
as for the Lord and not for men."
Colossians 3:23, DHE

To my wife, Kris:
Without your support, "none of this would have been at all possible."

PREFACE

Side impact motor vehicle crashes pose unique challenges for occupant protection, particularly with regard to torso injury mitigation. The minimal crush distance between the vehicle exterior and the occupant torso has necessitated advanced passive safety technologies in response to tightened regulatory requirements and increased public awareness of safety issues. In particular, lateral airbag restraints (side airbags) have undergone a rapid unregulated introduction in recent years, with US availability increasing to over 90% of new vehicles in 2010. As with frontal airbag restraints, the propensity for injury to occupants in close proximity to side airbag deployment remains a concern. While a commercial test protocol has been developed and approved by a collaboration of governments, industry members, and consumer safety advocates, its relevance to occupant injury risks in actual crashes has not been studied. To address this issue, the present study identified and characterized a mechanism of torso injury induced by close-proximity side airbag loading observed in drivers of vehicles involved in motor vehicle crashes.

Chapter 1 introduces the concepts and challenges associated with lateral impact vehicle crashworthiness and advanced inflatable restraint technologies. Chapter 2 provides the relevant human torso anatomy. Chapter 3 begins with an extensive review of existing torso injury criteria, their development, and their relevance to study objectives. Advanced computational research tools and injury mitigation efforts are also presented.

Chapter 4 presents an analysis of documented vehicle crashes from national US transportation databases. From the results of this examination, a parametric computational analysis is described in Chapter 5 which characterized the dependency of side airbag injury mitigation on occupant position and crash severity; a novel dynamic occupant scenario of close-proximity airbag loading is identified. Chapter 6 presents an experimental evaluation of this scenario as well as comparisons to stationary occupant loading and to unprotected blunt impact at similar severity. Deformations induced by close-proximity airbag and tissue responses are further examined in Chapter 7 through a comparative viscoelastic finite element analysis. Summary and potential limitations are provided in Chapter 8, and conclusions along with future directions are addressed in Chapter 9.

ACKNOWLEDGMENTS

Jason John Hallman

This research would not have been possible were it not for the counsel and assistance of many individuals. I offer my gratitude to my adviser, Dr. Frank Pintar, for his willing guidance of a young graduate student eager to enter the injury biomechanics field; and to Dr. Narayan Yoganandan, for insisting upon excellence and patiently cultivating it. I would also like to recognize my Dissertation Committee: Dr. Karen Brasel, Dr. Gerald Harris, and Dr. John LaDisa, Jr. Thank you for your suggestions, your enthusiasm, your leadership, and your dedication to my education. Each one of you has had a substantial contribution without which this work would not be complete.

Many thanks are due to the members of the Neuroscience-Biomechanics Laboratories at the Zablocki VA Medical Center: Christy Stadig (for countless conversations), Mark Meyer (for remaining with me during afterhours experiments), and John Humm (for willingly offering your knowledge and experience). Assistance was also provided by Jim Budzinski, Will Drobac, Paul Gromowski, Dale Halloway, Brad Peterson, Mike Rawski, Kristen Reichert, Mike Schlick, Steve Tilistyak, and Dr. Jiangyue Zhang. Each of you has contributed to this work in some fashion, and I will always be grateful. Further, I also owe my thanks to Dr. Brian Stemper for wisdom and encouragement when it was most needed and to my fellow students, David Barnes, Dr. Ronald Fijalkowski, and Steven Storvik, for ensuring that this process was not a lonely endeavor.

I am also grateful for the administrative and financial assistance from many organizations. These include the Medical College of Wisconsin Department of Neurosurgery, the Marquette University Department of Biomedical Engineering, the National Science Foundation Graduate Research Fellowship Program, the Tau Beta Pi Spencer Fellowship Program, the Association for the Advancement of Automotive Medicine Student Research Grant Program, the National Institutes of Health (R01AG024443), and the Department of Transportation (DTNH22-05-H-41001).

Finally, much personal support was provided by my friends and family, especially my wife Kristin, my parents John and Sandra, and my siblings Adam and Briana. Without your presence throughout my life and in this process, I would not have been able to accomplish this.

TABLE OF CONTENTS

PREFACE i

ACKNOWLEDGMENTS iii

LIST OF TABLES ix

LIST OF FIGURES xi

1. INTRODUCTION 1

2. THORACOABDOMINAL ANATOMY 10

2.1 External Anatomy 10

2.2 Skeletal Anatomy 11

2.3 Visceral Anatomy 15

2.4 Anatomic Variability 21

3. STATE OF THE ART: THORACOABDOMINAL TRAUMA IN SIDE IMPACT 23

3.1 Lateral Injury Metrics 24

3.1.1 Acceleration 26

3.1.2 Deflection Magnitude 29

3.1.3 Deflection Rate 31

3.2 Chestband Methods 33

3.3 Computational Methods 35

3.3.1 Finite Element Analyses 35

3.3.2 Multi-Body Analyses 40

3.4 Boundary Effects 43

3.4.1 Load Direction 43

3.4.2 Contact Interface Properties 45

3.5 Occupant-Airbag Interactions 47

3.5.1 Efficacy 48
3.5.2 Out-of-Position 50
3.6 Summary 53
4. INJURY PATTERNS FOLLOWING SIDE AIRBAG LOADING 54
4.1 Methodology 54
4.1.1 Data Description 54
4.1.2 Inclusion Criteria 55
4.1.3 Analysis Approach 56
4.2 Results 57
4.2.1 NASS Analysis 58
4.2.2 Case Examination 60
4.2.3 Case Descriptions 62
4.3 Discussion 69
5. DEFINING OUT-OF-POSITION DURING IMPACT 75
5.1 Methodology 75
5.1.1 Geometry and Boundary Conditions 76
5.1.2 Validation 78
5.1.3 Loading 79
5.2 Results 80
5.2.1 Validation 80
5.2.2 Position and ΔV 82
5.2.3 Comparison to Stationary Protocol 88
5.3 Discussion 93
6. EXPERIMENTAL EVALUATION OF SIDE AIRBAG LOADING 99
6.1 Methodology 100

6.1.1 Subject Preparation 100
6.1.2 Experimental Procedure 101
6.1.3 Data Collection and Processing 105
6.2 Results 108
6.2.1 Airbag Behavior 108
6.2.2 Injury Response 110
6.2.3 Chestband Analysis 115
6.3 Discussion 122
6.3.1 Injury Response 123
6.3.2 Injury Metrics 125
7. COMPARATIVE FINITE ELEMENT EVALUATION OF SIDE AIRBAG LOADING 132
7.1 Methodology 132
7.1.1 Geometry 133
7.1.2 Mesh Development 135
7.1.3 Material Properties 137
7.1.4 Validation 141
7.1.5 Loading 142
7.1.6 Output Parameters 146
7.1.7 Geometric Variations 149
7.2 Results 150
7.2.1 Mesh Density 150
7.2.2 Validation 152
7.2.3 Material Response Normalization 154
7.2.4 Analysis of Affected Areas 158
7.2.5 Biomechanical Correlation 163

7.3 Discussion 169

8. SUMMARY AND LIMITATIONS 175

8.1 Summary 175

8.2 Potential Limitations 179

9. CONCLUSIONS AND FUTURE DIRECTIONS 185

10. REFERENCES 188

APPENDIX A 217

LIST OF TABLES

Table 2.1. Volume distribution measured in cm^3 for adult normal population, normalized to subject height and weight. 22

Table 3.1. Relevant material properties of recent whole-body finite element models for impact. 39

Table 3.2. Summary of epidemiological findings regarding side airbag protection in lateral impacts. 50

Table 4.1. NASS population description 58

Table 4.2. Regression results for rib trauma 58

Table 4.3. Regression results for lung trauma 58

Table 4.4. Regression results for liver trauma 59

Table 4.5. Regression results for spleen trauma 59

Table 4.6. Torso airbag injury pattern from case occupants 68

Table 5.1. Metric sensitivity to occupant distance, raw and normalized to values at $\Delta V = 4$ m/s 88

Table 6.1. Subject specifications and test configuration. 105

Table 6.2. Subject injury results 111

Table 6.3. Peak deformations for four boundary conditions obtained from the xyphoid-level chestband at oblique vectors. 118

Table 6.4. Peak deformations for four boundary conditions obtained from the rib 10 level chestband at oblique vectors. 119

Table 6.5. Peak unconstrained responses, time of attainment, and angle of attainment from xyphoid level chestband. 122

Table 6.6. Contingency tests for injury dependence on dynamic OOP boundary condition 124

Table 6.7. Predictive ability of peak normalized deflection, peak deflection rate, and VCmax for spleen trauma and visceral trauma. 127

Table 7.1. Material properties chosen for the planar torso model. 141

Table 7.2. Normalized peak material response results for tests included in regression analyses. 156

Table 7.3. Geometries (5th, 50th, 95th) in which spleen areas were significantly ($p < 0.05$) greater for OOP dynamic subject. 163

Table 7.4. Correlation significance between peak oblique metrics and material response parameters for three model geometries. 164

Table 7.5. Maximum material response sensitivity to spleen parenchymal tissue properties.....173

Table A.1. Post mortem human subject testing sponsored by the National Highway Traffic Safety Administration and documented in the NHTSA Biomechanics Test Database. 217

LIST OF FIGURES

Figure 1.1. Event sequence for lateral vehicular impact: a) Initial contact, b) side structure deformation resulting in occupant-door contact, and c) final velocity....3

Figure 1.2. Side airbag protection and orientation options in contemporary automobiles. 6

Figure 1.3. Torso side airbag out-of-position testing procedures for seatback- and door-mounted modules with small female anthropometry. 7

Figure 2.1. External torso anatomical regions viewed in coronal plane from anterior. 11

Figure 2.2. External torso anatomical regions viewed in sagittal plane from left lateral....12

Figure 2.3. Torso cavities in mid-sagittal plane, viewed from right lateral. 12

Figure 2.4. Primary skeletal structures of the torso, viewed in coronal plane from anterior and posterior. 13

Figure 2.5. Ribcage cross-sectional unit, viewed from superior. 14

Figure 2.6. Axes of rib motion during respiration.....15

Figure 2.7. Visceral contents of the thoracic cavity, anterior and superior views. 16

Figure 2.8. Anterior view of progressive abdominal dissection: (a) Following removal of superficial tissues and abdominal wall; (b) Following removal of false ribs, greater omentum, and small intestine; (c) Following removal of liver, stomach, and partial large intestine. 17

Figure 2.9. Abdominal peritoneum viewed in transverse and sagittal sections. 19

Figure 2.10. Torso visceral contents in skeletal context, viewed in coronal plane. 20

Figure 3.1. Test methodologies in side impact biomechanical investigations. 25

Figure 3.2. Occupant local coordinate system endorsed by the Society of Automotive Engineers. 25

Figure 3.3. Accelerometer array developed by Robbins et al. (1976).....27

Figure 3.4. Probability of hard thorax trauma as a function of TTI.....29

Figure 3.5. NHTSA-SID currently employed for FMVSS 214 crashworthiness regulations. 29

Figure 3.6. Mechanical chest deflection components and transducers of the EuroSID. 31

Figure 3.7. Theoretical relationship between deflection and deflection rate for tissue failure. 32

Figure 3.8. Chestband determination of PMHS lateral deflection response 34

Figure 3.9. Logistic regression relationship between normalized chest deflection during sled impact and risk of hard thorax injury 35

Figure 3.10. Multi-body model for thoracic deflection response. 40

Figure 3.11. Exemplar 3D ellipsoidal multi-body model for left lateral impact. 41

Figure 3.12. MADYMO facet occupant model. 42

Figure 3.13. Oblique chestband deflection analysis methodologies. 45

Figure 3.14. Out-of-position child occupant test scenarios employed for seat- and door-mounted side airbag testing. 52

Figure 3.15. Out-of-position adult occupant test scenarios recommend for thoracoabdominal injury risk evaluation with seat- and door-mounted side airbags 52

Figure 4.1. PDOF inclusion criteria for NASS database query 56

Figure 4.2. Crash characteristics for splenic trauma without torso side airbag in the NASS database 60

Figure 4.3. Case 1 vehicle damage and airbag. 62

Figure 4.4. Case 2 vehicle damage and airbag. 63

Figure 4.5. Case 3 vehicle damage and airbag. 64

Figure 4.6. Case 4 vehicle damage and airbag. 65

Figure 4.7. Case 5 vehicle damage and airbag. 66

Figure 4.8. Abdominal radiology of splenic trauma in Cases 1-3 69

Figure 4.9. Seat and door airbag modules with respect to anatomical reference. 72

Figure 5.1. Facet occupant model in simulated sled geometry. 77

Figure 5.2. Initial conditions for parametric analysis. 80

Figure 5.3. Chest deflection, deflection rate, and viscous response of model and prior PMHS experiments at similar impact velocities. 81

Figure 5.4. Chest deflection, deflection rate, and viscous response of model subjected to rigid (no airbag) contact (left) and 2 cm airbag deployment (right) at $\Delta V = 7$ m/s. 83

Figure 5.5. Chest deflection, deflection rate, and viscous response of model subjected to 16 cm airbag deployment (left) and 20 cm airbag deployment (right) at $\Delta V = 7$ m/s. 84

Figure 5.6. Peak normalized chest deflection with respect to occupant distance from airbag for $\Delta V = 4$ and 9 m/s. 85

Figure 5.7. Defining points for peak normalized chest deflection, deflection rate, and viscous response at all ΔV with respect to occupant distance. 87

Figure 5.8. Normalized chest deflection, deflection rate, and viscous response of model subjected to stationary close-proximity torso airbag deployment. 89

Figure 5.9. Normalized chest deflection, deflection rate, and viscous response of model subjected to all ΔV with close-proximity airbag deployment. 91

Figure 5.10. Peak normalized chest deflection and VCmax of model subjected to all ΔV with rigid contact and close-proximity airbag deployment. 92

Figure 5.11. Comparative plot of critical distance ($\triangle$) and most protective distance ($\diamond$) defined by peak normalized deflection and VCmax. 94

Figure 5.12. Normalized biomechanical response to close-proximity airbag; that is, rigid 97

Figure 6.1. Bench seat apparatus with seat-mounted side airbag placement. 102

Figure 6.2. Instrumentation of specimens with respect to anatomy and airbags 103

Figure 6.3. RBandPC and post-processing methodologies for oblique chestband deflection analysis. 106

Figure 6.4. Stationary and dynamic airbag deployment scenarios. 109

Figure 6.5. Still frames from videography (frontal view) depicting variability in airbag deployment expansion for the four dynamic occupant tests. 110

Figure 6.6. Rib fracture patterns observed during post-test necropsy as viewed from left (L), posterior (P) and right (R) aspects. 113

Figure 6.7. Locations of splenic lacerations noted during necropsy. 114

Figure 6.8. Exemplar chestband contours demonstrating deformation patterns resulting from stationary and dynamic scenarios progressing from undeformed (U) to posterolateral airbag interaction (A) to maximum lateral deformation (M). 115

Figure 6.9. Exemplar normalized deflection traces for θ = 90° through 140°: Dynamic occupant (upper) and stationary occupant (lower). 116

Figure 6.10. Transient angle of deflection for stationary airbag, dynamic airbag, flat rigid wall and oblique load wall configurations. 121

Figure 6.11. Injured (upper) and normal (lower) subject MRI images overlaid with best metric measurement directions. 129

Figure 6.12. Probability of AIS 2+ trauma to posterolateral viscera with respect to peak normalized deflection (upper) and VCmax (lower) measured at θ = 130°. 130

Figure 7.1. Sectional image of Visible Male selected for model geometry. 134

Figure 7.2. Model geometry containing key features for mesh development. 135

Figure 7.3. Simplified model for mesh density investigation. 136

Figure 7.4. Chest wall compressive loading and corridor from PMHS tests. 139

Figure 7.5. Isolated whole liver stress-strain response plotted with range of experimental data. 140

Figure 7.6. Isolated whole-spleen stress-strain response plotted with range of experimental data. 140

Figure 7.7. Exemplar contour axes definition in undeformed and deformed states...143

Figure 7.8. SAE y-axis coordinate along exemplar chestband circumference: as measured (upper) and normalized to initial position and contour circumference (lower). 144

Figure 7.9. Exemplar chestband contours and resulting processed FE displacement contours for tests D-2 (left) and S-6 (right) at the xyphoid level in undeformed and deformed states. 145

Figure 7.10. Peak injury metric comparison between PMHS chestband result and FE loading input with respect to obliquity of measurement. 145

Figure 7.11. Geometric model variations corresponding to small (left) and large (right) visceral contents.....149

Figure 7.12. Model compliance for element side lengths considered. 150

Figure 7.13. Material response for element side lengths considered. 151

Figure 7.14. Resulting mesh density for the median viscera.....152

Figure 7.15. Pendulum loading at 60° with respect to anterior. 153

Figure 7.16. Force-deflection plots from PMHS and model pendulum impacts. 153

Figure 7.17. Model deformation response to boundary conditions: (a) dynamic OOP, (b) stationary OOP, (c) flat rigid, and (d) anterolateral oblique. ...155

Figure 7.18. Exemplar 5% area from which maximum material response was obtained. 156

Figure 7.19. Risk analyses with respect to peak material response after normalizing to 50% risk of PMHS injury. 157

Figure 7.20. Exemplar distributions of parenchymal strain, strain energy density, and capsular strain responses to loading from the four boundary conditions. 159

Figure 7.21. Refined spleen model and mesh density verification. 160

Figure 7.22. Mean affected area of 5th, 50th, and 95th percentile viscera models surpassing normalized material responses of strain energy density (upper), parenchymal strain (middle), and capsular strain (lower). 162

Figure 7.23. Coefficients of Determination (R^2) and PRESS statistics for correlations between oblique biomechanical parameters and tissue-level responses with median (50th) viscera model. 166

Figure 7.24. Coefficients of Determination (R^2) and PRESS statistics for correlations between oblique biomechanical parameters and tissue-level responses with large (95th) viscera model. 167

Figure 7.25. Coefficients of Determination (R^2) and PRESS statistics for correlations between oblique biomechanical parameters and tissue-level responses with small (5th) viscera model. 168

Figure 8.1. Transverse cross-sectional porcine anatomy at upper abdominal level corresponding to liver and spleen. 182

ONE

INTRODUCTION

Trauma resulting from motor vehicle crashes is a substantial problem in the United States. According to the Centers for Disease Control and Prevention (CDC), each year motor vehicle crashes are responsible for over 43,000 deaths and send another 2.7 million individuals to hospital emergency rooms (CDC, 2010). These annual fatalities and injuries cost an estimated $100 billion in lifetime medical spending and productivity losses (Naumann et al., 2010). Approximately 30% of crashes in the United States can be classified as lateral impacts (Dischinger et al., 1993; Roberts & Compton, 1993; Bedard et al., 2002; Samaha & Elliott, 2003; Nirula et al., 2005; Funk et al., 2008). Lateral impacts are uniquely characterized by (i) limited distance between the occupant and the vehicle interior, e.g., door panel or armrest, and (ii) limited vehicle structure between the occupant and the striking object, such as a stationary barrier or bullet vehicle (States & States, 1968; Viano et al., 1989a; Lau et al., 1991; Chung et al., 1999). Consequently lateral impacts have been associated with an increased risk of injury and doubled risk of mortality compared to similar energy vehicular impacts from frontal directions (Foret-Bruno et al., 1980; Dischinger et al., 1993; Siegel et al., 1993; McLellan et al., 1996; Zaouk et al., 2001; Bedard et al., 2002; Samaha & Elliott, 2003; Ryb et al., 2007; Nirula & Pintar, 2008).

The thorax and abdomen have been identified as particularly vulnerable to trauma in lateral motor vehicle crashes. Over half of lateral impact fatalities and serious injuries involve trauma to the thorax or abdomen (Hartemann et al., 1976a; Hartemann et al.,

1976b; Dischinger et al., 1993; Samaha & Elliott, 2003; Nirula et al., 2005). These injuries result primarily from occupant compartment intrusion during lateral impact. During impact (Figure 1.1), a striking object, e.g., a bullet vehicle, deforms the lateral vehicle structure, which intrudes into the occupant compartment. The magnitude and rate of intrusion are dependent upon the velocity, mass, and structural rigidity of the vehicle(s) involved. The occupant is generally theorized to maintain pre-event momentum until contacted by the lateral vehicle interior components as a result of deformation or struck vehicle translation. Consequently door contact is considered the primary mechanism of injury (States & States, 1968; Hartemann et al., 1976b; Cesari et al., 1978; Hartemann et al., 1979; Foret-Bruno et al., 1980; Siegel et al., 1993; Tencer et al., 2005a; Tencer et al., 2005b; Nirula & Pintar, 2008). The severity of contact is generally described by ΔV, the net change in velocity experienced by the vehicle occupant during the impact event.

Improvements to vehicle lateral impact crashworthiness have emphasized modulations to door contact parameters. When US vehicle crashworthiness regulations were updated between 1994 and 1998 to require dynamic lateral impact crash tests, automobile manufacturers generally employed side-structure stiffening and door panel padding to assure regulatory compliance (Kahane, 2007). These changes reduced biomechanical injury metrics (Section 3.1) as quantified by anthropomorphic test dummies to magnitudes permissible by regulations (Cesari et al., 1978; Deng, 1988; Olsson et al., 1989; Kiuchi et al., 1991; Lau et al., 1991; Hobbs, 1995; Lundell et al., 1995; Deng & Tzeng, 1996; McLellan et al., 1996; Igarashi et al., 1998; Schroeder et al., 1998; Kahane, 2007). With advancing passive safety technology and continued pressure

from consumer advocacy groups such as the Insurance Institute for Highway Safety (IIHS), inflatable restraint systems (airbags) have also been employed to reduce dummy injury metrics in crash tests.

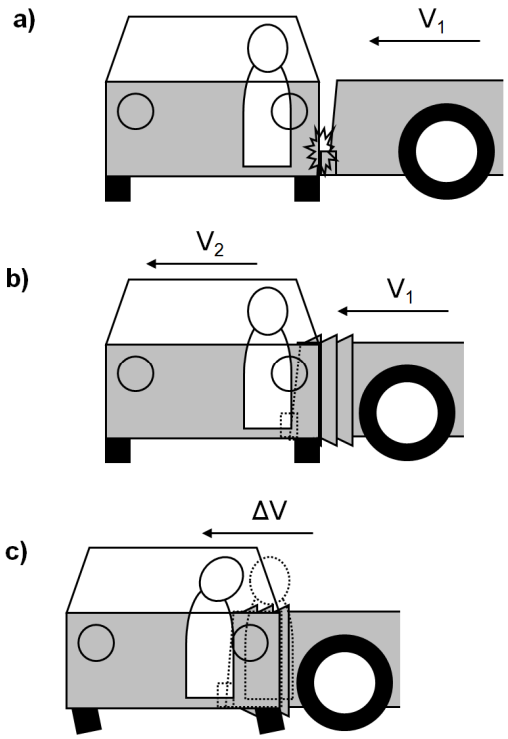

Figure 1.1. Event sequence for lateral vehicular impact: a) Initial contact, b) side structure deformation resulting in occupant-door contact, and c) final velocity.

First incorporated into vehicles in the 1970's (Smith, 1977), airbags for frontal impact protection were federally mandated in all passenger cars and light trucks sold in the US by the Federal Motor Vehicle Safety Standard (FMVSS) 208 (Hackney et al., 1984; NHTSA, 2001). Requirements dictated minimal protection to a 50th percentile unbelted male occupant in a 35 mph frontal collision, requiring inflation times and inflated volumes ranging 33-50 ms and 56-120 L, respectively (Hinch et al., 2001; NHTSA, 2001). Although retrospective studies have reported airbags to reduce frontal crash fatalities by 20% and overall crash mortality by 10% (NHTSA, 2001; Cummings et

al., 2002; Roselt et al., 2002; Olson et al., 2006), the propensity for airbag injury was not well understood prior to their implementation.

Utilizing controlled laboratory studies with preexisting dummy designs, frontal airbag systems were deemed safe to close-proximity, or "out-of-position," occupants (Hitchcock & Nash, 1980; Mertz et al., 1982; Morris, 1985; Backaitis & Roberts, 1987; Horsch et al., 1990; Melvin et al., 1993; Kent et al., 2005). Yet, investigational approaches for out-of-position scenarios utilized dummies originally designed for steering wheel hub loading to the sternum (Horsch et al., 1990; Melvin et al., 1993); field analyses incorrectly conjectured that "more children will be helped than harmed" (Hitchcock & Nash, 1980; Morris, 1985). Following the FMVSS 208 mandate, a collection of anecdotal reports accumulated which documented the traumatic injury risk to out-of-position pediatric and small female occupants (Weber, 1993; Coben, 1997; Kleinberger & Summers, 1997; Graham et al., 1998). With few case examples available, a pattern of injury for airbag loading was ascertained through a systematic process of case observation (Weber, 1993; Kleinberger & Summers, 1997), computational modeling of occupant kinematics (Berg et al., 1997; Kleinberger & Summers, 1997; Morris et al., 1998), and experimental replication (Mertz et al., 1982; Melvin et al., 1993; Berg et al., 1997; Kleinberger & Summers, 1997; Morris et al., 1998). In response to case studies and emerging research, the NHTSA again revised FMVSS 208 in 1997 to allow for "depowered" frontal airbags, shown safer to these at-risk occupants (NHTSA, 1997). Further, out-of-position test methods and modified child and small female dummies were developed to replicate injury mechanisms observed in actual case occupants (Crandall et al., 1998; Morris et al., 1998; Roychoudhury et al., 2000; Tylko & Dalmotas, 2001).

Continued retrospective analyses have confirmed elevated risk of injury to susceptible populations from older airbag designs (Kleinberger et al., 2000; Durbin et al., 2003; Kent et al., 2005; Newgard & Lewis, 2005; Quinones-Hinojosa et al., 2005; Donaldson et al., 2008). Yet, the NHTSA's response to these reports was effective. Although the NHTSA has confirmed 291 deaths attributable to frontal airbag deployment, over 75% occurred prior to 2001 and none were confirmed between 2006 and 2008 (NHTSA, 2008a).

The advent of lateral airbag restraints, i.e., side airbags, has been rapid but, unlike frontal airbags, unregulated. Side airbag technologies were not proposed publicly until the late 1980's (Olsson et al., 1989; Warner et al., 1989) and were first incorporated into vehicles in the mid-1990's (Yoganandan et al., 2007b). They are generally smaller than frontal airbags (~10 L) but, due to the limited distance between the occupant and intruding door, they must inflate substantially faster – within approximately 10 ms (Haland & Pipkorn, 1996). Side airbags are specific to vehicle model and exist in three primary configurations: head, torso, or combination head-and-torso (combo) airbags (Figure 1.2). Head side airbags are most commonly present as side curtains deploying from the roof rail or header. Torso and combo airbags are seat- or door-mounted, i.e., deploying from within the seat back or door panel lateral to the occupant. Because of the importance of thoracic and abdominal injury to the side impact injury pattern, torso-interacting airbags are particularly relevant to reducing morbidity and mortality in side impact crashes and are the focus of this study; torso airbags were already standard or available equipment in as many as 79% of 2010 model year vehicles in the US (IIHS, 2010).

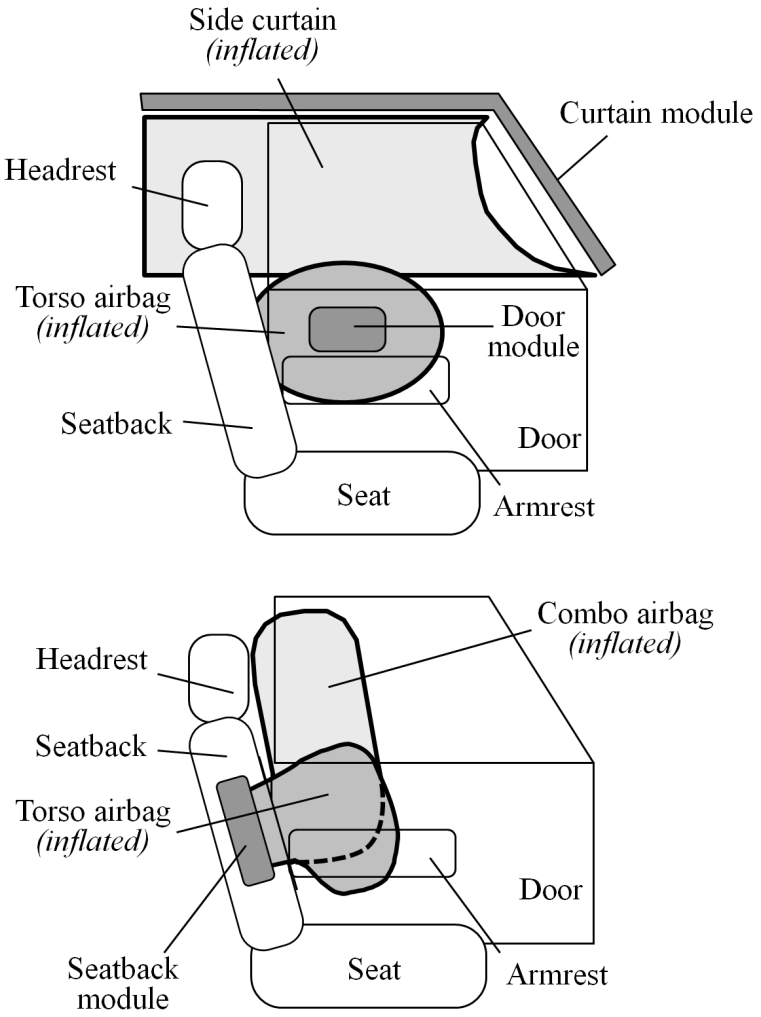

Figure 1.2. Side airbag protection and orientation options in contemporary automobiles.
Curtains may also be present with seatback-mounted torso airbags.

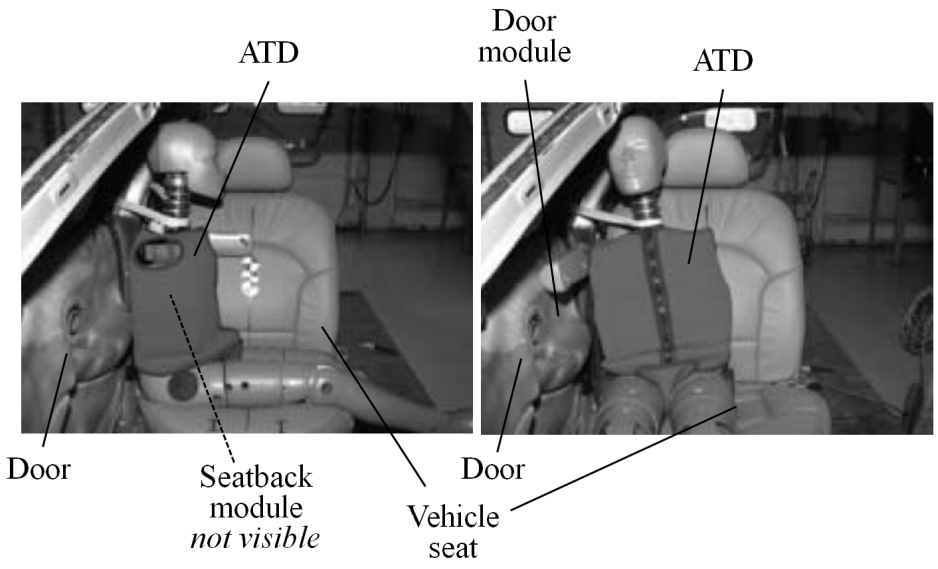

Figure 1.3. Torso side airbag out-of-position testing procedures for seatback- and door-mounted modules with small female anthropometry.
From IIHS (2003)

While epidemiological analyses of torso side airbag performance have reported inconsistent findings (Section 3.5.1), injury risks associated with out-of-position occupants have remained a concern. From lessons learned during frontal airbag implementation, studies attempted to preemptively identify and reduce injury risks from out-of-position scenarios to children and small adults (Khadilkar & Pauls, 1998; Schroeder et al., 1998; Pintar et al., 1999; Tylko & Dalmotas, 2000; Prasad et al., 2001; Duma et al., 2003a; Duma et al., 2003b; IIHS, 2003; Louden, 2007; Hallman et al., 2008; Hallman et al., 2009a; Hallman et al., 2009b). A Technical Working Group consisting of industry, government, and consumer organizations published a series of "Recommended Procedures" for assessing the out-of-position injury risk from side airbags available in US automobiles (Prasad et al., 2001; IIHS, 2003). As shown in Figure 1.3, these procedures employed female and child anthropometry dummies in close proximity to airbag

modules. Numerous orientations were conjectured to represent the "worst-case" scenarios for injury risk exposure; as many as practical were included in the Recommendations. Yet few studies have attempted to characterize injury patterns resulting from out-of-position side airbag deployment in real-world crashes (Section 3.5). Therefore the Recommended Procedures may not include scenarios relevant to injuries occurring in actual vehicle collisions. Further, side impact dummies developed prior to the introduction of side airbags may not be appropriate for close-proximity torso side airbag contact.

To address this issue, two study hypotheses of out-of-position side airbag loading were proposed. The study Hypothesis 1 was that ***thoracoabdominal deformation patterns resulting from out-of-position torso airbag interaction are morphologically different from lateral loading.*** Consequently, anthropomorphic test dummies designed for unprotected lateral thoracic loading may be incapable of a biofidelic response which may characterize out-of-position thoracoabdominal interaction. Because out-of-position deformation is hypothesized to induce unique deformation patterns, this boundary condition may also warrant unique biomechanical injury metrics (Section 3.1). Therefore study Hypothesis 2 was that ***thoracoabdominal injury response to out-of-position interaction with torso airbag is better predicted by a viscous metric than a deflection metric.***

The present study represents a heretofore neglected analysis of observed torso side airbag injuries. By identifying relevant injury patterns observed clinically, present out-of-position test protocols and dummies may be modified to accommodate injury mechanisms undetectable by present practices. Through this work, a thoracoabdominal

injury modality from torso side airbags, namely splenic trauma, was identified. The historical progression of frontal airbag out-of-position research, which the present study parallels, required the examination of real-world injuries (Hitchcock & Nash, 1980; Backaitis & Roberts, 1987; Mertz, 1988; Lancaster et al., 1993; Dalmotas et al., 1995), computational modeling of occupant dynamics in observed real-world scenarios (Berg et al., 1997; Kleinberger & Summers, 1997; Digges et al., 1998; Plank et al., 1998; Roychoudhury et al., 2000; Cheng et al., 2003), and controlled laboratory experiments and injury criteria development (Horsch & Culver, 1979; Mertz et al., 1982; Melvin et al., 1993; Berg et al., 1997; Hardy et al., 1997; Kleinberger & Summers, 1997; Crandall et al., 1998; Digges et al., 1998; Morris et al., 1998). This process was incorporated into the present study as four Specific Aims which are addressed in following chapters.

1. Identify unique thoracoabdominal injuries, as described by anatomical location and the Abbreviated Injury Scale, during documented side impacts involving torso-interacting side airbags.
2. Determine relationship between lateral thoracic biomechanical response and parameters of door intrusion velocity and occupant position to define “out-of-position” torso airbag interaction.
3. Characterize torso deformation and direction resulting from out-of-position side airbag interaction.
4. Quantify injury risk, as measured by Abbreviated Injury Scale and tissue-level material response, associated with out-of-position torso side airbag interaction with the thoracoabdominal region.

TWO

THORACOABDOMINAL ANATOMY

The torso encompasses the central component of many animal bodies. In humans, it serves as the core from which the neck, upper extremities, and lower extremities extend. In addition to its function as an anchor for these structures, it contains and shields the viscera within a hollow internal cavity. This internal cavity is subdivided by the diaphragm into two regions: thorax and abdomen. A third sub-cavity is often separated from the abdomen and termed the pelvic cavity. The following sections describe anatomy relevant to the aims of the present study. The reader is directed to the following references for further information, including physiology: Gray, 1918; Davies & Withrington, 1973; Chiles et al., 1975; Moss et al., 1981; Robertson et al., 2001; Bergman et al., 2002; Tablin et al., 2002; Geraghty et al., 2004; Rietzel et al., 2004; Drake et al., 2005; Iazzetti & Rigutti, 2005; Guyton & Hall, 2006; Netter, 2006; Liu et al., 2009.

2.1 EXTERNAL ANATOMY

Human anatomy is described by accepted medical convention (Gray, 1918). Primary anatomical planes are: sagittal, dividing left from right; coronal, dividing anterior from posterior; and transverse, dividing superior from inferior. As shown in Figure 2.1 and Figure 2.2, the torso is subdivided into regions by external landmarks, permitting thoracoabdominal anatomical description.

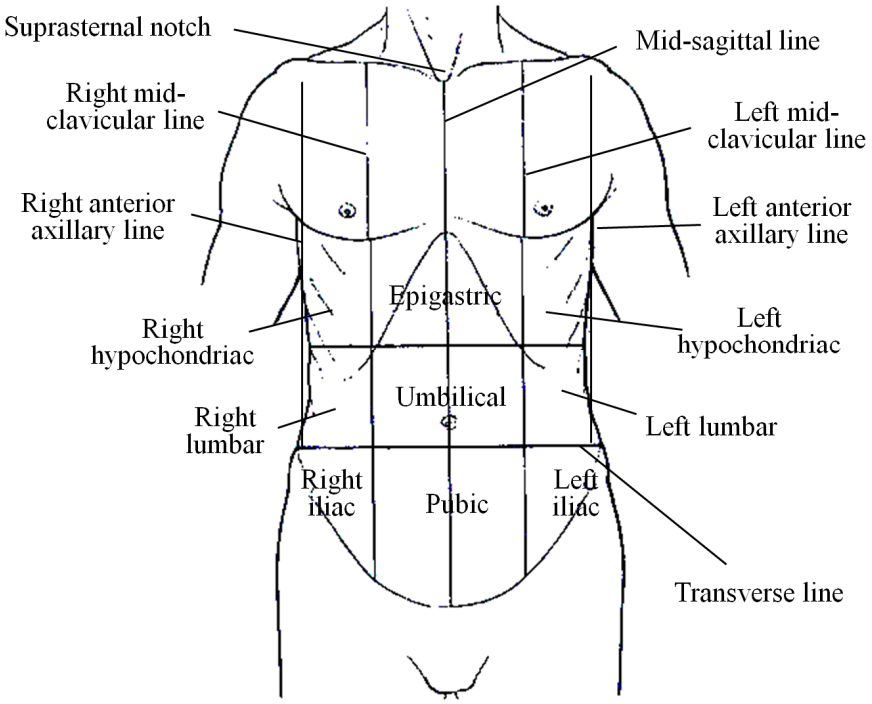

Figure 2.1. External torso anatomical regions viewed in coronal plane from anterior.
Modified from Gray (1918)

2.2 SKELETAL ANATOMY

The skeletal structures of the torso include all calcified tissues forming bone. The vertebral column composes the central support structure and, within the torso, can be subdivided into thoracic and lumbar regions (Figure 2.3). The thoracic region of the vertebral column is composed of twelve vertebral bodies, numbered T1 through T12. The lumbar region of the vertebral column is composed of five bodies, numbered similarly L1 through L5. Superior to T1 are the cervical vertebrae and skull, which compose the head/neck complex; inferior to L5 lies the sacrum, pelvis and lower extremities. These structures are not detailed here but are described in referenced texts.

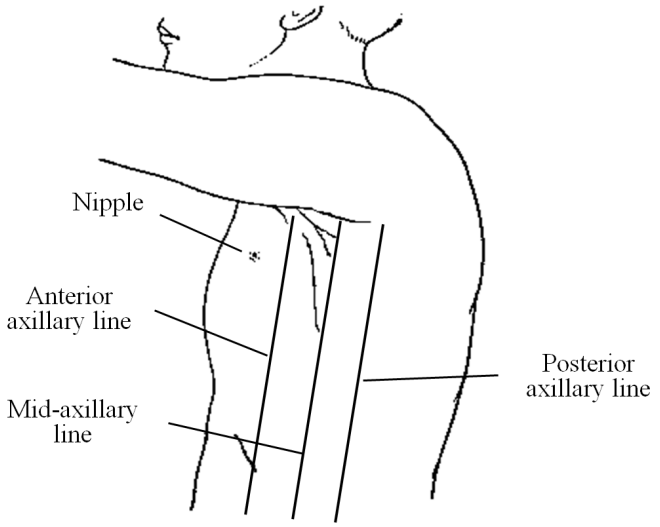

Figure 2.2. External torso anatomical regions viewed in sagittal plane from left lateral.
From Gray (1918)

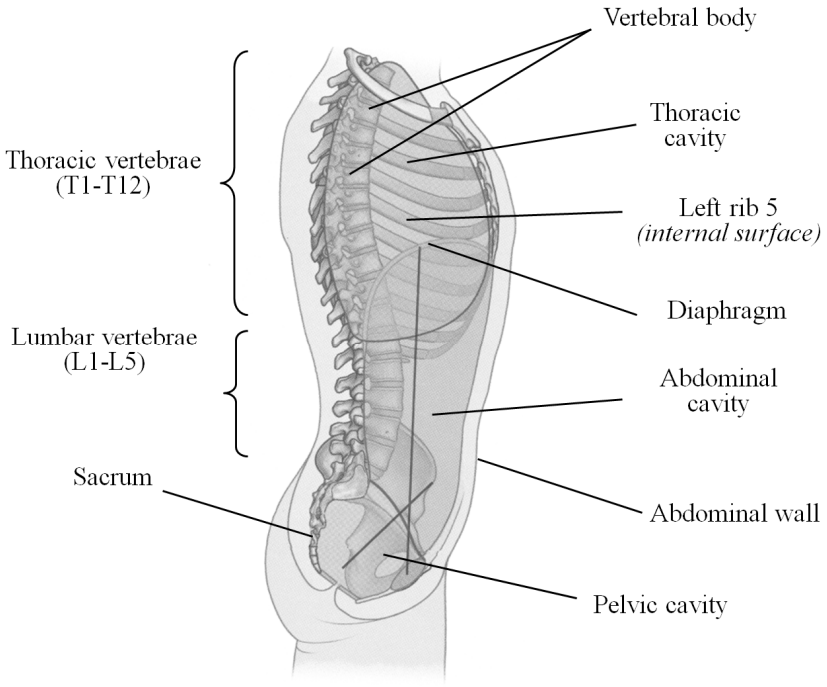

Figure 2.3. Torso cavities in mid-sagittal plane, viewed from right lateral.
From Drake et al (2005), used with permission

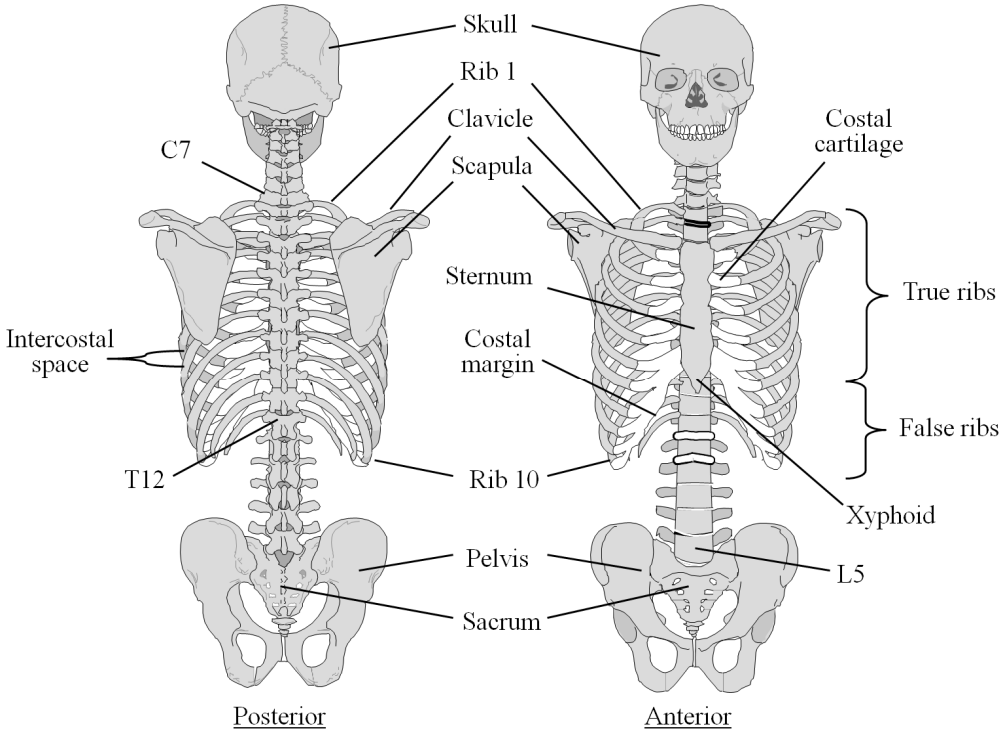

Figure 2.4. Primary skeletal structures of the torso, viewed in coronal plane from anterior and posterior.

Each thoracic vertebra is flanked by a pair of ribs (Figure 2.4), which are numbered rib 1 through rib 12 so as to correspond to the adjacent twelve thoracic vertebrae. Collectively these are referred to as the ribcage. Each rib projects posterolaterally from the thoracic spine at an angle oblique to all three primary anatomical planes. The ribs are broadly classified as true ribs and false ribs. True ribs, i.e., rib 1 through rib 7, extend anteriorly to articulate with the sternum by means of their respective costal cartilages (Figure 2.5). False ribs, consisting of rib 8 through rib 12, do not articulate directly with the sternum. The costal cartilages of rib 8 through rib 10 fuse anteriorly to form the costal margin, which articulates with the costal cartilage of rib 7. Rib 11 and rib 12 are also termed floating ribs because their costal cartilages do not articulate with other skeletal structures. Unlike the thorax, the abdomen has limited

skeletal structure anteriorly. However, the false ribs extend inferiorly to shield the lateral and posterior aspects of the most superior abdominal contents (Section 2.3).

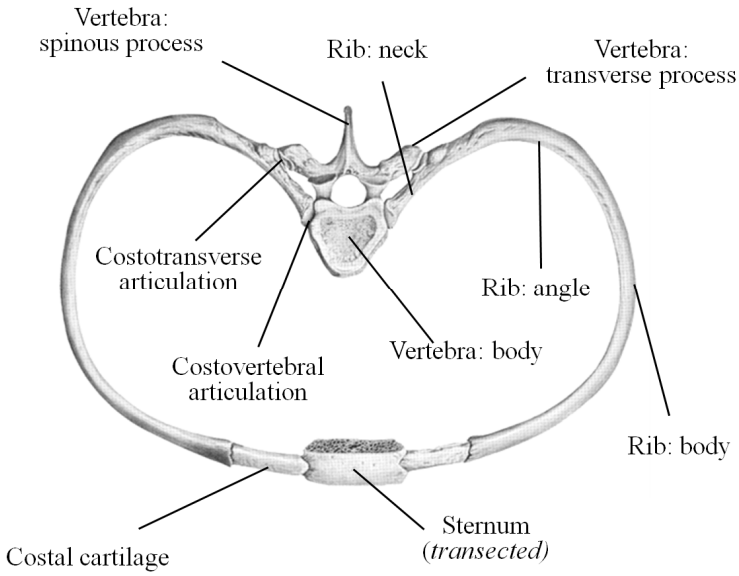

Figure 2.5. Ribcage cross-sectional unit, viewed from superior.
From Iazzetti et al. (2005), used with permission

In addition to providing structural support to the extremities and protection to the viscera from trauma, the ribcage serves a notable physiologic function during respiration. To cause inspiration, the ribcage increases in volume as rib obliquity is decreased with respect to both the sagittal and coronal planes (Figure 2.6). Although a singular articular movement, this inspiratory motion can be visualized as rotation about two axes. The first axis (A-A) increases the breadth of the thorax in the coronal plane; the second axis (B-B) raises the sternum and increases the depth of the thorax in the sagittal plane (Gray, 1918). Because of this function, each rib is comparatively flexible at the costovertebral junction and costal cartilage (posterior and anterior articulations).

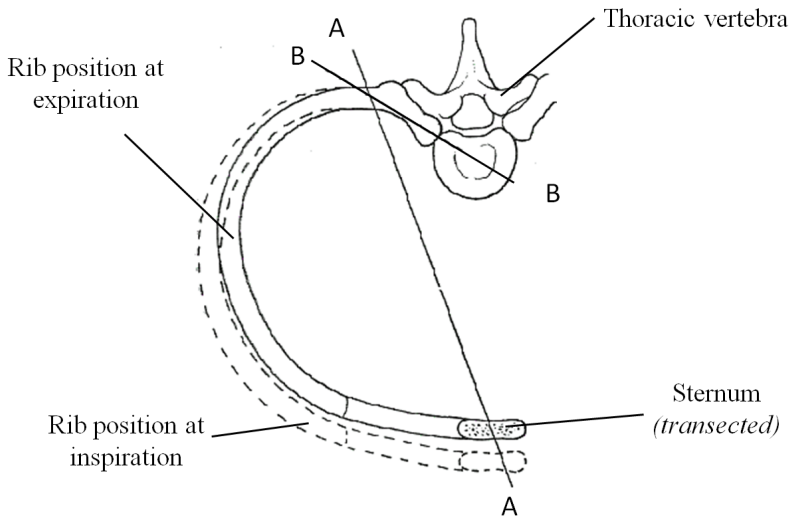

Figure 2.6. Axes of rib motion during respiration.
From Gray (1918)

2.3 VISCERAL ANATOMY

The visceral tissues within the thoracic and abdominal cavities vary widely with respect to function, vasculature, and physical properties; they are therefore asymmetric as well as inhomogeneous (Rouhana, 1993; Yoganandan et al., 2001).

The mediastinum and the lungs are entirely enclosed within the thoracic cavity (Figure 2.7). Deep to the sternum, the mediastinum is composed of the anatomical structures between the lungs, primarily the heart, great blood vessels, esophagus, and trachea. Bilateral to the mediastinum are the lungs. Each lung is contained within a pleural cavity, and a serous membrane provides lubrication between the lung and parietal pleura during respiratory motions (Section 2.2). During quiet respiration, the inferior margin of the lung crosses rib 6 at the mid-clavicular line and extends to T10 posteriorly. Inferior to the heart is the diaphragm, a broad muscular dome originating from the inferior thoracic cage and lumbar spine to seal and separate the thoracic and abdominal

cavities. As the diaphragm contracts during inspiration, it suppresses the abdominal contents to expand the thoracic cavity. As described in Section 2.2, the ribs also assist in expanding the thoracic cavity by means of the intercostal muscles.

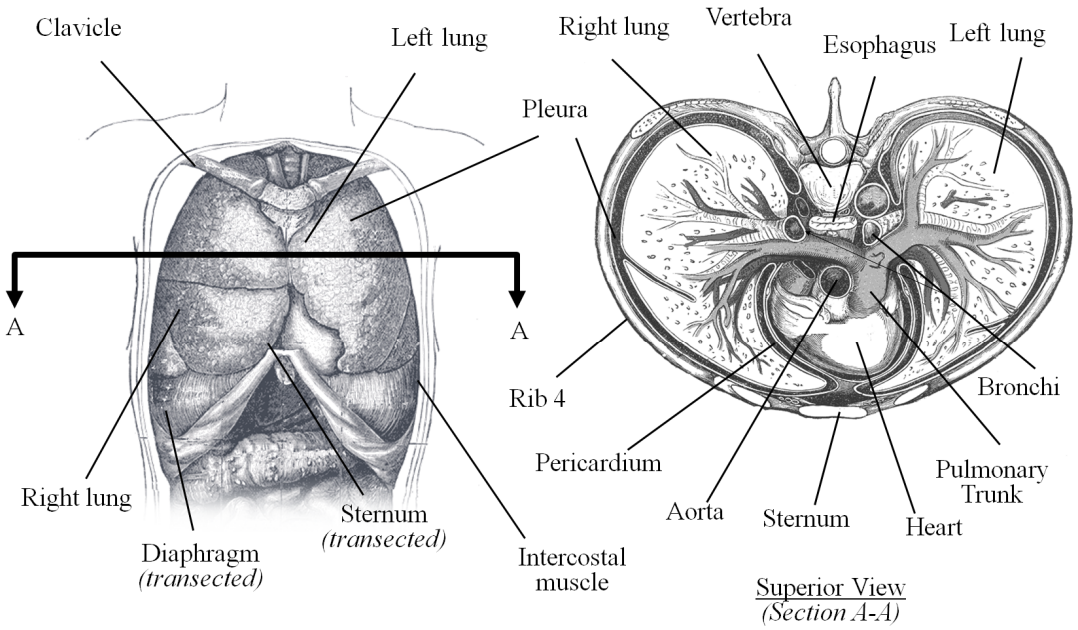

Figure 2.7. Visceral contents of the thoracic cavity, anterior and superior views.
From Gray (1918)

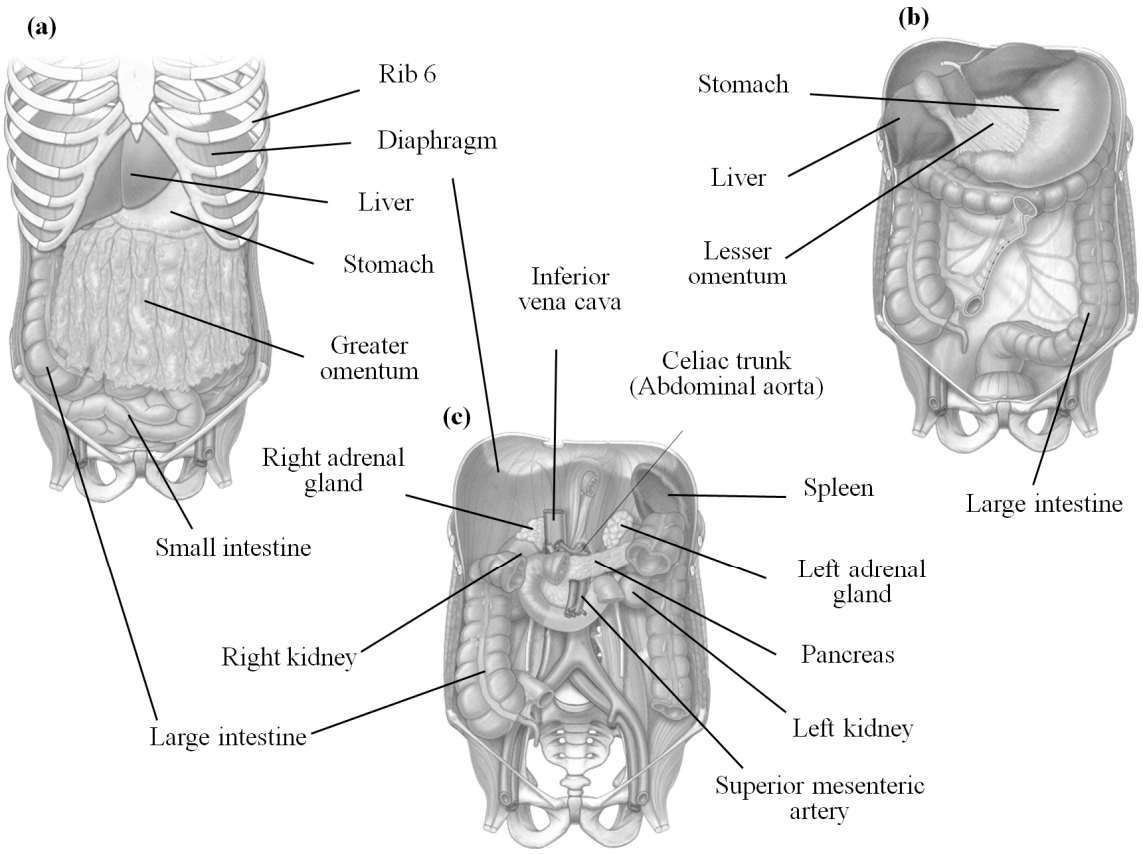

Figure 2.8. Anterior view of progressive abdominal dissection: (a) Following removal of superficial tissues and abdominal wall; (b) Following removal of false ribs, greater omentum, and small intestine; (c) Following removal of liver, stomach, and partial large intestine.
From Drake et al. (2005), used with permission

The contents of the abdominal cavity are heterogeneous and can be broadly subdivided into two categories: solid organs and hollow organs (Rouhana, 1993; Yoganandan et al., 2001). Solid organs consist of a metabolically active parenchyma surrounded by a thin fibrous capsule. Hollow organs exist primarily in the gastrointestinal tract and consist of serous, muscular, and epithelial tissue layers surrounding a central lumen (cavity). Shown in Figure 2.8 are anterior views of a progressive dissection of the abdominal cavity. The liver is a solid organ located in the right hypochondriac region. Weighing approximately 2,000 g, it is the largest visceral organ in the human and is responsible for many metabolic functions. Receiving

approximately 25% of the total resting blood-flow (cardiac output) from the abdominal aorta via the celiac trunk and from the portal vein (originating from the intestines—see below), it contains approximately 450mL (~10%) of blood volume at rest. In instances of cardiomyopathy it can expand to store as much as one liter of additional blood volume (Guyton & Hall, 2006). Inferior to both the liver and the diaphragm in the epigastric region lies the stomach. The greater omentum, a fold of fatty connective tissue, originates from the inferior surface of the stomach and drapes inferiorly between the abdominal wall and the abdominal viscera. The lesser omentum is similar in structure but originates from the opposing stomach surface and affixes to the inferior surface of the liver. Immediately deep to the greater omentum, approximately seven meters of hollow intestine extend from the stomach and are coiled primarily in the umbilical and pubic regions of the abdomen (Gray, 1918). Arterial blood-flow to the intestines is provided primarily from the superior and inferior mesenteric arteries and can account for 20% of resting cardiac output. Venous blood return from the intestines flows to the liver via the portal vein. The spleen, posterolateral to the stomach and inferior to the diaphragm, is a lobular highly vascular solid organ responsible for cardiovascular and immunological functions. At rest, splenic blood flow has been measured between 2% and 14% of the total cardiac output (Davies & Withrington, 1973; Guyton & Hall, 2006). Inferior to the spleen and liver, the left and right kidneys lie bilateral to the vertebral column and posterior to the other abdominal contents. These solid organs each are approximately 150 g and filter approximately 20% to 25% of resting blood circulation by means of the abdominal aorta, returning it to inferior vena cava (Guyton & Hall, 2006). The adrenal glands are superior to both kidneys and serve critical metabolic functions not detailed

here. These glands receive less than 1% of resting cardiac output, although this figure is disproportionately large considering their average mass (4 g) (Guyton & Hall, 2006).

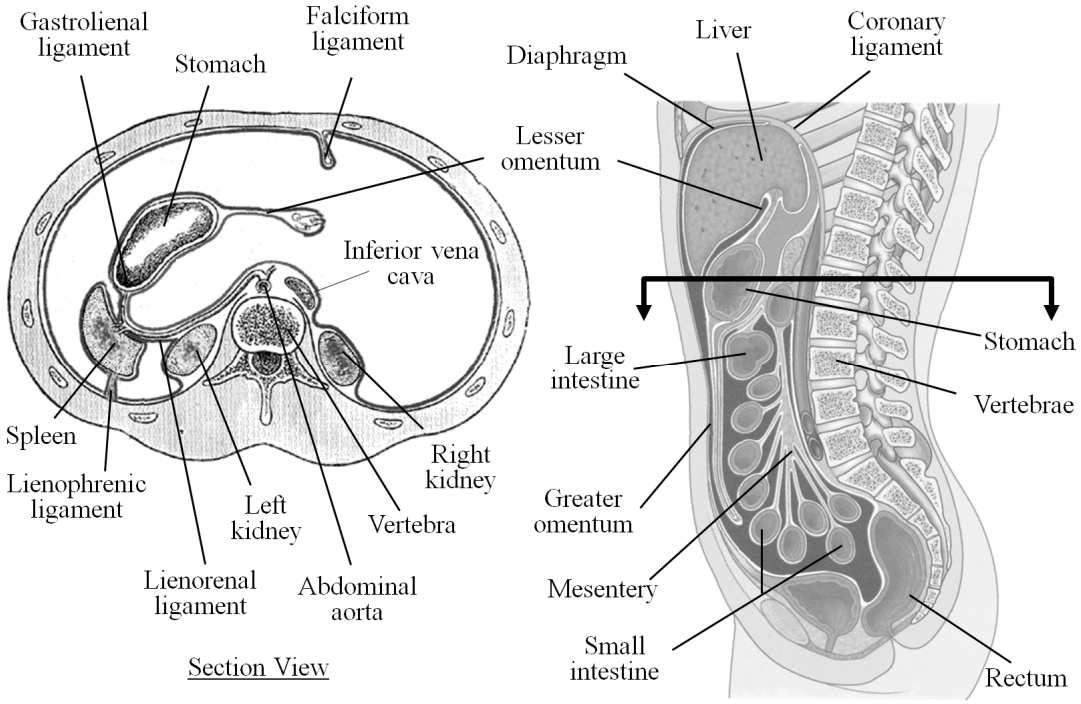

Figure 2.9. Abdominal peritoneum viewed in transverse and sagittal sections.
From Gray (1918) and Drake et al. (2005), use with permission

The peritoneum, a double-layered serous membrane, protects and suspends the intra-abdominal contents (Figure 2.9). The membrane anchors the surrounded abdominal tissues primarily to the posterior abdominal wall. Where the liver is attached superiorly to the diaphragm, the peritoneum is termed the coronary and falciform ligaments. The section of peritoneum which attaches the spleen to the stomach is the gastrolienal ligament; where the spleen is attached to the posterior abdominal wall, the lienorenal ligament; where the spleen is attached to the diaphragm, the lienophrenic ligament. Unlike the other intra-abdominal contents, the kidneys and adrenal glands are retroperitoneal.

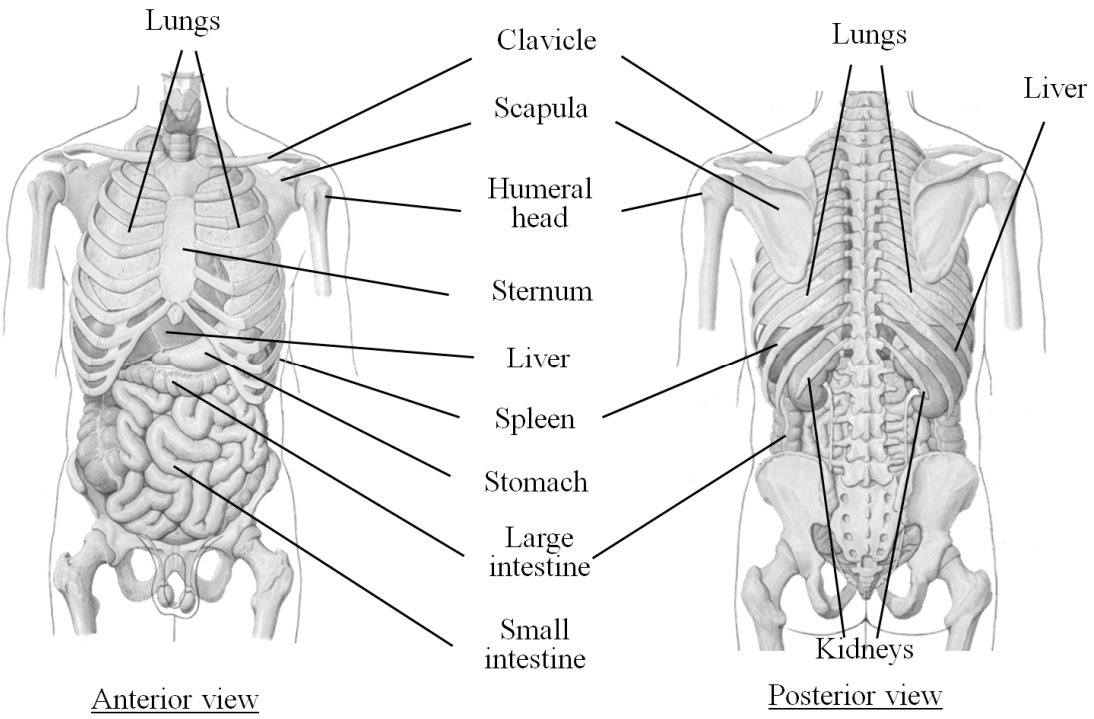

Figure 2.10. Torso visceral contents in skeletal context, viewed in coronal plane.
From Iazzetti et al. (2005), used with permission

Shown in Figure 2.10 are the thoracoabdominal viscera of the human torso in skeletal context. Superficial tissues, muscles, and greater omentum have been removed. The hollow organs, i.e., the stomach and intestines, are most superficial near the anterior abdominal wall. The solid organs are primarily posterior and adjacent to skeletal structures, i.e., the false ribs and vertebral column. With musculature absent, the liver is most apparent in the lateral and posterolateral regions of the ribcage, deep to ribs 7 through 10. The spleen is most apparent in the left posterolateral region of the ribcage, deep to the curvature of ribs 9 through 11. Because the liver and spleen are inferior to the diaphragm but partially within the thoracic cage, they have been categorized with thoracic anatomy as “hard thorax” structures for biomechanical injury metric development (see Section 3.1). The left and right kidneys are bilateral to the vertebral

column, deep and inferior to the floating ribs. Mildly asymmetric in the coronal plane, the left kidney is generally superior to the right kidney.

2.4 ANATOMIC VARIABILITY

Although general anatomic location is primarily consistent throughout the normophysiologic adult population, precise size and position of the thoracoabdominal contents has been demonstrated to be subject- and posture-specific (Geraghty et al., 2004; Rietzel et al., 2004; Kim et al., 2007; Beillas et al., 2009; Lafon et al., 2010). With Positional Magnetic Resonance Imaging (MRI) scanners, thoracoabdominal organ positions have been studied for standing, sitting, supine, and forward-flexed postures (Beillas et al., 2009; Lafon et al., 2010). Comparing standing to supine postures, organ locations deviated inferiorly between 31mm (left kidney) to 39mm (liver). With inferior motion of the abdominal contents, the thoracic cavity was found to expand approximately 20%; no statistically significant change in abdominal cavity volume was observed. Further, individual organ volumes did not vary with subject posture, although variations within subjects were observed. Normalized to sample mean, liver and kidney volumes varied approximately ± 20%; spleen volume was found to vary between -50% and +100% of sample mean. Kidney position demonstrated greatest variability in subject set, with centers of mass varying more than 115mm in the superior-inferior direction. Although these anatomic variations are wide, multivariate regression has demonstrated organ volume to approximate a normal distribution when scaled by subject gender, height, and mass (Geraghty et al., 2004). Volume distributions for liver, spleen, and left and right kidneys are shown in Table 2.1 for both males and females. As was found in many studies (Davies & Withrington, 1973; Moss et al., 1981; Skandalakis et al., 1993;

Robertson et al., 2001; Beillas et al., 2009; Liu et al., 2009), the spleen demonstrated greatest anatomical variability; masses from 50 g to over 800 g have been reported (Davies & Withrington, 1973). Patients characterized by abnormal spleen size (splenomegaly) and abnormal liver size (hepatomegaly) were excluded from the dataset.

Table 2.1. Volume distribution measured in cm^3 for adult normal population, normalized to subject height and weight.
From Geraghty et al. (2004)

Population	Liver	Spleen	Left Kidney	Right Kidney
5th Female	975	71	107	98
5th Male	1236	124	154	132
50th Female	1410	180	160	153
50th Male	1710	238	201	185
95th Female	1843	288	214	206
95th Male	2183	353	249	238

THREE

STATE OF THE ART:
THORACOABDOMINAL TRAUMA IN SIDE IMPACT

Past and present research has correlated traumatic injury response of human tissue, i.e., material or physiologic disruption, with external biomechanical response parameters. Biomechanical responses, e.g., acceleration or displacement measurements, provide biofidelity corridors for the development of mechanical occupant surrogates (dummies) implemented in full-scale vehicle crashworthiness assessments. Matched traumatic injury responses provide tolerance thresholds, i.e., injury criteria, for interpretation of dummy response data. Injury response of research subjects is generally reported in accordance with the holistic Abbreviated Injury Scale – AIS (Copes et al., 1990; AAAM, 2005). According to the AIS, minor injury is scored AIS 1 and unsurvivable injury is scored AIS 6. Intermediate levels are termed moderate (AIS 2), serious (AIS 3), severe (AIS 4), and critical (AIS 5). Scores are assigned to each organ or structure individually, e.g., thoracic cage, liver, aortic arch, etc. Scaling guidelines are explicitly defined by the Association for the Advancement of Automotive Medicine (AAAM, 2005).

This chapter summarizes published research regarding biomechanical injury tolerance of the thorax and abdomen in side impact vehicular crashes. Existing biomechanical injury metrics are described (Section 3.1). Developments in experimental methodologies through the Chestband device (Section 3.2) and in computational modeling (Section 3.3) are also addressed. Boundary condition effects are addressed

with regard to injury metrics and injury mechanisms in Section 3.4. Considerations necessary for injury mitigation through side airbags are explored in Section 3.5. The reader is referred to cited literature for further information.

3.1 LATERAL INJURY METRICS

Biomechanical injury correlates (metrics) have been developed in laboratory experiments for quantitative predictions of injury risk from biomechanical data. For simulation of lateral impact to the torso in laboratory settings, localized pendulum, gravity drop, and whole-body sled impacts have been employed (Figure 3.1). Injury observations are generally made by post-test full dissection necropsy; with postmortem subjects, noninvasive imaging methods such as ultrasound, computed tomography (CT), and magnetic resonance imaging (MRI) have not been shown effective in detecting visceral injury (Christe et al., 2009; Kendall et al., 2009). Biomechanical signal acquisition has been standardized by the Society of Automotive Engineers (SAE) in document J211: Surface Vehicle Recommended Practice. Channel Filter Classes (CFC) are specified by corridors with attenuation above 1000, 600, 180 or 60 Hz. Transducer orientations are standardized in the SAE occupant coordinate system (Figure 3.2). The following sections describe the development of accepted thoracoabdominal injury metrics for lateral impact and are subcategorized by mechanical derivation: acceleration (Section 3.1.1), deformation magnitude (Section 3.1.2), and deformation rate (Section 3.1.3).

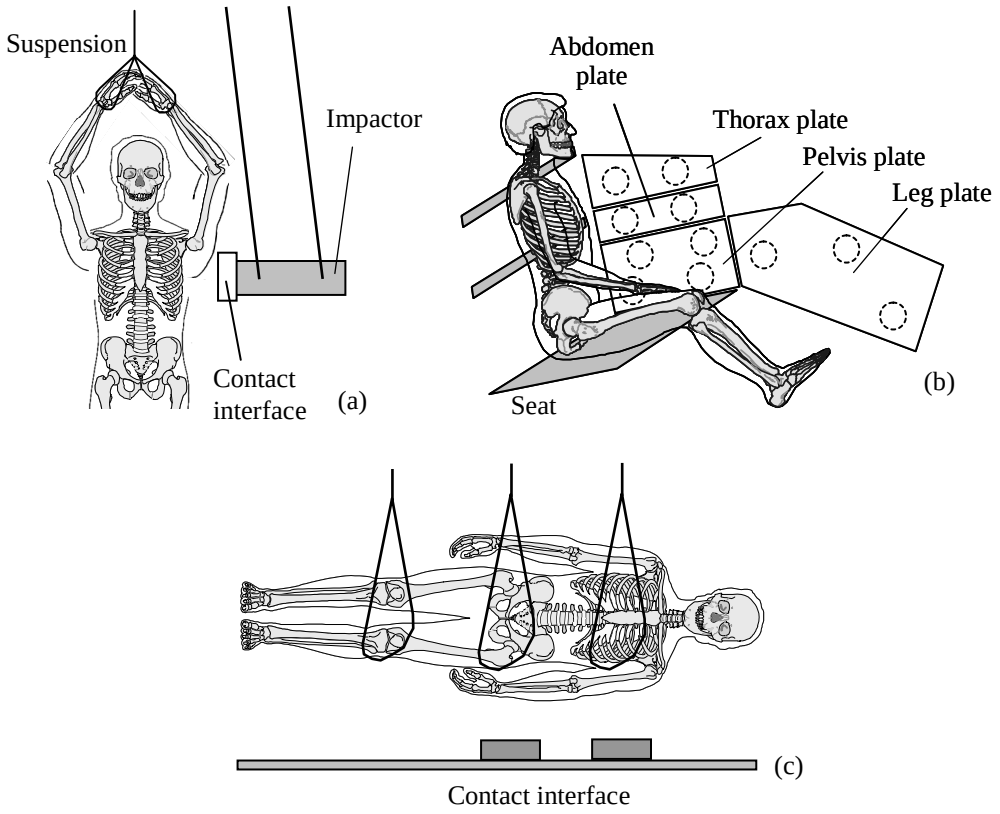

Figure 3.1. Test methodologies in side impact biomechanical investigations. (a) pendulum impact, (b) sled, (c) gravity drop.

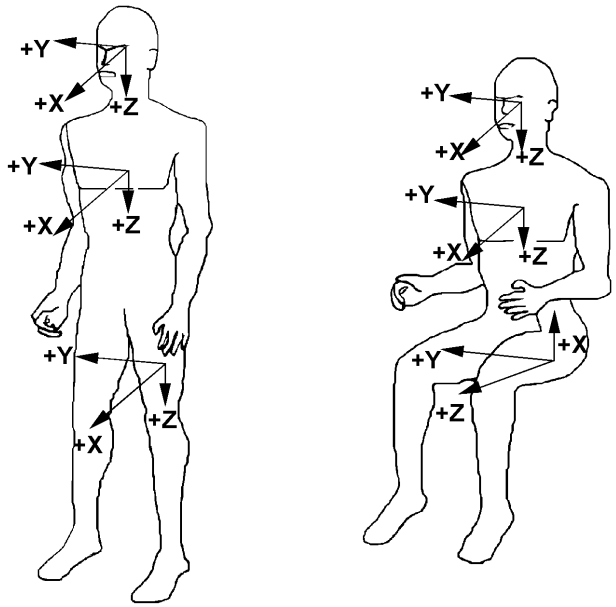

Figure 3.2. Occupant local coordinate system endorsed by the Society of Automotive Engineers.

3.1.1 ACCELERATION

Lateral impact tolerance was first investigated by military researchers utilizing healthy volunteers (Stapp, 1951; Zaborowski, 1964; Spark, 2003). Fully restrained subjects were oriented in forward- and rearward-facing seats and exposed to accelerations averaging from 98 to 392 m/s^2; subjects with lap belt restraints only were oriented in lateral facing seats and exposed to accelerations of 32 to 88 m/s^2. With forward orientation, average accelerations up to 340 m/s^2 were tolerated without lasting physiologic effect. In lateral exposure with lap belt restraint only, 50% of subjects reported persisting physical discomfort when accelerations were greater than or equal to 61 m/s^2. Orientation and restraint system contributed to the reduced acceleration tolerance, suggesting that tolerance to impact is reduced in lateral orientations and that restraint system is essential to mitigating injury (Zaborowski, 1964).

Using post-mortem human subjects (PMHS) and primate models, a thoracic accelerometer array (Figure 3.3) was developed for obtaining localized biomechanical data for injury criteria involving the hard thorax (Section 2.3) (Robbins et al., 1976). This array, which treated the thoracic cage as a deformable elliptical cylinder, included uniaxial accelerometers on the lateral and anterior boney structures (ribs 4 and 8, sternum), and triaxial accelerometer mounts on the spinous processes of T1 and T12.

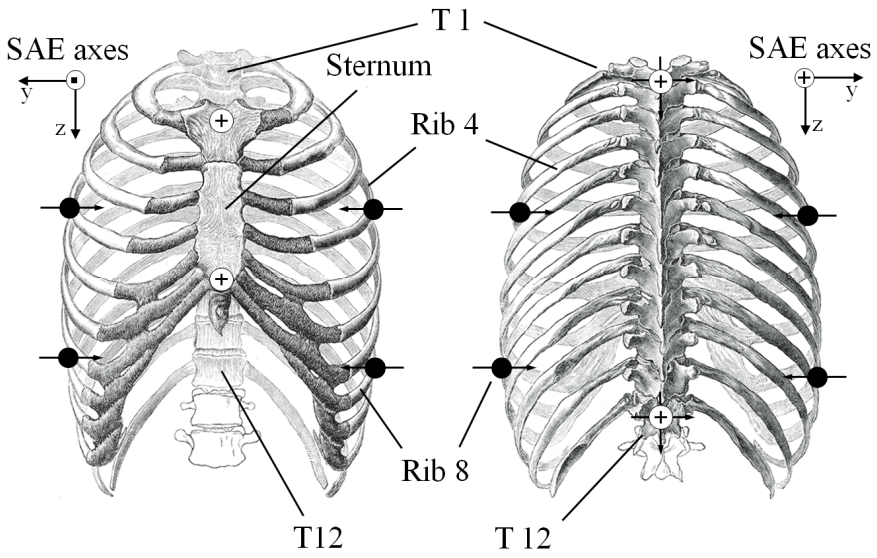

Figure 3.3. Accelerometer array developed by Robbins et al. (1976).

Continued use of this array permitted the development of a NHTSA-sponsored database of PMHS tests with standardized instrumentation utizing pendulum impacts (Melvin et al., 1976; Eppinger et al., 1978; Morgan & Waters, 1980; Cesari et al., 1981; Morgan et al., 1981; Nusholtz et al., 1983), drop impacts (Stalnaker et al., 1979; Tarriere et al., 1979), and sled impacts (Melvin et al., 1976; Eppinger et al., 1978; Robbins & Lehman, 1979; Morgan & Waters, 1980; Kallieris et al., 1981; Morgan et al., 1981; Cesari et al., 1983; Marcus et al., 1983). A compilation of test parameters and injury observations is presented in Appendix A for all NHTSA-sponsored lateral impact tests (Table A.1). Using 49 tests with accompanying accelerometer data, multivariate regression analysis identified an injury metric for risk of trauma to the hard thorax (Eppinger et al., 1984). This metric, termed the Thoracic Trauma Index (TTI), is shown in Eq. 3.1 (Eppinger et al., 1984; Morgan et al., 1986):

$$TTI = 1.4 \times \mathbf{Age} + 0.5 \times (\mathbf{T12_Y} + \mathbf{RIB_Y}) \times \mathbf{M} / 75 \qquad (3.1)$$

In Eq. 3.1, Age represents subject age, $T12_Y$ represents the peak signal from the T12 accelerometer oriented in the SAE y axis, RIB_Y represents the greatest of the peak signals from the rib 4 and rib 8 accelerometers, and M represents subject mass (kg). Risk curves for TTI are shown in Figure 3.4 for AIS 3+, 4+, and 5+ traumatic injuries to the hard thorax. An injury criterion of TTI = 145 g represented 25% risk of AIS 4+ hard thoracic injury. The NHTSA Side Impact Dummy (NHTSA-SID, Figure 3.5) was also developed to biofidelically measure occupant TTI for a 45 year old 75 kg (50th percentile) male during Federal regulatory crashworthiness assessments (Stalnaker et al., 1979). Minimum lateral protection standards are currently specified using the NHTSA-SID and TTI in Federal Motor Vehicle Safety Standard 214 for all consumer vehicles sold in the US (FMVSS 214, 1998).

Because of the accelerometer orientations, TTI and other acceleration-based injury metrics, e.g., Average Spine Acceleration (Cavanaugh et al., 1993), are subject to decreased sensitivity with increased load obliquity. Therefore, both TTI and ASA are valid for lateral and near-lateral impacts only. Similarly, the NHTSA-SID was developed to quantify occupant TTI response to lateral impact and may have questionable validity with other injury metrics or loading modalities.

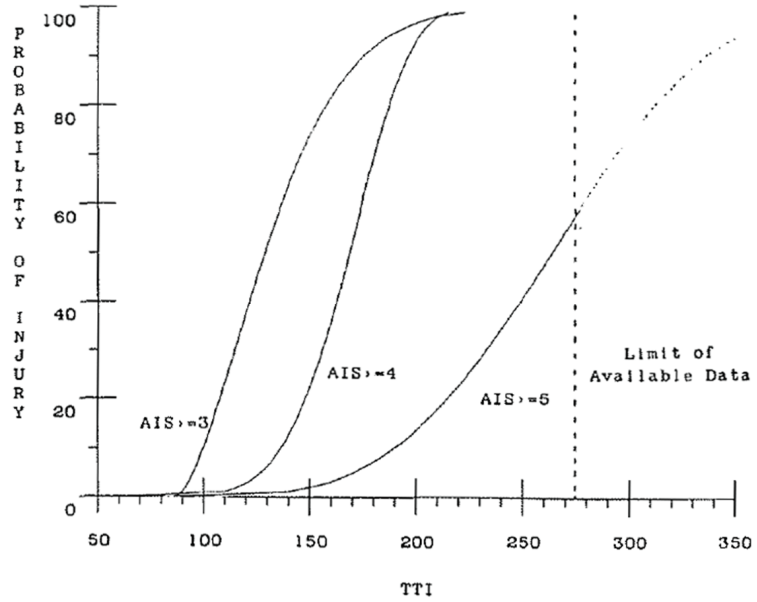

Figure 3.4. Probability of hard thorax trauma as a function of TTI.
From Marcus et al. (1986)

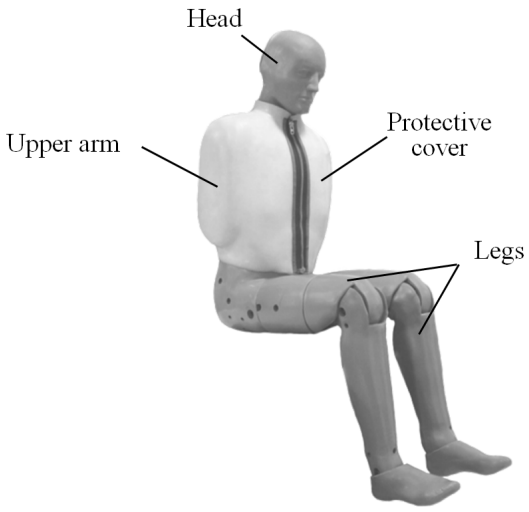

Figure 3.5. NHTSA-SID currently employed for FMVSS 214 crashworthiness regulations.

3.1.2 DEFLECTION MAGNITUDE

Magnitude of deformation (deflection) was identified as an injury correlate but has been historically difficult to quantify (McElhaney et al., 1971; Stalnaker et al., 1973). Using eight PMHS subjected to simulated automobile armrest impactors, lateral deflection of 6.7 cm was proposed as a limit to prevent rib fracture (Stalnaker et al.,

1973). Deflection was quantified by pre-limited linear impactor travel. From 26 drop tests, full-chest deflection of 30% and half-chest deflection of 35% were proposed as limits to prevent rib fracture (Stalnaker et al., 1979; Tarriere et al., 1979). Half-chest deflection was quantified using high speed videography and optical markers to measure between the sternum centerline and thorax contact surface. Full-chest deflection was recorded videographically by an invasive arrangement of rods through the chest cavity (Tarriere et al., 1979). Twelve PMHS were subjected to flat rigid and padded wall sled impacts with $\Delta V = 6.6 – 10.5$ m/s (Cavanaugh et al., 1990). Normalizing half-chest deflection to full chest breadth, logistic regression determined 0.31 (31%) corresponded to 50% risk of AIS 4+ thoracic injury. Half-chest deflection was measured from planar videographic analysis of optical markers fixed to the spine centerline, sternum centerline, and sled contact surface.

As with acceleration-based metrics, unilateral deflection transduction necessitates an assumption with regard to directionality. In simple blunt lateral trauma, peak deflection is determined along the direction of impact. Anthropomorphic dummies designed to quantify lateral thoracoabdominal deflection, e.g., European Side Impact Dummy (EuroSID, Figure 3.6), have incorporated linear transducers along pure lateral, i.e., 90° with respect to anterior, directions (Viano, 1994; Yoganandan & Pintar, 2008). Further, dummy mechanical degrees of freedom may constrain deflection modes to the lateral direction only. Yet the complexity of the vehicle crash environment suggests that occupant loading may not always align with the direction of greatest sensitivity. This is further addressed in Section 3.4.1.

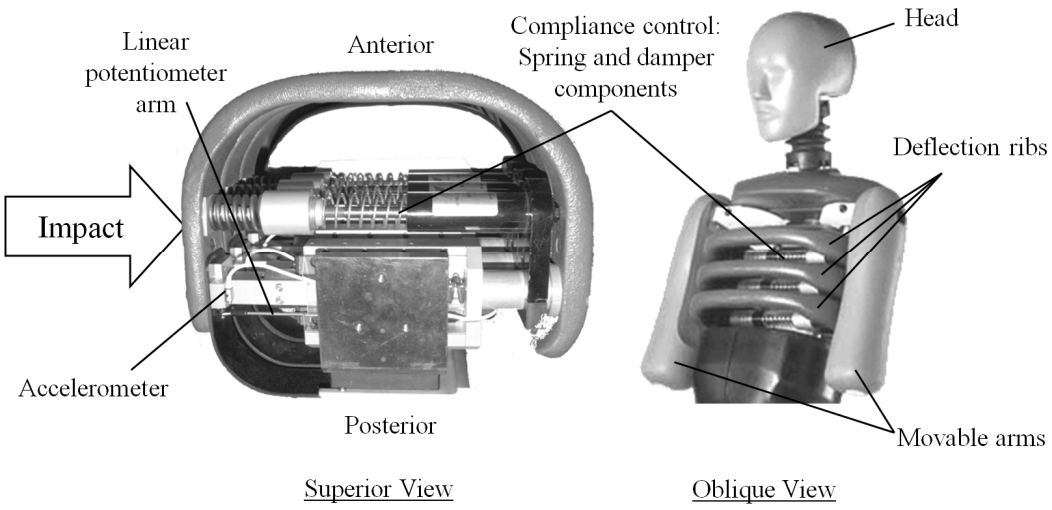

Figure 3.6. Mechanical chest deflection components and transducers of the EuroSID.

3.1.3 DEFLECTION RATE

Visceral injury was found to be dependent on viscous properties, i.e., rate effects, in animal models. With primates subjected to a 5.4 kg impactor, velocities greater than 9.1 m/s produced injury (McElhaney et al., 1971). Leporine subjects (n = 205) were exposed to rapid lateral chest deformation to induce lung trauma (Jonsson et al., 1979). With rates below 5 m/s, no lung injury was observed with deflections exceeding 50% full-chest breadth; rates surpassing 10 – 15 m/s commonly induced fatal injuries with deflections of only 15% full-chest breadth. Other leporine studies examining liver injury in abdominal impacts have reported similar rate dependence (Lau & Viano, 1981; Rouhana et al., 1985). Synthesizing these and other studies, a continuous relationship between injury risk, deflection, and deflection rate was theorized (Lau & Viano, 1986). Demonstrated in Figure 3.7, blunt trauma was categorized by three mechanisms of injury. Quasistatic deflection represented crushing tissue damage, while exceedingly high rate deflections ($\geq$ 20 – 30 m/s) represented blast tissue damage. The transition between these

mechanisms was termed the viscous region. The injury metric proposed for injury in this region was termed the Viscous Criterion (VC) and is shown in Eq. 3.4.

$$VC(t) = C(t) \cdot V(t) \tag{3.4}$$

where C(t) represents normalized deflection at time t and V(t) represents deflection rate (m/s) at time t.

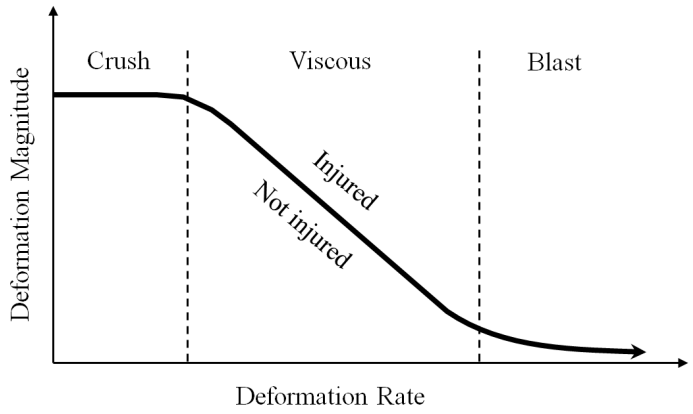

Figure 3.7. Theoretical relationship between deflection and deflection rate for tissue failure.
Concept from Lau & Viano (1986)

Thoracoabdominal injury to porcine subjects was correlated to maximum viscous response (VCmax) using a 23.4 kg pendulum impactor with high speed videography (Viano et al., 1989a). Using univariate logistic regression, a tolerance of VCmax = 0.89 m/s was determined for 25% risk of AIS 4+ injury, which included spleen lacerations, liver lacerations, and lung contusion. Using PMHS, only rib fractures were observed and VCmax = 1.47 m/s was determined for 25% risk of AIS 4+ injury (Viano et al., 1989b). The rarity of visceral injury in post-mortem subjects compared to *in vivo* subjects was attributed to the lack of physiologic vascular perfusion; this was also noted in laterally impacted canine and primate subjects (Nusholtz et al., 1980).

3.2 CHESTBAND METHODS

The "chestband," an external peripheral instrument, represented a notable improvement to quantifying chest deformation patterns. Prior studies utilized planar videography, depth-limited impactors, or invasive linear displacement transducers (Section 3.1.2). The chestband device consists of a flexible steel belt instrumented with resistive strain gages in an axially-compensated Wheatstone bridge configuration (Eppinger, 1989). Bridge time-traces represent band curvature at underlying points of known distances along the circumference. The discrete function of curvature values at known distances may be reconstructed into a continuous function for each instant by interpolating a cubic spline relationship between gage points (Eq. 3.5).

$$k_i(s,t) = a_i(t) + b_i(t) \cdot s + c_i(t) \cdot s^2 + d_i(t) \cdot s^3 \tag{3.5}$$

In Eq. 3.5, k_i represents curvature, s represents chestband distance, and a_i through d_i represent spline coefficients for spline segment i. Closed contours are created from the relationship between k and Φ, the total change in angle around a band of constant length L:

$$\Phi(s,t) = \int_0^L k(s,t)\, ds = 2\pi \tag{3.6}$$

Using RBandPC (Conrad Technologies, Washington DC), the simulation processor developed to reconstruct contours shapes, results were validated using sled experiments with a NHTSA-SID dummy (Pintar et al., 1996). The experimental use of the chestband facilitated direct PMHS deflection measurements without invasive instrumentation or videographic analysis and associated parallax error.

Chestbands were used on forty-two PMHS in rigid and padded wall sled impacts with ΔV = 6.7 or 8.9 m/s (Pintar et al., 1997; Kuppa et al., 2003). Distance was quantified between opposing contour points (Figure 3.8). Normalized to total chestband circumference, full-chest deflection time traces were calculated between 20% – 80%, 25% – 75%, and 30% – 70% pairings. Half-chest deflections were measured between left contour points and the mid-sagittal plane, defined by the line between the spine and sternum centerlines (S-S axis) palpated during testing. Peak normalized deflection, VCmax, and TTI values of 30%, 1.26 m/s, and 169 were correlated to 50% risk of AIS 4+ injury with p-values < 0.015 (Pintar et al., 1997). Incorporating an additional sixteen subjects into this dataset, normalized half-chest deflection was found to be the best predictor of thoracic injury (Kuppa et al., 2003). When standardized to chest breadth of 327 mm, 50% risk of AIS 3+ and AIS 4+ injury corresponded to lateral deflections of approximately 65 and 80 mm (Figure 3.9).

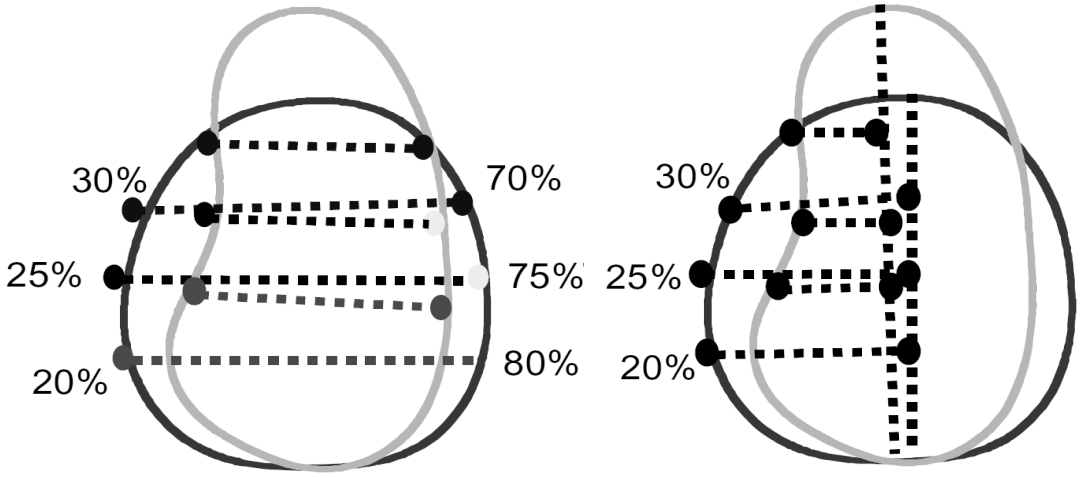

Figure 3.8. Chestband determination of PMHS lateral deflection response.
From Kuppa et al. (2003)

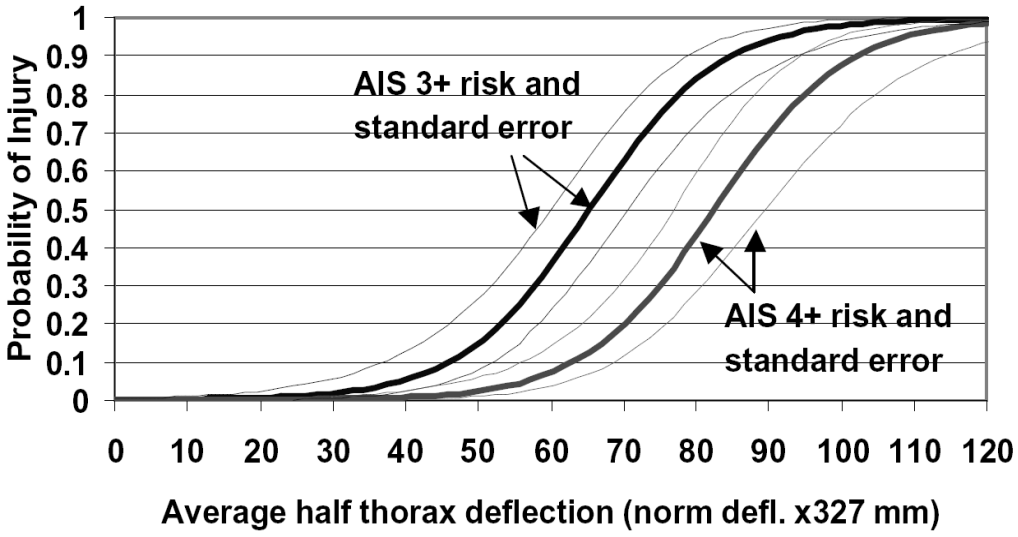

Figure 3.9. Logistic regression relationship between normalized chest deflection during sled impact and risk of hard thorax injury.
From Kuppa et al. (2003)

3.3 COMPUTATIONAL METHODS

Computational modeling represents a complementary investigational methodology by which thoracoabdominal loading parameters may be examined and injury metrics may be developed and validated. For thoracoabdominal injury prediction, modeling approaches may represent finite element analyses, multi-body formulations, or hybrid compositions thereof (Wismans et al., 2005).

3.3.1 FINITE ELEMENT ANALYSES

Although thoracoabdominal finite element (FE) models have been described in the literature for over thirty years (Sundaram & Feng, 1977), there remains a relative paucity of studies delineating their relationship to trauma observations in blunt lateral impact. Validation data represent blunt impact force-deflection corridors from cadaver

experiments (Section 3.1). Resulting stress or strain responses within tissues may be compared to injury observations. Given the quantity of materials present in the human thorax, the biological diversity of the human population, and the complexity of geometry, unique solutions to model composition do not exist. Due to problem complexity, finite element analyses of occupant lateral impact have generally involved one of only a few proprietary or consortium-developed whole-body and whole-torso human models. These include the Ford Motor Company Human Model, the Toyota Total Human Model for Safety (THUMS), and the European Human Model for Safety (HUMOS) (Lizee et al., 1998; Iwamoto et al., 2002; Behr et al., 2003; Ruan et al., 2003; Ruan et al., 2005; Hayashi et al., 2006; Ruan et al., 2006; Arnoux et al., 2008; Song et al., 2009).

Material properties have been identified by fitting material models to experimental measurements of tissue samples. In general, biological materials are viscoelastic (rate-dependent – Section 3.1.3), nonlinear, and anisotropic (Rouhana, 1993; Yoganandan et al., 2001; Wismans et al., 2005). However, if only the loading phase of an impact is considered, biological soft tissues may be approximated by a linear viscoelastic material model (Plank & Eppinger, 1991; Kuijpers et al., 1995; Deng et al., 1999; Furusu et al., 2001; Behr et al., 2003; Ruan et al., 2003; Ruan et al., 2005; Stitzel et al., 2005; Forbes et al., 2006; Hayashi et al., 2006; Murakami et al., 2006; Ruan et al., 2006; Roberts et al., 2007; Arnoux et al., 2008; Hayashi et al., 2008; Shen et al., 2008; Fijalkowski et al., 2009; Song et al., 2009) given by:

$$G(t) = G_{\infty} + \left(G_0 - G_{\infty}\right) e^{-\beta t} \tag{3.7}$$

G(t) represents the time-dependent shear response of the material, G_0 represents the short-duration shear response, G_{∞} represents the long-duration shear response, and β

represents the decay constant. Other important material properties are bulk modulus (K) and density (ρ). Bone may be approximated by a linear elastic material model (Plank & Eppinger, 1991; Kuijpers et al., 1995; Deng et al., 1999; Furusu et al., 2001; Behr et al., 2003; Ruan et al., 2003; Ruan et al., 2005; Stitzel et al., 2005; Forbes et al., 2006; Hayashi et al., 2006; Murakami et al., 2006; Ruan et al., 2006; Roberts et al., 2007; Arnoux et al., 2008; Hayashi et al., 2008; Shen et al., 2008; Fijalkowski et al., 2009; Song et al., 2009) given by:

$$\sigma = E\varepsilon \tag{3.8}$$

where σ represents material stress, ε represents material strain, and E represents the modulus of elasticity. Also relevant are ρ and the possion ratio (υ).

Fitted to quasistatic and dynamic experimental material responses, the material properties employed in the aforementioned proprietary models are diverse (Yamada, 1970; Melvin et al., 1973; Seki & Iwamoto, 1998; Carter et al., 2000; Carter et al., 2001; Nasseri et al., 2002; Stingl et al., 2002; Tamura et al., 2002; Kiss et al., 2004; Valtorta & Mazza, 2005; Balaraman et al., 2006; Jacquemoud et al., 2007; Kucharova et al., 2007; Saraf et al., 2007a; Saraf et al., 2007b; Nava et al., 2008; Rosen et al., 2008; Ahm & Kim, 2010). The relevant thoracoabdominal material properties utilized for the validated whole-body human models are shown in Table 3.1. Intuitively these material models do not account for failure mechanisms such as crack propagation or collagen fiber rupture. Therefore material failure must be discerned from stress and strain behavior within material model constraints. Most commonly, bone failure has been correlated to peak first principal strain (Stitzel et al., 2003; Forbes et al., 2006; Akiyama et al., 2009), while soft tissue failure has been correlated to maximum first principal strain and strain energy

density (Gilchrist et al., 2001; Snedeker et al., 2005a; Stitzel et al., 2005; Snedeker et al., 2007; Zou & Schmiedeler, 2008; Fijalkowski et al., 2009). Organ pressure has also been suggested as a predictor of soft tissue injury, but no significant relationship has been established (Ruan et al., 2005; Murakami et al., 2006; Hayashi et al., 2008).

Table 3.1. Relevant material properties of recent whole-body finite element models for impact.
(See text for sources)

Model: HUMOS

Material	ρ (kg/m^3)	K/E (MPa)	G_0 (MPa)	G_∞ (MPa)	υ
Liver	1100	0.166	0.045	0.036	-
Spleen	1100	0.25	0.054	0.04	-
Ometum	1000	0.001	0.036	0.027	-
Flesh	1210	0.01	0.045	0.036	-
Muscle	1210	0.2	0.154	0.086	-
Ribs (Cortical)	1800	13900	-	-	0.3
Ribs (Cancellous)	1800	450	-	-	0.3
Cartilage	1100	100	-	-	0.43

Model: THUMS

Material	ρ (kg/m^3)	K/E (MPa)	G_0 (MPa)	G_∞ (MPa)	υ
Liver	1100	0.0575	0.0295	0.002	-
Spleen	1100	0.0575	0.0295	0.002	-
Ometum	1000	0.0575	0.0295	0.002	-
Flesh	1210	100	0.35	0.17	-
Muscle	1210	1	-	-	0.49
Ribs (Cortical)	2000	50000	-	-	0.3
Ribs (Cancellous)	862	40	-	-	0.45
Cartilage	1000	24.5	-	-	0.4

Model: Ford

Material	ρ (kg/m^3)	K/E (MPa)	G_0 (MPa)	G_∞ (MPa)	υ
Liver	1100	2.875	0.23	0.044	-
Spleen	1100	2.875	0.23	0.044	-
Ometum	1100	0.5	0.054	0.04	-
Flesh	1100	1.33	0.14	0.04	-
Muscle	1100	2.1	0.35	0	-
Ribs (Cortical)	2000	9600	-	-	0.3
Ribs (Cancellous)	2000	9600	-	-	0.3
Cartilage	1500	53	-	-	0.4

3.3.2 MULTI-BODY ANALYSES

Multi-body formulations, i.e., rigid body or lumped-parameter, have been used to represent human whole-body kinematics as well as the deformable thorax and abdomen response during impact. The first computational thoracic model proposed a uniaxial human thorax with two inertial elements, representing external struck thorax mass and internal spine mass, interacting through viscous and elastic elements (Lobdell et al., 1973; Neathery & Lobdell, 1973). This model was modified for lateral loading (Figure 3.10) and was validated to PMHS pendulum impacts (Viano, 1978; Viano, 1987a; Viano, 1987b). A theoretical exercise of the Lobdell model governing equations established that the Viscous Criterion (Section 3.1.3) was analogous to the peak energy storage rate of the thoracoabdominal tissues (Wang, 1989). This model was also utilized in a parametric study of contact interface effects on injury metric response (Section 3.4.2).

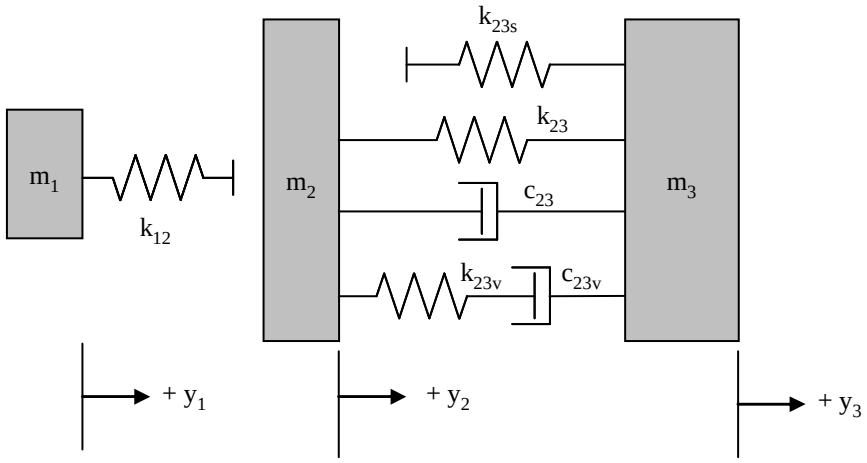

Figure 3.10. Multi-body model for thoracic deflection response. Mass elements: m_1 = impactor; m_2 = external inertia; m_3 = internal inertia.

Two and three dimensional multi-body models for side impact have employed ellipsoidal geometries (Deng, 1988; Deng, 1988; Deng, 1989; Huang et al., 1994; Deng

& Tzeng, 1996; Deng et al., 1998; Morris et al., 1999; Tencer et al., 2005a). These models were commercially developed for analyses of occupant kinematics and mimic the transducer response of dummies or instrumented PMHS (Figure 3.11). Multi-body motions were governed by three-dimensional elastic and viscoelastic joint restraints, and contacts were governed by force-penetration relationships.

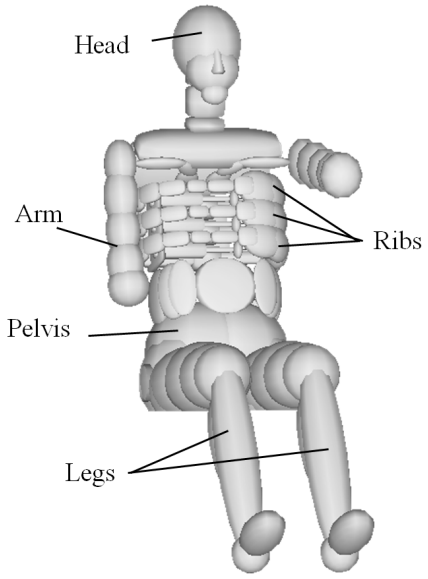

Figure 3.11. Exemplar 3D ellipsoidal multi-body model for left lateral impact. (MADYMO® EuroSID model, compare to Figure 3.6)

The MAthematical DYnamic MOdeling (MADYMO®, TNO-MADYMO, Livonia, Michigan) facet occupant model (Figure 3.12) was developed to replicate anthropometries more complex than possible with ellipsoids (Huang et al., 1994; Happee et al., 2000; de Lange et al., 2005; Tencer et al., 2005a; Mahangare et al., 2006). Consisting of head, neck, thorax, abdomen, and upper and lower extremities, each body region was modeled with rigid bodies of mass proportional to occupant anthropometry (Schneider et al., 1985). Masses were enclosed by massless facet surface skin to reproduce the complex human body geometries. Skeletal joint motions, including

extremity and vertebral column motions, were modeled as force-restrained rigid body joints (Happee et al., 2000).

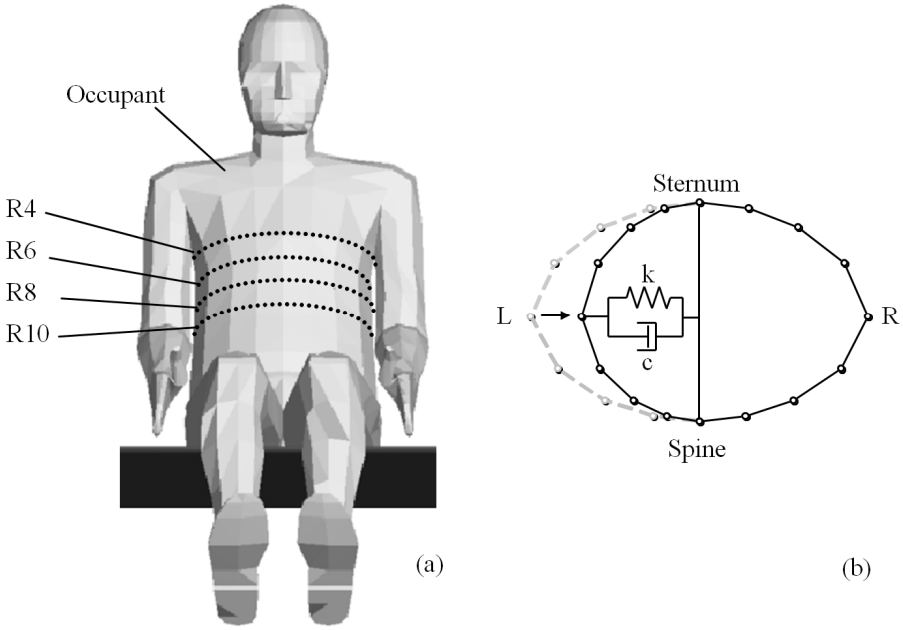

Figure 3.12. MADYMO facet occupant model.
(a) Anterior view of thoracic deformable bodies and corresponding levels; (b) Transverse view demonstrating lateral deformation in response to left contact force.

The thorax, the region of interest for this study, consisted of four discrete deformable structures (Figure 3.12). The nodes of these elliptical structures defined the circumference of the thorax and abdomen facet surface. Progressing inferiorly, thoracic structures were located at lateral levels of the fourth, sixth, eighth, and tenth rib (levels R4, R6, R8, and R10). Deformation response to lateral forces occurred through medial superposition of nodes. Thoracic deformation compliance was defined by nonlinear elastic and viscoelastic restraints between the spine and lateral nodes (*k* and *c*). Restraints were also defined between superior and inferior deformable structures. The biomechanical response of the thorax was validated to a variety of boundary conditions (Irwin et al., 1993; Lizee et al., 1998; Talantikite et al., 1998; Happee et al., 2000; de

Lange et al., 2005; Douglas et al., 2007; Hallman et al., 2010). Free pendulum tests utilized a 23.4 kg mass with velocities between 3.3 and 9.9 m/s. Drop tests utilized rigid contact at impact velocites between 4.3 and 6.3 m/s. Sled impacts utilized rigid contact at ΔV = 6.7 and 9.1 m/s. Force-deflection, force-time, and acceleration-time responses were compared to PMHS tests. Model biofidelity was also evaluated using standards as published in ISO TR9790 (ISO, 1999; de Lange et al., 2005), in which environmental reaction forces were validated. In all, model response was demonstrated to be a good predictor of cadaveric biomechanical response for impact velocities ranging ΔV = 3.3 – 9.7 m/s.

3.4 BOUNDARY EFFECTS

To improve vehicle crashworthiness and reduce occupant injury risks, studies have delineated the potential for altered boundary conditions to modulate accepted injury metrics. Altered boundary conditions may mitigate or elevate injury risk with respect to rigid lateral loading scenarios. Both experimental and parametric computational methods have been employed.

3.4.1 LOAD DIRECTION

Due to thoracoabdominal heterogeneity and asymmetry (Chapter 2), biomechanical and injury response is dependent on loading direction. Anatomical structures near the site of contact are generally more susceptible to localized strains (Rouhana & Kroell, 1989; Yoganandan et al., 2001). In primate subjects, right-side impact velocity tolerance was 20% below left-side tolerance (McElhaney et al., 1971). Comparing similar anterolateral pendulum impacts, i.e., 15° – 60°, to anterior or pure

lateral loading, peak forces were generally reduced while measured deflections were elevated (Yoganandan et al., 1996; Yoganandan et al., 1997; Shaw et al., 2006; Trosseille et al., 2008). Accelerations between anterior, lateral and 45° oblique impacts also exhibited direction dependence in magnitude and time response (Nusholtz et al., 1983). With strain gages mounted directly to the ribs, strain profiles were found to vary uniquely with each loading condition, contributing to differing injury response, primarily observed by rib fracture patterns (Trosseille et al., 2009). Greatest rib strains were noted during anterolateral loading compared to lateral and anterior loading.

Chestband analysis methods presented in Section 3.2 are not relevant to the obliquely loaded torso. Consequently two alternative methodologies have been utilized in the literature (Figure 3.13). Seven PMHS were subjected to a 23 kg impactor at 2.5 m/s in pure lateral (270° or 90°) and oblique (60° or 300°) angles (Shaw et al., 2006). Chestband deflection was quantified across the full-chest depth along the direction of impact (Figure 3.13a). Oblique biomechanical compliance was up to 39% greater than lateral compliance. In another series, sled experiments were conducted at $\Delta V = 6.7$ m/s using 20° and 30° oblique wall impacts using four PMHS (Yoganandan et al., 2008). Half-chest deflection was quantified to the point of maximum deformation regardless of direction (Figure 3.13b). From three chestbands placed at the axillary, xyphoid, and tenth rib levels, a statistically significant ($p < 0.05$) difference in mass-scaled deflections (Eppinger et al., 1984) was noted between oblique deflections and rigid lateral impact at two of three chestband levels. Anterolateral deformations have also been reported from chestband data in full scale side impacts into narrow objects (Pintar et al., 2007).

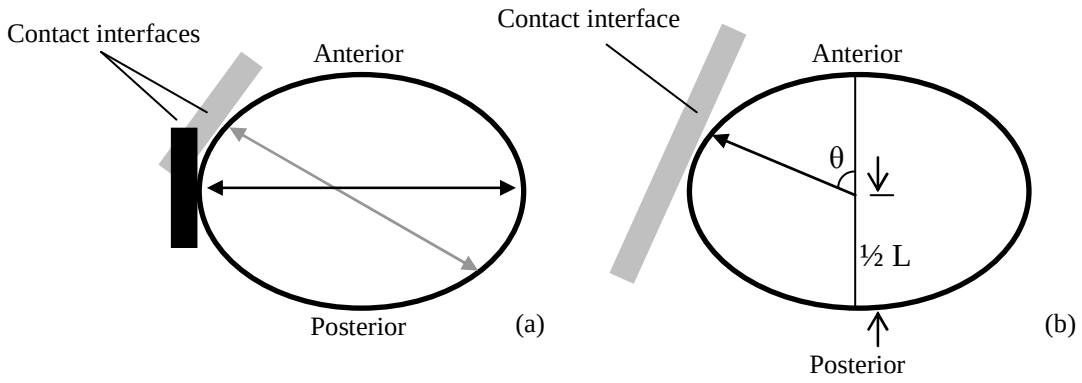

Figure 3.13. Oblique chestband deflection analysis methodologies.
(a) Shaw et al. (2006) and (b) Yoganandan et al. (2008).

In contrast with anterolateral thoracoabdominal loading, few studies have attempted to characterize the biomechanical response of the thorax and/or abdomen to posterolateral loading. One study varied impact angle posteriorly by 15° for anthropomorphic test device validation and quantified only spinal accelerations (Morgan & Waters, 1980). While crashes resulting in 4 - 5 or 7 - 8 o'clock principal directions of force (see Figure 4.1) are rarer than other lateral impact variants (Dischinger et al., 1993; Zaouk et al., 2001), the deployment of seat-mounted side airbags may provide a common posterolateral thoracic and abdominal loading mechanism and are relevant to the present study.

3.4.2 CONTACT INTERFACE PROPERTIES

Contact interface properties modulate injury metrics and affect injury risk. Using the Lobdell uniaxial thorax model (Section 3.3.2), deflection and viscous injury metrics were evaluated with constant crush force or linear elastic interfaces of 5 or 10 cm finite depth (Viano, 1987a; Viano, 1987b). Results demonstrated that viscous response was more sensitive than deflection to interfaces properties, achieving reductions of up to 60% compared to 30%. Further, metrics exhibited a dual response in time domain: (i) initial

interface contact followed by (ii) rigid contact when finite interface depth was exhausted. Peak injury metrics were minimized when dual responses were equivalent. Intuitively, interfaces of sufficient stiffness mimicked rigid contact.

In lateral impact sled tests (ΔV = 8.9 m/s), padding thickness affected injury mitigation (Marcus et al., 1983). Maximum AIS in the hard thorax (MAIS) decreased with increased padding thickness from 2.47 ± 0.50 (mean ± SE) with 9 cm padding to 0.81 ± 0.44 with 14 cm. MAIS was 3.42 ± 0.31 in rigid wall impact. Using an analytical model, padding effectiveness was found to be dependent upon both loading mechanism and biomechanical metrics (Deng, 1989). In simulated free-flight impact, padding introduction reduced rib and spine accelerations, peak deflection rate, and VCmax; peak chest deflection remained unaffected. During sled pulse simulations, identical padding reduced chest wall velocity while increasing VCmax and peak chest deflection. Other analytical models have reported similarly inconsistent metric reduction from padding (Huang et al., 1994). Using eight PMHS impacts of varying padding configurations, it was reported that padding stiffness of 131 kPa may increase MAIS injury compared to rigid wall during sled impact at ΔV = 8.9 m/s (Cavanaugh et al., 1993). Average MAIS = 4.0 from rigid wall tests; average MAIS = 2.3 from 55 kPa padding; average MAIS = 4.7 from 131 kPa padding. At impact velocities between 5.6 and 9.1 m/s, peak deflection and VCmax were increased up to 25% and 50%, respectively, by the addition of stiff padding (100 – 200 kPa) to the boundary condition (Pintar et al., 1997; Chung et al., 1999). Risk analyses further suggested that inappropriate padding may increase injury (Cavanaugh et al., 1993).

3.5 OCCUPANT-AIRBAG INTERACTIONS

Side airbag technologies, proposed in the 1980's (Olsson et al., 1989; Warner et al., 1989), were introduced to mitigate injury metrics by modulating boundary conditions during lateral impact. Although padding stiffness and depth must be tuned appropriately for torso injury mitigation (Section 3.4.2), airbags are further complicated by added parameters. These parameters include airbag volume, inflated depth, inflation pressure in time domain, and ventilation area (Kiuchi et al., 1991; Lundell et al., 1995; Malczyk & Adomeit, 1995; Haland & Pipkorn, 1996; Pipkorn & Haland, 1996; Tanavde et al., 1997; Deng et al., 1998; Igarashi et al., 1998; Khadilkar & Pauls, 1998; Tylko & Dalmotas, 2000; Mao & Appel, 2001; Tylko & Dalmotas, 2001). At ΔV = 10 m/s, varying ventilation area from 0 to 15 cm^2 reduced chest deflection from 50 to 30 mm and VCmax from 0.6 to 0.3 m/s. In contrast, at ΔV = 12 m/s deflection and VCmax were reduced from 70 to 50 mm and from 1.4 to 0.7, respectively (Haland & Pipkorn, 1996), indicating that injury metric mitigation was not equivalent at all ΔV. Other airbag parameters identified to affect biomechanical response include stowage folding pattern, fabric permeability, activation time, direction of gas release, and ambient conditions (Malczyk & Adomeit, 1995; Miller & Gu, 1997; Tanavde et al., 1997; Digges et al., 1998; Plank et al., 1998; Smith et al., 2003).

3.5.1 EFFICACY

Complexities from these airbag characteristics may have contributed to inconsistent findings from epidemiological analyses of torso side airbag performance. These analyses have employed NHTSA-administered vehicle crash databases such as the Crash Injury Research and Engineering Network (CIREN), the Special Crash

Investigations (SCI) database, the National Automotive Sampling System (NASS) database, and the Fatality Analysis Reporting System database (NHTSA, 1999; Scally et al., 1999; McKay, 2003). These databases are sanitized of personally identifiable data. The CIREN database, formed in 1996, is a collaboration of clinicians and engineers at up to twelve Level 1 Trauma Centers in the US. Enrolled cases generally involve AIS 3+ (or multiple AIS 2) injuries occurring in late model vehicle crashes. The SCI program began in 1972 and collects data nationally from crashes involving special circumstances or emerging safety technologies. The FARS is a census of all crashes resulting in at least one fatality within the US. Data have been collected annually since 1975, and the resulting fatality must have occurred within 30 days of the event. The NASS database is composed of cases selected from a statistical sample of police crash reports in which at least one vehicle was towed from the scene. Sampling design ensures cases are a representative random sample of the hundreds of thousands of minor, serious and fatal crashes occurring annually in the US. Approximately 5,000 cases are sampled annually within regions selected from over 1,000 population-based sampling units. Each sampled case is assigned a Ratio Inflation Factor, a weight which allows National estimates to be made based upon sampled cases.

Analyses have evaluated torso airbag efficacy with varying levels of statistical significance (Langwieder et al., 1998; Baur et al., 2000; Dalmotas et al., 2001; Kirk & Morris, 2003; McGwin et al., 2003; Braver & Kyrychenko, 2004; McGwin et al., 2004; Weber et al., 2004; Yoganandan et al., 2005; McCartt & Kyrychenko, 2007; Yoganandan et al., 2007b; Yoganandan et al., 2007c). A summary of these studies is shown in Table 3.2. Analyses of FARS data (1997-2001) have suggested statistically insignificant effects

from torso airbags for adult occupants and detrimental effects for elderly occupants (McGwin et al., 2003; Braver & Kyrychenko, 2004). NASS analyses have reported conflicting conclusions regarding efficacy (McGwin et al., 2004; Yoganandan et al., 2007c). Analysis of UK data has suggested an increased torso injury risk with torso airbag deployment (Morris et al., 2005), particularly rib fractures in the lower posterolateral thorax and one severe splenic laceration. More recent FARS analysis (1999-2004) suggested mortality risk reductions for occupants in airbag-equipped vehicles, but morbidity was not considered (McCartt & Kyrychenko, 2007). Studies consistently found head protection to be more beneficial than torso protection. Further, a recent NHTSA analysis of improved crashworthiness regulations found torso airbag protection to reduce mortality rate by 5%, compared to a 24% reduction from side structure improvements alone (Kahane, 2007). These results suggest that torso airbag protection is not effective compared to head protection despite the thorax injury rate in nearside impacts (Hartemann et al., 1976a; Hartemann et al., 1976b; Dischinger et al., 1993; Samaha & Elliott, 2003; Nirula et al., 2005). Torso airbag performance may be complicated by occupant position with respect to the device, an elusive parameter in real-world crash data.

Table 3.2. Summary of epidemiological findings regarding side airbag protection in lateral impacts.

Database	Outcome	Data Years	Head Protection*	Torso Protection*	Reference
FARS	Mortality	1999-2001	0.4-0.71 RR	0.79-1.01 RR	(Braver & Kyrychenko, 2004)
FARS	Mortality	1999-2004	0.56-0.71 RR	0.66-0.84 RR	(McCartt & Kyrychenko, 2007)
NASS	AIS 1+	1998-2001	0.08-0.79 RR	0.11-0.91 RR	(McGwin et al., 2004)
NASS	AIS 3+	1997-2000	0.78-1.72 RR		(McGwin et al., 2003)
NASS	Case study	1994-2004	"Torso and [combo] bags do not clearly decrease severity of injuries. However, the separate system of torso and curtain appears to offer improved protection."		(Yoganandan et al., 2005)
NASS	AIS 2+	1997-2004	Without side airbag, 90% of AIS 2+ at ΔV < 39 km/hr. With airbag, 90% of AIS 2+ at ΔV < 37 km/hr.		(Yoganandan et al., 2007c)
UK/France	AIS 3+	1998-2004	0.44-1.85 RR	0.37-1.88 RR	(Page et al., 2006)
UK	AIS 4+	2001-2003	Injury rate with airbag higher than without: (22.4% vs. 10.2%, insignificant)		(Kirk & Morris, 2003; Morris et al., 2005)
FARS	Mortality	1994-2004	26% reduction (significant)	5% reduction (not significant)	(Kahane, 2007)
			24% reduction from side structure improvements alone		

* RR = Relative Risk with 95% confidence interval.

3.5.2 OUT-OF-POSITION

Airbags are designed to mitigate injury metrics for occupants in normal postures. Normal pretest occupant positioning is in the mid-seat position for side impact crashworthiness tests according to the United States (NCAP) and European (EuroNCAP) specifications (EuroNCAP, 2004a; NHTSA, 2008b). When a vehicle occupant deviates from a normal posture, an out-out-position (OOP) scenario may result. OOP injuries can generally be attributed to two loading mechanisms: “punch-out” and “membrane” loading (Melvin et al., 1993; Hardy et al., 1997; Kleinberger & Summers, 1997; Digges et al., 1998). The punch-out mechanism arises from the forceful airbag stowage release, often required to break or tear vehicle cosmetic trim pieces and permit airbag deployment. The

membrane loading mechanism arises after punch-out as the airbag rapidly expands to a fully inflated volume.

Side airbag OOP studies employed methodologies similar to frontal airbag investigations (Chapter 1). Without observed injury patterns resulting from side airbag interaction, proposed OOP scenarios relied upon conjecture. With three- and six-year-old child dummies, 15 different OOP scenarios were identified in which head accelerations, neck forces and moments, and chest deflection injury metrics may potentially exceed injury criteria values (Pintar et al., 1999; Tylko & Dalmotas, 2000; Prasad et al., 2001). These scenarios required precise stationary dummy placement; position deviation of 2 cm reduced injury metrics by over 75% (Pintar et al., 1999). Exemplar child scenarios are shown in Figure 3.14 . Computer simulations were employed in which small female occupants were positioned in five close-proximity scenarios; none indicated high risk of head, neck, extremity, and thorax injury (Khadilkar & Pauls, 1998; Duma et al., 2003b). The currently accepted commercial side airbag protocol published by the Insurance Institute for Highway Safety (IIHS) employs not less than 35 test scenarios by which out-of-position risks from side airbags are evaluated (IIHS, 2003). These conjectured scenarios were intended to identify and prevent injurious scenarios before they occurred. Recommended test scenarios for adult occupants with torso-interacting airbags are shown in Figure 3.15. All scenarios employ stationary occupants and involve the measurement of lateral thoracoabdominal deflection, VCmax, and accelerations. Yet the relevance of these stationary “inadvertent deployment” scenarios and their associated injury mechanisms has not been addressed. Further, results from padded boundary conditions (Section 3.4.2) suggest that impact loading events may exist in which airbag presence

exacerbates rather than mitigates injury. Nonuniform cushion depth may also induce load obliquity, shown to increase biomechanical response in lateral impact (Section 3.4.1). These mechanisms of injury are not addressed by current protocols.

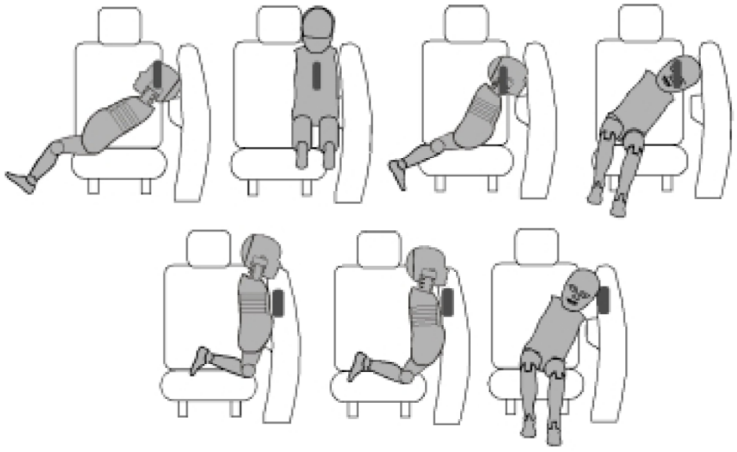

Figure 3.14. Out-of-position child occupant test scenarios employed for seat- and door-mounted side airbag testing.
From Pintar et al. (1999)

Figure 3.15. Out-of-position adult occupant test scenarios recommend for thoracoabdominal injury risk evaluation with seat- and door-mounted side airbags.
From IIHS (2003)

Increasing side airbag popularity has increased the availability of data regarding torso airbag performance in actual crashes. While much attention has been devoted to upper extremity interaction with torso side airbags (Duma et al., 1998; Duma et al., 2003a; McGwin et al., 2008), field studies have not yet identified consistent thoracoabdominal injury patterns attributable to OOP side airbag interaction. Studies of crashes in the United Kingdom have suggested that airbag deployment is associated with an increased thoracoabdominal injury severity; results were not significant (Kirk & Morris, 2003; Morris et al., 2005). Further, the spleen was identified in two independent cases as specifically susceptible to injury from airbag deployment (Kirk & Morris, 2003; Weber et al., 2004). Yet no further case studies or biomechanical analyses have been published concerning this injury.

3.6 SUMMARY

Through use of multiple biological models, injury criteria have been developed consisting of biomechanical correlates to thoracoabdominal injury response in lateral impact (Section 3.1). Using the chestband device (Section 3.2) or other experimental methodologies, these injury criteria exhibited directional dependence (Section 3.4.1) and were modulated by boundary conditions (Section 3.4.2). Computational models have also been developed to numerically evaluate thoracoabdominal injury risks (Section 3.3), but these have not been widely employed. Although side airbags have been introduced to mitigate thoracoabdominal injuries through modulation of boundary conditions (Section 3.5.1), the propensity for out-of-position injury has been inadequately addressed (Section 3.4.2), particularly with regard to torso injury mechanisms observed in actual crashes.

FOUR

INJURY PATTERNS FOLLOWING SIDE AIRBAG LOADING

Specific Aim 1: Identify unique thoracoabdominal injuries, as described by anatomical location and the Abbreviated Injury Scale, during documented side impacts involving torso-interacting side airbags.

The present study was initiated with an examination of clinical observations following side impact crashes. Occupants in motor vehicle crashes with and without torso-interacting airbags were identified, and an evaluation of injury patterns was employed to identify divergences from expected patterns possibly induced by airbag interaction.

4.1 METHODOLOGY

A query of crash injury databases was designed to retrieve case occupants in lateral impacts with and without torso side airbag deployment. Cases involving airbag deployment were examined for recurrent patterns of thoracoabdominal injury which may characterize detrimental interaction.

4.1.1 DATA DESCRIPTION

Individual motor vehicle crash reports were examined in the Crash Injury Research and Engineering Network (CIREN), Special Crash Investigations (SCI), and National Automotive Sampling System (NASS) databases. The CIREN and SCI

databases represent case reports detailing abnormal conditions, injuries, or emerging vehicular safety technologies; NASS represents a statistical annual sample of crashes in the US. See Section 3.5.1 for detailed descriptions.

4.1.2 INCLUSION CRITERIA

The NASS database was queried for years 1998 through 2008; vehicle model years prior to 1998 were excluded due to updated FMVSS 214 requirements (Section 3.1.1). Crash characteristics represented left- and right-side impacts with Principal Direction of Force (PDOF) = 1 – 4 o'clock or 8 – 11 o'clock (Figure 4.1) and door designated as the primary damage region. Crashes involving rollover were excluded, and crash characteristics of ΔV and intrusion magnitude were obtained. Because the NASS dataset designated side airbag deployment as "other airbag" without further information, photos from all cases were examined individually to segregate torso-interacting airbags from curtains providing only head protection (Chapter 1). Case occupants were belted non-ejected adults (≥16 years) in front nearside seat positions, i.e., drivers in left-side impacts, right-front passengers in right-side impacts. Age, body mass index (BMI), and gender were obtained for each case occupant. Presence of thoracoabdominal injuries was delineated by AIS injury codes assigned to the liver, spleen, ribcage, and lungs.

Detailed case review was performed on all crashes from the NASS, SCI, and CIREN databases with documented side airbag deployment. Because the CIREN and NASS database inclusion criteria (AIS ≥ 3 and towed vehicle, respectively) biased cases toward high-severity crashes, CIREN and NASS cases were selected for individual review only if $\Delta V \leq 27$ km/h. Low ΔV ensured that airbag deployment energy was a proportionally greater component of the total crash event. Vehicle photos were examined

to determine airbag type and deployment status; vehicles with airbags offering torso protection were identified.

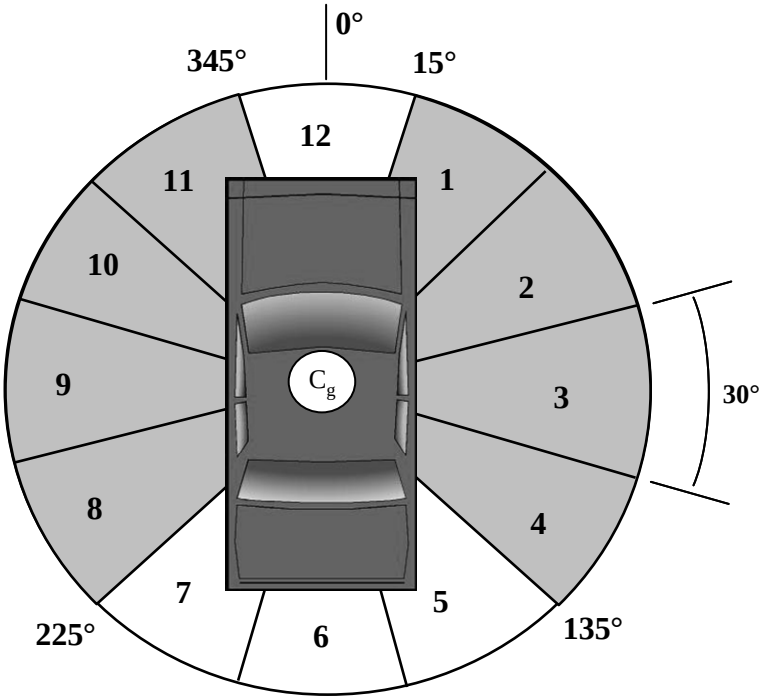

Figure 4.1. PDOF inclusion criteria for NASS database query.

4.1.3 ANALYSIS APPROACH

To evaluate injury patterns, crash and occupant characteristics were compared between airbag and non-airbag groups. Using the NASS database, case occupants were stratified by injury presence and airbag presence for four analyses: spleen trauma, liver trauma, rib fracture, and lung trauma. Because of anatomical considerations (Section 2.3), spleen trauma analysis examined only left-side impacts, and liver trauma analysis examined only right-side impacts. Multivariate logistic regression (SAS Institute Inc., Cary, NC) was performed for each injury controlling for effects from the following categorical predictors: occupant age, gender, and airbag presence. Continuous predictors

were occupant BMI, crash ΔV, and intrusion. Because intrusion was categorical in the NASS dataset, each intrusion category was assigned the lowest value within the assigned categorical range. For each predictor, the Odds Ratio (OR), OR 95% Confidence Interval (CI), and Rao-Scott χ^2 significance were determined.

For the SCI and CIREN individual cases, injury types and AIS scores from each case with airbag deployment were compared to the NASS side impact dataset. CIREN lateral impact cases without airbag were also examined to confirm similarities between CIREN and NASS source data. Thoracoabdominal injuries with side airbag which were outside of typical distributions for the given crash severity were identified ($\Delta V \leq 27$ km/h or minimal compartment intrusion).

4.2 RESULTS

The NASS query yielded 2,489 raw cases which were weighted to a national estimate of 882,100. Drivers subjected to left-side impact accounted for 84.9% of (weighted) case occupants, and front passengers subjected to right-side impact accounted for the remainder. Thoracoabdominal injuries were present as follows: rib fracture = 4.3%; lung trauma = 1.2%; liver trauma = 0.6%; spleen trauma = 1.0%. Other dataset details are depicted in Table 4.1.

Cases selected for individual review totaled 338. Cases with deployed side airbag totaled 272, distributed among databases as follows: 161 from SCI, 45 from CIREN, and 66 raw cases from NASS. Injuries demonstrated in radiology and case description were compared to cases without airbag deployment.

Table 4.1. NASS population description.

Predictor	Group	Raw Count	Weighted Count	Percent
Gender	Male	1166	452,808	51.3
	Female	1323	429,292	48.7
Airbag	Yes	287	62,409	7.1
	No	2202	819,691	92.9
Aspect	Left	1993	749,266	84.9
	Right	496	132,835	15.1
Intrusion (cm)	int.≤2	978	525,705	59.6
	2<int.≤7	249	100,715	11.4
	7<int.≤14	322	106,760	12.1
	14<int.≤30	466	106,820	12.1
	30<int.≤45	319	31,848	3.6
	45<int.≤60	116	7,746	0.9
	int.≥61	36	2,451	0.3
Injury	Rib	386	37,725	4.3
	Lung	182	10,908	1.2
	Liver	34	772	0.6
	Spleen	118	7,823	1.0

4.2.1 NASS ANALYSIS

Regression results are shown in Table 4.2 through Table 4.5. Significant predictors of anatomical trauma are bolded.

Table 4.2. Regression results for rib trauma.

Effect	OR	CI	p-Value
Airbag	1.97	0.61 - 6.33	0.2571
ΔV	**1.06**	**1.04 - 1.08**	**<0.0001**
Intrusion	**1.08**	**1.06 - 1.10**	**<0.0001**
Gender	0.74	0.33 - 1.70	0.4836
BMI	1.04	0.99 - 1.09	0.1578
Age	**1.04**	**1.03 - 1.05**	**<0.0001**

Table 4.3. Regression results for lung trauma.

Effect	OR	CI	p-Value
Airbag	2.10	0.85 - 5.21	0.1087
ΔV	**1.09**	**1.07 - 1.11**	**<0.0001**
Intrusion	**1.07**	**1.06 - 1.09**	**<0.0001**
Gender	0.86	0.43 - 1.72	0.6664
BMI	**1.05**	**1.01 - 1.09**	**0.0126**
Age	**1.02**	**1.01 - 1.03**	**0.0024**

Table 4.4. Regression results for liver trauma.

Effect	OR	CI	p-Value
Airbag	1.73	0.36 - 8.40	0.4975
ΔV	**1.14**	**1.07 - 1.21**	**<0.0001**
Intrusion	**1.09**	**1.04 - 1.14**	**0.0003**
Gender	4.07	0.80 - 20.63	0.0899
BMI	**1.15**	**1.04 - 1.28**	**0.0081**
Age	1.03	1.00 - 1.05	0.0533

Table 4.5. Regression results for spleen trauma.

Effect	OR	CI	p-Value
Airbag	4.19	0.88 - 20.0	0.0726
ΔV	**1.05**	**1.03 - 1.07**	**<0.0001**
Intrusion	**1.12**	**1.09 - 1.15**	**<0.0001**
Gender	**3.89**	**1.26 - 12.0**	**0.0181**
BMI	**0.91**	**0.87 - 0.94**	**<0.0001**
Age	0.97	0.94 - 1.01	0.1314

Airbag deployment was associated with an increased OR for all injuries but was not significant for any anatomical injury at $\alpha = 0.05$. With $\alpha = 0.1$, airbag deployment was a significant predictor for spleen trauma. For all traumatic injuries analyzed, crash characteristics of ΔV and intrusion magnitude were found to be significant. Contributory effects from increased age were observed for rib and lung trauma (OR = 1.02 – 1.04) but not liver or spleen trauma. Increased BMI was a significant predictor of lung and liver trauma (OR = 1.05 – 1.15) but was inversely related to spleen trauma (OR = 0.91). Gender was only significant for spleen trauma.

A closer examination of NASS revealed 3,551 weighted occupants with splenic trauma in left side impacts without airbag (1998-2007). Crash characteristics for this subset are shown in Figure 4.2. Within this subset, no splenic trauma was observed below $\Delta V = 14$ km/h. Additionally, 85% of weighted cases occurred at $\Delta V > 27$ km/h,

and 94% of weighted cases occurred with compartment intrusion ≥ 15 cm. These data provided a baseline to which individual case reports were compared.

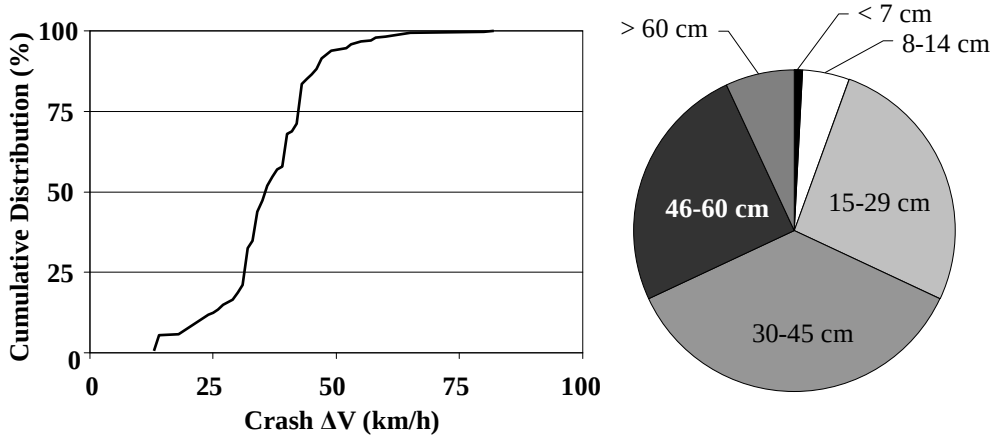

Figure 4.2. Crash characteristics for splenic trauma without torso side airbag in the NASS database.
(left) Cumulative distribution of crash ΔV and (right) compartment intrusion

4.2.2 CASE EXAMINATION

Individual CIREN case occupants involved in low severity side impacts without side airbags sustained injuries distributed as follows: trauma to head/neck (35%), thorax (69%), abdomen (15%) and extremities (15%). Of thorax cases, 62% included rib fracture and 31% included lung trauma. Given the anatomic location of the spleen (Section 2.3) and NASS results (Section 4.2.1), particular attention was given to individual cases of splenic trauma. Fifteen percent of returned CIREN case occupants without airbag sustained splenic trauma scored AIS ≥ 2; all were associated with at least 1 rib fracture. Average door intrusion for all left side CIREN cases was 17 cm. Door intrusion in splenic trauma sub-group averaged 21 cm with a minimum of 17 cm.

Of the 272 cases with a deployed side airbag, injury patterns demonstrated partial similarity with non-airbag cases. However, five case occupants sustained splenic trauma

in crashes which deviated from the “typical” crash characteristics. These case occupants presented with splenic laceration and contusion following seat-mounted airbag deployment. In these cases, door intrusion was not present, and mean lateral ΔV was 8 km/h (max = 14 km/h). In addition to these five cases, five secondary case occupants were identified as presenting with possible airbag splenic injuries. Higher ΔV (mean = 20 km/h) and intrusion (mean = 13 cm) precluded more conclusive determination.

The following section details the circumstances surrounding suspected airbag-induced splenic trauma. Cases are summarized in Table 4.6.

4.2.3 CASE DESCRIPTIONS

Case 1. The case vehicle, a minivan, was involved in a sideswipe collision. The left side of a compact pickup in the opposing lane contacted the left side of the case vehicle. The case vehicle came to a controlled stop. The impact was classified as minor, no intrusion into the occupant compartment was documented, and ΔV could not be calculated without measureable intrusion (Figure 4.3). The case occupant, the 44 year-old, 170 cm, 52 kg, female driver of the minivan, was reportedly using a three-point belt and the seat-mounted combination side airbag deployed. She sustained a left pulmonary contusion, posterior fractures to left ribs 9 and 11, a left posterior chest wall contusion, and a severe (AIS 4) splenic laceration. Other occupants of the case vehicle (three, ages 9 to 11) were using the available three-point belts, were not subject to airbag deployments, and were not injured.

Figure 4.3. Case 1 vehicle damage and airbag.

Case 2. The case vehicle, a four door sport-utility vehicle, lost control over ice on a one way limited access highway. The left front followed by the left rear struck a concrete barrier on the left shoulder of the roadway. The vehicle continued a counter-clockwise rotation before coming to rest facing oncoming traffic. The lateral ΔV was calculated to be 5 km/h and no occupant compartment intrusion occurred (Figure 4.4). The case occupant, the 34 year-old, 175 cm, 76 kg, male driver, was reportedly wearing a three-point belt and the seat-mounted combo side airbag deployed (Figure 4.4). The occupant, who drove the case vehicle to his residence following the incident, was reportedly jogging the subsequent morning before the onset of abdominal pain. Upon hospital arrival, he was diagnosed with a severe (AIS 4) splenic laceration.

Figure 4.4. Case 2 vehicle damage and airbag.

Case 3. The case vehicle, a compact SUV, was struck laterally by a 2003 mid-sized four door sedan in a four-way intersection. Following a counter-clockwise rotation, the case vehicle came to rest within the roadway facing the opposing direction. The lateral ΔV was calculated to be 14 km/h and maximum intrusion (below occupant hip level) was 10 cm (Figure 4.5). The case occupant, the 56 year-old, 163 cm, 88 kg, male driver, was restrained by a three-point belt and the seat-mounted combination side airbag deployed through an overlaid sweatshirt (Figure 4.5). He suffered contusions to left back and scapula, non-displaced fractures to left ribs 6 through 11, minimally-displaced fracture to rib 10, left unilateral lower lobe pulmonary contusion, and splenic laceration (AIS 3).

Figure 4.5. Case 3 vehicle damage and airbag.

Case 4. The case vehicle, a compact SUV, was struck by a sub-compact coupe in a four-way intersection. The front right of the striking vehicle made contact with the front left of the case vehicle; both vehicles initiated opposing rotations causing a "side-slap" contact. The lateral ΔV was calculated to be 10 km/h and no intrusion occurred (Figure 4.6). The case occupant, the 48 year-old, 163 cm, 66 kg, female driver, was restrained by a three-point belt and the seat-mounted combination side airbag deployed (Figure 4.6). She was initially diagnosed with rib contusion (AIS 1) and abdominal skin contusion (AIS 1). While under care she developed abdominal pain with rapid onset of hypovolemic shock. She was diagnosed with a fractured spleen (not further specified); the injury was likely AIS 3+ because treatment was surgical.

Figure 4.6. Case 4 vehicle damage and airbag.

Case 5. The case vehicle, a minivan, lost control while negotiating a left curve on a wet six-lane divided highway. The vehicle departed the roadway to the right in a clockwise yaw, struck a large wooden two-post roadway sign laterally, and came to rest entangled in a chain link fence. The vehicle contacted the signposts forward of the A-pillar (adjacent to windshield) and aft of the B-pillar (divides front and rear doors). The lateral ΔV was calculated as 11 km/h, and no intrusion occurred in the vicinity of the case occupant (Figure 4.7). The case occupant, the 61 year-old, 185 cm, 79 kg, male driver, was restrained by a three-point belt and the seat-mounted torso airbag deployed (Figure 4.7). He sustained a splenic contusion and laceration (AIS 3), fractures of between 2 and 3 ribs (AIS 2), and abrasions and contusions to the chest and abdomen (AIS 1). He was hospitalized for five days.

Figure 4.7. Case 5 vehicle damage and airbag.

Possible Trauma. Five additional cases involving deployed side airbags were noted in which injury patterns were consistent with the preceding pattern. These cases, shown in Table 4.6, included four seat-mounted torso airbags and one seat-mounted combination airbag. Because the severity of impact, i.e., ΔV and/or intrusion, was similar to cases of splenic trauma in absence of airbag, conclusive determination of the energy source could not be made.

Summary. In addition to splenic trauma, *Cases 1*, *3*, *4*, and *5* demonstrated posterolateral injury to ribs which varied from chest wall contusion (*Case 4*) to six total rib fractures including minimal rib displacement (*Case 3*). *Cases 1* and *3* also included lung contusion to the posterior aspect of the lower left lobe. These injuries resulted from low severity impacts with little or no intrusion. Intrusion was reported only in *Case 3* (10 cm) but was below both occupant abdomen and hip. Although one case did not include a calculation of crash velocity, all other cases were calculated between ΔV = 5 km/h and 14 km/h. Contrast-enhanced imaging of splenic trauma (Figure 4.8) was available in three of five reports included in this study (*Cases 1 – 3*).

Table 4.6. Torso airbag injury pattern from case occupants.

Case	Age, Gender	Height, Weight	ΔV	Int. (cm)	Rib Injury	Lung Injury	Spleen Injury
1	44, F	170 cm, 52 kg	N/A	0	2 fx (posterior)	contusion	Laceration (AIS 4)
2	34, M	175 cm, 76 kg	5 km/h	0	*	*	Laceration (AIS 4)
3	56, M	163 cm, 88 kg	14 km/h	10	6 fx (posterior)	contusion	Laceration (AIS 3)
4	48, F	163 cm, 66 kg	10 km/h	0	contusion	*	Fracture (NFS)
5	61, M	185 cm, 79 kg	11 km/h	0	2-3 fx	*	Laceration & contusion (AIS 3)
The following cases suggest airbag-related trauma:							
6	42, M	175 cm, 88 kg	N/A	0	4 fx (posterior)	L basilar pneumothorax	Laceration (AIS 2)
7	51, M	157 cm, 65 kg	N/A	20	*	*	Contusion (AIS 2)
8	22, F	165 cm, 77 kg	26 km/h	12	*	*	Laceration (AIS 4)
9	23, F	163 cm 50 kg	27 km/h	17	4 fx (posterior)	Contusion	Laceration (AIS 2)
10	43, F	158 cm, 48 kg	N/A	13	2+ fx, displaced	*	Laceration (AIS 2)

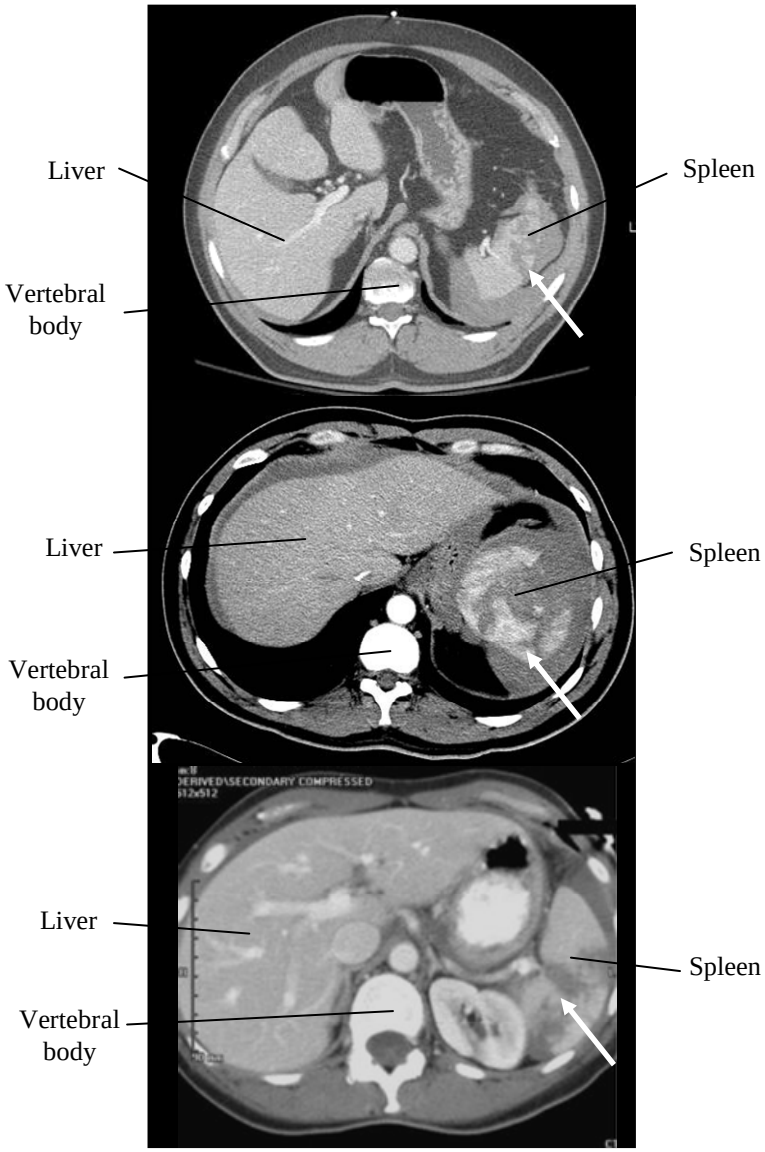

Figure 4.8. Abdominal radiology of splenic trauma in Cases 1-3.
Injury is indicated by white arrows.

4.3 DISCUSSION

The present study examined clinical observations following lateral impacts involving torso-interacting airbags. Five cases were identified in which case occupants presented with splenic trauma. These injuries were suspect because they occurred (i) at ΔV less than all cases of side impact splenic trauma found within the CIREN and NASS

databases and (ii) in absence of substantial occupant compartment intrusion. An additional five cases were identified in which occupants presented with similar injury patterns but did not meet both criteria (i) and (ii) simultaneously.

From multivariate regression analysis, airbag deployment was not significantly associated with any hard thorax injuries at a 95% confidence level. This observation is consistent with previous examinations of torso airbag efficacy in which results were not significant (Langwieder et al., 1998; Baur et al., 2000; Dalmotas et al., 2001; Kirk & Morris, 2003; McGwin et al., 2003; Braver & Kyrychenko, 2004; McGwin et al., 2004; Weber et al., 2004; Yoganandan et al., 2005; McCartt & Kyrychenko, 2007; Yoganandan et al., 2007b; Yoganandan et al., 2007c). Yet, splenic trauma was significantly associated with torso airbag deployment at a 90% confidence level. This suggested that airbag deployment was associated with an increased risk of splenic trauma after controlling for crash intrusion and ΔV as suggested by other analyses (McCartt & Kyrychenko, 2007). In contrast, the five CIREN cases presented in this study were marked definitively by low crash severity.

Other sources of injury in these five cases were considered unlikely. These sources included other occupants, belt pretensioners, vehicle yawing and excessive ΔV. Of the five cases presented in this study, two case vehicles contained more than one occupant. All occupants were restrained by three-point belts, reducing likelihood of occupant torso interaction. Although belt pretensioners were present in three vehicles, none appeared to be activated. Vehicle yawing, shown to affect occupant kinematics (Marine & Werner, 1998), may have contributed to crash severity. However, yaw rate demonstrated in these five cases was not consistent in presence or direction. Accuracy of

reported ΔV was also considered. A previous comparison of ΔV, reconstructed by computer algorithms using vehicle crush profiles, and onboard Event Data Recorders (EDR) demonstrated ΔV to underestimate actual impact severity in frontal scenarios (Niehoff & Gabler, 2006). Conversely, examination of reconstructed ΔV and lateral crash tests has revealed algorithmic overestimations averaging 10 km/h (Johnson et al., 2009). Despite possible error in reported ΔV, cases demonstrated minimal vehicle crush and lack of compartment intrusion. By these measures, impacts could still be classified validly as minor.

Although not uncommon in motor vehicle crashes, splenic trauma has not been associated heretofore with low ΔV near-side impacts involving side airbag deployment. Epidemiological analyses of splenic trauma have identified door interior contact as the most probable injury mechanism in lateral impact (Siegel et al., 1993; Reiff et al., 2001). Reported by Reiff et al., splenic injury risk increased five-fold when intrusion was > 30 cm as compared to intrusion of 1 – 30 cm magnitude. Biomechanical assessments have also identified intrusion as the primary mechanism of injury in lateral impact (Cesari et al., 1978). Regression analyses in this study of the NASS database are in agreement with these findings. The lack of intrusion reported during these individual airbag cases, in combination with low ΔV, may indicate the presence of a contrasting injury mechanism.

Shown in Figure 4.9 are representative seat- and door-mounted airbag module locations in relationship to spleen location *in situ* (Gray, 1918). The thoracoabdominal region containing the spleen is nearest to the site of airbag deployment. Therefore, this region may be more susceptible to injury if occupant posture deviates toward the airbag module. Lateral postural deviation is not abnormal; unaware subject variations have been

reported in excess of 22 cm under normal driving conditions (Dinas & Fildes, 2002). A fiftieth percentile male exemplar occupant is also shown in Figure 4.9. The airbag location in this vehicle seat was palpated manually and marked, demonstrating the preferred installation region within the seatback of vehicles sold in the US. If the occupant deviated laterally in this exemplar vehicle, the posterolateral torso likely would be exposed to airbag deployment forces.

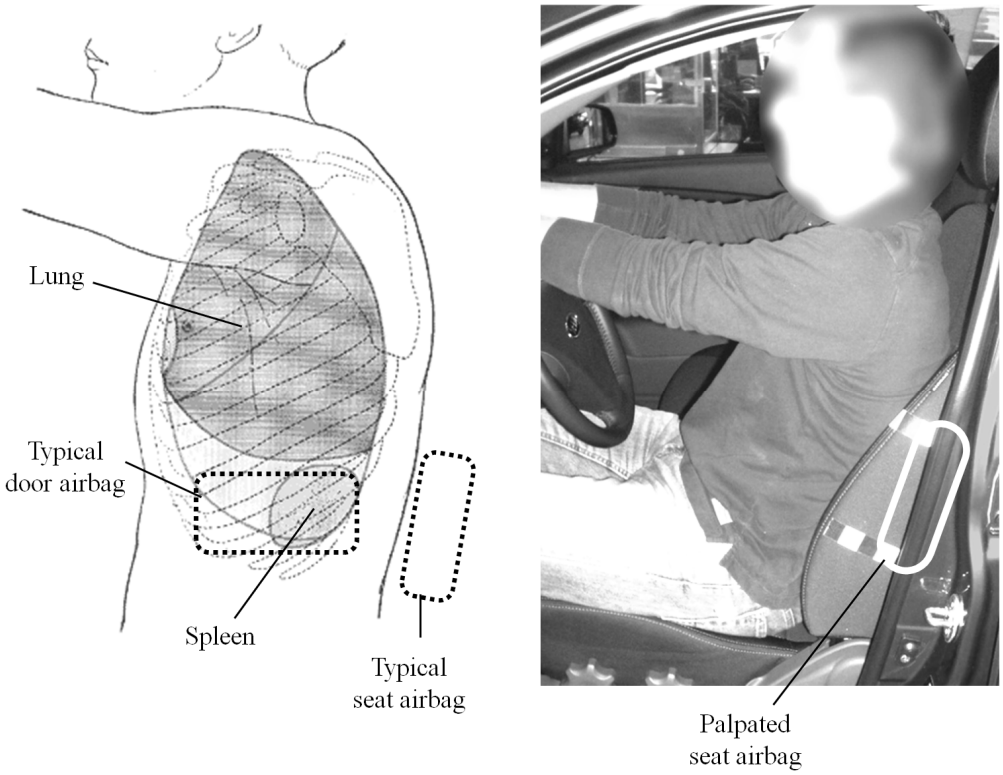

Figure 4.9. Seat and door airbag modules with respect to anatomical reference. Left: Spleen *in situ* with common airbag module locations. Right: Exemplar vehicle and occupant with seat airbag indicated.
Modified from Gray (1918)

The possibility of splenic trauma from airbag deployment is clinically important. The vascular nature of the spleen and its location *in situ*, deep to the posterolateral curvature of left ribs 9-11, exposes it to deflection and viscous injury from blunt trauma

(Yoganandan et al., 2000; Yoganandan et al., 2001). Acute splenic trauma can be life-threatening, and active hemorrhaging requires immediate medical intervention (Arden et al., 1981; Harbrecht et al., 2007). Although treatment course is increasingly non-operative in the absence of shock, as many as one-third of cases still necessitate splenectomy (Mustard et al., 1984; Glass & Gilbert, 1996; Dissanaike & Frezza, 2006; Kotsanas et al., 2006; Harbrecht et al., 2007). This procedure has been associated with a lifelong risk of overwhelming sepsis (Naylor et al., 1974; Shatney, 1987; Deodhar et al., 1993; O'Sullivan et al., 1994; Waghorn, 2001; Vasef & Platz, 2002; Hartnett et al., 2003; El-Alfy & El-Sayed, 2004; Harbrecht et al., 2007; Harbrecht et al., 2008; Davies et al., 2009).

One case presented in this study demonstrated the potential latency of splenic hemorrhage induced by airbag deployment. As many as one-third of patients presenting with acute splenic trauma suffer from "delayed rupture" (Naylor et al., 1974; Leppaniemi et al., 1988; O'Sullivan et al., 1994; Parithivel et al., 2002; Ruffolo, 2002; Rubin, 2003; Shah et al., 2008; Davies et al., 2009). This condition is characterized by hemorrhaging which does not manifest for at least 48 hours (Parithivel et al., 2002). During this latency, even contrast-enhanced abdominal imaging scans may appear normal (Leppaniemi et al., 1988). Reported delays are commonly two to ten days (Leppaniemi et al., 1988; Parithivel et al., 2002). Although many mechanisms may contribute to this condition (Parithivel et al., 2002), delayed rupture poses unique complications to treatment. The onset of splenic hemorrhaging can present with "explosive suddenness" and can rapidly develop into hypovolemic shock (Wooldridge, 1969; Ruffolo, 2002). Although the latency period reported in this study was insufficient to be characterized as

a delayed rupture (twelve hours), the case occupant was participating in strenuous exercise prior to seeking medical treatment, subjecting himself to further risk of complication.

While torso airbag efficacy and resulting injury patterns have been studied using real-world motor vehicle crash data from multiple datasets, inconsistent results have been reported (Section 3.5.1). While this may be attributable to limited sample size as many authors have noted, the complexity of side impact boundary conditions may also obscure results. Torso airbag performance is complicated by occupant position with respect to the device, an elusive parameter in real-world crash data. A parametric analysis is appropriate to delineate the relationship between occupant position, crash severity, and risk of lateral thoracic injury.

FIVE

DEFINING OUT-OF-POSITION DURING IMPACT

Specific Aim 2: Determine the relationship between lateral thoracic biomechanical response and parameters of door intrusion velocity and occupant position to define "out-of-position" torso airbag interaction.

All previous out-of-position considerations of thoracoabdominal injury have neglected the contribution of crash severity (Section 3.5.2). To delineate the relationship between occupant position, crash severity, and risk of lateral torso injury, a computational parametric analysis was completed with a generalized torso side airbag. This analysis varied occupant distance from the deploying airbag and door intrusion velocity with respect to the occupant.

5.1 METHODOLOGY

Thoracic biomechanical response was quantified in simulated sled impact with and without a torso-protecting side airbag. Lateral biomechanical response parameters of normalized chest deflection and the Viscous Criterion (Sections 3.2.2 and 3.2.3) were quantified using the standardized facet occupant model in MADYMO (R6.3, TNO-MADYMO, Livonia, MI) simulations.

5.1.1 GEOMETRY AND BOUNDARY CONDITIONS

An introductory model description can be found in Section 3.3.2. The lateral contact boundary condition was an impact device representing a Heidelberg-type sled identical to that utilized in previous laboratory experiments (Foret-Bruno et al., 1980; Melvin et al., 1980; Monk et al., 1980; Kallieris et al., 1981; Pintar et al., 1997). This device replicated side impact by simulating the intrusion velocity at which the vehicle interior door contacts the occupant laterally (Figure 1.1). This intrusion velocity has been demonstrated to approximate crash ΔV at the instant of occupant contact (Melvin et al., 1980; Monk et al., 1980; Lau et al., 1991). The sled model was positioned on a zero-friction bench seat with a 15° seat pan and a 68° seat back angle (Figure 5.1). For simulating nearside impact, a rigid wall was positioned such that the occupant left side contacted the boundary at a predefined impact velocity. This rigid wall rose 40 cm above the midpoint of the seat and terminated just inferior to the shoulder complex of the occupant.

The occupant was positioned with the head Frankfort plane horizontal, legs stretched forward and parallel in a normal driving posture, and spine in normal seated curvature. The arms were oriented forward and away from the torso such that the lateral thorax was fully exposed to impact. For this analysis, lateral chest deflections, deflection rates, and viscous responses (Section 3.1) were quantified from the thoracic deformable structures. The mid-thorax line was defined between nodes overlying the spinal column centerline and the mid-sternum. Half-chest deflection was quantified as the distance between the lateral node and the mid-thorax line (Section 3.3.2).

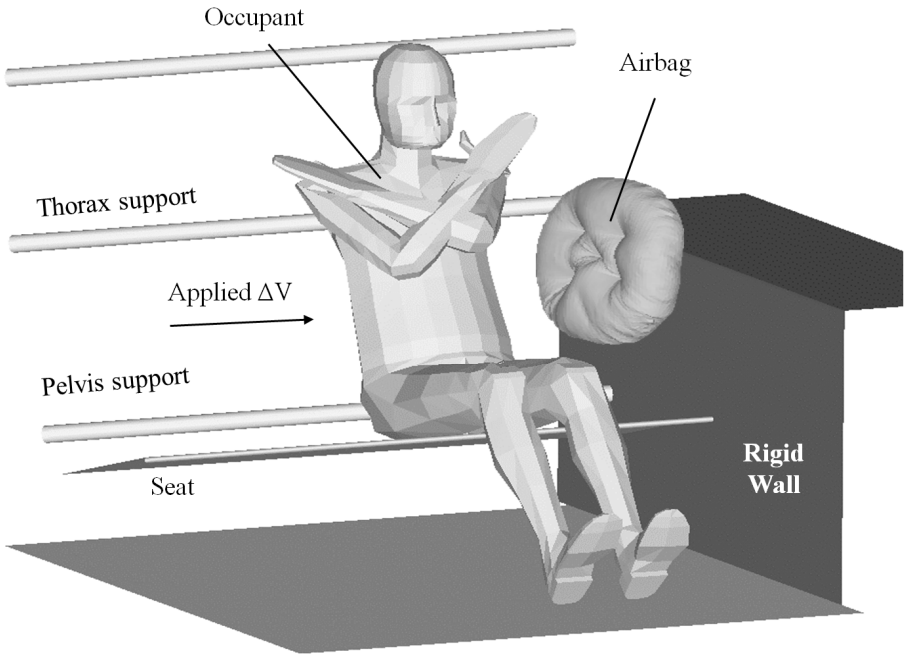

Figure 5.1. Facet occupant model in simulated sled geometry.

The generalized torso side airbag consisted of a modified finite element (FE) frontal airbag provided standard with the MADYMO software package. Because of the facet occupant model design (Figure 3.12), thoracic deformation sensitivity was greatest from the pure lateral direction. Therefore a door-mounted torso side airbag was simulated to load the model in the most sensitive direction. The FE mesh was tethered by line elements to an inflated depth of 18 cm and inflated volume of 13 L. This airbag volume was reasonable, as side airbags of 12 L have been reported (Pipkorn & Haland, 1996). The airbag fabric consisted of two circular halves composed of 13,000 triangular membrane elements with 0.5 mm thickness. Fabric material properties were unaltered from previous studies (Sieveka et al., 2001; Power et al., 2002). Inflation behavior was defined by a mass inflow function with isothermal expansion. The airbag required 14 ms

to inflate. Characterized in a standardized 60 L tank test (Wang, 1991; Ruff et al., 2007), the prescribed inflator achieved 95 kPa maximum pressure and 5 kPa/ms maximum onset rate. This maximum tank test pressure was realistic for a torso-interacting side airbag (Pintar et al., 1999). Airbag aggressivity was conservative as measured by the inflator tank pressure onset rate; onset rates 300% greater than specified in this analysis have been reported (Pintar et al., 1999). Thermodynamic calculations utilized a lumped-parameter approach, assuming uniform pressure throughout the airbag volume. Inflator nozzle gas flow was approximated by applying additional momentum to fabric nodes within a defined nozzle outflow stream using an Idelchik nozzle diffusion approximation (Idelchik, 1986). This method improved early stage airbag deployment simulation (Roychoudhury et al., 2000; Petit et al., 2003; Park & Hong, 2005). Surface-to-surface contacts were defined between the airbag fabric, the rigid impact wall, and the occupant facet surface skin.

5.1.2 VALIDATION

The model response was validated using data from seven PMHS tests conducted with a Heidelberg-type sled device similar to the simulation geometry and previously published (Pintar et al., 1997; Kuppa et al., 2003). Briefly, thoracic injury metrics were derived from two 40-channel or 59-channel chestbands at the level where the fourth and eighth ribs intersect the mid-axillary line. Half-chest deflections were quantified from chestband contours (Section 3.2). Chest deflection rate, used to calculate the viscous response, was obtained by numerical differentiation of chest deflection and application of a CFC 180 filter in accordance with SAE J211 (Section 3.1).

5.1.3 LOADING

The occupant was positioned in a forward-facing posture with the lateral thorax adjacent to the airbag and wall. In this orientation, the occupant model was subjected to six door velocities and thirteen occupant distances. Door velocity was incremented from ΔV = 4.0 to 9.0 m/s in 1.0 m/s intervals, a range chosen to represent the middle 50% of side impacts in the US (Zaouk et al., 2001). At each velocity, the side airbag was activated at the instant the occupant was within a predetermined distance from rigid wall (Figure 5.2). This occupant distance was incremented from 2.0 to 24.0 cm in steps of 2.0 cm. Each ΔV was also repeated without airbag deployment. Finally, the airbag was deployed into the stationary occupant thorax to mimic the current OOP protocol as defined by §3.3.4.5 the *Recommended Procedures for Evaluating Occupant Injury Risk from Deploying Side Airbags* (Sections 1 and 3.5.2) (IIHS, 2003).

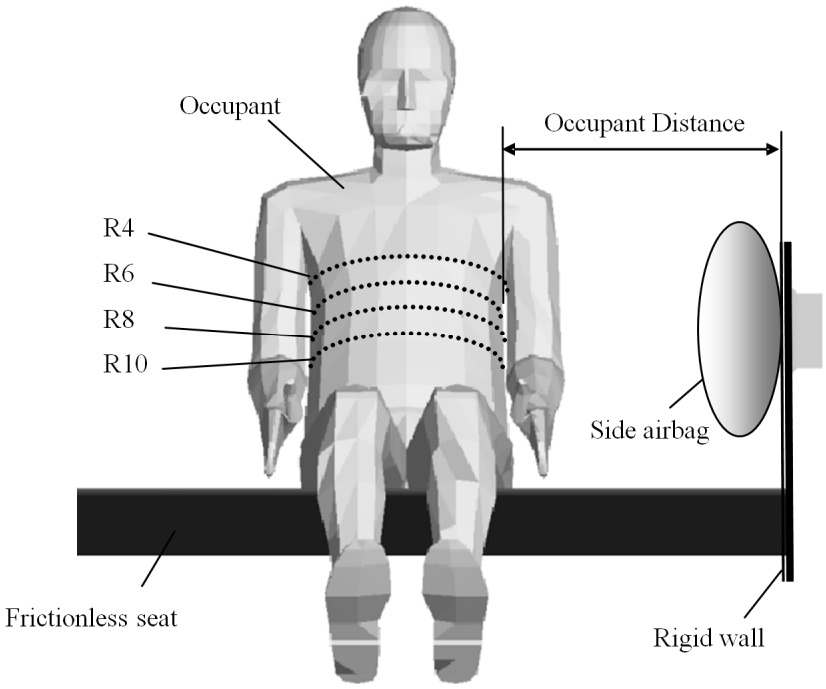

Figure 5.2. Initial conditions for parametric analysis.
NOTE: Arms were oriented as in Figure 5.1 for simulations.

5.2 RESULTS

A total of 79 simulations were completed. Thirteen impacts were simulated at each ΔV, which corresponded to simulations without airbag and at distances from 2.0 to 24 cm.

5.2.1 VALIDATION

Results from previous PMHS tests were compared to computational simulation results for validation purposes. Individual time responses from PMHS were scaled according to subject mass using accepted techniques (Eppinger et al., 1984) prior to aggregation. Obtained at the eighth rib level chestband, the traces demonstrated that simulated responses from computation model were similar to PMHS response in

magnitude and in morphology. Simulated response was within ± 1 SD from PMHS data during the loading phase of impact.

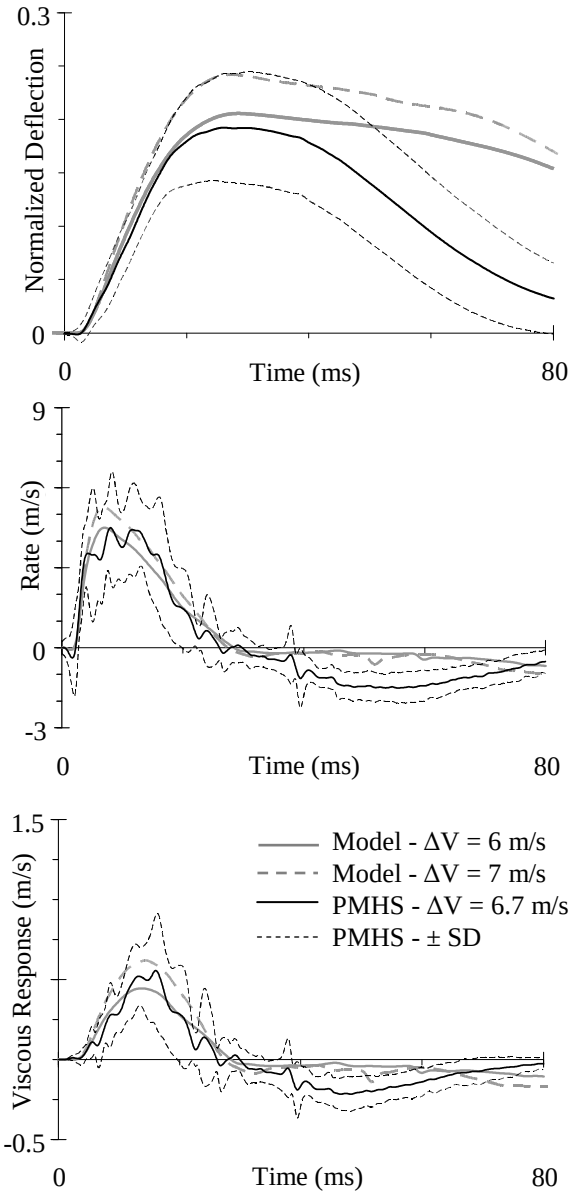

Figure 5.3. Chest deflection, deflection rate, and viscous response of model and prior PMHS experiments at similar impact velocities.

5.2.2 POSITION AND ΔV

Shown in Figure 5.4 and Figure 5.5 are exemplar metric time histories for ΔV = 7.0 m/s for each contour level; similar trends were apparent at other ΔV. Scenarios shown are unprotected (rigid) contact and airbag protection with activation at occupant distances corresponding to greatest biomechanical response (2 cm), least deflection (16 cm), and least viscous response (20 cm). For each plot, t = 0 indicates simulation time at which first thorax contact occurred; for simulations without airbag t = 0 represents contact with the rigid wall. For the non-airbag scenarios, overall peak response was consistently observed at the R4 level, immediately inferior to the shoulder complex (Figure 5.2). This was contrasted by airbag deployment at 2 cm during which greatest responses were observed at the R8 level for all ΔV. This level corresponded to the airbag module location. With increasing occupant distance, the exhaustion of airbag gases following impact permitted rigid boundary interaction from behind the airbag fabric and elevated response was observed at the R4 and R6 levels (Figure 5.5). As occupant distance increased from nearest location to distances further from the airbag, biomechanical response at all levels decreased as a result of decreased airbag loading. Yet, excessive distances led to insufficient airbag pressures and eventual increases in biomechanical response. Without sufficient airbag cushion pressure, rigid interaction from behind airbag fabric induced a marked increase in response traces at the upper thorax levels later in impact duration. This response demonstrated a “dual impact” scenario of protected lateral impact: (i) airbag contact followed by (ii) wall contact. Biomechanical response initially represented airbag only contact; after airbag gases were

exhausted time traces demonstrated response to interaction with wall from behind airbag fabric.

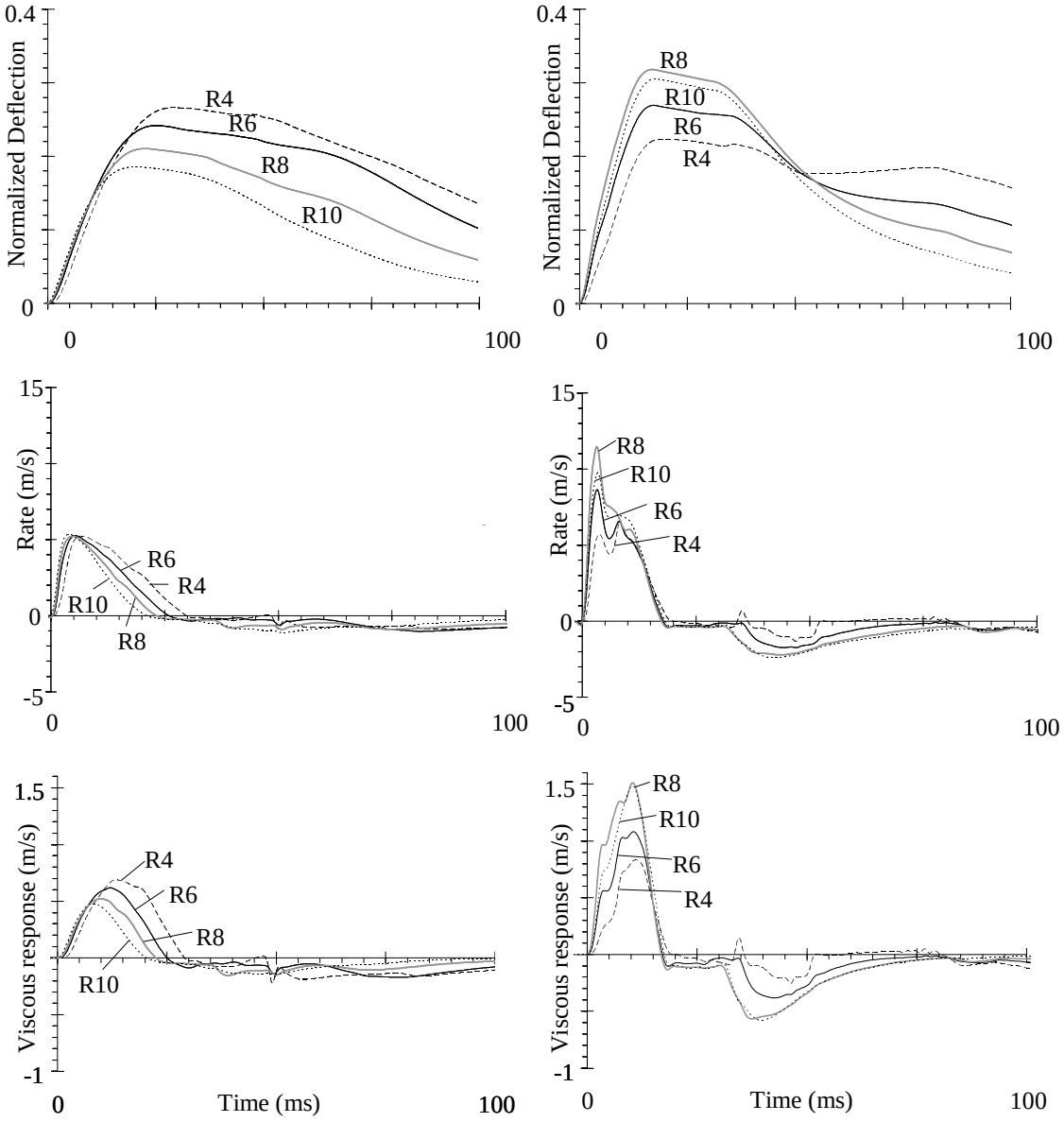

Figure 5.4. Chest deflection, deflection rate, and viscous response of model subjected to rigid (no airbag) contact (left) and 2 cm airbag deployment (right) at ΔV = 7 m/s.

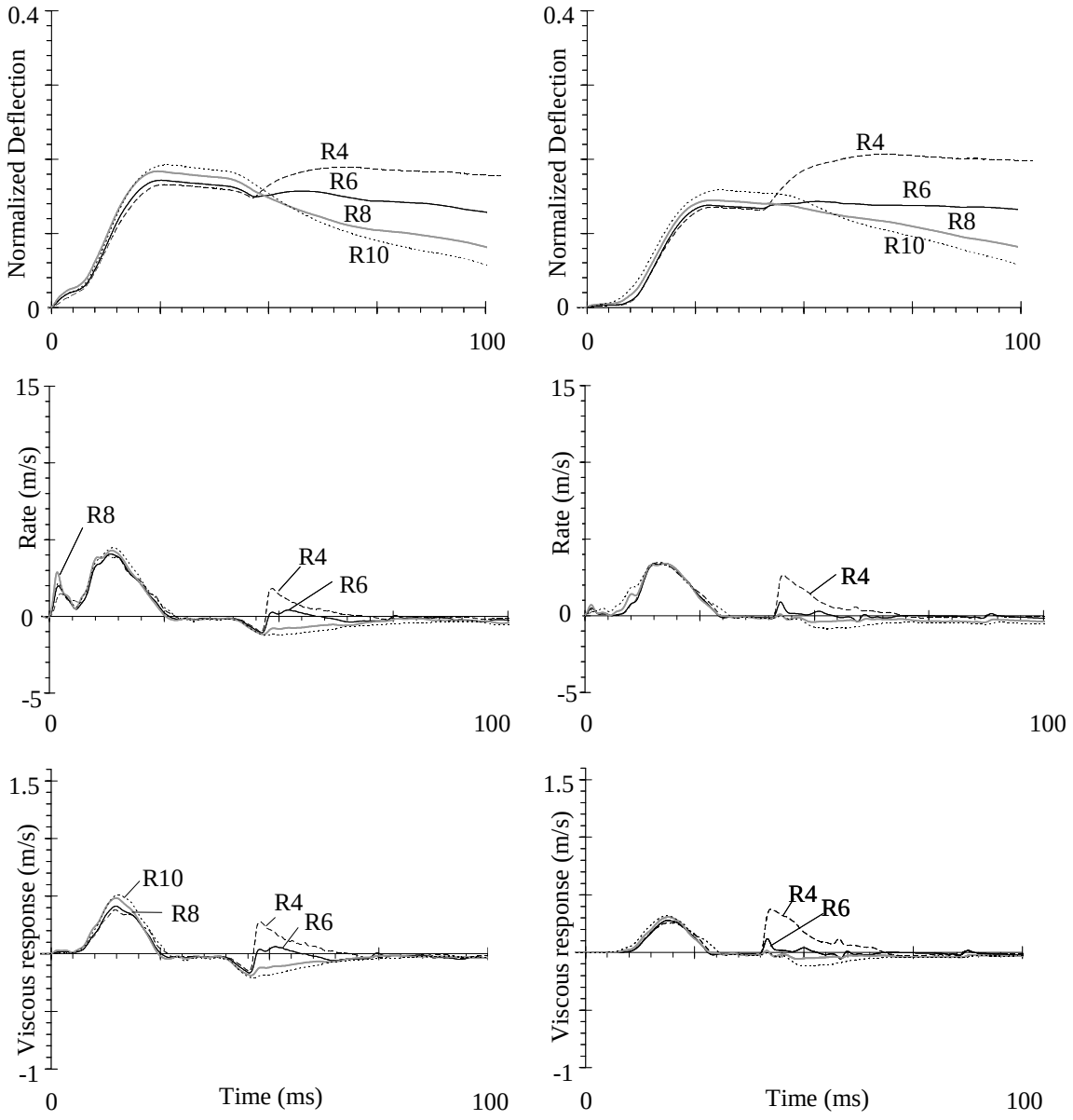

Figure 5.5. Chest deflection, deflection rate, and viscous response of model subjected to 16 cm airbag deployment (left) and 20 cm airbag deployment (right) at ΔV = 7 m/s.

Trends in gross peak responses were compared as a function of occupant distance at the instant of airbag activation. An exemplar plot representing peak normalized deflection is shown in Figure 5.6. Trend lines are punctuated by three points of interest. Square markers indicate the points demonstrating the maximum biomechanical injury metrics, i.e., most harmful occupant distance. For each ΔV, this point corresponded to

the nearest occupant distance examined with side airbag and exceeded response magnitudes obtained from unprotected rigid contact. Triangular markers denote the distance at which peak responses with airbag interaction were equivalent to metrics obtained from unprotected door contact, hereafter referred to as the critical distance. This distance was quantified using linear interpolation of adjacent points. Diamond markers indicate occupant distance of greatest airbag protection, denoted by the greatest reductions in biomechanical response at each ΔV.

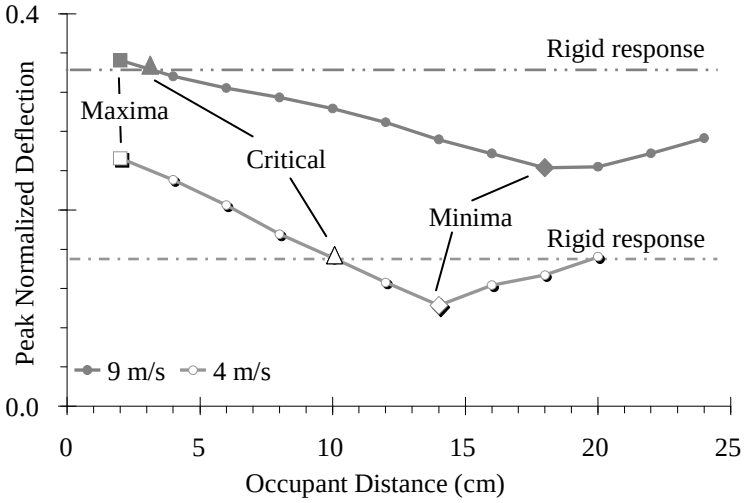

Figure 5.6. Peak normalized chest deflection with respect to occupant distance from airbag for ΔV = 4 and 9 m/s.

Shown in Figure 5.7 are the aforementioned defining points from normalized deflection, deflection rate, and viscous response trends for all ΔV considered in this analysis. Minimum deflections (plotted as diamonds) were achieved when occupant distance was between 14 and 18 cm, at which deflections were reduced approximately 30% compared to rigid contact. The critical distance (plotted as triangles) deviated from 10.1 to 3.2 cm with increasing ΔV. Maximum deflection for each ΔV was observed when occupant was nearest the airbag at deployment. These deflections ranged between

103% and 168% of deflections attained during rigid interaction. Peak rate and viscous response trends were quantitatively different from trends in deflection response. Minimum viscous responses (plotted as diamonds) were attained when occupant distance was between 16 and 24 cm. At these distances, responses were between 49% and 64% of peaks attained during rigid contact. Unlike deflection, the viscous critical distance varied by less than 1.0 cm with increasing ΔV. Maximum response for each ΔV was observed when occupant distance was minimized. Metrics ranged between 140% and >400% of values attained during rigid interaction.

Injury metric sensitivity to airbag deployment also varied with ΔV. Sensitivity was defined as the slope of the peak biomechanical response trends (Figure 5.6) evaluated at the critical occupant distance. Resulting values are shown in Table 5.1. Additionally, relative values are shown, representing both deflection and viscous response sensitivities normalized to value at $\Delta V = 4$ m/s. Sensitivity of deflection decreased with increasing ΔV by approximately one-third. Rate and viscous response sensitivity increased with ΔV by nearly two-fold.

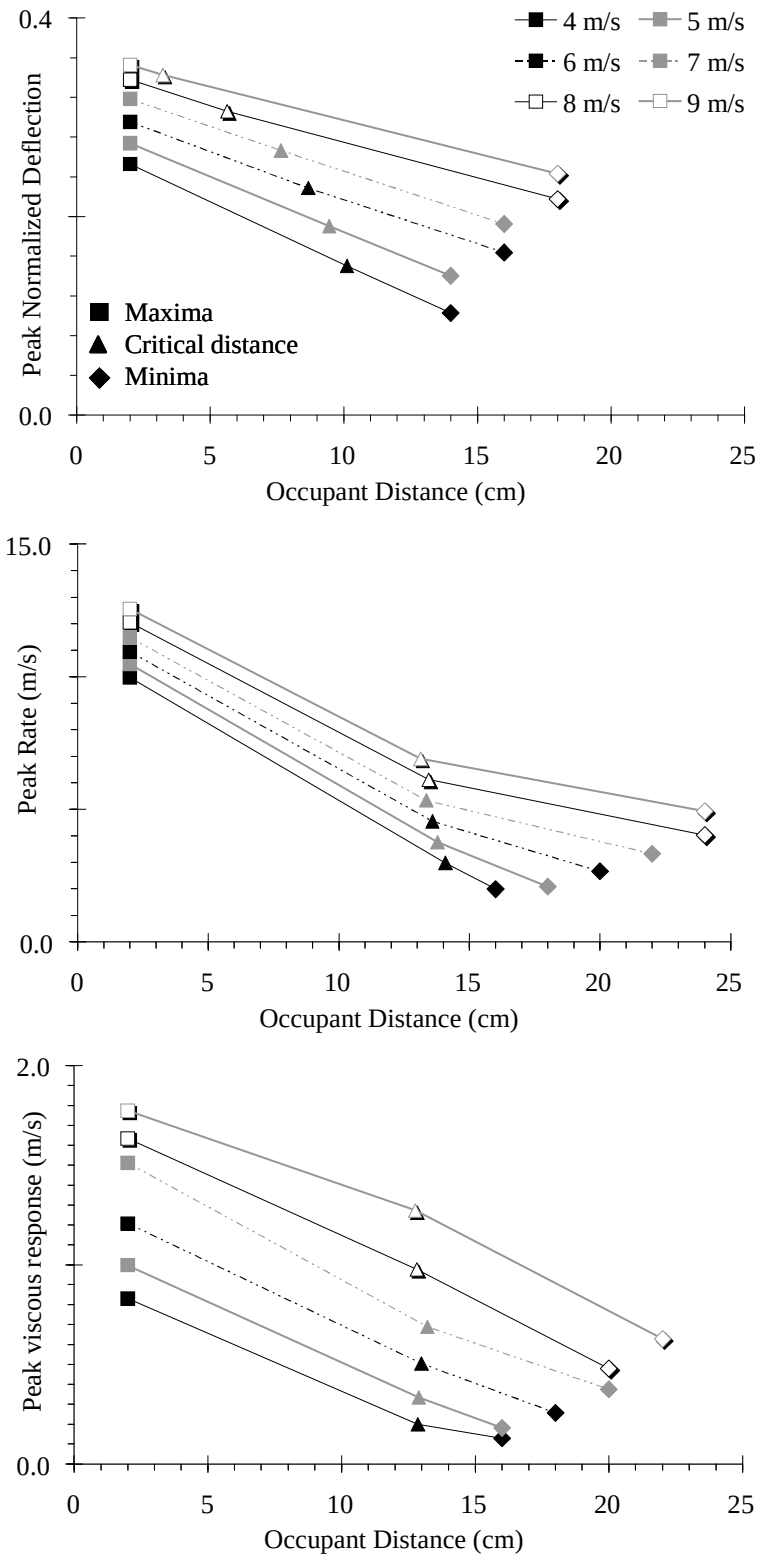

Figure 5.7. Defining points for peak normalized chest deflection, deflection rate, and viscous response at all ΔV with respect to occupant distance.
Lines are drawn for clarity.

Table 5.1. Metric sensitivity to occupant distance, raw and normalized to values at ΔV = 4 m/s

ΔV (m/s)	Deflection (cm^{-1})	Deflection (Norm) (cm^{-1})	VCmax $(m(s\ cm)^{-1})$	VCmax (Norm) (cm^{-1})
4	-0.013	1.00	-0.046	1.00
5	-0.011	0.91	-0.051	1.10
6	-0.010	0.81	-0.064	1.39
7	-0.010	0.76	-0.070	1.51
8	-0.006	0.48	-0.074	1.59
9	-0.008	0.64	-0.086	1.86

5.2.3 COMPARISON TO STATIONARY PROTOCOL

Simulated biomechanical response resulting from a stationary occupant is shown in Figure 5.8. The countour at R4 indicated the lowest peak metrics, followed by R6 and R10. Overall peak responses were demonstrated at R8; this location corresponded to the level of the airbag module. In stationary conditions, peak normalized deflections were between 0.13 (R4) and 0.19 (R8). Viscous response peaks ranged 0.3 – 0.7 m/s at these respective contours.

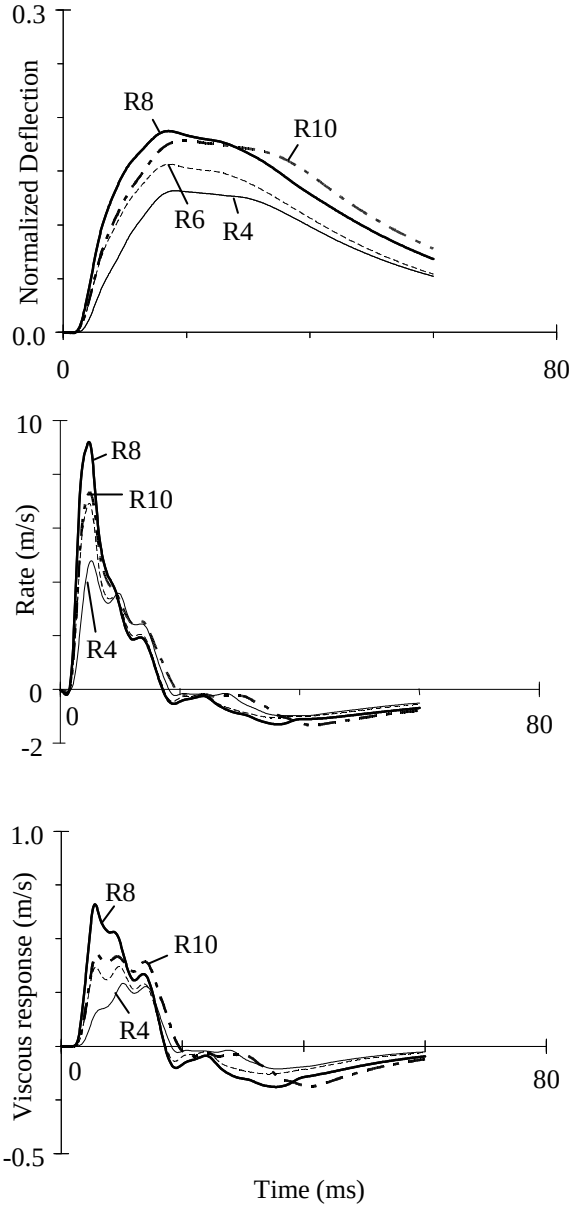

Figure 5.8. Normalized chest deflection, deflection rate, and viscous response of model subjected to stationary close-proximity torso airbag deployment.

Biomechanical response time traces are shown in Figure 5.9 for stationary and dynamic close-proximity (2 cm) occupant at all ΔV; only the thoracic level demonstrating peak response for each ΔV is depicted. Occupant position was equivalent at airbag activation (t = 0). During the initial three milliseconds following airbag contact, injury metrics from stationary and dynamic occupants differed by less than five percent. With

impact progression, biomechanical responses increased with ΔV. Further, time of peak viscous response also deviated with increased ΔV. For all simulations, peak deflection occurred between 17.1 and 20 ms following airbag activation. Similarly, peak rate occurred at t = 5.0 ms independent of ΔV. Maximum viscous response from the stationary occupant was observed at t = 5.6 ms, less than 1 ms following peak rate. With increased ΔV, peak viscous response lagged peak rate, occurring between 9.2 – 12.6 ms.

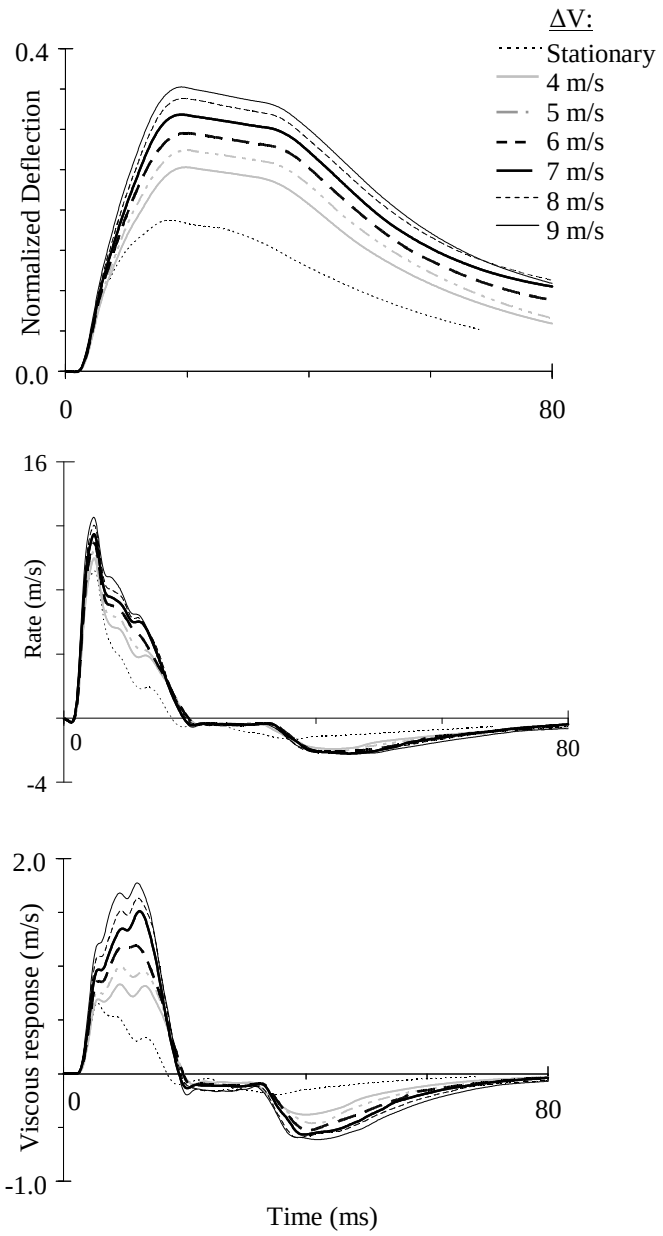

Figure 5.9. Normalized chest deflection, deflection rate, and viscous response of model subjected to all ΔV with close-proximity airbag deployment.

Shown in Figure 5.10 are peak biomechanical metrics with rigid wall and close-proximity boundary conditions. Without airbag, normalized deflection ranged from 0.15 (ΔV = 4.0 m/s) to 0.35 (9.0 m/s); viscous response ranged from 0.2 to 1.3 m/s. With close-proximity boundary condition and ΔV, deflection ranged 0.21 – 0.44 and viscous

response ranged 0.8 – 1.8 m/s. Also indicated in Figure 5.10 are increases in biomechanical response induced by close-proximity boundary condition compared to rigid contact. Close-proximity airbag induced biomechanical response greater than rigid boundary conditions at all ΔV considered. Deflection increase resulting from airbag ranged 0.01 – 0.10, and viscous increase ranged 0.5 – 0.8 m/s. The greatest increase in deflection response occurred at ΔV = 4.0 m/s; the greatest viscous response increase occurred at ΔV = 7.0 m/s.

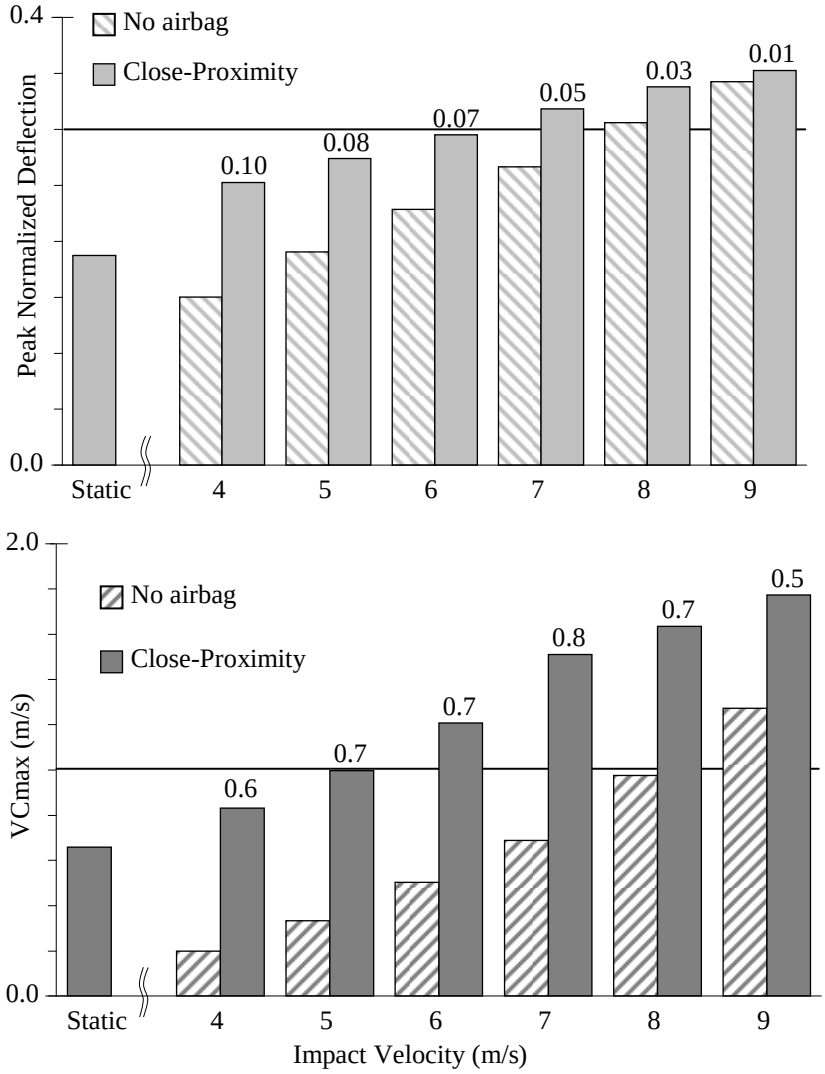

Figure 5.10. Peak normalized chest deflection and VCmax of model subjected to all ΔV with rigid contact and close-proximity airbag deployment.
Adjacent numerals indicate increases over rigid contact.

5.3 DISCUSSION

The purpose of this analysis was to assess the dependency of thoracic biomechanical response on occupant distance and door velocity with a generalized torso side airbag. These biomechanical metrics (peak deflection and VCmax) represent the injury metrics currently evaluated during commercial side airbag out-of-position testing (IIHS, 2003). Trends were identified using three points of interest: the critical distance, the most protective distance, and the least protective distance.

Torso interaction with airbag demonstrated a "dual impact" pattern in which metrics responded to airbag contact followed by rigid contact. Studies of padded lateral impact have made similar observations (Section 3.4.2). Viano (1987a and 1987b) described the effects of constant crush-force and linear elastic padding materials using a lumped parameter thorax model. Metric minima were reported when material properties led to equal response magnitudes to padding interaction and subsequent through-padding rigid contact.

With increased occupant distance, greater time lapsed between airbag activation and thorax contact. This greater duration allowed airbag pressure losses to venting, reducing the influence of the airbag contact on the total biomechanical response. The most protective distance resulted when airbag and through-airbag rigid interactions were equivalent. This distance varied with ΔV, deviating away from the airbag module with increased ΔV, up to 10 cm across the ΔV range in this study. Depicted in Figure 5.11 are positions of least deflection response overlaid with positions of least viscous response; linear fit lines are also shown for clarity. Minimized deflection consistently required distances 2 cm closer to the airbag than minimized viscous response for the same ΔV.

Further, injury metrics were not reduced equivalently at all ΔV. Peak compression was reduced by approximately 30% compared to values without airbag regardless of ΔV. In contrast, viscous response was reduced by 35% at the least ΔV and by 50% at the greatest ΔV. This finding is in agreement with other studies of thoracic injury mitigation, in which padding was more mitigative of viscous response than of deflection (Deng, 1989; Deng & Tzeng, 1996).

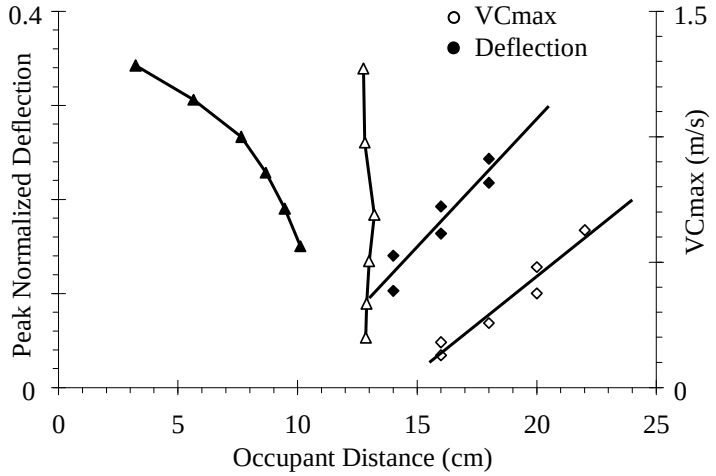

Figure 5.11. Comparative plot of critical distance (△) and most protective distance (◇) defined by peak normalized deflection and VCmax.

Although a previous study found excessively stiff padding to be equivalent to rigid contact (Viano, 1987a), early airbag contact was more complex than stiff padding response. Early stages of airbag deployment resulted in additional energy from fabric momentum and transient gas pressure. Thus, unlike padded contact with constant material properties, the net energy imparted to the thorax by the airbag contact may be greater than unprotected rigid contact (Haland & Pipkorn, 1996; Smith et al., 2003; Yoganandan et al., 2007b; Yoganandan et al., 2007c). Studies of close-proximity airbag deployment have demonstrated high forces imparted to test subjects (Horsch et al., 1990; Lau et al., 1993). Yet, parametric analyses tuning airbag parameters to meet deflection-,

viscous-, and acceleration-based thoracic injury criteria (Section 3.1) have neglected the role of the inflation phase in airbag-occupant interaction which was included in the present analysis (Haland & Pipkorn, 1996; Pipkorn & Haland, 1996; Deng et al., 1998; Khadilkar & Pauls, 1998; Sieveka et al., 1998; Vaidyaraman et al., 1998).

The critical distance was the nearest distance at which peak thoracic injury metrics with airbag were equivalent without airbag deployment. From this threshold, airbag deployment was detrimental to a closer occupant and beneficial to a farther occupant. Critical distances for deflection and viscous metrics are depicted on the same axes in Figure 5.11 for all ΔV. A minimum occupant distance was required (approximately 13 cm) for the airbag to mitigate viscous response regardless of ΔV. In contrast, critical distances for deflection varied approximately 7.0 cm closer to the airbag as ΔV increased, indicating a reduction in airbag influence with increased ΔV. In other words, an occupant could be closer to the device and still benefit from deployment. This observation regarding deflection is also supported by sensitivity values (Table 5.1). With increasing ΔV, deflection response demonstrated decreased sensitivity to occupant distance while VCmax demonstrated a two-fold greater sensitivity.

Because of the complexity of side airbag interaction with a dynamic torso, the stationary OOP test protocol may be inadequate. In Figure 5.10, accepted biomechanical tolerances for 25% risk of AIS 4+ injury are indicated by a bold line (Sections 3.1.2 and 3.1.3). Under the stationary test condition, metrics did not exceed injury tolerances. Without a side airbag, deflection and viscous responses achieved or exceeded tolerance when $\Delta V > 7$ m/s. With close-proximity airbag deployment, responses achieved or exceeded biomechanical tolerance as low as $\Delta V = 5$ m/s, exceeding the peak responses

from the stationary protocol. Therefore, between $\Delta V = 5$ and ~8 m/s, biomechanical tolerances were exceeded because of airbag deployment. This velocity range suggests a scenario for torso airbags in which their deployment can exacerbate injury. Yet, the airbag did not induce metrics in excess of tolerances under the accepted stationary evaluation procedure.

Shown in Figure 5.12 are the response differences between close-proximity airbag and rigid contact after normalizing to stationary response. Airbag deployment exhibited a monotonically decreasing influence on deflection with increasing ΔV: linear fit to peak deflection differences demonstrated $R^2 > 0.997$. In contrast, airbag viscous effects were not linear; the airbag boundary condition exhibited increasing influence on VCmax up to $\Delta V = 7.0$ m/s. At this ΔV, normalized response increase was greater than 1.0, indicating that airbag deployment increased response by a magnitude greater than that which resulted from the stationary out-of-position test. In other words, the collective effect of close-proximity airbag and dynamic impact exceeded the linear summation of their independent effects. This observation may be explained by a theoretical interpretation of the Viscous Criterion. Mathematically, VCmax is proportional to the peak energy storage rate of the thorax (Wang, 1989). While the total energy imparted may not have increased beyond linear summation, the combined energy from the airbag and impact was imparted without an increase in duration. However, the proportional contribution of the airbag to total impact energy decreased with increasing ΔV. At ΔV beyond those investigated here, severity of impact would obscure airbag effects.

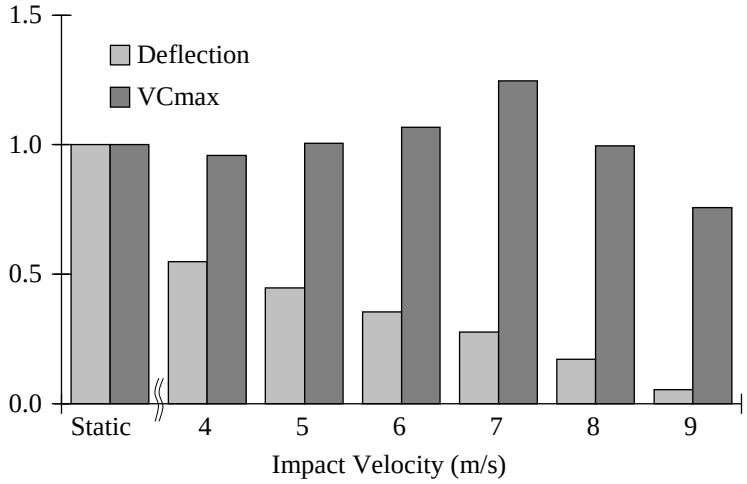

Figure 5.12. Normalized biomechanical response to close-proximity airbag; that is, rigid response subtracted from close-proximity response.

These results further suggested that visceral organs in close proximity to the airbag during deployment may be more susceptible to trauma in close-proximity side airbag scenarios. Recall that viscous response is generally associated with visceral injury (Section 3.1.3), and peak deflection is generally associated with rib fracture (Section 3.1.2). Viscous sensitivity suggests that injury resulting from torso airbag may be more likely visceral trauma. Real-world observations have found this to be the case (Chapter 4; Kirk & Morris, 2003), noting abnormal visceral injury following dynamic impacts with torso airbag deployment. Further, because the critical distance for VCmax was as little as 2 cm from the distance of least deflection at lower ΔV (Figure 5.11), reasonable postural variations may greatly influence soft tissue injury risk.

This analysis was limited by the availability of a vehicle-specific coupled fluid-structure side airbag model. Therefore a generalized door-mounted torso side airbag was simulated to load the model in the most sensitive lateral direction (Figure 3.12). This analysis delineated the broader trends by which torso airbag deployment may cause injury in actual crashes. A dynamic out-of-position definition is therefore required for

side airbag testing. Further, maximal airbag influence was suggested at $\Delta V = 7$ m/s. Yet because this model was constrained to lateral deformations only, no information could be obtained with regard to patterns of deformation due to OOP airbag loading. To address Specific Aims 3 and 4, laboratory testing was required to characterize the deformation patterns induced by close-proximity airbag deployment during dynamic side airbag interaction.

SIX

EXPERIMENTAL EVALUATION OF SIDE AIRBAG LOADING

Specific Aim 3: Characterize torso deformation and direction resulting from out-of-position side airbag interaction.

Specific Aim 4: Quantify injury risk, as measured by Abbreviated Injury Scale and tissue-level material response, associated with out-of-position torso side airbag interaction with the thoracoabdominal region.

Kinematic computational modeling demonstrated that dynamic occupants may be more susceptible than stationary occupants to injury from torso side airbag out-of-position (OOP) interaction. Injury risk to dynamic occupants may not be identified through stationary testing. Further, injuries resulting from side airbag interaction may most likely involve soft tissues, specifically splenic trauma. To address Specific Aims 3 and 4, sled experiments utilizing postmortem human subjects (PMHS) were designed to evaluate the thoracoabdominal deformation patterns and injury response to OOP side airbag interaction in dynamic and stationary experiments. A sled velocity of $\Delta V = 6.7$ m/s was chosen to represent a dynamic OOP definition based on computational modeling (Chapter 5) and the availability of comparable PMHS test data at this velocity with identical sled geometry (Maltese et al., 2002; Kuppa et al., 2003; Yoganandan et al., 2008). Unlike the computational multi-body model, these tests employed a seat-mounted torso airbag consistent with field observations (Chapter 4).

6.1 METHODOLOGY

The protocol was designed to characterize thoracoabdominal response to seat-mounted torso-interacting side airbags.[1] Stationary and dynamic (sled) test setups were developed in which PMHS were exposed to out-of-position torso side airbag contact. An airbag was selected from a subset of popular vehicles as determined by US sales (Automotive News, 2008). The chosen airbag inflated from a spiral fold pattern to a volume of approximately 11 L within 14 ms following activation. The bag fabric had no vent holes, extended approximately 44 cm from the inflator, and measured 40 cm in the occupant SAE z-axis (Figure 3.2). To characterize the potential loading capabilities of the airbag, a previous study deployed a variety of bags against an instrumented rigid surface at a distance of 6 cm (Hallman et al., 2009b). The chosen airbag exerted 4 kN peak force against this surface, which was the maximum tested and > 60% greater than the mean.

6.1.1 SUBJECT PREPARATION

Unembalmed PMHS were screened for HIV and Hepatitis A, B, and C. Anthropomorphic data and pre-test radiographs were obtained according to established procedures (Pintar et al., 1997). Specimens were dressed in tight-fitting leotards and masked to cover the head and face. Following surgical exposure of the femoral artery within the femoral triangle, a Foley catheter was inserted proximally through the iliac artery and fixed in the abdominal aorta by inflating the balloon. A tracheostomy was performed and pulmonary edematous fluid was removed. Carotid arteries were occluded

[1] This research was reviewed and approved by the Institutional Review Board at all participating institutions.

by ligature. Accelerometers (7264C-2K, Endevco Inc., San Juan Capistrano, CA) were rigidly fixed to the spine at the locations of T1, T12, and the sacrum; axes were in accordance with SAE J211.

6.1.2 EXPERIMENTAL PROCEDURE

PMHS were subjected to stationary airbag deployment or dynamic lateral impact with close-proximity airbag boundary condition. In both instances, subjects were placed on a Teflon-coated bench seat with 2.5 cm square tubular supports for the lumbar and thoracic regions. The seat assembly included a 15° seat pan angle and a 68° seat back angle (Figure 6.1). Further details have been described in the literature (Yoganandan et al., 2007a). Prior to testing, chestbands (Section 3.2) were placed on the torso circumferentially. For stationary tests, one 59-channel chestband (Denton ATD, Inc., Rochester Hills, MI) was placed at the xyphoid level. In dynamic tests, two 59-channel chestbands were placed at levels corresponding to the xyphoid and tenth rib (Figure 6.2). In one dynamic test, a chestband was placed at the axilla level in lieu of the tenth rib level. Using palpation, the band locations overlying the spine and sternum centerlines were determined. Chestbands were wrapped with metallic shielding and sealed with conductive adhesive tape. This treatment minimized signal interference from electrostatic discharge induced by rapid airbag fabric deployment. Shielding was overlaid with a cotton garment to maintain realistic interaction between the subject and the deploying airbag. After the chestbands and overlying materials were in place, subjects were positioned upright on the seat assembly in a normal forward-facing posture. Care was taken to ensure that the head Frankfort plane was horizontal, legs were extended forward in a normal driving posture, and the dorsal spine maintained normal

curvature. To maximize thoracic exposure to airbag deployment characteristics, both arms were oriented forward and away from the lateral thorax. This maintained an unprotected thorax throughout the event. Specimen vasculature was pressurized to normal mean arterial pressure (approximately 90 mmHg) with a heparin and dye solution by means of the Foley catheter; lungs were exercised immediately prior to testing and left open to atmosphere.

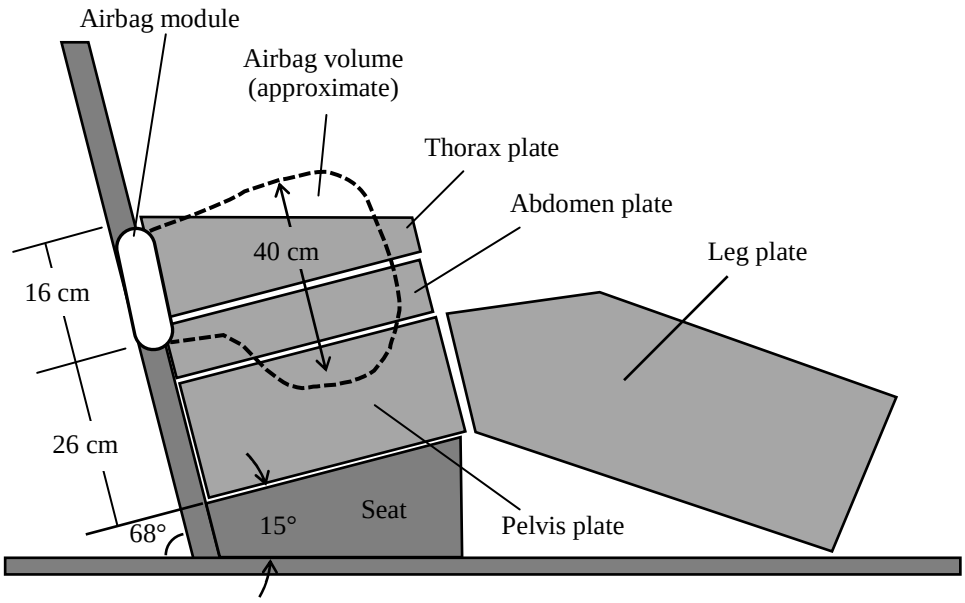

Figure 6.1. Bench seat apparatus with seat-mounted side airbag placement.
Additional details provided in Yoganandan et al. (2007).

For stationary airbag deployments, a rigid wall was attached to the seat assembly such that the superior edge was at a height of 450 mm above the seat. This corresponded to a level just inferior to the shoulder complex. The torso side airbag was mounted approximately 150 mm away from the wall. Subjects were positioned adjacent to the wall with the unmodified folded airbag approximately 1.0 cm from the posterolateral thorax between the T6 and L1 levels. No trim pieces or seat subcomponents were

included. The airbag was the only source of energy to interact with the subject. Left- and right-side deployments were performed on each subject.

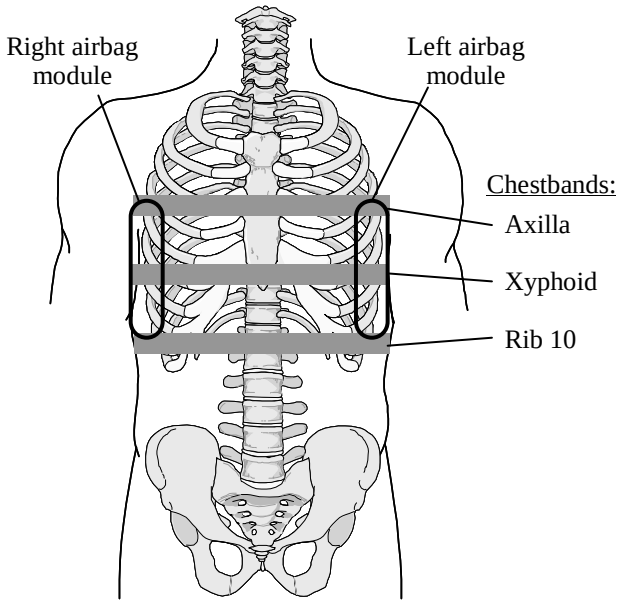

Figure 6.2. Instrumentation of specimens with respect to anatomy and airbags.
Stationary test specimens included xyphoid-level only; dynamic test specimens included xyphoid level and either axilla- or rib 10-level chestband.

For dynamic impacts, the bench seat and back support were fixed to the platform of an acceleration sled with pneumatic actuation and hydraulic control (ServoSled®, Seattle Safety, Kent, WA). A four-plate load wall configuration was located on the left end of the seat assembly (Figure 6.1) and has been described elsewhere (Yoganandan et al., 2007a). Wall adjustments were made to ensure the superior edge of the thorax plate corresponded to a level just inferior to the shoulder complex for all specimens. Thus, no shoulder engagement occurred. The unmodified torso side airbag was mounted posterior to the subject at a distance of 150 mm from the wall. The subjects were positioned 400 mm from the load wall, a distance sufficient for the sled to achieve and maintain ΔV = 6.7 m/s between airbag activation and subject contact with wall. Sled acceleration was recorded using a uniaxial accelerometer. In accordance with multi-body modeling

(Chapter 5), the side airbag was activated when the distance between the occupant and the wall was minimized. To identify this scenario with a seat-back mounted torso airbag, an iterative test series was conducted with an anthropomorphic test dummy. From this test series, it was determined that the side airbag should be activated when the outboard edges of the module and subject torso were coincident in the frontal plane (Figure 6.2). This deployment time also caused airbag interaction with the posterolateral region of the subject thorax and abdomen.

Ten tests were completed (Table 6.1). Three PMHS were subjected to stationary airbag deployment with both aspects exposed (six tests), and four PMHS were subjected to dynamic lateral impacts with airbag. Mean subject age was 60.6 yrs; mean height and mass were 170 cm and 72.1 kg. Following testing, radiographs were taken and full-dissection necropsy was performed in consultation with an experienced board-certified pathologist to obtain a detailed assessment of trauma to hard and soft tissues. Injuries were recorded and scaled in accordance with the AIS 2005 edition (AAAM, 2005).

Table 6.1. Subject specifications and test configuration.

PMHS	ID	Config.	Sex	Age (yrs)	Height (cm)	Weight (kg)	Chest depth* (cm)	Chest breadth* (cm)
1	S-1 S-2	Static, L Static, R	M	37	166	64	27.5	34.3
2	S-3 S-4	Static, L Static, R	M	83	174	86	29.7	38.4
3	S-5 S-6	Static, R Static, L	F	50	164	57	22.9	30.8
4	D-1	Dynamic	F	81	150	50	25.7	33.7
5	D-2	Dynamic	M	64	176	84	28.9	38.9
6	D-3	Dynamic	M	63	162	56	24.9	30.5
7	D-4	Dynamic	M	46	201	108	29.5	41.3

* Measured at the xyphoid level.

6.1.3 DATA COLLECTION AND PROCESSING

All signals were gathered at 12.5 kHz with the TDAS PRO data acquisition system (Diversified Technical Systems Inc., Seal Beach, CA) in accordance with SAE J211 specifications. High speed videography (Redlake-IDT, Tallahassee, FL) was recorded at a minimum of 2.5 kHz from four views: frontal, front oblique, overhead, and rear oblique. Accelerometer signals and load wall reaction forces were acquired for possible future use but were not included in this study.

Chestband signals were filtered according to CFC180 to remove airbag electrostatic interference and processed using RBandPC software (ver. 3.0a, Conrad Technologies, Washington, DC). As defined in RBandPC (Section 3.2), the spine and sternum locations represent unique contour boundary conditions. The spine location is constrained at the contour origin. The sternum location is constrained at $y = 0$ (as defined by spine) but may rotate and translate in the SAE x-axis. For solution stability in posterolateral loading, artificial spine and sternum locations were assigned in RBandPC processing as follows. Contour locations overlying subject spine and sternum locations

were identified. When imported into RBandPC, artificial spine and sternum locations were offset from subject spine and sternum in the contralateral direction by 10% of total chestband circumference (Figure 6.3). This methodology ensured that no boundary artifacts were generated by posterolateral loading in the vicinity of the subject spine location. Validation of this approach is addressed further in this section. Contours were generated at frequencies of 12.5 kHz throughout the event.

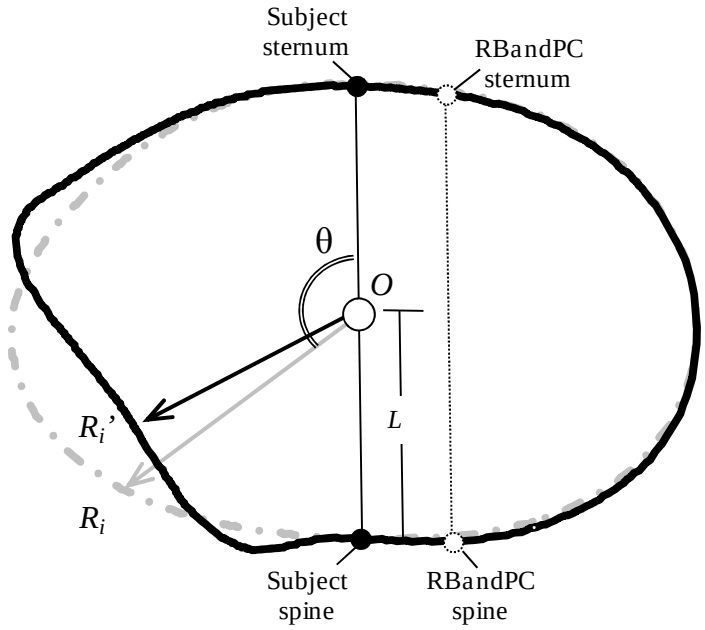

Figure 6.3. RBandPC and post-processing methodologies for oblique chestband deflection analysis.

Contour outputs from RBandPC were postprocessed using custom software developed with Matlab (The MathWorks, Natick, MA). The spine and sternum contour locations were returned to the centerlines of the subject spine and sternum; the spine-sternum (S-S) axis was defined by these anatomical locations (Figure 6.3). Contour origin (*O*) was defined as the midpoint between the spine and sternum contour locations in the undeformed state (t = 0). As deformation progressed, *O* remained coincident with the S-S axis and maintained a fixed distance (*L*) from the spine. Vectors for deflection

measurement were defined between *O* and points around the perimeter of the contour. Discrete points were obtained at approximately 2 mm intervals circumferentially (R_i). Deflections were quantified as the scalar subtraction of the instantaneous vector $O'R_i'$ from the initial undeformed vector OR_i. Deflections were normalized to chest breadth and a CFC180 filter was applied. The deformation direction for each point R_i was defined as the non-reflex angle ($\theta = 0 – 180°$) between the S-S axis and each initial vector OR_i, measured from the forward (anterior) direction. Left-side impacts were measured in the counterclockwise direction; right-side impacts were measured in the clockwise direction. Time traces of normalized deflection vectors were examined between $\theta = 90°$ and 140°. Deflection rate and its instantaneous product with normalized deflection, i.e., VC (Section 3.1.3), were also calculated.

Biomechanical and injury responses were compared to other boundary conditions from previously reported sled tests to delineate boundary effects. These tests utilized an identical side impact sled device and ΔV but boundary conditions represented flat rigid impacts [i.e., non-airbag (n = 7)] or 20° and 30° anterolateral oblique rigid impacts (n = 4) (Pintar et al., 1997; Maltese et al., 2002; Kuppa et al., 2003; Yoganandan et al., 2007a; Yoganandan et al., 2008). Chestband data were reanalyzed according to the methodology presented in this study. Biomechanical comparisons employed ANOVA and Fisher's post-hoc test to identify differences in normalized deflection and viscous responses along oblique measurement angles using the Matlab Statistical Analysis Toolbox (The Mathworks, Natick, MA). Additionally, two flat rigid tests were selected to validate the novel RBandPC methodology through comparison to "traditional" chestband analysis methods (Pintar et al., 1996). The traditional methodology required that the anatomical

spine and sternum chestband locations be maintained when RBandPC reconstructions are generated. Resulting injury metrics were compared between this approach and the 10% offset method described for this analysis.

6.2 RESULTS

6.2.1 AIRBAG BEHAVIOR

High-speed videography was examined to verify airbag boundary conditions. In stationary tests, the inflating airbag first contacted the posterolateral torso approximately between the T6 and L1 levels. As inflation progressed, the bag fabric unfolded in the forward and lateral directions around the torso where the bag contacted the rigid boundary (Figure 6.4). In dynamic tests, PMHS were first contacted by the airbag in a manner similar to stationary deployments. Following initial contact, the airbag fabric unfolded forward and lateral around the torso into the space between the subject and the load wall. Relative motion continued between the subject and the impact apparatus. This motion narrowed the space between the torso and the load wall as the airbag was simultaneously expanding within this space. Shown in Figure 6.5 are videographic frames from the four dynamic tests and the degree of forward airbag expansion into the lateral space. Despite similar deployment conditions, deployment variability was observed. In tests D-1 and D-2, the bag fabric completely surrounded the thoracoabdominal region and, in D-2, preventing direct load wall contact. Tests D-3 and D-4 exhibited less expansion before the moving torso obstructed further forward movement; in these tests airbag coverage extended approximately to the mid-axillary

line. As load wall interaction was maximized, airbag gases were exhausted and rigid contact occurred through the deflated fabric.

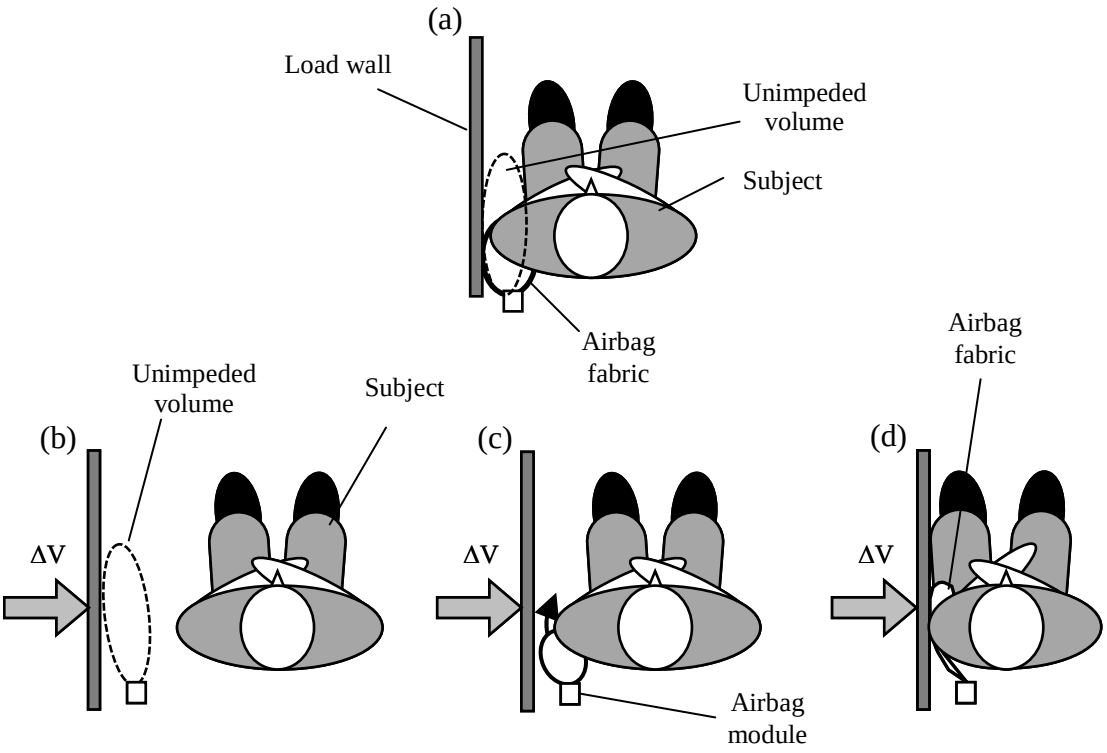

Figure 6.4. Stationary and dynamic airbag deployment scenarios. (a) stationary interaction, (b) dynamic scenario prior to airbag activation, (c) dynamic posterolateral interaction with airbag, and (d) through-fabric wall interaction with subject following gas exhaustion.

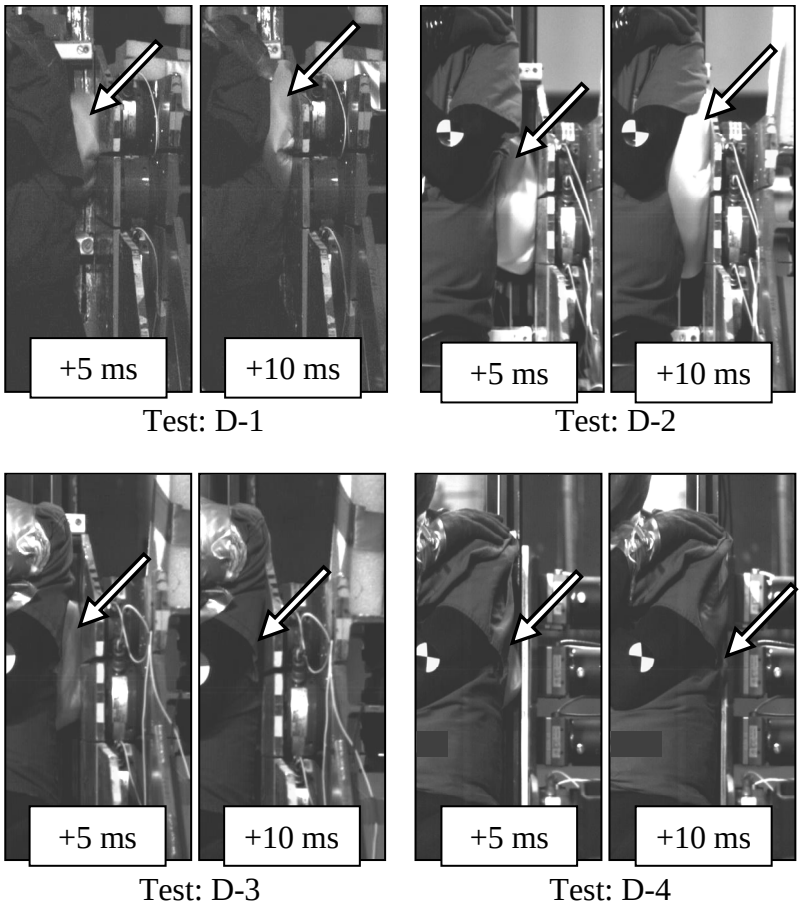

Figure 6.5. Still frames from videography (frontal view) depicting variability in airbag deployment expansion for the four dynamic occupant tests
Duration following airbag activation is noted. Arrows indicate visible airbag fabric.

6.2.2 INJURY RESPONSE

Shown in Table 6.2 are the injuries observed during necropsy and AIS scores. Skeletal injuries were observed in PMHS 2 and 3 (stationary tests) and PMHS 4, 6, and 7 (dynamic tests). Rib fractures are indicated anatomically in Figure 6.6. In stationary tests, rib fractures were noted in posterolateral region between ribs 7 – 12; skeletal injury was AIS 3 for two of three tests. In dynamic tests, rib fractures ranged from none (PMHS 5) to twenty rib fractures (bilateral) with probable flail chest (PMHS 4).

Table 6.2. Subject injury results

PMHS	Config.	Injury Description	Skeletal AIS	Visceral AIS
1	Static L & R	None	0	0
2	Static L & R	6 left rib fxs	3	0
3	Static L & R	2 left rib fxs; 3 right rib fxs; splenic lac: 0.3 cm	3	2
4	Dynamic	18 left rib fxs w/ flail chest and pleural tear; 2 right rib fxs; 3 splenic lac: 2.8 cm, 1.9 cm, 1.1 cm left inferior labrum tear	4	3
5	Dynamic	Renal lac: 1.3 cm	0	2
6	Dynamic	11 left rib fxs; left clavicle fx	4	0*
7	Dynamic	4 left rib fxs; splenic lac: 1.1 cm	3	2

* Subject perimortem splenectomy

Visceral injuries were observed in PMHS 3 (stationary test) and PMHS 4, 5, and 7 (dynamic tests). A left kidney laceration in PMHS 5 consisted of a 1.3 cm capsular disruption on the posterior lip of the renal cortex oriented in the medial-lateral direction. Splenic injuries were observed on the diaphragmatic surface in PMHS 3, 4, and 7 (Figure 6.7). Because PMHS 6 underwent a perimortem splenectomy, hypothetical splenic injury response was not known. In PMHS 4, three splenic lacerations were observed and ranged 1.1 – 2.8 cm in length. Two of these lacerations were near the anterior border and were oriented perpendicular to the superior border in the cranial-caudal direction. The longest laceration was near the posterior end and was parallel to the superior border in the medial-lateral direction. In PMHS 7, a single capsular tear was noted on the apex of the posterior end. The tear measured 1.1 cm and was oriented in the cranial-caudal direction. In PMHS 3, a laceration was noted near the anterior end; this laceration measured 0.3 cm and was oriented in the cranial-caudal direction.

Thoracoabdominal injury response from the flat rigid and anterolateral oblique boundary conditions has been reported (Pintar et al., 1997; Kuppa et al., 2003;

Yoganandan et al., 2008). Briefly, PMHS subjected to flat rigid boundary condition sustained between 7 and 11 rib fractures (AIS 3-4); three subjects did not sustain injury. PMHS subjected to anterolateral oblique loading sustained between 4 and 8 rib fractures; one subject sustained an anterior left lung contusion and diaphragm laceration.

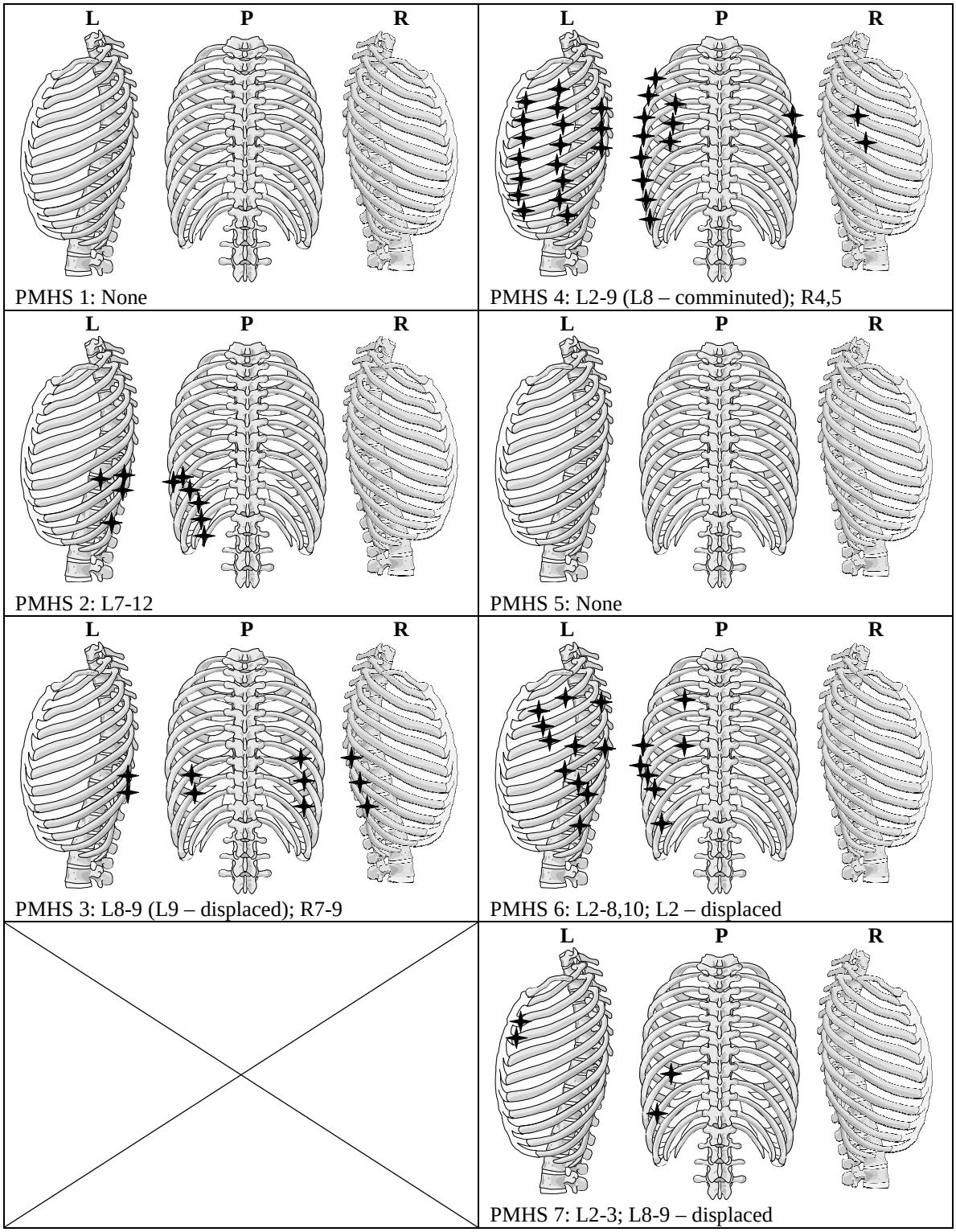

Figure 6.6. Rib fracture patterns observed during post-test necropsy as viewed from left (L), posterior (P) and right (R) aspects.

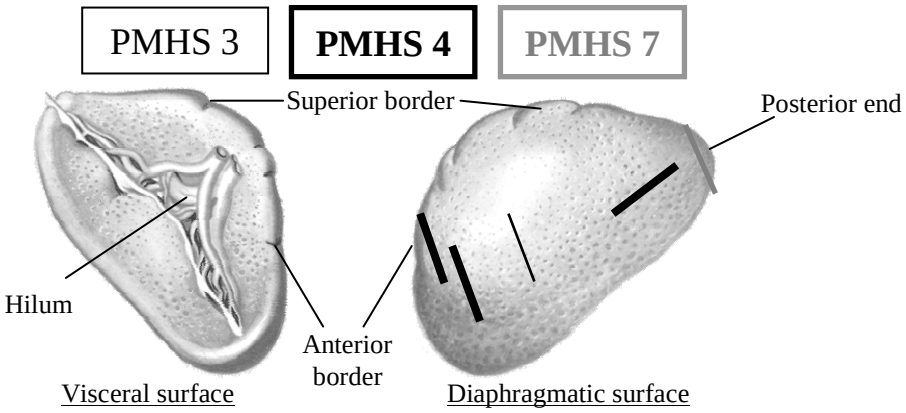

Figure 6.7. Locations of splenic lacerations noted during necropsy.
Modified from Internet Encyclopedia of Science (2001-2010), used with permission

6.2.3 CHESTBAND ANALYSIS

Shown in Figure 6.8 are exemplar chestband contours. Deformations initially occurred in the posterolateral region of the thorax and abdomen in similar manners for stationary and dynamic test results. With dynamic impact progression, the airbag expanded between the thorax and load wall until inflator gases were fully exhausted. Following gas exhaustion, wall contact governed the chest deformation in the lateral region through deflated airbag fabric.

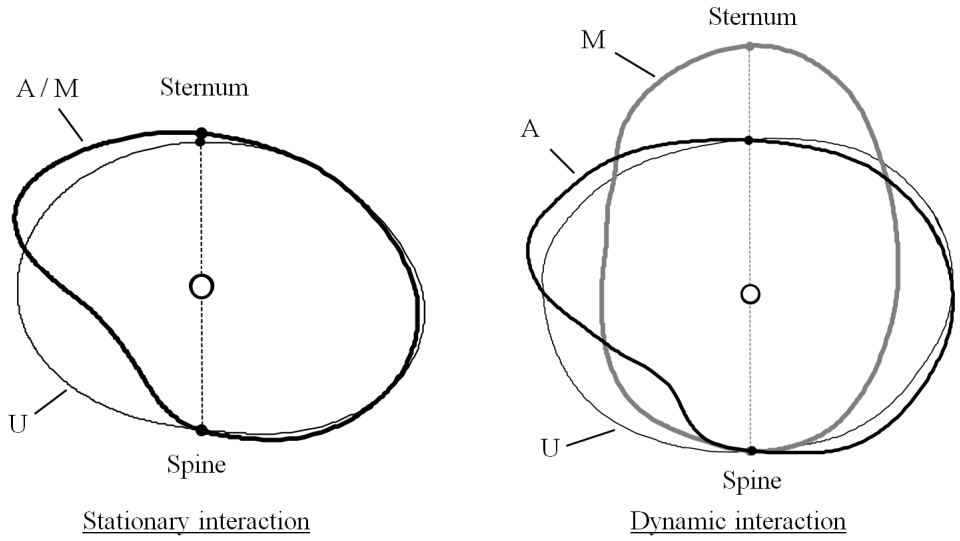

Figure 6.8. Exemplar chestband contours demonstrating deformation patterns resulting from stationary and dynamic scenarios progressing from undeformed (U) to posterolateral airbag interaction (A) to maximum lateral deformation (M).

Normalized deflections were quantified along vectors between 90° and 140° in 5° increments. Exemplar plots are shown in Figure 6.9; time zero was considered airbag activation. Deflections were characterized by two phases: initial contact ($t < \sim 10$ ms) and maximum deflection response ($t > 10$ ms). During initial contact, greater deflections were observed with oblique angles, i.e., $\theta > 110°$; these are indicated by paler lines in Figure 6.9. In dynamic airbag interaction, deflections along lateral angles, i.e., $\theta < 110°$,

surpassed posterolateral deflection as airbag deployment progressed (t > 10 ms). Overall peak deflections were typically observed between 100° and 110° in dynamic tests and between 115° and 135° in stationary tests.

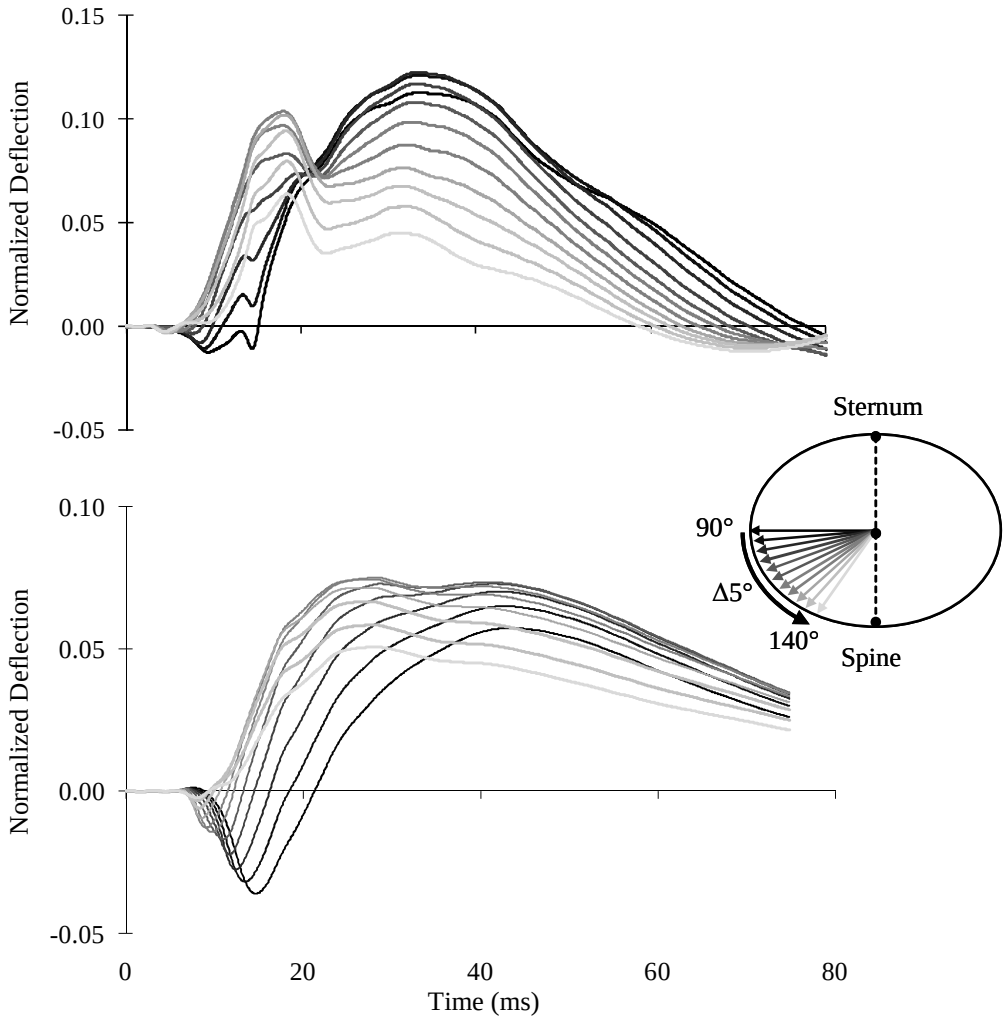

Figure 6.9. Exemplar normalized deflection traces for θ = 90° through 140°: Dynamic occupant (upper) and stationary occupant (lower).

Table 6.3 and Table 6.4 contain peak normalized deflection, peak deflection rate, and VCmax in increments of 5°; mean and standard error (SE) are listed for each boundary condition. Validation of RBandPC chestband analysis with 10% spine-sternum offset indicated that peak normalized deflection deviated by less than 1% and VCmax deviated by 4.0%. Peak normalized deflection and VCmax were considered because

previous analysis identified these metrics to be significant predictors of hard thoracic trauma (Section 3.1); peak deflection rate was included because VCmax is derived from deflection rate.

Statistical analysis concentrated on the xyphoid-level chestband, from which the greatest biomechanical responses were obtained during airbag interaction. ANOVA identified differences in all biomechanical responses ($p<0.05$). Using Fisher's post-hoc test, significance ($p<0.05$) was identified between dynamic OOP and flat rigid boundary conditions for normalized deflection and VCmax when measured at $\theta \geq 110°$. Although not significant, normalized deflection at $\theta = 90°$ from dynamic airbag tests was reduced compared to flat rigid wall and approximately equal to the anterolateral boundary condition. Stationary airbag tests induced minimal deflection at $\theta = 90°$ compared to other boundary conditions, but stationary and dynamic OOP occupant responses were statistically equivalent when $\theta \geq 125°$.

Table 6.3. Peak deformations for four boundary conditions obtained from the xyphoid-level chestband at oblique vectors.

Peak normalized deflection

Angle	Dynamic OOP		Stationary OOP		Flat Rigid		Anterolateral	
	Mean	SE	Mean	SE	Mean	SE	Mean	SE
140°	0.112	0.009	0.101	0.019	0.039	0.005	0.006	0.004
135°	0.131	0.008	0.108	0.019	0.047	0.007	0.007	0.005
130°	0.149	0.010	0.112	0.017	0.059	0.008	0.008	0.006
125°	0.166	0.013	0.109	0.015	0.075	0.009	0.010	0.008
120°	0.183	0.017	0.101	0.013	0.093	0.011	0.014	0.011
115°	0.198	0.021	0.091	0.011	0.113	0.013	0.024	0.015
110°	0.207	0.025	0.078	0.010	0.133	0.015	0.045	0.016
105°	0.207	0.029	0.064	0.011	0.153	0.016	0.070	0.018
100°	0.199	0.034	0.055	0.010	0.170	0.015	0.099	0.019
95°	0.186	0.038	0.045	0.010	0.183	0.014	0.129	0.021
90°	0.172	0.037	0.035	0.010	0.190	0.012	0.159	0.022

Peak deflection rate (m/s)

Angle	Dynamic OOP		Stationary OOP		Flat Rigid		Anterolateral	
	Mean	SE	Mean	SE	Mean	SE	Mean	SE
140°	9.10	2.85	6.23	1.09	4.31	0.40	1.26	0.58
135°	8.97	2.65	6.94	1.34	4.90	0.45	1.40	0.57
130°	8.66	2.41	7.15	1.30	5.51	0.56	1.49	0.49
125°	8.99	2.01	6.56	0.91	6.16	0.69	1.61	0.40
120°	8.79	1.75	5.64	0.79	6.72	0.82	1.72	0.30
115°	8.88	1.57	5.50	0.76	7.18	0.90	2.14	0.41
110°	9.61	1.71	4.79	0.50	8.24	1.21	2.54	0.53
105°	11.10	1.60	3.67	0.25	8.91	1.69	2.99	0.66
100°	12.12	1.59	3.02	0.50	8.70	1.71	3.50	0.82
95°	12.58	1.71	2.54	0.60	7.80	1.36	3.90	0.86
90°	12.42	1.92	2.16	0.51	6.82	0.93	4.36	0.86

VCmax (m/s)

Angle	Dynamic OOP		Stationary OOP		Flat Rigid		Anterolateral	
	Mean	SE	Mean	SE	Mean	SE	Mean	SE
140°	0.39	0.06	0.33	0.07	0.13	0.03	0.05	0.01
135°	0.54	0.09	0.39	0.07	0.17	0.04	0.06	0.01
130°	0.70	0.16	0.42	0.08	0.22	0.05	0.06	0.01
125°	0.87	0.26	0.39	0.08	0.25	0.05	0.06	0.01
120°	1.04	0.37	0.33	0.08	0.29	0.06	0.06	0.01
115°	1.29	0.44	0.25	0.05	0.39	0.07	0.06	0.02
110°	1.51	0.51	0.16	0.04	0.49	0.09	0.07	0.03
105°	1.65	0.57	0.10	0.03	0.61	0.11	0.12	0.05
100°	1.72	0.59	0.07	0.02	0.71	0.11	0.21	0.08
95°	1.61	0.58	0.06	0.02	0.75	0.10	0.30	0.10
90°	1.36	0.53	0.07	0.02	0.73	0.08	0.40	0.12

Table 6.4. Peak deformations for four boundary conditions obtained from the rib 10 level chestband at oblique vectors.

Peak normalized deflection

Angle	Dynamic OOP		Flat Rigid		Anterolateral	
	Mean	SE	Mean	SE	Mean	SE
140°	0.089	0.010	0.042	0.012	0.058	0.043
135°	0.106	0.011	0.050	0.013	0.055	0.039
130°	0.117	0.012	0.058	0.014	0.051	0.034
125°	0.123	0.014	0.068	0.016	0.047	0.027
120°	0.128	0.020	0.077	0.017	0.048	0.018
115°	0.131	0.025	0.092	0.016	0.052	0.014
110°	0.137	0.026	0.107	0.014	0.070	0.016
105°	0.138	0.028	0.123	0.012	0.096	0.018
100°	0.136	0.030	0.139	0.012	0.123	0.019
95°	0.131	0.031	0.155	0.011	0.150	0.020
90°	0.121	0.032	0.168	0.010	0.177	0.019

Peak deflection rate (m/s)

Angle	Dynamic OOP		Flat Rigid		Anterolateral	
	Mean	SE	Mean	SE	Mean	SE
140°	5.28	0.11	4.47	1.13	2.78	1.80
135°	5.40	0.20	5.00	1.04	2.90	1.81
130°	5.26	0.29	5.41	1.06	2.99	1.78
125°	4.99	0.27	5.69	1.19	3.20	1.63
120°	4.90	0.02	5.77	1.27	3.44	1.41
115°	4.91	0.25	5.92	1.35	3.68	1.12
110°	4.97	0.49	6.30	1.39	4.00	0.92
105°	5.04	0.72	6.86	1.39	4.35	0.93
100°	5.01	1.01	7.42	1.36	4.95	0.94
95°	5.77	0.82	7.82	1.30	5.32	1.05
90°	6.54	1.00	7.93	1.22	5.81	1.05

VCmax (m/s)

Angle	Dynamic OOP		Flat Rigid		Anterolateral	
	Mean	SE	Mean	SE	Mean	SE
140°	0.30	0.04	0.23	0.13	0.10	0.03
135°	0.39	0.05	0.24	0.12	0.10	0.04
130°	0.44	0.04	0.26	0.13	0.10	0.04
125°	0.46	0.02	0.28	0.13	0.10	0.05
120°	0.45	0.03	0.31	0.12	0.10	0.07
115°	0.42	0.06	0.31	0.11	0.13	0.08
110°	0.37	0.08	0.35	0.11	0.17	0.09
105°	0.35	0.07	0.40	0.10	0.22	0.09
100°	0.33	0.06	0.46	0.10	0.31	0.09
95°	0.31	0.07	0.53	0.11	0.43	0.11
90°	0.29	0.08	0.59	0.09	0.56	0.13

Chestband deformation patterns demonstrated a transient location of maximum response (deflection locus). To represent this transient locus, a novel "unconstrained" deflection time trace was defined by the instantaneous peak deflection for each sample time. The location of this instantaneous peak was defined by $\theta(t)$, which characterized the angle between the anterior direction and the transient deflection locus (Figure 6.3). Mean $\theta(t)$ response was determined for stationary and dynamic occupants with close-proximity airbag as well as the flat rigid and anterolateral boundary conditions (Figure 6.10). Time zero represented deformation onset, i.e., point at which measured deflection from at least one chestband first exceeded 4 mm. Corridors represent instantaneous average angle response for all contours ± standard deviation (SD). Angle of deformation onset was 141 ± 4° (mean ± SE) for contours from stationary tests and 122 ± 2° for contours from dynamic tests. At deflection onset, mean deflection angle resulting from dynamic airbag interaction was 35° greater (Student's t-test; $p < 0.001$) than flat or anterolateral oblique contact. Further, both stationary and dynamic airbag interaction demonstrated transient deflection loci varying 20° and 30° over the first 60 ms of impact, respectively; deflection angles resulting from flat and anterolateral rigid interaction did not vary more than 5°. Following initial airbag contact in stationary tests, deflection angle deviated toward 120° with respect to the S-S axis. Airbag contact during sled OOP tests induced deformations which deviated toward pure lateral, i.e., 90° with respect to S-S axis, with impact progression.

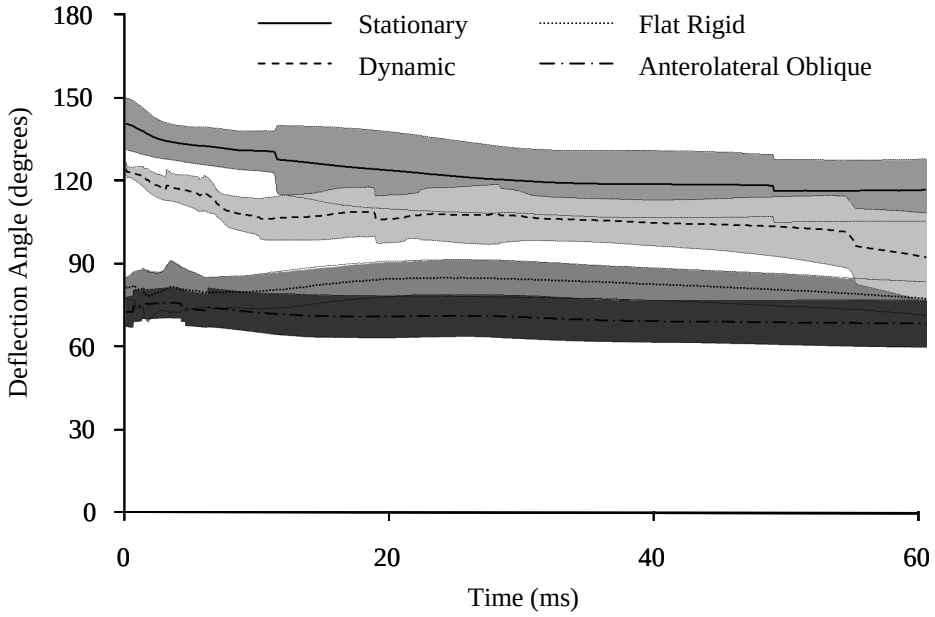

Figure 6.10. Transient angle of deflection for stationary airbag, dynamic airbag, flat rigid wall and oblique load wall configurations.
Shading denotes ±SD corridors.

Assembled into a single array, this unconstrained deflection time trace was differentiated to obtain deflection rate and viscous response. Peak normalized deflection, peak deflection rate, and VCmax were determined by this analysis approach and are shown for each test in Table 6.5. Comparing transient xyphoid-level responses among sled tests, OOP airbag induced greater peak deflection rate than rigid unprotected contact ($p < 0.02$); trends indicated increased normalized deflection and VCmax but these were not significant. Angles of peak normalized deflection, peak rate, and VCmax were dependent on boundary condition ($p < 0.005$).

Table 6.5. Peak unconstrained responses, time of attainment, and angle of attainment from xyphoid level chestband.

Test ID	Deflection			Deflection Rate			Viscous Response		
	Peak	Time (ms)	Angle (degrees)	Peak (m/s)	Time (ms)	Angle (degrees)	Peak (m/s)	Time (ms)	Angle (degrees)
S-1	0.119	12.7	135	6.1	7.2	134	0.57	7.5	133
S-2	0.085	19.1	99	16.9	0.1	130	0.48	0.5	130
S-3	0.144	19.8	132	5.8	0.1	151	0.31	6.4	140
S-4	0.111	10.4	128	7.6	0.1	138	0.40	4.9	129
S-5	0.075	17.4	116	2.9	3.4	124	0.12	5.8	123
S-6	0.171	14.8	128	5.2	7.1	131	0.59	9.9	130
D-1	0.200	26.1	103	15.4	1.3	121	0.86	12.2	105
D-2	0.297	20.0	99	14.7	16.1	98	3.23	16.7	98
D-3	0.179	14.8	110	6.1	5.0	110	0.62	10.8	109
D-4	0.167	19.1	108	12.8	8.5	104	1.32	8.9	103
Flat 1	0.223	20.2	80	5.5	8.6	78	0.82	10.3	78
Flat 2	0.211	27.4	87	5.1	14.1	86	0.79	14.2	86
Flat 3	0.196	17.3	92	6.7	2.8	102	0.72	8.0	92
Flat 4	0.199	29.4	88	6.7	3.7	82	0.60	8.3	82
Flat 5	0.143	14.8	84	5.5	5.7	83	0.51	9.4	82
Flat 6	0.244	26.1	95	6.0	12.2	90	1.06	12.8	91
Flat 7	0.159	34.4	91	7.6	4.4	82	0.49	4.7	82
Oblique 1	0.203	20.2	76	5.2	6.7	78	0.60	8.9	76
Oblique 2	0.287	34.0	71	7.0	6.2	73	0.98	16.2	71
Oblique 3	0.227	33.7	59	4.4	2.1	65	0.57	11.3	63
Oblique 4	0.249	30.3	67	5.8	6.0	67	0.73	10.1	68

6.3 DISCUSSION

Out-of-position side airbag boundary conditions were uniquely characterized by deformations oblique with respect to the lateral direction and with respect to other lateral impacts. In previous experimental designs, thoracoabdominal loading direction was controlled by test setup. Oblique direction was controlled via subject orientation with respect to the impactor motion (Nusholtz et al., 1983; Viano et al., 1989b; Yoganandan et al., 1997; Chung et al., 1999; Shaw et al., 2006) or boundary orientation with respect to the subject motion (Pintar et al., 2007; Yoganandan et al., 2007a; Yoganandan et al.,

2008). In this study, direction was not controlled directly by the experimental design. Because deformation was initiated by airbag deployment, the direction was influenced by airbag-subject interaction resulting primarily from independent airbag deployment characteristics. Obliquity deviated toward lateral with impact progression.

Previous studies have reported that padded impact does not consistently reduce biomechanical response of PMHS (Cavanaugh et al., 1993; Pintar et al., 1997; Chung et al., 1999). At impact velocities between 5.6 and 9.1 m/s, peak deflection and VCmax were increased up to 25% and 50%, respectively, by the addition of stiff padding (100 – 200 kPa crush strength) to the boundary condition. Softer padding (55 kPa) was shown effective at reducing biomechanical response (Cavanaugh et al., 1993; Kuppa et al., 2003). The present study was in agreement with these results: OOP occupants sustained significantly increased peak deflection rate (Table 6.5), and trends further suggested that peak normalized deflection and VCmax may also be elevated compared to unprotected lateral loading.

6.3.1 INJURY RESPONSE

One previous study examined biomechanical response to OOP airbag in a dynamic sled environment. This study involved only one PMHS in a sled test with ΔV = 15 m/s (Schroeder et al., 1998). Although no change in thoracic injury response was reported, the excessive ΔV may have obscured airbag effects. Previous stationary PMHS tests with side airbags emphasized upper extremity injury risks but posterolateral fractures to ribs 8 – 10 were also reported (Duma et al., 1998). Although Duma et al. did not indicate if a visceral examination was performed, findings from stationary airbag deployments in this study are consistent. Although rib fractures induced by sled impacts

with OOP airbag interaction were similar to other sled boundary conditions, apparently unique visceral trauma occurred in these tests. One stationary subject and three dynamic subjects were characterized by lacerations to kidney or, particularly, the spleen. During necropsy, the dynamic test subject without visceral trauma was determined to have undergone a perimortem splenectomy. Because airbag deployment was the only experimental variation between OOP and flat rigid sled impacts, χ^2 contingency tests were performed for lacerations to spleen, kidney, or all viscera (Table 6.6). Significant dependencies were found between visceral trauma and OOP boundary conditions, particularly splenic lacerations; presence of kidney laceration(s) was not significant. Further, examination of the NHTSA biomechanics database (Section 3.1 and Table A.1) revealed that visceral injuries are rare in PMHS. Among 80 tests below $\Delta V = 8$ m/s, only one subject sustained splenic trauma and kidney lacerations were only present with abdominal or thoracic offsets. More than 80% of all subjects sustained no visceral trauma. Studies utilizing animal subjects, which exibit visceral trauma with greater frequency (Section 3.1.3), have also noted the propensity for splenic trauma induced by localized changes to boundary conditions, namely protruding or gapped interfaces (Rouhana & Kroell, 1989).

Table 6.6. Contingency tests for injury dependence on dynamic OOP boundary condition.

Laceration	χ^2	p-Value
Spleen	5.83	0.0157
Kidney	1.93	0.1653
Viscera	10.00	0.0016

A contingency test was also performed for visceral injury dependence on impact velocity, comparing both out-of-position airbag boundary conditions. Significance was found ($p < 0.1$) for visceral trauma, suggesting that dynamic occupants are more likely

than stationary occupants to sustain visceral trauma with out-of-position airbag interaction.

Visceral lacerations were oriented in both cranial-caudal and medial-lateral (transverse) directions. The cranial-caudal lacerations may have resulted from shearing induced by overlying rib fracture displacement (Section 2.3). The spleen, deep to the posterolateral curvature of ribs 9 – 11 and posterior to the mid-axillary line (Bergman et al., 2002), may be particularly sensitive to rib fractures in this region (Figure 2.10). Yet, in all tests the lack of observed trauma to the diaphragm, which separates the spleen from the chest wall, suggests that direct interaction with fractured ribs may not be the likely injury mechanism.

The absence of underlying visceral trauma reported in the literature suggests that, in the present study, the visceral injury mechanism may be unique to this boundary condition and more complex than rib fracture interaction. The capsular tears to the posterior ends of the spleen observed in PMHS 7 and in PMHS 4, and to the kidney observed in PMHS 5 were not located in the vicinity of any rib fractures. These lacerations were oriented in a medial-lateral (transverse) direction in PMHS 4 and 5 and may have resulted from a viscous failure mechanism (Section 3.2.3). This mechanism cannot be ruled out in PMHS 3 or in other lacerations observed in PMHS 4.

6.3.2 INJURY METRICS

In OOP tests with dynamic subjects, overall peak metrics were observed consistently at the xyphoid level chestband (T11 level posteriorly), corresponding to the site of maximum airbag interaction (Table 6.3 and Table 6.4). The upper abdominal location of visceral lacerations is also consistent with these regions of deformation.

Therefore a causative relationship between visceral trauma and posterolateral biomechanics can be inferred from this research.

Univariate logistic regression was employed to identify biomechanical predictors of AIS 2+ trauma to spleen (n = 17) or posterolateral viscera (n = 21). Due to anatomical considerations, right-sided stationary tests and OOP sled test D-3 were excluded from spleen analysis. Peak biomechanical responses were considered at vectors between 90° and 140° (Table 6.3). Model fit was assessed with Wald's statistic, the Deviance, and the Goodman-Kruskal gamma using the Matlab Statistical Analysis Toolbox (Table 6.7). Wald's statistic tested the null hypothesis of covariate independence, i.e., $p < 0.1$ indicated that the predictor was significant (Kuppa & Eppinger, 1998). Deviance was analogous to a generalized residual sum of squares and was determined for purposes of model comparison; lower deviance values indicated better whole-model fit (McCullagh & Nelder, 1990). The gamma value was analogous to a linear R^2 as an alternative assessment of data correlation (Kuppa & Eppinger, 1998).

Table 6.7. Predictive ability of peak normalized deflection, peak deflection rate, and VCmax for spleen trauma and visceral trauma.

	Splenic Trauma			Visceral Trauma		
	Normalized Deflection			Normalized Deflection		
Angle (°)	*Wald's*[a]	*Deviance*	*Gamma*[b]	*Wald's*[a]	*Deviance*	*Gamma*[b]
140	**0.091**	8.82	**0.821**	**0.042**	11.85	0.853
135	0.154	7.96	**0.744**	**0.095**	9.48	**0.882**
130	0.155	7.62	**0.795**	**0.097**	6.32	**0.971**
125	**0.088**	8.55	**0.821**	**0.098**	5.87	**0.971**
120	**0.089**	10.09	**0.821**	**0.097**	5.81	**0.941**
115	0.120	12.14	**0.795**	**0.086**	8.18	**0.912**
110	0.190	13.77	0.641	**0.050**	11.61	0.853
105	0.395	15.05	0.385	**0.057**	14.56	0.647
100	0.797	15.79	0.256	0.101	17.06	0.559
95	0.668	15.63	-0.051	0.254	19.03	0.353
90	0.324	14.78	-0.385	0.595	20.16	0.118
	Deflection Rate			Deflection Rate		
	Wald's[a]	*Deviance*	*Gamma*[b]	*Wald's*[a]	*Deviance*	*Gamma*[b]
140	0.144	6.97	**0.812**	**0.085**	14.13	**0.779**
135	0.175	8.72	**0.744**	**0.086**	15.74	**0.779**
130	0.174	11.60	0.692	**0.093**	16.70	**0.779**
125	0.145	12.59	0.675	**0.087**	15.55	**0.765**
120	0.178	13.53	0.709	**0.056**	14.65	**0.809**
115	0.364	14.94	0.658	**0.061**	15.75	**0.765**
110	0.510	15.68	0.521	0.123	17.81	0.676
105	0.311	15.21	0.368	**0.062**	16.22	0.603
100	0.196	15.11	0.316	**0.080**	16.89	0.574
95	0.136	14.29	0.111	**0.042**	15.18	0.456
90	0.114	13.53	-0.128	**0.030**	13.68	0.353
	VCmax			VCmax		
	Wald's[a]	*Deviance*	*Gamma*[b]	*Wald's*[a]	*Deviance*	*Gamma*[b]
140	**0.066**	7.03	**0.846**	**0.026**	10.76	**0.824**
135	**0.096**	8.11	**0.782**	**0.050**	7.23	**0.843**
130	**0.089**	11.51	0.705	**0.063**	7.36	**0.833**
125	0.229	14.07	0.679	**0.081**	7.88	**0.814**
120	0.489	15.30	0.705	**0.100**	10.36	**0.814**
115	0.619	15.57	0.667	**0.089**	10.32	**0.794**
110	0.570	15.51	0.538	**0.058**	11.20	0.725
105	0.589	15.56	0.410	**0.067**	12.60	0.657
100	0.696	15.71	0.333	**0.098**	14.16	0.608
95	0.900	15.83	0.141	0.129	15.41	0.471
90	0.834	15.79	-0.077	0.155	16.52	0.363

a. Significant values are bolded

b. Results within 0.1 of best statistic are bolded.

From the resulting test statistics, metrics at $\theta = 90°$ were not good predictors of visceral injury and in some cases were inversely related to injury risk. Normalized deflection was a significant predictor of visceral trauma for $\theta \geq 105°$ and was associated with the smallest deviance and the largest gamma for $\theta = 120 – 130°$. Considering only splenic trauma, normalized deflection was significant for $\theta = 120$, 125, and 140°; gamma and deviance were optimized at $\theta = 125°$. While peak deflection rate was the most significant predictor of visceral trauma, deviance and gamma statistics for peak rate were poor in comparison to other metrics. VCmax was predictive of splenic trauma for $\theta \geq 130°$. VCmax was predictive of general visceral trauma for $\theta \geq 100°$ with optimized deviance and gamma statistics at $\theta \geq 125°$. Overall greatest gamma and deviance statistics resulted from peak normalized deflection between $\theta = 120$ and 130°.

MRI slices from injured (Chapter 4) and normophysiologic subjects are overlaid with these angles in Figure 6.11. From an anatomic perspective, these angles intersect with a wide region of the spleen cross-section in these subjects. Based on this analysis, a posterolateral metric measured within these angles may be most relevant to predict underlying visceral trauma. Probability of visceral trauma with respect to normalized deflection and VCmax at $\theta = 130°$ are shown in Figure 6.12. Approximately 50% risk of injury was represented by deflection of 0.140 or VCmax of 0.55 m/s. For the average subject chest breadth (354 mm), this deflection corresponded to 49.6 mm. PMHS 6, which did not contain a spleen, was subjected to deflection and VCmax of 0.128 and 0.42 m/s, respectively, at $\theta = 130°$. Therefore the present analysis suggests that this subject, if intact, had a hypothetical 20 - 28% risk of splenic trauma.

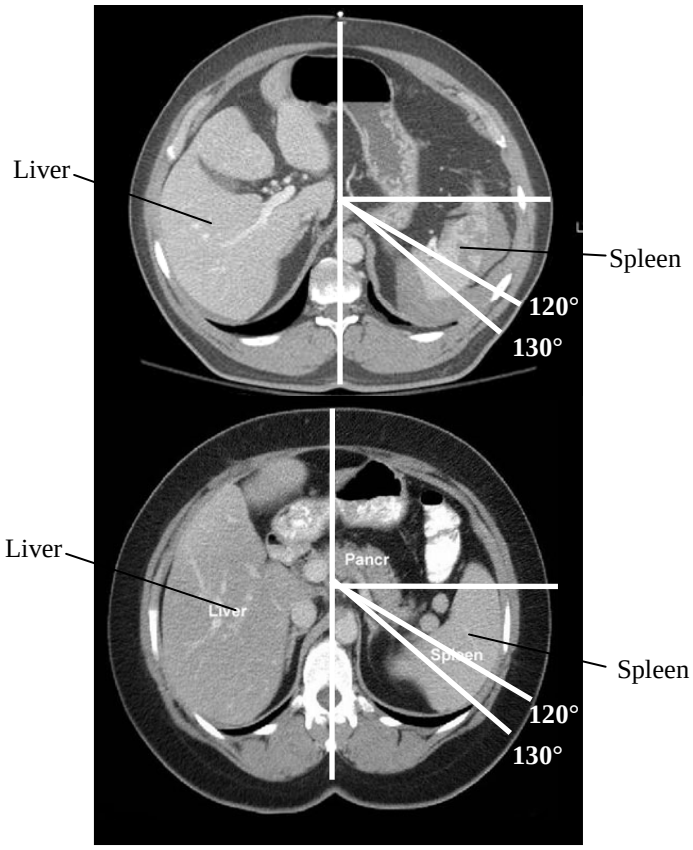

Figure 6.11. Injured (upper) and normal (lower) subject MRI images overlaid with best metric measurement directions.
From Drake et al. (2005), used with permission

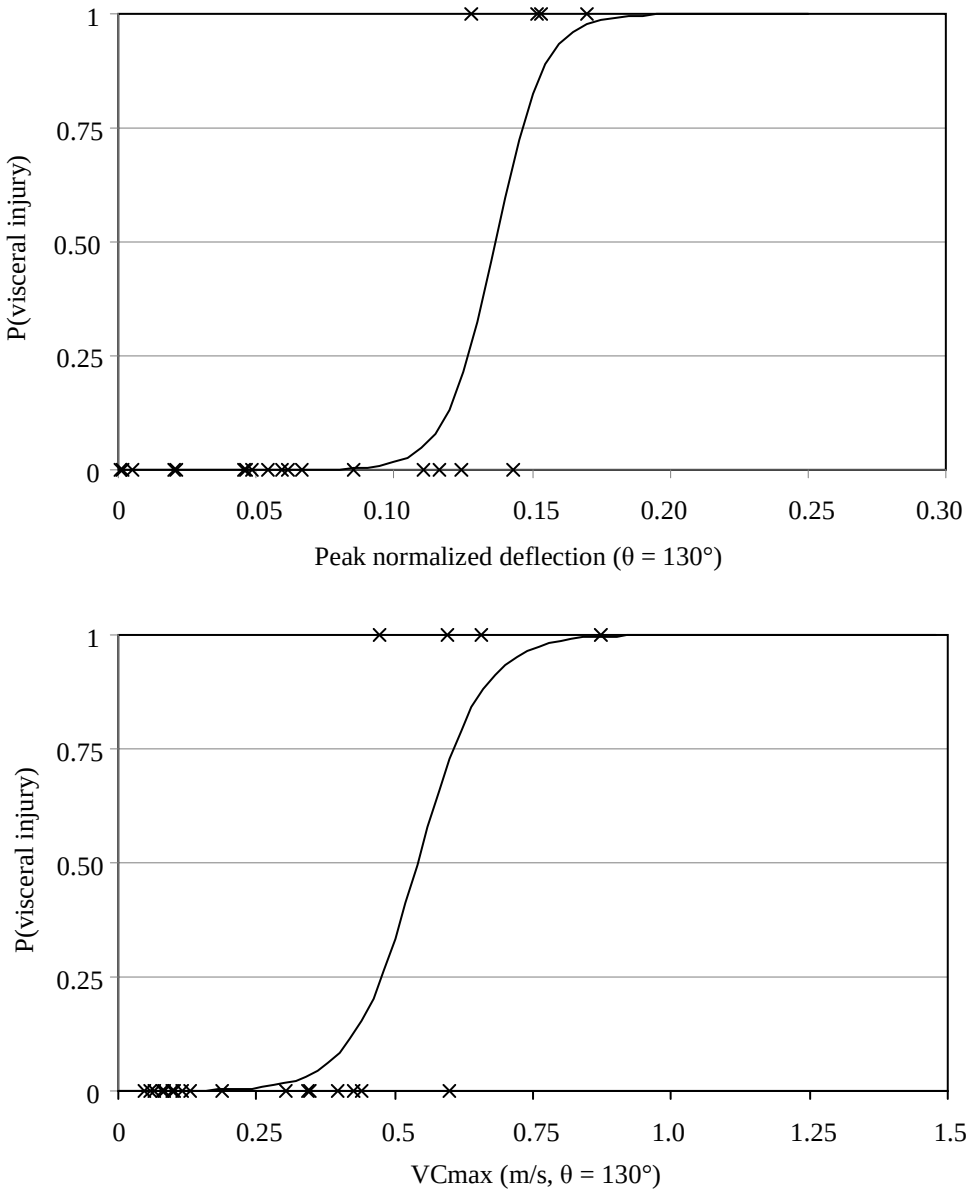

Figure 6.12. Probability of AIS 2+ trauma to posterolateral viscera with respect to peak normalized deflection (upper) and VCmax (lower) measured at θ = 130°.

Previously these injury metrics, i.e., normalized deflection and VCmax, have been associated with substantially greater tolerances when measured from the pure lateral direction (Section 3.1). Normalized deflection tolerances of 0.30 – 0.31 were reported for 50% risk of AIS 4+ skeletal injury (Cavanaugh et al., 1993; Pintar et al., 1997). VCmax tolerances of 0.89 and 1.26 m/s have been reported for 25% and 50% risk of AIS

4+ injury (Viano et al., 1989a; Cavanaugh et al., 1993; Pintar et al., 1997). Although lower severity injuries were considered for regressions in this analysis (AIS 2+ vs. AIS 4+), the lack of visceral injuries with flat rigid torso loading suggests this alone may not account for the tolerance discrepancy. Anterolateral loading has demonstrated the dependence of biomechanical and injury response on load direction: Anterolateral loading induces increased deflections compared to lateral loading (Nusholtz et al., 1980; Nusholtz et al., 1983; Shaw et al., 2006; Yoganandan et al., 2008; Trosseille et al., 2009) along with differing injury patterns (Nusholtz et al., 1980; Pintar et al., 2007; Yoganandan et al., 2008; Trosseille et al., 2009). It is therefore likely that biomechanical tolerances are reduced with oblique airbag interaction.

Multi-body analysis (Chapter 5) found VCmax to be most sensitive to airbag interaction. Because *in vivo* studies have demonstrated VCmax to better predict visceral trauma than deflection metrics (Section 3.1.3), the visceral trauma observations in this experimental series are consistent with anticipated airbag injuries. Yet in this analysis oblique normalized deflection was also a good predictor of posterolateral visceral trauma. This may have been due to the small injured sample size in this dataset (n = 4) and the binomial nature of the injury data. Therefore, it was not possible to definitively select a viscous metric despite its association with soft tissue injury. To delineate the relationship between tissue-level material behavior and externally measured biomechanical response, a finite element analysis was conducted and is presented in the following chapter.

SEVEN

COMPARATIVE FINITE ELEMENT EVALUATION OF SIDE AIRBAG LOADING

Specific Aim 4: Quantify injury risk, as measured by Abbreviated Injury Scale and tissue-level material response, associated with out-of-position torso side airbag interaction with the thoracoabdominal region.

To identify external biomechanical injury metrics for internal tissue-level material response with close-proximity side airbag, a viscoelastic finite element (FE) analysis was conducted with a comparative approach. As with other comparative analyses, this approach emphasized response changes induced by loading and geometry variations (Farke, 2008; Tomaszewski et al., 2010; Viscardi et al., 2010). Because side airbag loading was known to induce posterolateral visceral injury for the set of postmortem human subject (PMHS) experiments described in this study (Chapter 6), material response parameters which mirror tissue injury may assist in conclusively identifying the injury metric necessary for prediction of injuries due to adverse side airbag interaction.

7.1 METHODOLOGY

A plane strain FE model was developed for the LS-DYNA (Livermore Software Technology Corporation, Livermore, CA) dynamic large strain finite element solver. Plane strain formulation was chosen to constrain tissue deformations to the transverse plane. This assumption eliminated the complexity of three-dimensional relative

translations of the intra-abdominal contents which occur during thoracoabdominal impact; these are as yet poorly understood (Nusholtz et al., 1980; Yoganandan et al., 2001; Kent et al., 2003). Further, external deformation responses from experimental procedures were only determined in the transverse plane through the chestband device (Sections 3.2 and 6). Consequently, the planar deformation constraint permitted comparative assessments of tissue response while eliminating confounding out-of-plane response. This formulation was employed to delineate chest wall stress response to incremental load distributions (Khaewpong et al., 1991; Campbell et al., 2005; Campbell & Tannous, 2007).

7.1.1 GEOMETRY

Sectional images of a human torso were obtained from the Visible Human Project (National Library of Medicine, National Institutes of Health, Bethesda, MD). High resolution images were acquired from an adult male donor through a process previously described (Spitzer et al., 1996). Uncompressed thoracoabdominal images were imported into the image thresholding program Mimics (Materialise, Leuven, Belgium). The image corresponding to the level of the middle T11 vertebral body was identified (Figure 7.1). Key anatomical structures were segmented, and boundary curves were exported in Initial Graphics Exchange Specification (IGES) format for the following features: vertebral body, chest wall, sternum, liver, spleen, omentum and hollow intra-abdominal structures, and external “flesh” tissue. IGES curves were imported into the Solidworks design sketcher (Dassault Systèmes SolidWorks Corp., Concord, MA) and rendered with simple line and arc geometries.

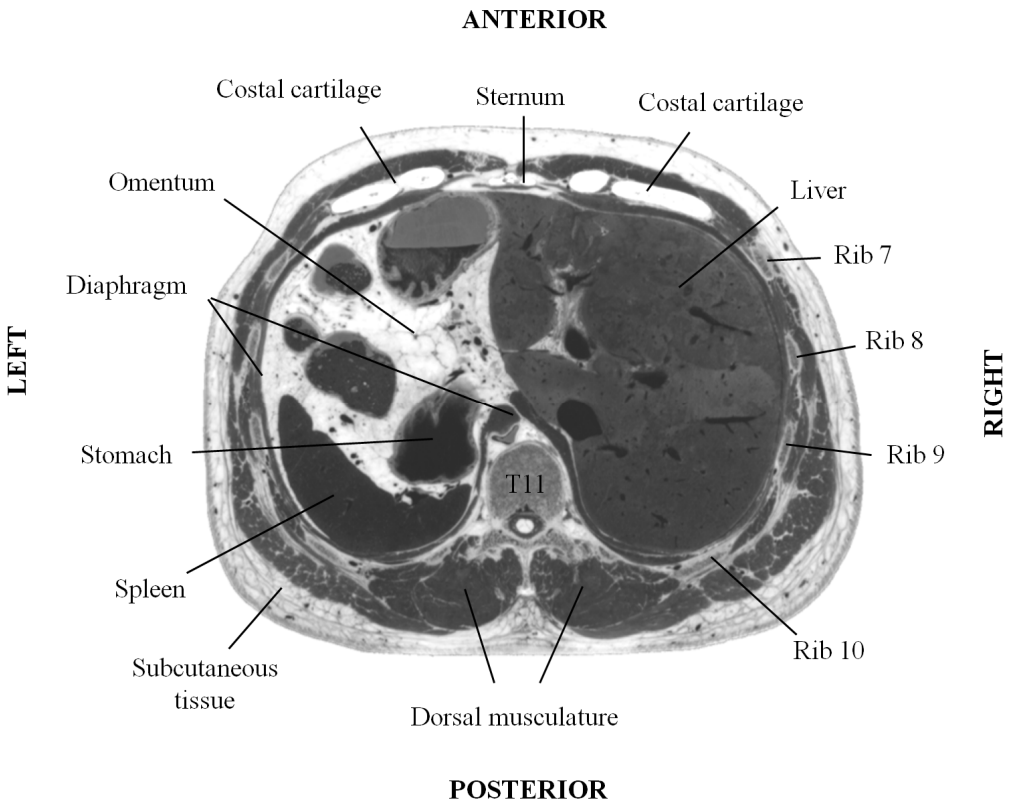

Figure 7.1. Sectional image of Visible Male selected for model geometry.

Visceral volumes follow a normal distribution when scaled to subject gender and standardized height and weight (Geraghty et al., 2004) according to Eq. 7.1.

$$V_{\text{corrected}} = V_{\text{measured}} + F_{\text{ht}}(H_{\text{std}} - H_{\text{j}}) + F_{\text{wt}}(W_{\text{std}} - W_{\text{j}}) \tag{7.1}$$

V corresponds to organ volume, H_j and W_j are height and weight for subject j, H_{std} and W_{std} are standardized height and weight, and F_{wt} and F_{ht} are correction coefficients determined by the study. The standardized 50th percentile male anthropometry represents H_{std} = 1.76 m and W_{std} = 73.0 kg. Using liver and spleen volume measurements from Mimics, the Visible Male was determined to contain a 33rd percentile liver and a 47th percentile spleen. By assuming that organ dimensional

changes occur proportionally in three dimensions, cross-sectional areas were scaled to the 50th percentile male according to Eq. 7.2:

$$A_{\text{corrected}} = A_{\text{measured}} \left(\frac{V_{\text{corrected}}}{V_{\text{measured}}} \right)^{2/3} \tag{7.2}$$

where A represents cross-sectional area and V represents volume. The resulting geometry (Figure 7.2) represented the 50th percentile (median) male viscera with simple geometries and was again exported as IGES curves.

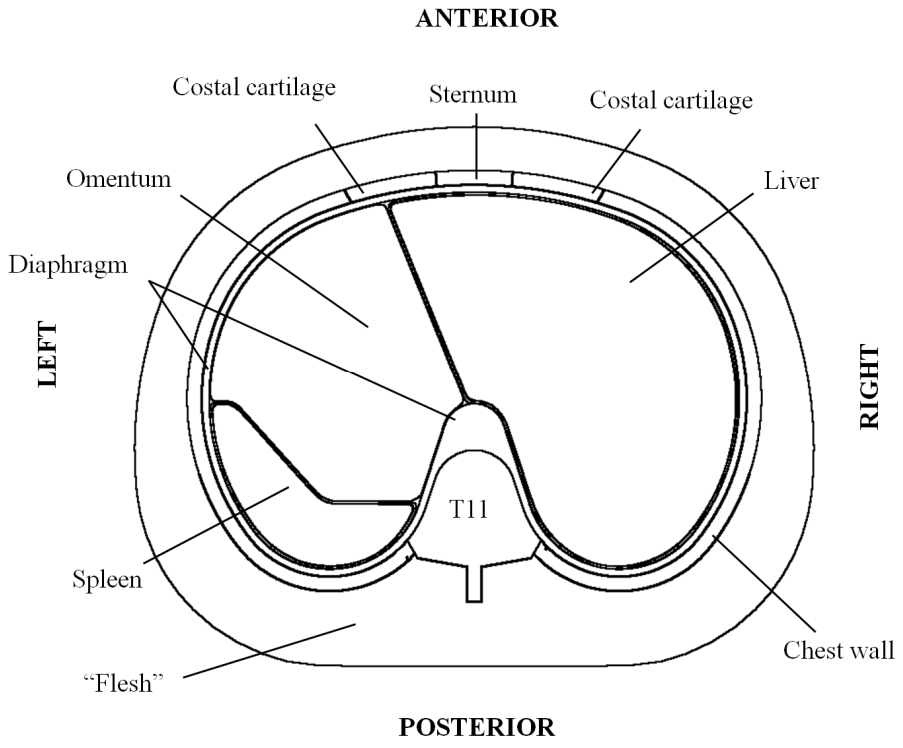

Figure 7.2. Model geometry containing key features for mesh development.

7.1.2 MESH DEVELOPMENT

Curves were imported into the LS-DYNA preprocessor LS-PrePost (Livermore Software Technology Corporation, Livermore, CA) for discretization. Geometries were

represented by regular four node shell elements with translational and rotation degrees of freedom. To identify element size appropriate for chest loading, an initial model was developed with homogeneous visceral contents (Figure 7.3). This model was discretized with meshes of decreasing element side length. Four models were developed, consisting of average element side lengths of 10, 5, 2.5, and 1 mm. During anterior loading, model deflection compliance as well as peak tissue responses were compared to identify the element side length appropriate for deflection response analysis. Results of this analysis are presented in Section 7.2.1.

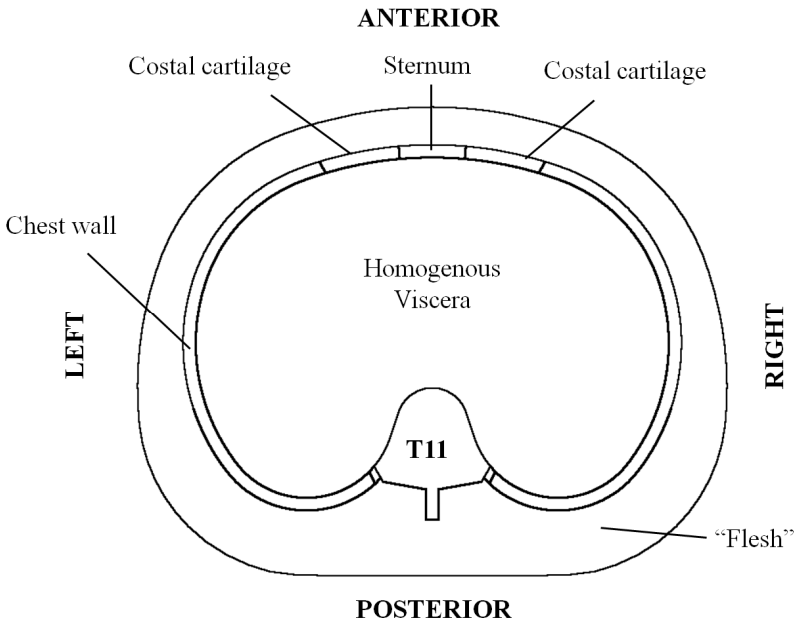

Figure 7.3. Simplified model for mesh density investigation.

For simulating out-of-position side airbag boundary conditions, a visceral model was developed which included spleen and liver geometries (Figure 7.2). The omentum and hollow organs were represented by a generalized visceral material. Initial element side length obtained from the homogenous model was applied to the meshing of the detailed model but was verified with a subsequent examination (Section 7.2.4). In all

meshes, self-contacts were defined between all nodes to prevent self-penetration. Frictionless surface-to-surface contacts were defined between all intra-abdominal contents and the chest wall. Relative motion is known to occur between layers of subcutaneous tissues in mammals such as humans (Kawamata et al., 2003). This motion was represented by a single sliding-only contact defined between the subcutaneous flesh and the chest wall.

7.1.3 MATERIAL PROPERTIES

Material properties were selected according to the literature and from iterative tuning to published biomechanical experiments. The vertebral body and sternum were assumed to be rigid. The generalized chest wall, costal cartilage, and costovertebral tissues were assumed to be linear elastic materials. Subcutaneous flesh, liver, spleen, and omentum were assumed to be linear viscoelastic materials. Although other material models were considered, these material models reduced the number of necessary parameters while maintaining adequate response similarities to biological tissues during material loading (Section 3.3.1). Further, the majority of computational impact analyses have employed these material models (Bandak & Eppinger, 1994; Deng et al., 1999; Furusu et al., 2001; Gilchrist et al., 2001; Jost & Nurick, 2001; Lee & Yang, 2001; Iwamoto et al., 2002; Behr et al., 2003; Kimpara et al., 2005; Mizuno et al., 2005; Wismans et al., 2005; Forbes et al., 2006; Arnoux et al., 2008; Hayashi et al., 2008; Shen et al., 2008; Fijalkowski et al., 2009). Final properties are given in Table 7.1, and the selection methodology was as follows.

Because ribs were oblique with respect to the model section plane, a generalized chest wall of thickness of 8 mm represented ribs as well as overlying and intercostal

tissues (Figure 7.1 and Figure 7.2). Chest wall material properties were obtained from the literature (Section 3.3) but adapted to model geometry. The experimentally determined rib bending modulus (Yoganandan & Pintar, 1998) was scaled according to two parameters: (i) fractional representation of bone in the total chest wall cross-section and (ii) bending thickness variation between the total chest wall and ribs. Ribs are approximately 30% of the total chest wall cross-sectional area (Schneider et al., 1985; Mohr et al., 2007). Further, elementary beam theory demonstrates that deflection stiffness is proportional to the cubed height of the cross-section. Because the average rib thickness (6.5 mm) is less than the gross chest wall thickness (Yoganandan & Pintar, 1998; Mohr et al., 2007), the chest wall elastic modulus was determined from Eq. 7.3:

$$E_{\text{wall}} = 0.3\left(\frac{h_1}{h_2}\right)^3 E_{\text{rib}} \tag{7.3}$$

where h_1 and h_2 represent the rib and chest wall bending thicknesses, respectively, and E_{rib} represents the experimentally measured rib bending modulus (Yoganandan & Pintar, 1998). Material density and cartilage properties were similarly scaled to account for their proportional components within the chest wall shared with intercostal tissues (Section 2.3). The resulting chest wall geometry was validated to eviscerated PMHS chest compression experiments (Murakami et al., 2006; Kent, 2008), shown in Figure 7.4. Application of an appropriate mesh is addressed in Section 7.2.1.

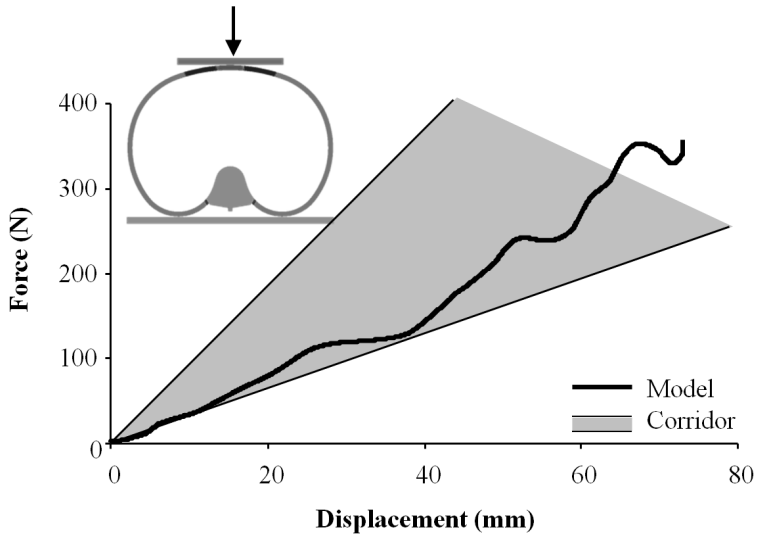

Figure 7.4. Chest wall compressive loading and corridor from PMHS tests.

Initial liver and spleen material properties were obtained from human finite element models (Lizee et al., 1998; Iwamoto et al., 2002; Behr et al., 2003; Ruan et al., 2003; Ruan et al., 2005; Hayashi et al., 2006; Ruan et al., 2006; Arnoux et al., 2008; Song et al., 2009) and tuned to experimental results. Both the liver and spleen were surrounded by a capsular layer. The liver shear response properties were identical to that used in the Ford Human Body Model (Ruan et al., 2003). Because experiments have quantified the liver capsule to be approximately 30% stronger than the parenchyma (Seki & Iwamoto, 1998; Carter et al., 2001; Stingl et al., 2002), this relationship was incorporated in the shear response of the capsular material. Following mesh refinement (Section 7.2.1), model response was comparable to dynamic compression experiments with perfused whole primate livers loaded at 2.5 s^{-1} strain rate (Figure 7.5; Melvin et al., 1973). Compared to the liver, spleen parenchyma is more compliant (Seki & Iwamoto, 1998; Carter et al., 2000; Carter et al., 2001; Stingl et al., 2002; Tamura et al., 2002). Therefore the spleen parenchyma viscoelastic shear properties were 70% lower than the liver and nearer to that used in the HUMOS model (Behr et al., 2003). Because

experiments have quantified the spleen capsule to be approximately 500% stronger than the spleen parenchyma (Seki & Iwamoto, 1998; Davies et al., 2002; Stingl et al., 2002), this relationship was assumed. Following mesh refinement (Sections 7.2.1 and 7.2.4), spleen response was comparable to compression experiments with 0.5 s^{-1} strain rate (Figure 7.6; Tamura et al., 2002). Shear properties of the remaining omental tissue were selected from existing models (Ruan et al., 2003). All intra-chest wall tissues were assigned identical bulk moduli (K = 0.5 MPa) and shear decay constants (β = 1 ms^{-1}).

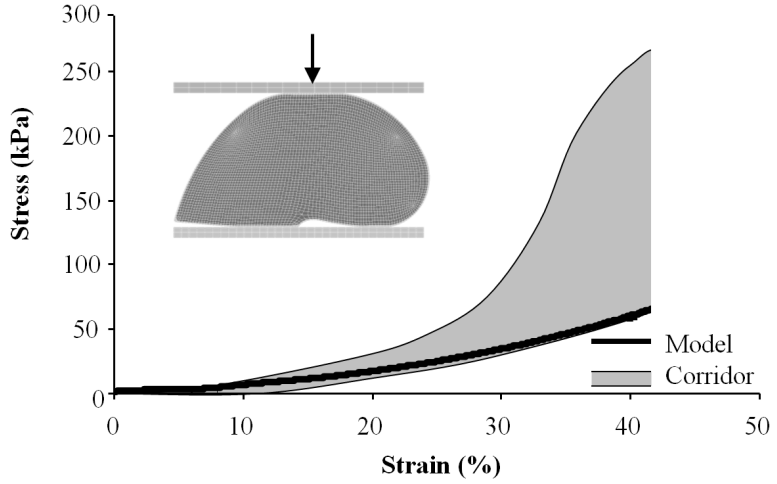

Figure 7.5. Isolated whole liver stress-strain response plotted with range of experimental data.
Data from Melvin et al. (1973)

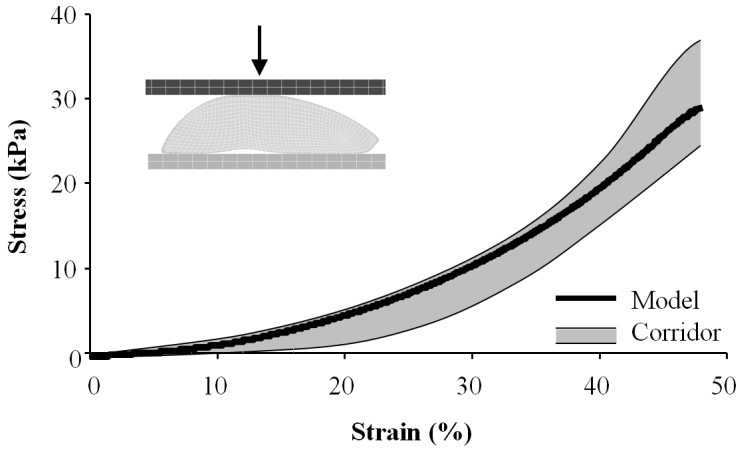

Figure 7.6. Isolated whole-spleen stress-strain response plotted with range of experimental data.
Data from Tamura et al. (2002)

Table 7.1. Material properties chosen for the planar torso model.

Material	ρ kg/m^3	K/E (MPa)	G_0 (MPa)	G_∞ (MPa)	poisson
Flesh	1100	0.5	0.350	0.170	
Chest Wall	1310	350	-	-	0.3
Costal Cartilage	1200	25	-	-	0.4
Costovertebral Junction	1200	50	-	-	0.4
Omentum	1100	0.5	0.054	0.040	-
Diaphragm	1100	0.5	0.400	0.100	-
Liver: Parenchyma	1100	0.5	0.230	0.044	-
Liver: Capsule	1100	-	0.300	0.065	-
Spleen: Parenchyma	1100	0.5	0.069	0.013	-
Spleen: Capsule	1100	-	0.345	0.065	-

7.1.4 VALIDATION

The model response was validated to lateral and oblique PMHS pendulum impacts (Viano et al., 1989a; Viano, 1989; Shaw et al., 2006). With a rigid pendulum, impacts were simulated with velocities of 2.5 m/s, 4.5 m/s, and 6.5 m/s along left lateral and 60° (left of anterior) vectors. The model was free to translate in response to impact. Force response was obtained from the contact interface; deflection response was obtained from the relative translation between opposing exterior subcutaneous nodes parallel to the impact direction. Two-dimensional model force responses were scaled to the contact area from PMHS experiments according to Eq. 7.4:

$$F_{\text{scaled}} = F_{\text{model}} \frac{A}{L} \tag{7.4}$$

where L corresponds to model contact interface length and A corresponds to PMHS contact interface area. Scaled force-deflection cross plots were compared to PMHS

response in accordance with accepted validation procedures (Iwamoto et al., 2002; Behr et al., 2003; Ruan et al., 2003).

7.1.5 LOADING

The model was exercised with subject-specific loading parameters from PMHS experiments (Chapter 6). In order to apply complex loading patterns observed in posterolateral side airbag boundary conditions, displacement-driven loading definitions were created from experimental xyphoid-level chestband results. Because initial chestband contours were subject-specific due to external torso dimensions, e.g., depth, breadth (Table 6.1), deformation results were systematically scaled to the 50th percentile model geometry using custom software developed in Matlab (The MathWorks, Natick, MA). Each chestband contour was discretized throughout the circumference into approximately 2 mm intervals (R_i). Contour circumference was normalized with respect to four points identified during each experiment: spine centerline (0), sternum centerline (0.5), and the half-distance between spine and sternum on the left (0.25) and right (0.75) sides. A chestband local coordinate system (CS) was created from these four chestband locations (Figure 7.7). This CS was redefined for each sample time and contour. Because of the geometric dependency of the CS definition and contour shape transience, axes were not necessarily orthogonal. Using this CS, coordinate pairs were determined for all discretized contour points R_i (in 2 mm intervals) which were time-dependent and unique for each point along the circumference. Expressed as a function of chestband circumference (Figure 7.8), x- and y-coordinates were independently normalized to their initial position. Raw circumference was also replaced with normalized circumference. Using the normalized deformation history of each chestband contour, a moderately

dissimilar geometry may be given a resembling deformation pattern. Potential deformation rate variations induced by geometry changes were tempered by accepted scaling relationships (Eppinger et al., 1984).

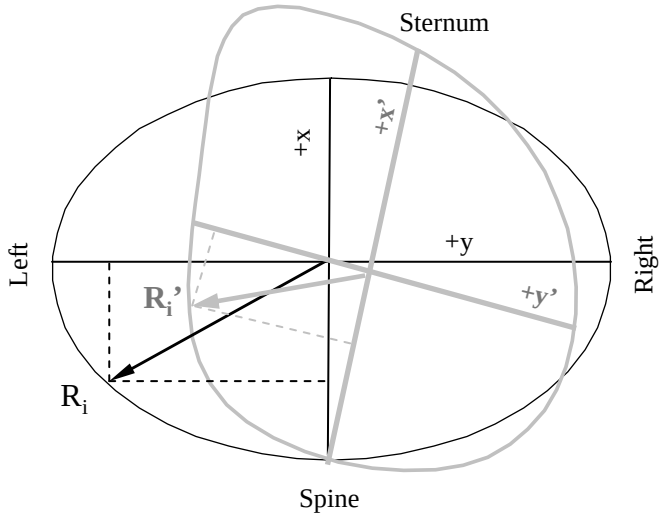

Figure 7.7. Exemplar contour axes definition in undeformed and deformed states.

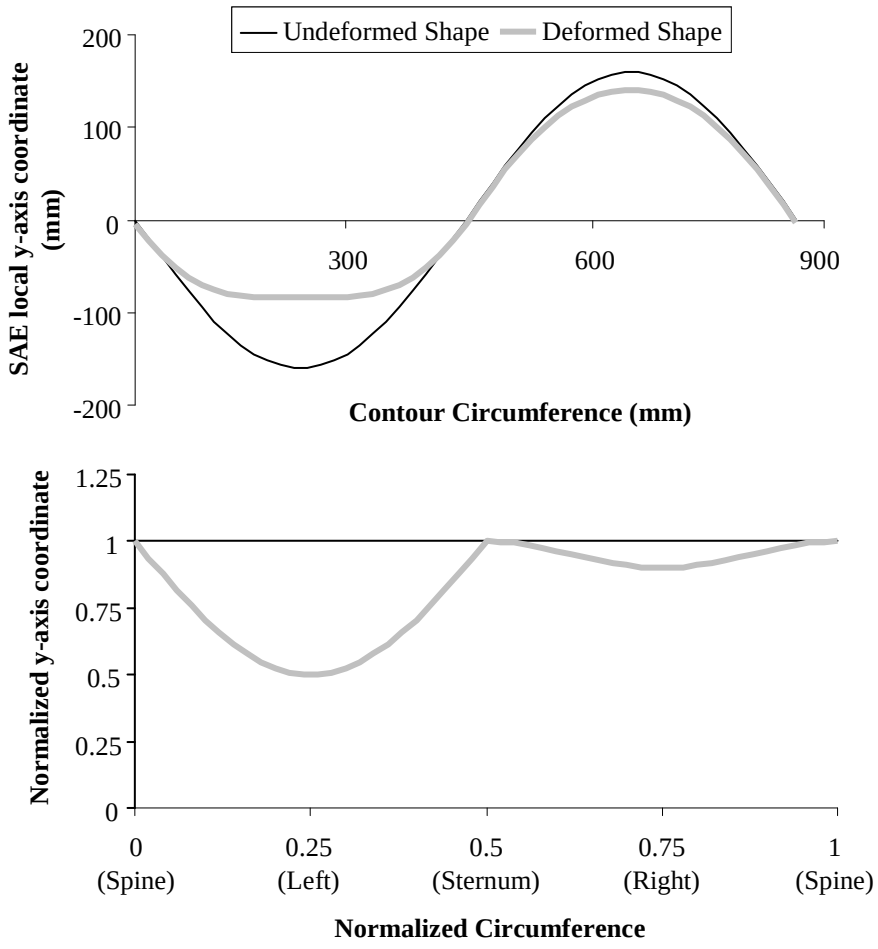

Figure 7.8. SAE y-axis coordinate along exemplar chestband circumference: as measured (upper) and normalized to initial position and contour circumference (lower).

The FE model was loaded by a displacement-driven FE mesh chestband. The chestband mesh consisted of a single layer of 192 four node shell elements with 192 nodes in contact with the model flesh. Identical to experimental chestband contours, the FE chestband CS was defined locally. For each imported chestband and each sample time, normalized contour positions (Figure 7.8) were interpolated onto the FE chestband nodes. This algorithm generated a time-dependent deformation pattern for the FE model which preserved the deformation patterns from the experimental results (Figure 7.9). Peak injury metrics obtained from experimental results and FE input (normalized

deflection and VCmax) demonstrated favorable agreement (Figure 7.10). Surface-to-surface contact without sliding was defined between the FE chestband and the model flesh.

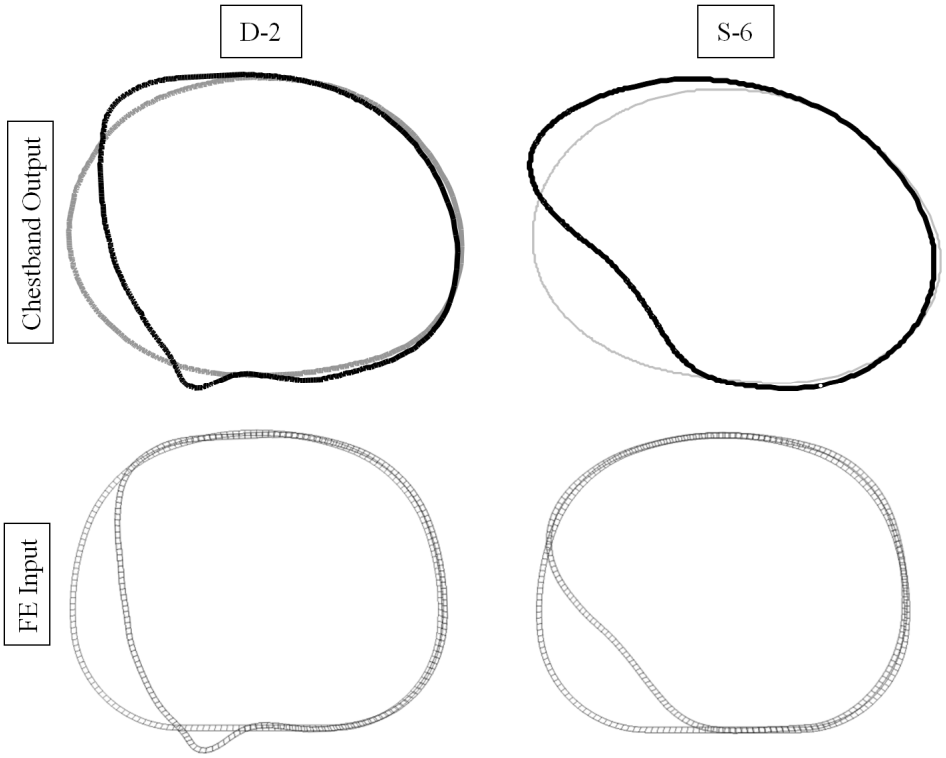

Figure 7.9. Exemplar chestband contours and resulting processed FE displacement contours for tests D-2 (left) and S-6 (right) at the xyphoid level in undeformed and deformed states.

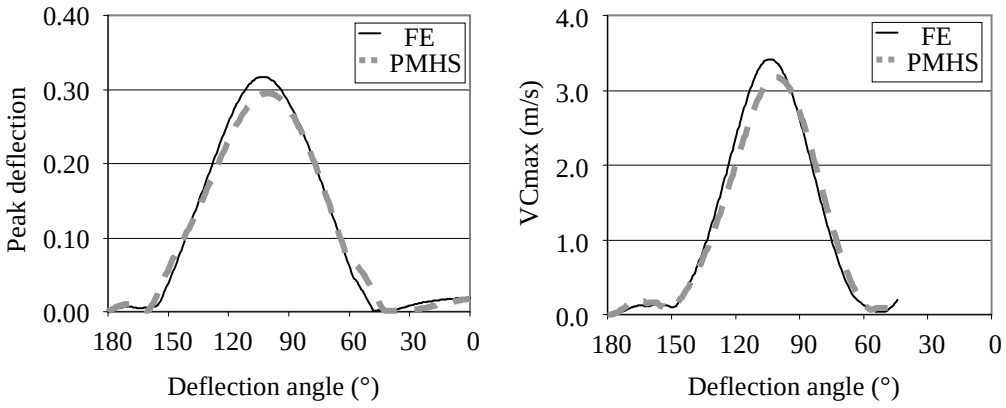

Figure 7.10. Peak injury metric comparison between PMHS chestband result and FE loading input with respect to obliquity of measurement.

For this analysis, four torso boundary conditions were examined. These boundary conditions, identical to the analysis presented in Chapter 6, included (1) out-of-position airbag contact with $\Delta V = 6.7$ m/s, (2) stationary out-of-position airbag contact, (3) flat unprotected rigid contact at $\Delta V = 6.7$ m/s, and (4) anterolateral oblique rigid contact at $\Delta V = 6.7$ m/s. From these boundary conditions, 21 complete subject-specific loading sets were obtained. To maintain realistic material inertial response, an acceleration field was applied to the model nodes in the x and y directions as obtained from T12 spinous process accelerometers during each test (Chapter 6). Acceleration magnitudes and durations were scaled to subject mass in accordance with accepted procedures (Eppinger et al., 1984).

7.1.6 OUTPUT PARAMETERS

Biological tissue failure is known to result from mechanisms of material stress and strain (Yamada, 1970). For a variety of soft tissues, studies have correlated first principal strain and strain energy density with observed failure (Yamada, 1970; Snedeker et al., 2005a; Snedeker et al., 2005b; Stitzel et al., 2005; Fijalkowski et al., 2009; Brunon et al., 2010). Based upon experimental observations (Chapter 6) and clinical experiences (Chapter 4), the present analysis considered injury to splenic tissue only. Trauma observations consisted of capsular tears or parenchymal hematomas and lacerations. To identify these in the model, three spleen material response parameters were investigated. Parenchymal maximum principal strain (ε_1) and parenchymal and capsular strain energy density (NRG) have been suggested in the literature (Yamada, 1970; Snedeker et al., 2005a; Snedeker et al., 2005b; Stitzel et al., 2005; Fijalkowski et al., 2009; Brunon et al., 2010). A third parameter, capsular longitudinal (circumferential) strain (ε_C), was also

investigated, as capsular tearing may occur independent of parenchymal failure (Snedeker et al., 2005b; Schmitt & Snedeker, 2006; Snedeker et al., 2007). Using the LS-PrePost software, these values were exported in time domain for each element. An algorithm was developed in Matlab to import time traces for further analysis. Maximum values represent mean response of a contiguous area containing the overall peak and composing 5% of total spleen area.

Following a systematic normalization to facilitate a comparative analysis, two analyses were completed using these three material responses (ε_1, NRG, and ε_C). First, the dependence of whole-spleen response on boundary condition was examined through an analysis of total affected cross-sectional areas. Second, maximum spleen material responses were correlated with obliquely measured external biomechanical responses (normalized deflection and VCmax). These are elaborated further in this section.

Normalization. From each simulation, the locations of peak ε_1, NRG, and ε_C were obtained. A contiguous area encompassing the peak response element and equal to 5% of total spleen cross-sectional area was identified; maximum response was considered to be the average material response obtained from this area at the instant the peak was obtained. Injury results from matched cadaveric experiments were used to apply logistic regression models to the maximum ε_1, NRG, and ε_C obtained. Injuries to any left-side viscera were considered. Right-sided stationary airbag test subjects and the subject found to have undergone a splenectomy were excluded from this analysis. 50% risk of observed injury was chosen as the normalizing parameter and was applied to the following analyses.

Affected Area. For this analysis, all 21 subjects were included; right-sided stationary airbag tests were inverted about the SAE x-axis (Figure 3.2) to simulate left-sided airbag loading. Using normalized responses (ε_1, NRG, and ε_C), "affected area" was defined as the proportion of total spleen area exceeding an arbitrary response threshold. For quantitative comparison between the four boundary conditions, affected areas surpassing normalized ε_1, NRG, and ε_C of 0.2, 0.6, and 1.0 were examined. The non-parametric Kruskal-Wallis analysis of variance by ranks was employed to identify correlation ($p < 0.05$) between affected area and boundary condition. The Mann-Whitney Rank Sum test was applied as a post-hoc analysis between the dynamic OOP and the flat rigid boundary condition as well as between the dynamic OOP and the stationary OOP boundary condition.

Biomechanical Correlation. The relationship between splenic tissue material response and external biomechanical parameters were evaluated using the ten PMHS side airbag tests employing dynamic and stationary occupants. From each model simulation, the locations of peak ε_1, NRG, and ε_C were obtained. A contiguous area encompassing the peak response element and equal to 5% of total spleen cross-sectional area was identified; maximum response was considered to be the average material response obtained from this area at the instant the peak response was obtained. Biomechanical parameters of peak normalized deflection and VCmax were quantified at $\theta = 90° – 140°$ with respect to the spine-sternum line. These were found to be predictive of visceral injury in PMHS experiments (Chapter 6). The significance, Coefficient of Determination (R^2), and the Predicted Sum of Squares (PRESS) statistic were computed to assess the relationship between maximum normalized responses (ε_1, NRG, and ε_C) and external

biomechanical response parameters. The R^2 is bounded by [0 1] and represents the proportion of material response variance for which the biomechanical parameter is predictive. The PRESS statistic quantifies the degree to which the resulting regression may be generalized to a larger dataset; lower values indicate better generalizability.

7.1.7 GEOMETRIC VARIATIONS

Two anatomical variations were considered to identify any geometric dependencies between external biomechanical parameters and material responses. Using Eqs. 7.1 and 7.2 with human population data described in Section 2.4 (Geraghty et al., 2004), visceral geometries were altered to coincide with the human 5th percentile (small) and 95th percentile (large) liver and spleen volumes (Figure 7.11). Material properties and loading were identical to the median model. These geometries were included in the affected area analysis and biomechanical correlations.

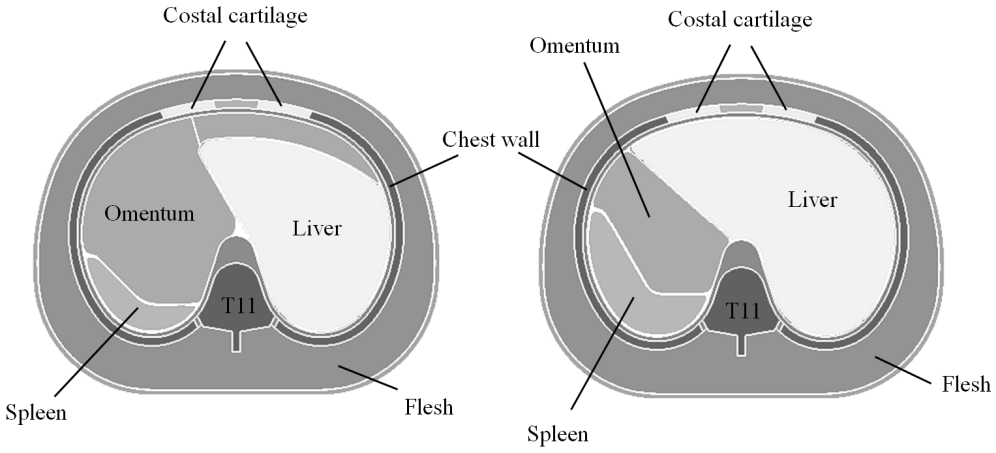

Figure 7.11. Geometric model variations corresponding to small (left) and large (right) visceral contents.

7.2 RESULTS

7.2.1 MESH DENSITY

Deflection compliance for all mesh densities is shown in Figure 7.12. Deflection traces varied by 20% between 10 mm and 5 mm element sizes. Force-deflection traces with 5 mm and 2.5 mm elements deviated by 7%; variability was less than 2% between 2.5 mm and 1 mm.

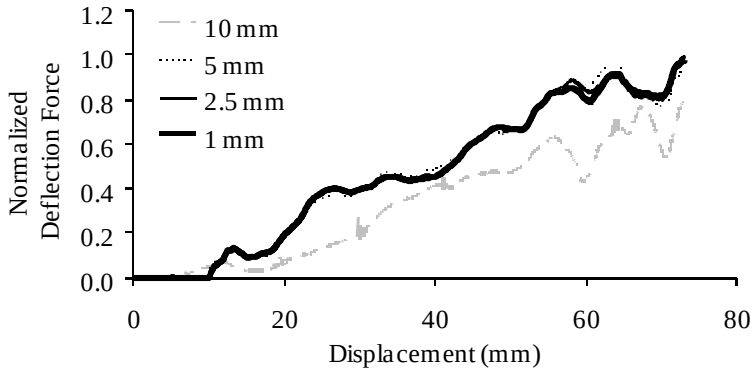

Figure 7.12. Model compliance for element side lengths considered.

Maximum strain and maximum strain energy density from the viscera are shown in Figure 7.13. Maximum responses were averaged over areas of 400 mm^2 (1% of total viscera) containing the peak overall response element. Results were within 4% between 5 mm and 2.5 mm element side length and within 1% between 2.5 mm and 1 mm element side length.

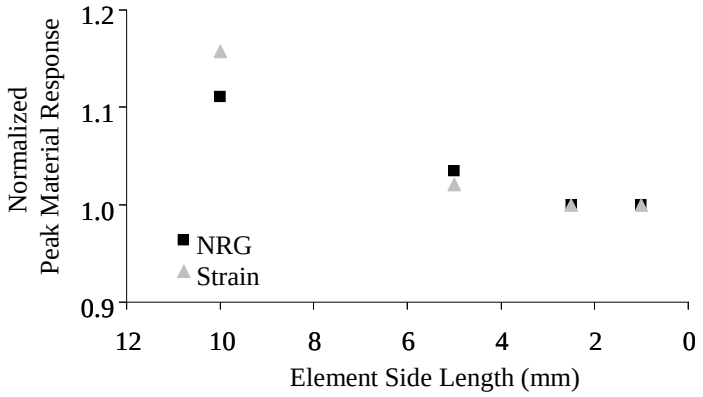

Figure 7.13. Material response for element side lengths considered.

Results from initial mesh study determined the parameters for the detailed model meshes. Because model external flesh was most relevant for deflection only, it was composed of elements with an average 5 mm side length. Chest wall and visceral contents of liver, spleen, and omentum were composed of elements averaging 2.5 mm side length. The resulting mesh (Figure 7.14) was composed of 11,438 elements. 91.1% of element aspect ratios were less than 2 and 99.3% of element quadratic angles were between 45° and 135°.

The altered viscera geometry models were meshed similarly. The 5th percentile model was composed of 11,382 elements, 90.0% of which were characterized by aspect ratios less than 2. No less than 98.5% of element quadratic angles were between 45° and 135°. The 95th percentile model was composed of 11,680 elements, 90.9% of which were characterized by aspect ratios less than 2. No less than 98.6% of element quadratic angles were between 45° and 135°.

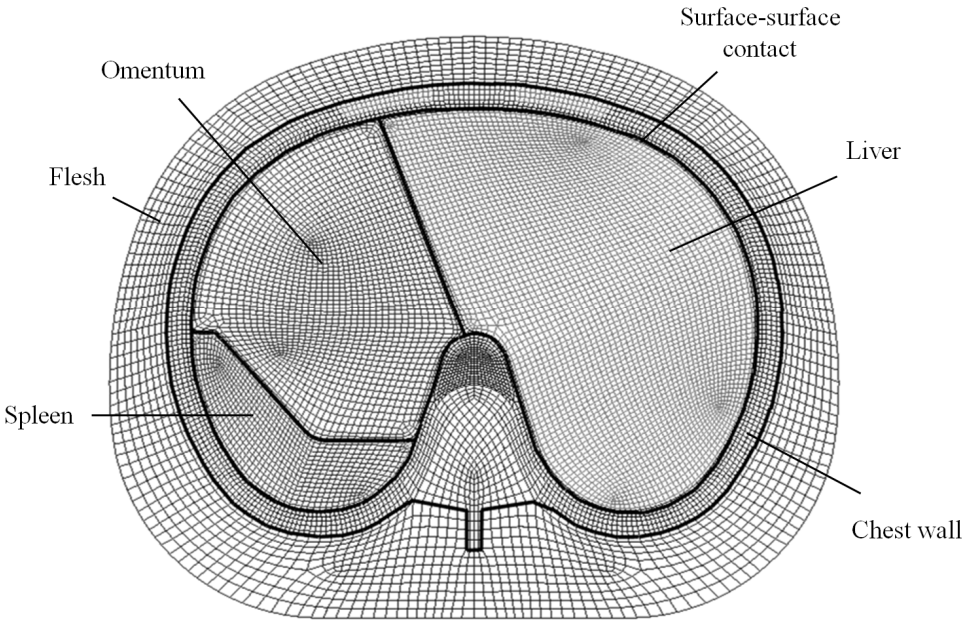

Figure 7.14. Resulting mesh density for the median viscera.

7.2.2 VALIDATION

An exemplar image of the pendulum-loaded computational model is depicted in Figure 7.15 with axis of deflection measurement. Force-deflection plots are shown in Figure 7.16 from PMHS experiments. Peak model response compared favorably with reported experimental results. Peak forces and peak deflections were within the ranges of peaks obtained from PMHS experiments. Further, force-deflection response was generally within corridors bounded by ranges of individual responses.

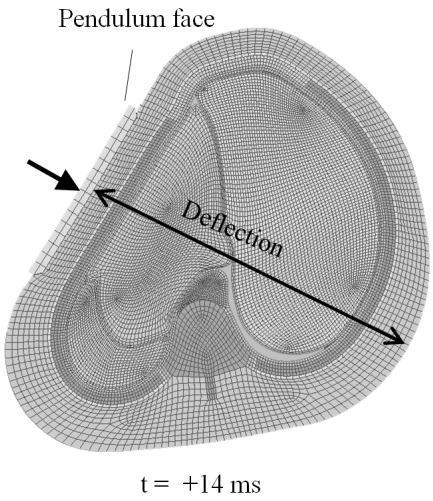

Figure 7.15. Pendulum loading at 60° with respect to anterior.

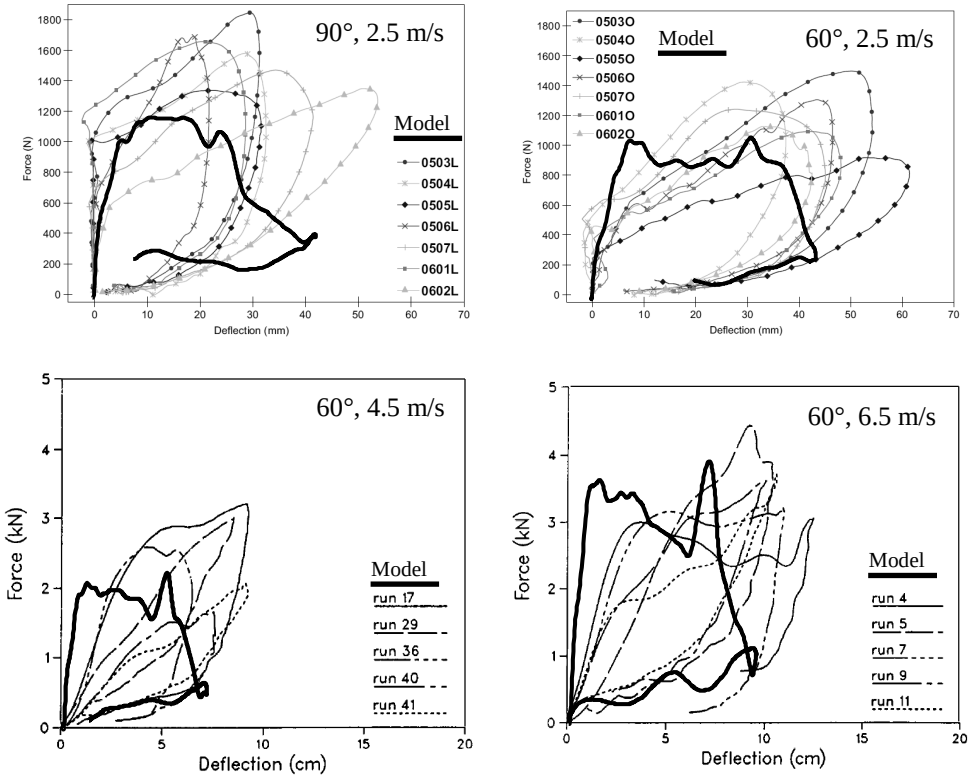

Figure 7.16. Force-deflection plots from PMHS and model pendulum impacts.
From Viano (1989) and Shaw et al. (2006)

7.2.3 MATERIAL RESPONSE NORMALIZATION

Shown in Figure 7.17 are exemplar images of deformation response to four boundary conditions representing (a) out-of-position airbag contact with $\Delta V = 6.7$ m/s, (b) stationary out-of-position airbag contact, (c) flat unprotected rigid contact at $\Delta V = 6.7$ m/s, and (d) anterolateral oblique rigid contact at $\Delta V = 6.7$ m/s. From 21 chestband loading simulations with the planar model, 17 were incorporated into logistic regression analyses. Recall that maximum values represent mean response of a contiguous area containing the overall peak and composing 5% of total spleen area (Figure 7.18). Shown in Figure 7.19 are risk functions of maximum material responses and experimental injury data (Chapter 6). Regression p-values were at or below $p = 0.1$ for each of the three material responses (ε_1, NRG, and ε_C). Shown in Table 7.2 are the normalized maximum values obtained from each of 21 test simulations. Three of the four highest NRG and ε_1 values were obtained from chestband loadings which induced visceral injury (D-1, D-2, and D-4); two of the four highest ε_C values corresponded to subjects sustaining visceral injury (D-1 and D-2).

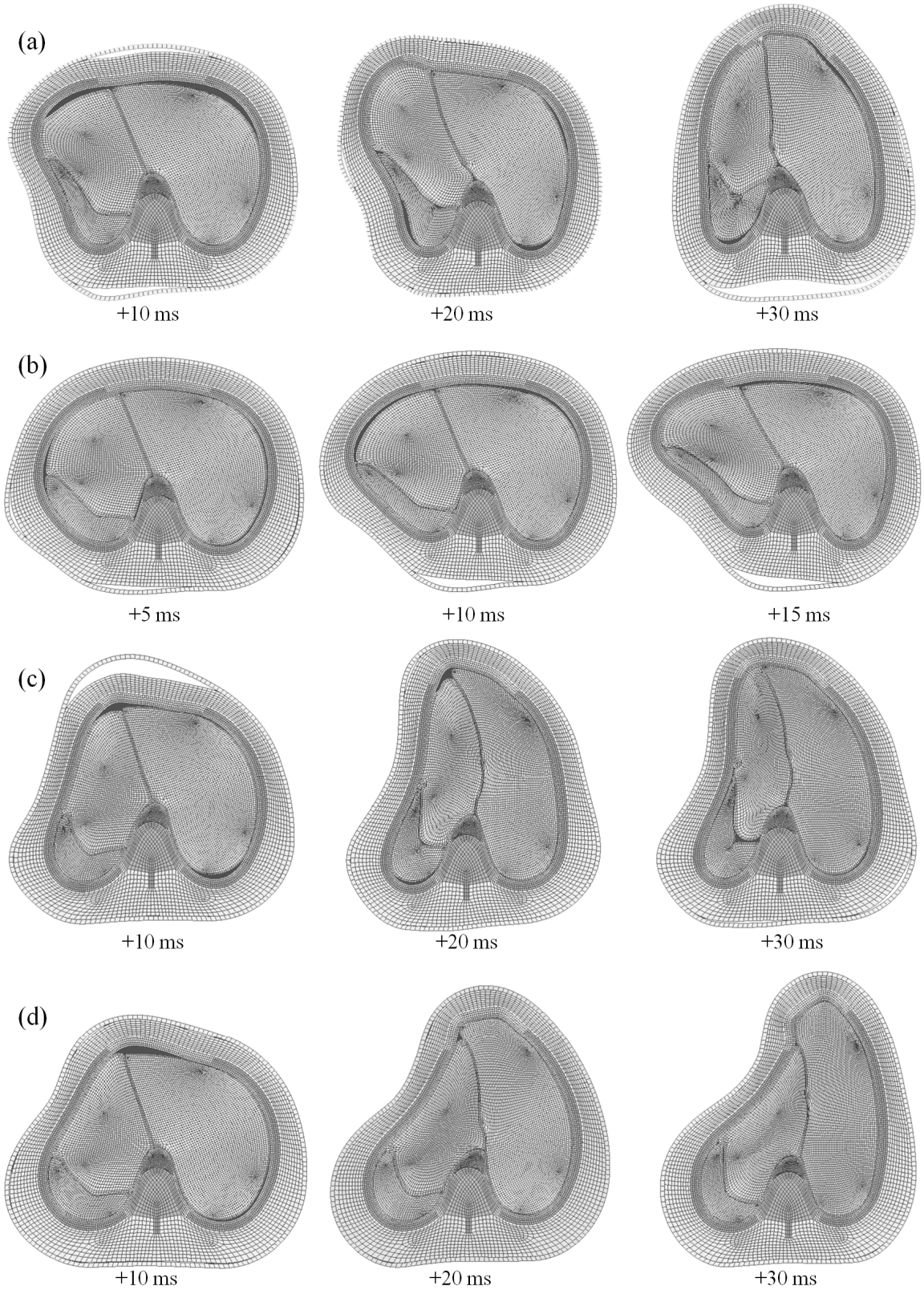

Figure 7.17. Model deformation response to boundary conditions: (a) dynamic OOP, (b) stationary OOP, (c) flat rigid, and (d) anterolateral oblique.

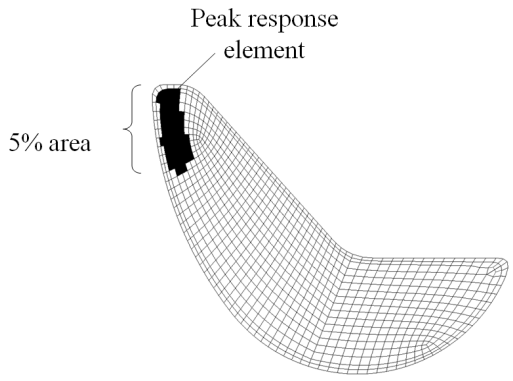

Figure 7.18. Exemplar 5% area from which maximum material response was obtained.

Table 7.2. Normalized peak material response results for tests included in regression analyses.

Test ID	NRG	Capsular Strain (ε_C)	Parenchymal Strain (ε_1)
D-1	1.736	1.862	1.999
D-2	1.318	1.150	1.620
D-3*	0.437	0.537	1.502
D-4	1.267	0.508	1.176
S-1	0.304	0.650	0.381
S-2*†	0.419	0.343	0.408
S-3	0.308	0.594	0.374
S-4*†	0.300	0.548	0.355
S-5*†	0.201	0.315	0.224
S-6	0.415	0.948	0.587
Flat 1	0.699	0.261	0.871
Flat 2	0.472	0.471	0.694
Flat 3	0.468	0.407	0.727
Flat 4	1.083	0.315	0.698
Flat 5	0.615	0.289	0.677
Flat 6	0.475	0.412	0.650
Flat 7	0.719	0.412	1.035
Oblique 1	0.415	0.496	0.798
Oblique 2	0.652	0.455	0.634
Oblique 3	0.150	0.148	0.242
Oblique 4	0.288	0.165	0.427

* Denotes simulations excluded from regression analyses.
† Denotes inverted right-side test.

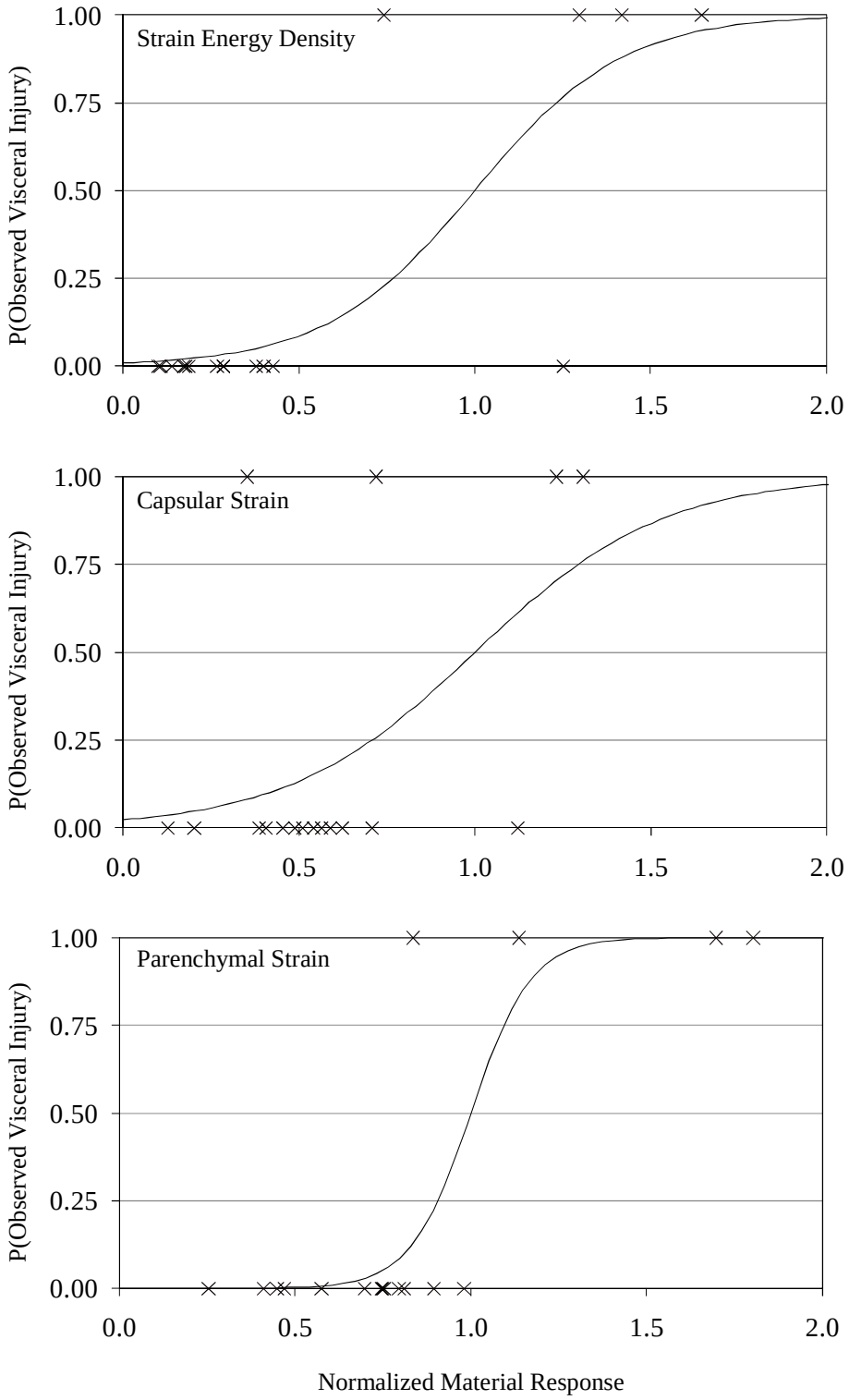

Figure 7.19. Risk analyses with respect to peak material response after normalizing to 50% risk of PMHS injury.

7.2.4 ANALYSIS OF AFFECTED AREAS

Material response parameters ε_1, NRG, and ε_C were evaluated for each element in time domain. To compare whole-spleen response between each boundary condition, the total area surpassing response thresholds of 0.2, 0.6, and 1.0 was quantified. The material response distributions resulting from these simulations (Figure 7.20) compared favorably to observed injuries in clinical imaging from case studies of side airbag injury (Chapter 4) and from observed laceration patterns observed in experimental subjects (Chapter 6). Namely, simulations of injured subjects exhibited diffuse parenchymal areas of elevated strain energy density and strain response as well as elevated capsular strain on the diaphragmatic surface near the anterior and posterior ends.

Affected area analysis was chosen to verify spleen mesh density (Figure 7.14). Using the D-1 subject loading, affected area results were compared to a refined spleen mesh density of halved (1 mm) element side length (Figure 7.21). NRG response was chosen as the parameter most sensitive to mesh refinement. Examining affected area responses in time domain, area results did not differ by more than 4.1% throughout simulation time; final results differed by less than 2%. Therefore the chosen mesh density (Section 7.2.1) was considered sufficient.

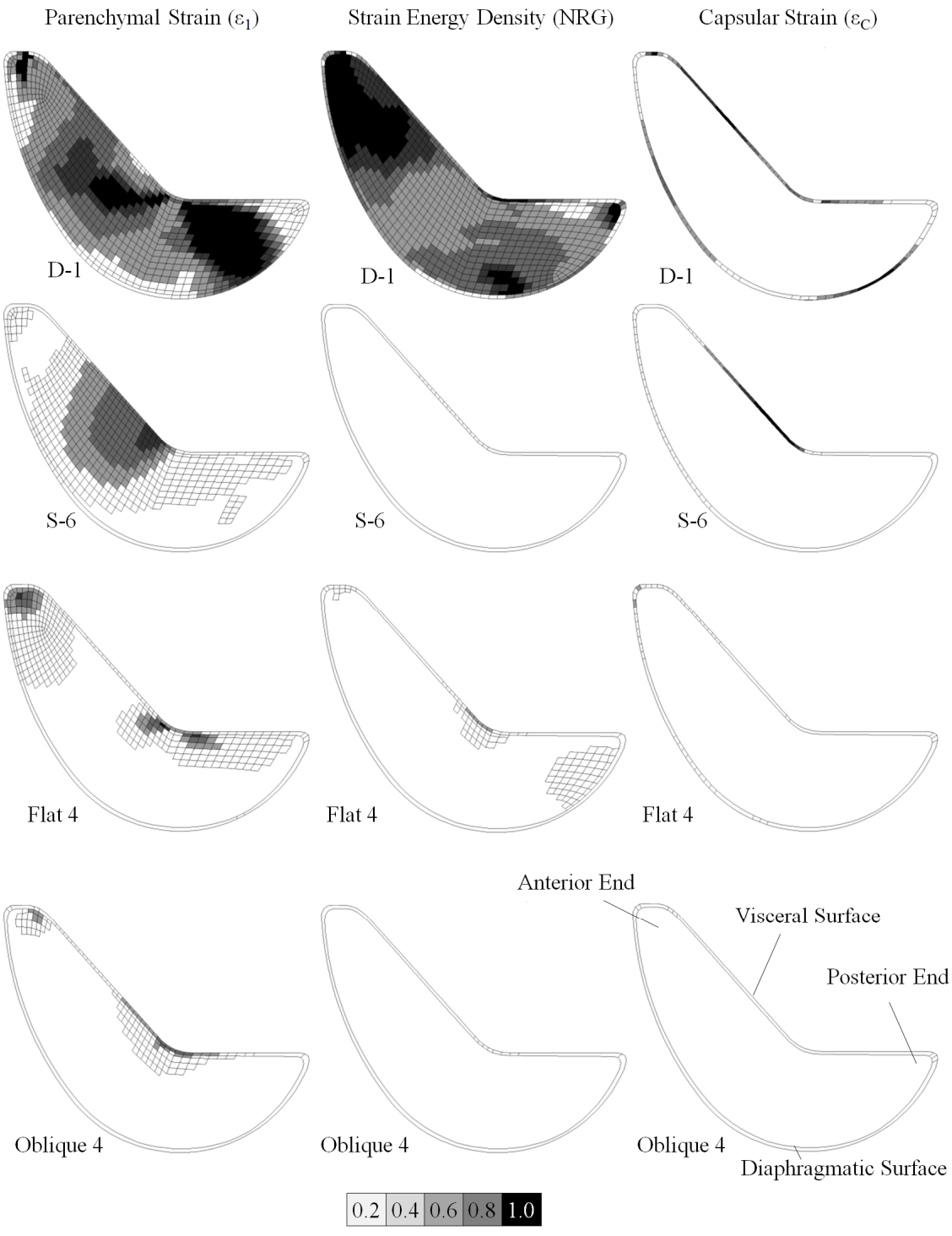

Figure 7.20. Exemplar distributions of parenchymal strain, strain energy density, and capsular strain responses to loading from the four boundary conditions.

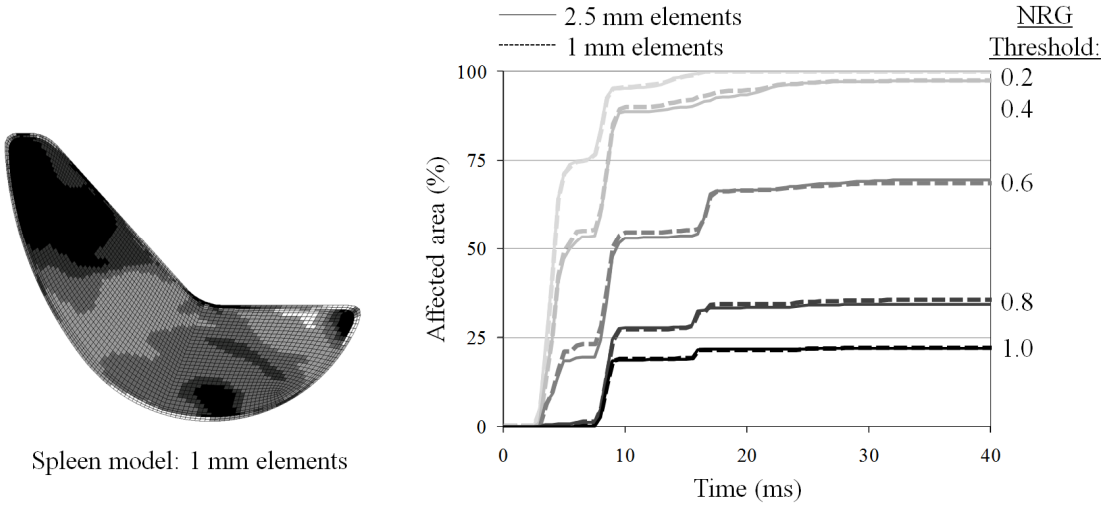

Figure 7.21. Refined spleen model and mesh density verification.

Shown in Figure 7.22 are the mean affected areas surpassing incremental material response thresholds for ε_1, NRG, and ε_C. Results are aggregated by the four boundary conditions and the three visceral geometries. Using the non-parametric Kruskal-Wallis analysis of variance by ranks, significant differences ($p < 0.05$) were found in affected areas between the four boundary conditions. Therefore, whole spleen material response was dependent upon boundary condition. This was consistent for the three visceral geometries.

As a post-hoc analysis, the Mann-Whitney Rank Sum test was used to identify differences in affected area between the sled impacts ($\Delta V = 6.7$ m/s with rigid or OOP airbag contact) and between the two OOP scenarios (Table 7.3). For NRG, differences between sled boundary conditions were significant ($p < 0.05$) with all geometries only for affected areas surpassing 1.0 NRG. For ε_1, significance was found between sled impacts for all magnitudes with 5th and 50th percentile geometries. Comparing the two OOP boundary conditions, results were significantly different for all geometries and boundary conditions considering NRG and ε_1. Capsular strain results were different considering $0.2 – 0.6\ \varepsilon_C$.

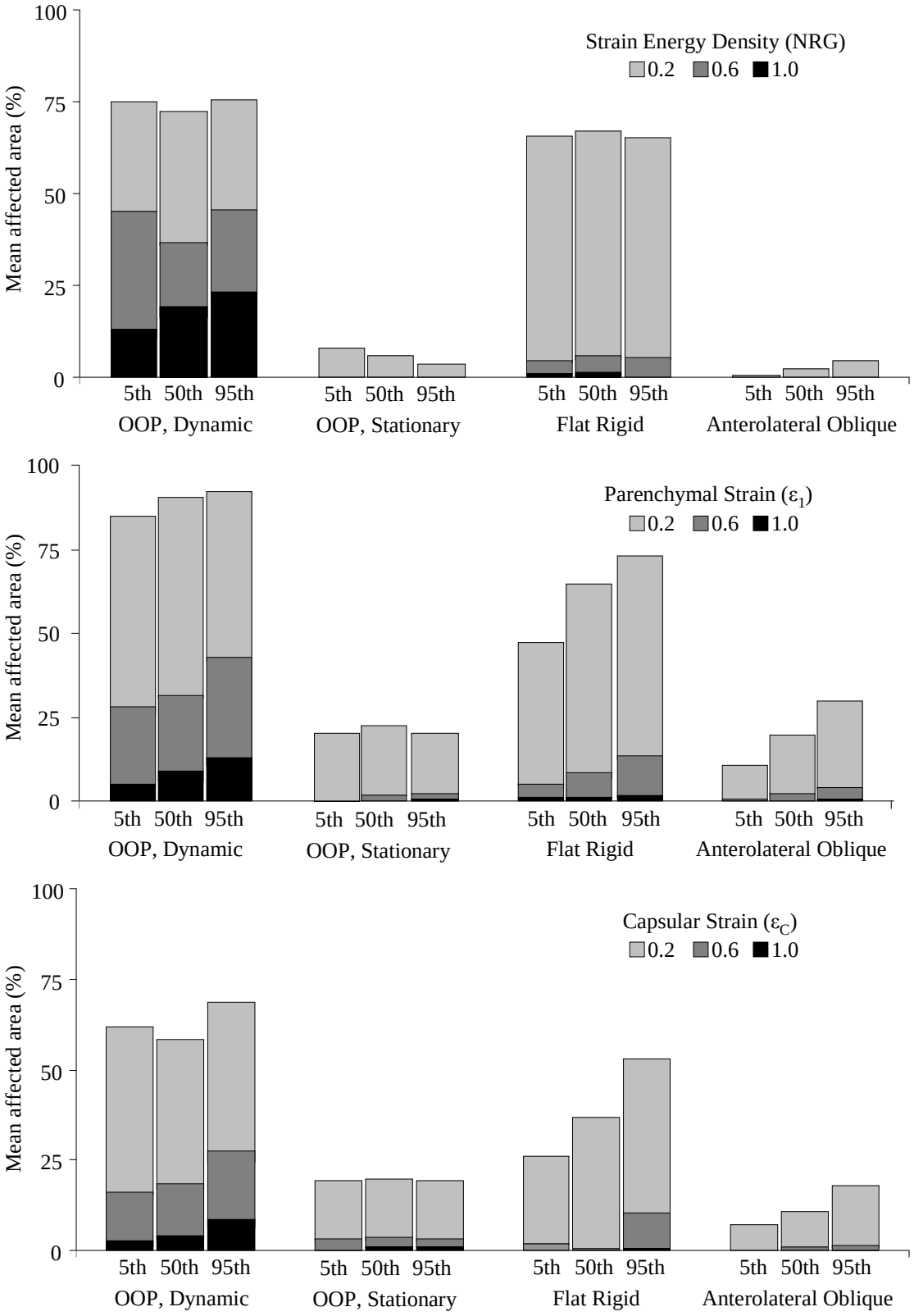

Figure 7.22. Mean affected area of 5th, 50th, and 95th percentile viscera models surpassing normalized material responses of strain energy density (upper), parenchymal strain (middle), and capsular strain (lower).

Table 7.3. Geometries (5th, 50th, 95th) in which spleen areas were significantly ($p < 0.05$) greater for OOP dynamic subject.

OOP Dynamic Subject compared to:	Response Magnitude	Strain Energy Density	Parenchymal Strain	Capsular Strain
Flat Rigid	0.2	-	5,50,95	5
	0.6	-	5,50,95	5,50,95
	1	5,50,95	5,50	5,50
OOP Stationary Subject	0.2	5,50,95	5,50,95	5,50,95
	0.6	5,50,95	5,50,95	5,50,95
	1	5,50,95	5,50,95	-

7.2.5 BIOMECHANICAL CORRELATION

Correlations between external mechanical parameters and splenic tissue responses were evaluated using the ten out-of-position side airbag scenarios. Contained in Table 7.4 are the significance values from a correlation matrix between maximum material responses and peak posterolateral metrics of normalized deflection and VCmax (Table 6.3). Correlations were not significant at $\theta = 140°$ for any geometry or at $\theta = 135°$ for small viscera geometry. Further, strain energy density appeared least correlated with posterolateral biomechanics; results were significant only at $\theta \leq 120°$ (115° for the small viscera geometry).

Table 7.4. Correlation significance between peak oblique metrics and material response parameters for three model geometries.

5th Percentile (Small) Model						
Angle	NRG		ε_C		ε_1	
	NormD	VCmax	NormD	VCmax	NormD	VCmax
140 °	*0.864*	*0.633*	*0.180*	*0.109*	*0.870*	*0.643*
135 °	*0.773*	*0.314*	*0.062*	*0.055*	*0.389*	*0.151*
130 °	*0.396*	*0.223*	0.014	0.036	*0.089*	0.019
125 °	*0.193*	*0.230*	0.004	0.058	0.018	0.011
120 °	*0.070*	*0.163*	0.003	0.055	0.001	0.003
115 °	0.034	*0.056*	0.006	0.034	0.000	0.000
110 °	0.019	0.026	0.011	0.031	0.000	0.000
105 °	0.012	0.016	0.016	0.036	0.000	0.000
100 °	0.010	0.014	0.018	0.041	0.000	0.000
95 °	0.009	0.015	0.021	0.053	0.000	0.000
90 °	0.009	0.020	0.026	0.063	0.000	0.000
50th Percentile (Median) Model						
Angle	NRG		ε_C		ε_1	
	NormD	VCmax	NormD	VCmax	NormD	VCmax
140 °	*0.978*	*0.477*	*0.060*	*0.072*	*0.868*	*0.683*
135 °	*0.612*	*0.224*	0.006	0.008	*0.387*	0.203
130 °	*0.271*	*0.165*	0.000	0.000	*0.083*	0.038
125 °	*0.117*	*0.186*	0.000	0.000	0.015	0.026
120 °	0.036	*0.122*	0.000	0.001	0.001	0.008
115 °	0.015	0.038	0.002	0.003	0.000	0.002
110 °	0.008	0.017	0.010	0.009	0.000	0.001
105 °	0.005	0.012	0.023	0.017	0.000	0.001
100 °	0.004	0.011	0.031	0.023	0.000	0.002
95 °	0.003	0.012	0.043	0.031	0.000	0.003
90 °	0.003	0.016	0.058	0.034	0.000	0.005
95th Percentile (Large) Model						
Angle	NRG		ε_C		ε_1	
	NormD	VCmax	NormD	VCmax	NormD	VCmax
140 °	*0.868*	*0.401*	*0.177*	*0.170*	*0.481*	*0.291*
135 °	*0.508*	*0.183*	0.031	0.015	*0.141*	0.024
130 °	*0.200*	*0.133*	0.001	0.000	0.016	0.000
125 °	*0.077*	*0.158*	0.000	0.000	0.002	0.000
120 °	0.020	*0.100*	0.000	0.000	0.000	0.000
115 °	0.009	0.032	0.001	0.000	0.000	0.000
110 °	0.005	0.015	0.003	0.001	0.000	0.000
105 °	0.003	0.012	0.008	0.003	0.000	0.000
100 °	0.002	0.012	0.011	0.004	0.000	0.000
95 °	0.002	0.014	0.015	0.006	0.001	0.000
90 °	0.002	0.018	0.022	0.007	0.001	0.000

Values in italics are not significant.

Shown in Figure 7.23 through Figure 7.25 are R^2 values overlaid with corresponding PRESS statistics for all material responses evaluated in this analysis. Recall that the R^2 value represents the proportion of material response variance for which the biomechanical parameter is predictive. Recall that the PRESS statistic quantifies the degree to which the resulting relationship may be generalized to a larger dataset. Therefore the best metric demonstrates maximal R^2 and minimal PRESS. In general, the angles yielding the lowest PRESS values were in agreement with the angles yielding the greatest R^2 values. Strain energy density (NRG) was least correlated with the external biomechanical parameters compared to ε_1 and ε_C: Only for the large viscera geometry with normalized deflection at $\theta = 90° – 100°$ was $R^2 > 0.7$. By comparison, capsular strain indicated highest correlation of these material responses for the median and large viscera geometries; parenchymal strain indicated highest correlation only for the small viscera geometry.

With increased spleen size, PRESS and R^2 values indicated improved correlations. Highest overall R^2 values were observed for capsular and parenchymal strains in the large (95th percentile) model between $\theta = 115° – 125°$ (Figure 7.24). For this geometry, VCmax was preferable to normalized deflection. For median geometry (Figure 7.23), R^2 and PRESS values indicated normalized deflection was preferable to VCmax, but at angles similar to the large geometry. Comparatively, spleen material response in the small geometry did not correlate as well with external biomechanical metrics. Yet considering maximum parenchymal strain, $R^2 \approx 0.85$ for peak normalized deflection and VCmax at $\theta = 110°$.

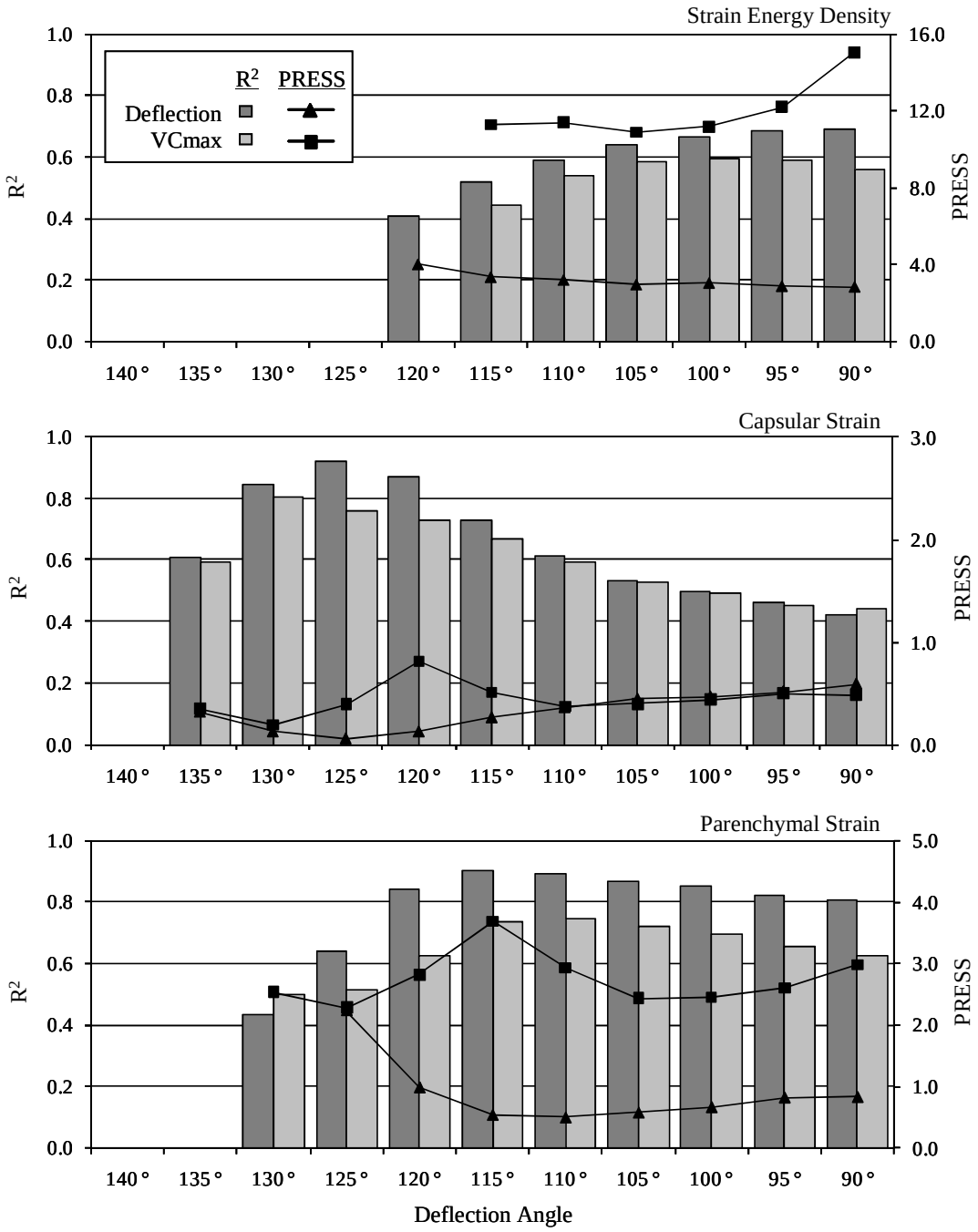

Figure 7.23. Coefficients of Determination (R^2) and PRESS statistics for correlations between oblique biomechanical parameters and tissue-level responses with median (50th) viscera model.

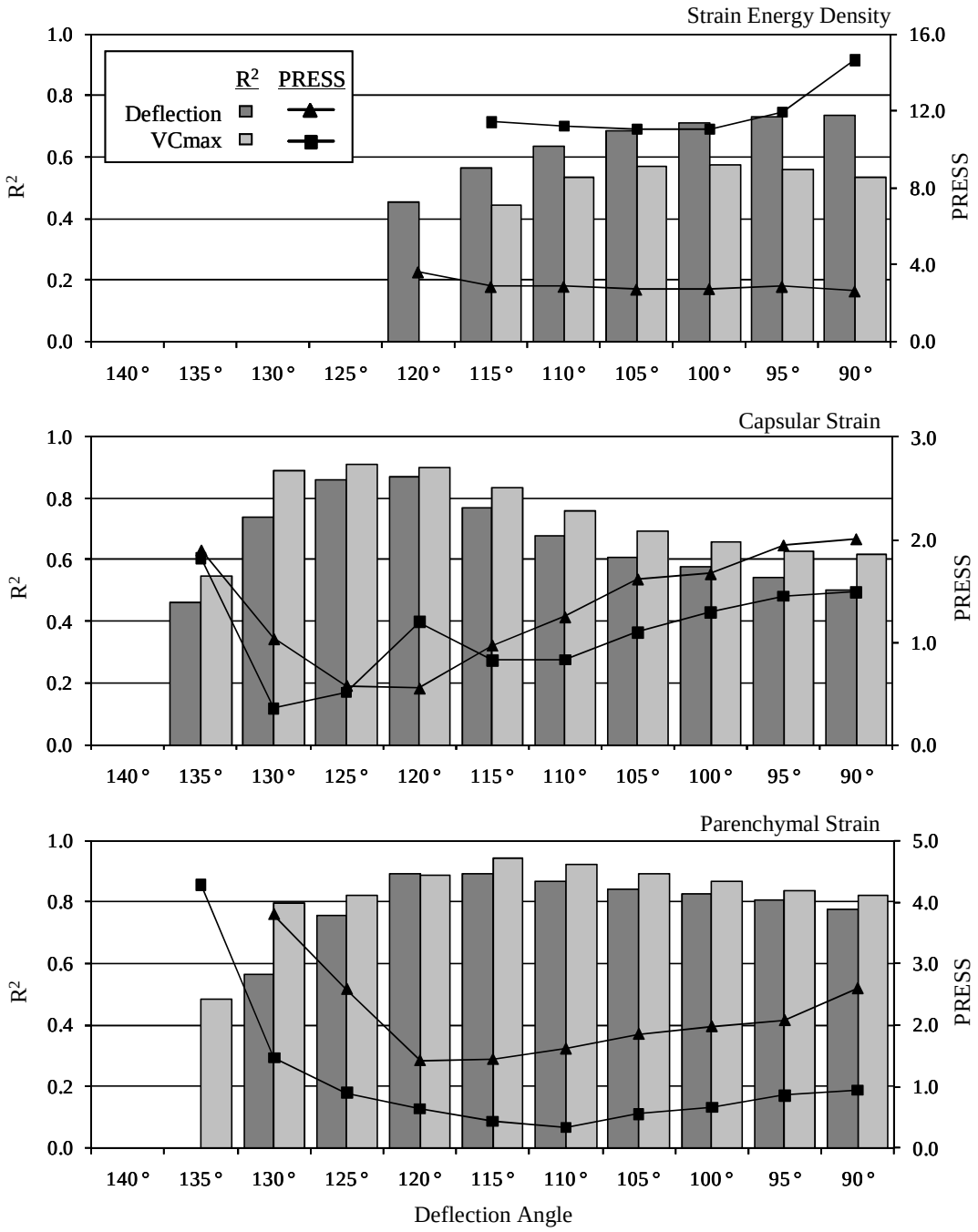

Figure 7.24. Coefficients of Determination (R^2) and PRESS statistics for correlations between oblique biomechanical parameters and tissue-level responses with large (95th) viscera model.

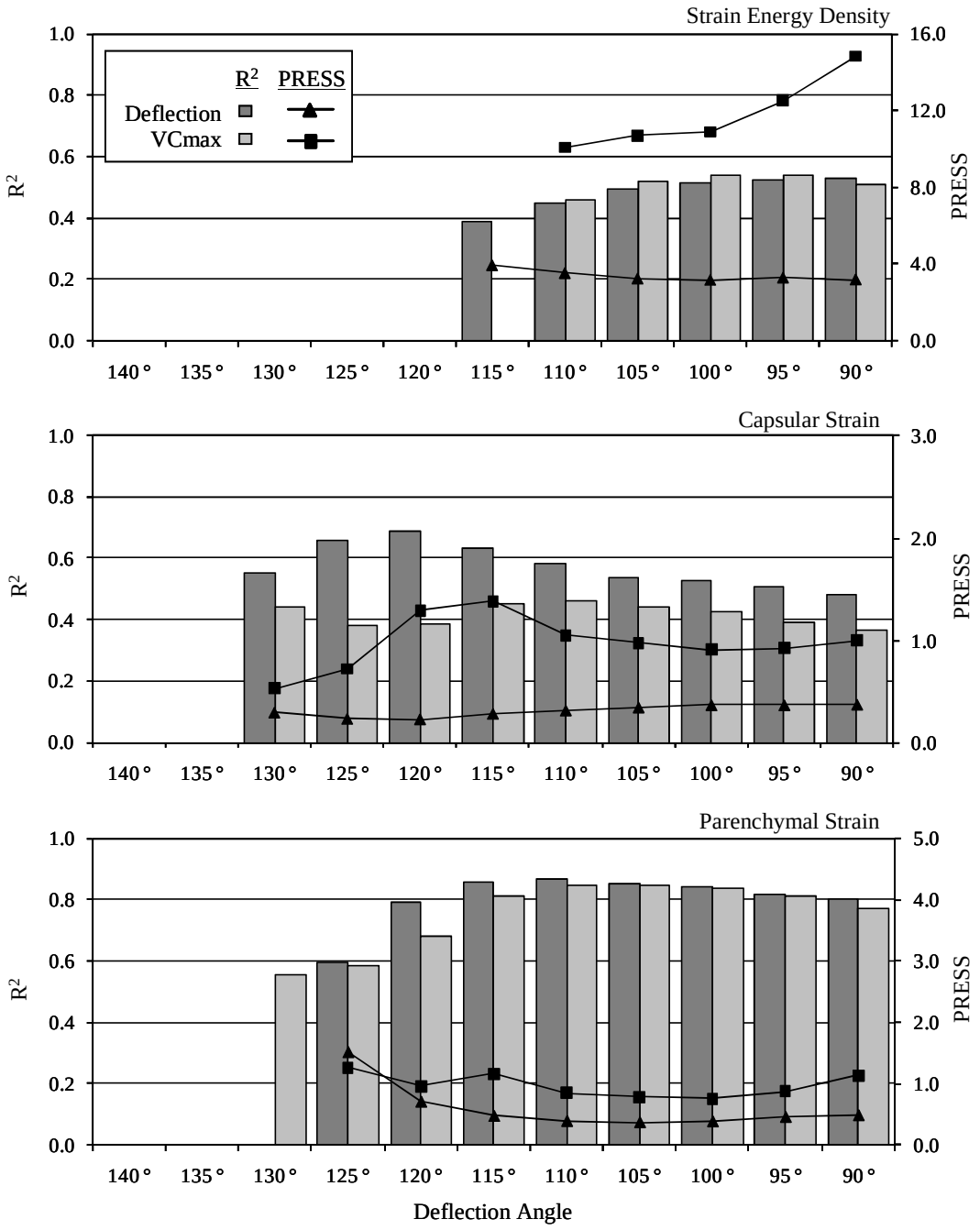

Figure 7.25. Coefficients of Determination (R^2) and PRESS statistics for correlations between oblique biomechanical parameters and tissue-level responses with small (5th) viscera model.

7.3 DISCUSSION

This comparative subject-specific loading analysis demonstrated that tissue-level spleen responses is dependent on boundary condition and correlated with external thoracoabdominal biomechanics. Further, loadings which demonstrated the greatest normalized deflections and viscous metrics were also associated with greatest material response parameters of parenchymal strain (ε_1), capsular strain (ε_C), and strain energy density (NRG) in the finite element spleen.

Although a material response-based injury metric has not been developed for splenic trauma, parameters of parenchymal maximum principal strain, capsular longitudinal strain, and strain energy density are mechanically justified. Material strain and rate-dependent strain energy density are important parameters of tissue failure in blunt trauma (Yamada, 1970; Tong & Fung, 1993). Trauma to renal capsule and parenchyma was correlated to maximum strain energy density in a viscoelastic finite element model of an *ex vivo* perfused porcine kidney (Snedeker et al., 2005a; Schmitt & Snedeker, 2006; Snedeker et al., 2007). Derivations of maximum principal strain were correlated to neural trauma as identified by rodent unconscious time and histological evaluations (Bandak & Eppinger, 1994; Fijalkowski et al., 2009). Maximum principal strain was correlated to lung contusion in blunt impacts to rodent subjects (Stitzel et al., 2005). The diversity of these tissues validated the extension of response criteria to spleen tissue. Rib fracture was not considered by the model. Rather, the generalized chest wall material was linearly elastic without failure. Rib fractures have been considered by element erosion (deletion) with failure strain value (Hayashi et al., 2008; Song et al.,

2009). Yet component analysis (Figure 7.4) and pendulum validation have demonstrated the present formulation to be sufficiently physiologic for this analysis.

The plane strain formulation was appropriate for this analysis which considered only in-plane deformations and in-plane material responses. The spleen and liver are constrained to the diaphragm *in vivo* by the splenophrenic and coronary ligaments, respectively. Although postural and respiratory motions may change the sagittal plane orientation of these structures (Rietzel et al., 2004; Brandner et al., 2006; Beillas et al., 2009; Lafon et al., 2010), studies of *in vivo* liver kinematics during impact have suggested that the transverse plane is the primary plane of visceral motion (Nusholtz et al., 1980; Miller, 1989; Viano et al., 1989a; Arnoux et al., 2008; Cheynel et al., 2009). Further, material response parameters were significantly correlated ($p < 0.1$) with visceral injury observations in matched tests, supporting model formulation.

Validation was in accordance with previous finite element models for blunt impact. Validation procedures have employed simulations of pendulum (Lee & Yang, 2001; Tannous et al., 2003; Campbell et al., 2005; Ruan et al., 2006; Snedeker et al., 2007) or sled impacts (Furusu et al., 2001; Iwamoto et al., 2002; Ruan et al., 2003; Forbes et al., 2006; Ruan et al., 2006) with force-deflection comparisons. Further, individual model components, i.e., spleen, liver and chest wall, were independently demonstrated to conform to available published experimental data (Melvin et al., 1973; Viano, 1989; Tamura et al., 2002; Shaw et al., 2006; Kent, 2008).

Boundary condition was a determinant of diffuse spleen response for all model geometries (5th, 50th, and 95th percentiles). From Figure 7.22, dynamic out-of-position loading was associated with an increase in affected areas for all magnitudes of material

response (ε_1, NRG, and ε_C) compared to other boundary conditions. This analysis revealed that the OOP boundary condition subjected the organ diffusely to greater material deformations. Because prior research has associated tissue deformation with tissue failure (Yamada, 1970; Kiss et al., 2004; Jacquemoud et al., 2007; Saraf et al., 2007a; Ahm & Kim, 2010; Brunon et al., 2010), this observation further supports the conclusion that a dynamic OOP boundary condition subjects the posterolateral viscera to a greater risk of trauma than an unprotected lateral impact (Chapter 6). Comparing between visceral geometries in this boundary condition, the spleen size also increased the affected areas associated with ε_1, NRG, and ε_C response, but primarily for magnitudes surpassing 1.0. For example, total affected area surpassing 0.2 NRG was not associated with geometry (remaining approximately 75%) but affected area surpassing 1.0 NRG was nearly doubled (from 12% to 25%). This suggested that, while proportional involvement of the organ did not increase, the larger size elevated the magnitude of tissue deformations, likely increasing injury risk. Because acute splenomegaly (spleen enlargement) is associated with increased risk of splenic rupture (Naylor et al., 1974; Arden et al., 1981; Glass & Gilbert, 1996; Harbrecht et al., 2007; Zissin et al., 2007), present results are in agreement with the literature. With flat rigid and anterolateral oblique impacts, large spleen geometries increased affected areas for ε_1 and ε_C response. This finding primarily resulted from the anterior end of the spleen extending anteriorly (Figure 7.11) where it was exposed to increased deformation from lateral chest deflection. Similarly, the smaller geometry reduced spleen interaction with lateral chest deflection and decreased affected area. Notably, strain energy density was unaffected by

geometric changes to spleen in these non-airbag boundary conditions, suggesting that this may not be the most appropriate correlate to injury.

Clinical data has associated acute splenomegaly with increased risk of splenic rupture, particularly during infection (Rutkow, 1978; Putukian et al., 2008). Large spleen geometry in this study was associated with increased parenchymal and capsular strain as well as increased affected area (Figure 7.22); NRG was also increased but affected area was not increased. Yet cases of chronic splenomegaly have not been associated with increased risk of trauma (Pottakkat et al., 2006), possibly due to fibrotic changes in splenic tissue composition. To address such material changes, a sensitivity analysis was conducted which examined the relationship between material responses (ε_1, NRG, and ε_C) and splenic tissue material properties (Table 7.5). The chestband loading chosen for this sensitivity analysis corresponded to the most severe splenic trauma case (D-1). Spleen parenchymal tissue properties of density (ρ), bulk modulus (K), and shear moduli (G_0 and G_∞) were arbitrarily varied by 50% ($\pm$ 25%). All material response parameters were most sensitive to K, a finding in agreement with the literature (Shen et al., 2008). Strain energy density was highly sensitive to ρ, but this was due primarily to the derivation of this response parameter. Increased G_0 and G_∞ induced increases in capsular strain and decreases in parenchymal strain. In light of this analysis, material property changes induced by chronic splenomegaly likely included increased shear and bulk moduli. Splenic capsular material changes were not addressed by this analysis but likely include similar fibrotic stiffening. Computational analysis has suggested a stiffening relationship between biological tissue perfusion and material bulk response (Bilston, 2002). Therefore during acute splenomegaly, capsular material changes would be unlikely, but

inflammation may increase the parenchymal bulk modulus (K), elevating both capsular and parenchymal strains.

Table 7.5. Maximum material response sensitivity to spleen parenchymal tissue properties.

Property ±25%	Capsular Strain ε_C	Parenchymal Strain ε_1	Strain Energy Density NRG
ρ	2% / -6%	2% / -6%	19% / -21%
G_0	8% / -5%	-9% / 4%	<1% / <1%
K	19% / -1%	9% / -15%	-20% / 32%
G_∞	9% / <1%	-3% / 6%	<1% / <1%

Visceral geometry was a determinant of external biomechanical correlation. Comparing PRESS and R^2 values, material responses in small viscera geometry correlated poorly in comparison to other geometries. Highest overall R^2 values occurred in the large geometry model. For this geometry, VCmax was a better predictor of maximum parenchymal and capsular strain than normalized deflection. In the median geometry normalized deflection was preferable for ε_1 and ε_C. Clinical evidence has suggested that splenomegaly and hepatomegaly may be associated with increased risk of trauma (Wooldridge, 1969; Rutkow, 1978; Arden et al., 1981; Rubin, 2003; Putukian et al., 2008; Shah et al., 2008). Therefore, larger geometries may be more relevant to out-of-position test protocols and injury risk reductions, suggesting the use of VCmax. Yet observed injury patterns (Chapter 4) were limited to normophysiologic patients who may be more indicative of median visceral geometries. Therefore results suggested that normalized deflection and VCmax should be used concurrently in injury risk assessments. These parameters should be obtained from angles between $\theta = 115° – 125°$ with respect to the anterior direction.

These results are consistent with cadaveric experiments (Chapter 6), clinical observations (Chapter 4) and multi-body analysis (Chapter 5). Yet, both the model and

the PMHS experiments did not differentiate peak normalized deflection from the VCmax response as an injury metric. This suggests that, for this posterolateral boundary condition, both are appropriate. A study of anterior PMHS loading reported a similar conclusion (Kent et al., 2001). Specifically, it was observed that VCmax injury criteria (thresholds) were exceeded in conjunction with normalized deflection criteria in all dynamic loading scenarios. However, this was not observed with the multi-body analysis (Chapter 5), in which VCmax was exceeded prior to normalized deflection with incrementally increasing ΔV. Therefore, as current procedures suggest that both metrics be quantified in vehicle crashworthiness assessments (IIHS, 2003; EuroNCAP, 2004b; IIHS, 2008; NHTSA, 2008b), these results support such a practice.

EIGHT

SUMMARY AND LIMITATIONS

8.1 SUMMARY

The hypotheses for this study were that torso-protecting side airbags induce morphologically different thoracoabdominal deformation patterns in out-of-position occupants compared to lateral loading. Further, it was hypothesized that a viscous injury metric is more sensitive than a deflection injury metric. In investigating these hypotheses, this study identified and described the heretofore unknown biomechanical and injury response of an out-of-position, i.e., close-proximity, occupant to a torso-protecting side airbag system in a dynamic impact environment. This boundary condition represented the torso impeding full inflation of the airbag within the space between the occupant and the intruding door. Four Specific Aims were addressed.

1. *Identify unique thoracoabdominal injuries, as described by anatomical location and the Abbreviated Injury Scale, during documented side impacts involving torso-interacting side airbags.*

Clinical results from the NASS database demonstrated that torso airbag deployment was predictive with 90% confidence of splenic trauma, suggesting the possibility of a causal relationship. Further, five individual case occupants from the CIREN, NASS, and SCI databases were analyzed in which splenic trauma was associated with torso-interacting side airbag deployment; five additional cases followed a similar injury pattern. Findings from the NASS and from the literature indicated that, in absence of torso side airbag, the probability of splenic injury in these particular cases was

minimal. Anatomic considerations were discussed, noting that the preferred torso airbag stowage region was in close-proximity to the posterolateral region of the "hard thorax" occupied by the spleen. An occupant impeding airbag deployment would be contacted in this region by the airbag. This injury was considered substantial because acute splenic trauma can be life-threatening, and active hemorrhaging requires immediate medical intervention (Glass & Gilbert, 1996; Harbrecht et al., 2007; Harbrecht et al., 2007). Although treatment course is increasingly non-operative, as many as one-third of cases still necessitate splenectomy (O'Sullivan et al., 1994; Pottakkat et al., 2006; Harbrecht et al., 2007). This procedure has been associated with a lifelong risk of overwhelming sepsis (Naylor et al., 1974; Shatney, 1987; Deodhar et al., 1993; Waghorn, 2001; El-Alfy & El-Sayed, 2004; Zissin et al., 2007).

2. *Determine relationship between lateral thoracic biomechanical response and parameters of door intrusion velocity and occupant position to define "out-of-position" torso airbag interaction.*

Through a parametric examination of occupant distance and door velocity, the side airbag mitigation of deflection, deflection rate, and viscous injury metrics was characterized using the MADYMO facet human model. Three points of interest were identified: most protective occupant distance, critical distance, and least protective distance. Distance demonstrating most airbag protection, i.e., lowest injury metrics, increased with increasing ΔV. Least protection, i.e., highest metrics, resulted when occupant was nearest the airbag at all ΔV. Critical distance, i.e., equivalent metrics with and without airbag, occurred between distances of least and most protection. Critical distance only varied considering deflection metrics, from 3 to 10 cm, but did not vary

when rate or viscous metrics were considered. While previous out-of-position testing of torso-interacting airbags has utilized dummies in stationary orientations, dynamic impact with close-proximity airbag deployment was found to induce metrics greater than the linear summation of stationary deployment and dynamic rigid contact. A dynamic out-of-position scenario was proposed at $\Delta V \approx 7$ m/s.

3. *Characterize torso deformation and direction resulting from out-of-position side airbag interaction.*

Seven PMHS were exposed to ten airbag deployments. Subjects were positioned in out-of-position scenarios such that the deploying airbag first contacted the posterolateral thorax between T6 and L1 while stationary (n = 3 x 2 aspects) or while subjected to left lateral sled impact at $\Delta V = 6.7$ m/s (n = 4). Chestband contours were analyzed to quantify deformation direction in the thoracic x-y plane, deflection, rate, and viscous response. Results were compared to unprotected wall lateral impacts (n = 7) and obliquely mounted anterolateral wall impacts (n = 4). Unlike unprotected wall or anterolateral boundary conditions, deformation direction with airbag was transient during out-of-position sled impact and during stationary out-of-position deployment. At onset, deflection angle was posterolateral ($p < 0.001$) and progressed laterally 30° at maximum deflection. Out-of-position interaction induced peak deflection rates significantly greater than unprotected contact; trends suggested that normalized deflection and VCmax were also greater. Posterolateral deflections were not significantly different between dynamic and stationary airbag deployments when $\theta > 125°$ and deflections were significantly greater in the dynamic out-of-position scenario when $\theta > 105°$.

4. Quantify injury risk, as measured by Abbreviated Injury Scale and tissue-level material response, associated with out-of-position torso side airbag interaction with the thoracoabdominal region.

Skeletal injuries were consistent with posterolateral contact; visceral injuries consisted of renal (n = 1) or splenic (n = 3) lacerations. Presence of posterolateral visceral trauma was significantly associated ($p < 0.002$) with this dynamic out-of-position scenario compared to unprotected impact; presence of splenic trauma in particular was significant ($p < 0.02$). Because of deflection angle transience and localized injury response, a posterolateral injury metric was required for this boundary condition in addition to traditional lateral biomechanical response. Logistic regression of posterolateral responses found peak deflection normalized to chest breadth as well as VCmax best correlated to visceral injury at oblique angles corresponding to $\theta = 120° – 130°$. Measured at $\theta = 130°$, normalized deflection = 0.140 and VCmax = 0.55 m/s corresponded to 50% risk of visceral trauma. Planar finite element modeling confirmed the elevation of splenic parenchymal strain, capsular strain, and strain energy density in out-of-position compared to unprotected impact. Further, geometric enlargement of the spleen increased parenchymal strain, capsular strain, and strain energy density compared to median and small viscera geometries. Correlations between external biomechanical parameters and these three splenic material responses identified $\theta = 115° – 125°$ as best predictors of capsular strain and parenchymal strain response, particularly for 50th and 95th percentile geometries; strain energy density response was least correlated with external biomechanical response. Results further indicated that this injury mechanism did not necessitate the choice of a viscous metric over a deflection metric. Yet,

parametric analysis of occupant position and door velocity suggested that viscous response was more sensitive to airbag deployment parameters and was therefore preferable for this boundary condition.

8.2 POTENTIAL LIMITATIONS

A number of potential limitations should be considered when interpreting the results of this study. The following section addresses these limitations in the order in which the study was presented.

The case study relied upon database composition. To be included in the CIREN database, an occupant should have sustained one AIS 3+ or multiple AIS 2+ injuries. To be included in the NASS database, at least one vehicle must require a tow as a result of the crash. This requirement may skew the data sample toward increased severity crashes. Therefore statistical analyses were only performed on the NASS dataset. A secondary concern remains the possibility of acute splenic trauma presenting as “delayed rupture” (Leppaniemi et al., 1988). This condition is characterized by splenic trauma from which hemorrhaging does not manifest for at least 48 hours (Parithivel et al., 2002). During this latency, even contrast-enhanced abdominal imaging scans may appear normal (Leppaniemi et al., 1988). Given reported latencies (Leppaniemi et al., 1988; Parithivel et al., 2002), it is not unfeasible that latent splenic trauma at presentation may be diagnosed incorrectly as spontaneous splenic rupture (Rutkow, 1978; Parithivel et al., 2002; Ruffolo, 2002; Putukian et al., 2008). For such patients the association between injury response and side airbag interaction would be overlooked.

With the parametric multi-body model and the PMHS experiments, lateral impact was simplified using a “Heidelberg-type” sled which impacted with controlled constant

door velocity (Kallieris et al., 1981; Marcus et al., 1983). In contrast, lateral motor vehicle crashes exhibit complex door velocity time-traces with variable door crush profiles (Lau et al., 1991; Kent et al., 2001; Tencer et al., 2005a). Yet, controlled door velocities have been utilized previously in sled devices to simulate lateral motor vehicle crashes and develop injury metrics and injury criteria (Pintar et al., 1997; Maltese et al., 2002; Yoganandan & Pintar, 2005). Such simulations demonstrated door velocity to correlate with crash ΔV (Dargaud & Bourdillon, 1986; Pintar et al., 1997; Watson et al., 2009). Although the scenario in this study neglected variable door velocity and geometry due to the crash, this methodology isolated side airbag affects. Because door velocity and therefore energy transfer remained unchanged with variable occupant distance, only changes in airbag-occupant interactions affected biomechanical response.

The generalized side airbag incorporated into the multi-body analysis was also a limitation of this study. No independently validated side airbag model was available, as these are generally proprietary. Yet, use of a vehicle-specific side airbag model may have confounded the generalizability of this analysis. The modified airbag in this study accommodated a reasonable approximation to torso side airbag characteristics. The maximum tank test pressure was realistic for a torso-interacting side airbag (Pintar et al., 1999). Airbag aggressivity was conservative as measured by the maximum tank pressure onset rate; onset rates 300% greater than specified in this study have been reported with door-mounted side airbags (Pintar et al., 1999). Lumped-parameter analysis was employed, assuming uniform pressure and temperature throughout the airbag control volume. Advances in coupled fluid-structure algorithms have demonstrated that the contribution of gas dynamics to the early stages of airbag inflation can affect deployment

kinematics (Marklund & Nilsson, 2002; Pyttel et al., 2007; Ruff et al., 2007). Yet, studies have demonstrated lumped-parameter airbag models to reasonably approximate close-proximity occupant interactions (Roychoudhury et al., 2000; Petit et al., 2003; Park & Hong, 2005). The use of this generalized side airbag model confirmed the complexity of side airbag protection in lateral impact and the sensitivity of the viscous injury metric to side airbag boundary conditions. These trends were in agreement with other study findings; namely, the propensity of out-of-position side airbag boundary condition to induce visceral injury.

Visceral trauma is reportedly less frequent in cadaveric specimens as well as difficult to identify compared to *in vivo* experiments at similar impact severities (Nusholtz et al., 1980; Rouhana, 1993; Yoganandan et al., 2001). Although this suggested that an *in vivo* model may be necessary to confirm splenic injury observations, this approach was ultimately rejected because of anatomic variations between species. Porcine subjects represent the most common animal surrogate for studies of thoracoabdominal biomechanics due to anatomical and mass distribution similarities (Trollope et al., 1973). Yet, porcine geometry differs substantially for the spleen, the primary organ of interest in this study (Figure 8.1). The long ribbon-like porcine spleen extends beyond the mid-axillary line and is directly loaded by chest wall deformation even in lateral impact (Horn et al., 2005). Further, the narrow thoracic cage geometry reduces the posterolateral exposure of the visceral contents. The use of post-mortem human subjects preserved anatomical similarity with vehicle occupants.

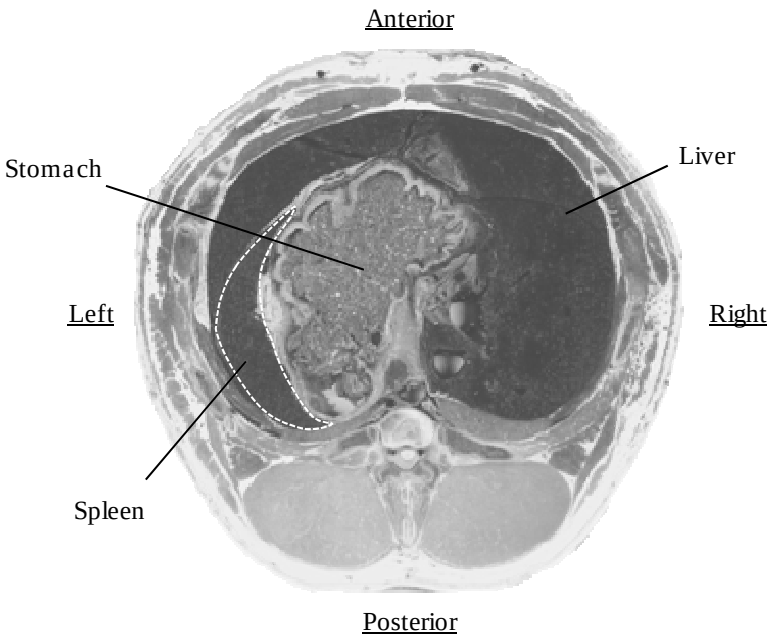

Figure 8.1. Transverse cross-sectional porcine anatomy at upper abdominal level corresponding to liver and spleen.
From Horn et al. (2005), used with permission

The absence of vehicle-specific seat and door trim pieces may affect the injury response correlation for this airbag boundary condition, as these have been shown to affect biomechanical response (Mertz et al., 1982; Horsch et al., 1990; Melvin et al., 1993). Similarly, the current test series employed only one side airbag design judged to be the most aggressive available in a representative subset of the US consumer vehicle fleet (Hallman et al., 2009b). Due to subject availability, no cadaveric tests were conducted without chestbands in place. The highly fluid nature of airbag deployment suggests that the chestband may affect biomechanical or injury response during close-proximity airbag interaction. The chestband may reduce punch-out effects (Section 3.5.2) by distributing forces over a larger area or increase membrane effects by introducing focal loads to the underlying anatomy. While previous chestband studies

have not observed localized chestband effects (Morgan et al., 1994; Pintar et al., 1997; Shaw et al., 2006), noninstrumented subjects may be warranted for conclusive characterization of injury response.

The plane strain model employed in this study constrained element deformations to planar response only. This approach has been employed previously for computational examination of thoracoabdominal injury response with chestband contours (Tannous et al., 2003; Campbell et al., 2005; Campbell & Tannous, 2007). Yet the model constraints prevented direct application of resulting strain magnitudes to the human occupant. Rather, a comparative analysis of boundary conditions identified relative material response changes induced by out-of-position torso airbag contact compared to unprotected lateral impact. Further, the homogenous treatment of splenic tissue in this study did not consider devascularization injuries seen clinically (Tulikoura et al., 1999; Shackford, 2002; Madoff et al., 2005; Dissanaike & Frezza, 2006; Harbrecht et al., 2007; Tinkoff et al., 2008). Yet devascularization is rare in absence of other parenchymal damage to which the model composition was sensitive (Arden et al., 1981; Mustard et al., 1984; Tulikoura et al., 1999). Similarly, rib fracture was not considered by the elastic chest wall model. This injury pattern, although present in PMHS subjects, was not necessarily unique to the boundary condition, and visceral shearing by fractured rib ends represents a self-evident injury mechanism. Finally, as with all computational models of trauma, assumption with regard to material models may affect results. Complex nonlinear tissues were assumed to be linear elastic and viscoelastic materials such that study aims were achievable. While previous studies have suggested linear viscoelasticity and elasticity to represent an appropriate material model for impact (Arnoux et al., 2008;

Arnoux et al., 2008; Shen et al., 2008; Fijalkowski et al., 2009), select studies have suggested that more complex material models may better correlate with experimental results (Lee & Yang, 2001; Snedeker et al., 2007).

NINE

CONCLUSIONS AND FUTURE DIRECTIONS

This study identified splenic lacerations to result from close-proximity torso airbag interaction in normophysiologic vehicle occupants. These results were corroborated by injury observations in PMHS and biomechanical response in multi-body and finite element simulations. In PMHS experiments, torso biomechanical response was uniquely oblique with respect to anatomy, subjecting the posterolateral viscera to greater injury risk than unprotected lateral loading. Injury risk and viscoelastic tissue response was best correlated to deflection and viscous responses measured at 115° – 130° with respect to anterior direction, suggesting that dummy lateral instrumentation should be augmented by posterolateral response measurements. Further, results revealed that crash severity affected biomechanical and injury response, necessitating a dynamic out-of-position consideration beyond stationary tests currently employed.

The results of this study suggest that a number of future directions should be pursued. These research opportunities include expanded experimental methods, *in vivo* and *ex vivo* visceral response characterization, and computational parametric evaluation of loading gradations. These recommendations are briefly addressed in the remainder of this section.

An expansion of the experimental protocol is necessary to address dynamic occupants subjected to right side airbag loading. While right front passengers accounted for only 15% of NASS cases retrieved for analysis in this study (Chapter 4), 28% of

roadways worldwide carry traffic in a left-hand drive configuration (Kincaid, 1986), which typically places the driver on the right side of the vehicle. Observed asymmetry in biomechanical tolerance (Stalnaker et al., 1973) suggests the translation of injury metrics developed in this study to right side impact maybe not be direct. While no right side visceral lacerations, particularly to the liver, were observed in stationary posterolateral airbag loading, study results suggest that a dynamic occupant subjected to out-of-position right side impact may have increased exposure to visceral trauma risk compared to unprotected impact.

Torso compliance in this posterolateral region is not well understood. Pendulum impacts may assist in characterizing the biomechanical response of this region for dummy development and biofidelity. While typical pendulum impacts have employed 23.4 kg masses with moderate velocities, e.g., $\Delta V = 4.5 – 8.9$ m/s (Nusholtz et al., 1983; Viano, 1989; Yoganandan et al., 1996), deflection rates observed in this study exceeded 15 m/s. Therefore in addition to traditional pendulum impacts, posterolateral experiments also should employ high-rate low-mass impacts. These conditions would ensure that corridors were appropriate for airbag loading as observed in this study. Previous work has utilized small projectile testing to evaluate risk of lung contusion (Shen et al., 2005). Similar methodology may be appropriate.

An anatomically appropriate *in vivo* model may also delineate biomechanical injury risk functions with greater significance. Although the commonly utilized porcine model was rejected for this study (Chapter 8), other species may provide sufficient anatomic similarity to vehicular occupants. *In vivo* experiments also permit the observation of progressive degradation often associated with splenic trauma, as delayed

presentation is not uncommon (Parithivel et al., 2002; Ruffolo, 2002; Harbrecht et al., 2007; Davies et al., 2009). Similarly, an *ex vivo* experimental design should be undertaken to describe the response of this organ to blunt trauma in isolation. Prior work has employed surgically mobilized and saline-perfused viscera but has neglected the spleen beyond quasistatic loading (Fazekas et al., 1972; Melvin et al., 1973; Snedeker et al., 2005a). Also unknown is the quantitative relationship between splenic inflammation and the biomechanical and injury response of the organ. Perfusion pressures beyond accepted mean arterial pressure may be appropriate as a surrogate for physiologic inflammation. Because inflammation is associated with an increased risk of laceration (Rutkow, 1978; Rubin, 2003; Putukian et al., 2008; Shah et al., 2008), a quantitative injury risk study may delineate appropriate criteria for inclusion in dynamic posterolateral out-of-position test protocols. Resulting data would also be useful for material property measurement and further finite element model refinement.

A parametric loading study without airbag may delineate the relationship between visceral injury and varying gradations of posterolateral deformation. Such parametric studies are more befitting of computational methods, and the planar model developed in this study would be appropriate. Graded increases in deflection magnitude or deflection rate may induce complex material responses leading to the refinement of injury criteria presented. Greater complexity of loading may also define intra-abdominal visceral kinematics, which may play a role in injury mechanisms. Because these were partially neglected by the planar model, an expansion of the present model to three dimensions could be employed.

TEN

REFERENCES

AAAM. (2005). *Abbreviated injury scale - 2005 edition*. Barrington, IL: Association for the Advancement of Automotive Medicine.

Ahm, B., & Kim, J. Measurement and characterization of soft tissue behavior with surface deformation and force response under large deformations. *Medical Image Analysis*, 14(2), 2010, 138-148.

Akiyama, A., Okamoto, M., Ito, O., & Takahashi, Y. Development of omni-directional injury criteria for a pedestrian dummy for evaluating rib fracture. *SAE Trans. 2009-01-1210*. Warrendale, PA: Society of Automotive Engineers. 2009.

Arden, G. P., Christian, M. S., & Williams, E. J. Traumatic rupture of the spleen. *International Surgery*, 66(2), 1981, 149-153.

Arnoux, P. J., Serre, T., Cheynel, N., Thollon, L., Behr, M., Baque, P., & Brunet, C. Liver injuries in frontal crash situations a coupled numerical - experimental approach. *Computer Methods in Biomechanics and Biomedical Engineering*, 11(2), 2008, 189-203.

Automotive News. (2008, U.S. car sales by nameplate. *Automotive News*,

Backaitis, S. H., & Roberts, J. V. Occupant injury patterns in crashes with airbag equipped government sponsored cars. *31st Stapp Car Crash Conference*, New Orleans, Louisiana. 1987. 251-266.

Balaraman, K., Mukherjee, S., & Chawla, A. Inverse finite element characterization of soft tissues using impact experiments and taguchi methods. *SAE Trans. 2006-01-0252*. Warrendale, PA: Society of Automotive Engineers. 2006.

Bandak, F. A., & Eppinger, R. H. A three-dimensional finite element analysis of the human brain under combined rotational and translational accelerations. *38th Stapp Car Crash Conference*, Ft. Lauderdale, FL. 1994. 145-163.

Baur, P., Lange, W., Messner, G., Rauscher, S., & Pieske, O. Comparison of real world side impact/rollover collisions with and without thorax airbag/head protection system: A first field experience study. *Annual Proceedings of the Association for the Advancement of Automotive Medicine*, 44, 2000, 187-201.

Bedard, M., Guyatt, G. H., Stones, M. J., & Hirdes, J. P. The independent contribution of driver, crash, and vehicle characteristics to driver fatalities. *Accident; Analysis and Prevention,* 34(6), 2002, 717-727.

Behr, M., Arnoux, P. J., Serre, T., Bidal, S., Kang, H. S., Thollon, L., Cavallero, C., Kayvantash, K., & Brunet, C. A human model for road safety: From geometrical acquisition to model validation with radioss. *Computer Methods in Biomechanics & Biomedical Engineering,* 6(4), 2003, 263.

Beillas, P., Lafon, Y., & Smith, F. W. The effects of posture and subject-to-subject variations on the position, shape and volume of abdominal and thoracic organs. *Stapp Car Crash Journal,* 53, 2009, 127-154.

Berg, F. A., Schmitt, B., Epple, J., & Mattern, R. Dummy-loadings caused by an airbag in simulated out-of-position situations. *1997 International IRCOBI Conference,* Hannover, Germany. 1997. 419-431.

Bergman, R. A., Heidger, P. M., & Scott-Conner, C. E. H. (2002). The anatomy of the spleen. In A. J. Bowdler (Ed.), *The complete spleen* (2nd ed., pp. 3-10). USA: Humana Press.

Bilston, L. E. The effect of perfusion on soft tissue mechanical properties: A computational model. *Computer Methods in Biomechanics and Biomedical Engineering,* 5(4), 2002, 283-290.

Brandner, E. D., Wu, A., Chen, H., Heron, D., Kalnicki, S., Komanduri, K., Gerszten, K., Burton, S., Ahmed, I., & Shou, Z. Abdominal organ motion measured using 4D CT. *International Journal of Radiation Oncology, Biology, Physics,* 65(2), 2006, 554-560.

Braver, E. R., & Kyrychenko, S. Y. Efficacy of side air bags in reducing driver deaths in driver-side collisions. *American Journal of Epidemiology,* 159(6), 2004, 556-564.

Brunon, A., Bruyere-Garnier, K., & Coret, M. Mechanical characterization of liver capsule through uniaxial quasi-static tensile tests until failure. *Journal of Biomechanics,* in press.

Campbell, J. Q., Tannous, R. E., Takhounts, E. G., Martin, P. G., Eppinger, R. H., & Nguyen, T. On the development of a theoretically based, statistically justified, thoracic injury criterion. *19th International Technical Conference on the Enhanced Safety of Vehicles,* Washington, DC. 2005.

Campbell, J. Q., & Tannous, R. E. Using a finite element model to predict thoracic injuries. *IFMBE Proceedings,* 18, 2007, 690-692.

Carter, F. J., Frank, T. G., Davies, P. J., & Cuschieri, A. Puncture forces of solid organ surfaces. *Surgical Endoscopy*, 14(9), 2000, 783-786.

Carter, F. J., Frank, T. G., Davies, P. J., McLean, D., & Cuschieri, A. Measurements and modelling of the compliance of human and porcine organs. *Medical Image Analysis*, 5(4), 2001, 231-236.

Cavanaugh, J. M., Walilko, T. J., Malhotra, A., Zhu, Y., & King, A. I. Biomechanical response and injury tolerance of the thorax in twelve sled side impacts. *34th Stapp Car Crash Conference*, Orlando, FL. 1990. 23-38.

Cavanaugh, J. M., Zhu, Y., Huang, Y., & King, A. I. Injury and response of the thorax in side impact cadaveric tests. *37th Stapp Car Crash Conference*, San Antonio, TX. 1993. 199-221.

CDC. Injury preventiona and control: Data and statistics. Washington, DC: U.S. Centers for Disease Control and Prevention. 2010.

Cesari, D., Ramet, M., & Herry-Martin, D. Injury mechanisms in side impact. *22nd Stapp Car Crash Conference*, Ann Arbor, MI. 1978. 431-447.

Cesari, D., Ramet, M., & Bloch, J. Influence of arm position on thoracic injuries in side impact. *25th Stapp Car Crash Conference*, San Francisco, CA. 1981. 271-297.

Cesari, D., Zac, R., & Johnson, A. Evaluation of side impact protection in barrier to car tests. *27th Stapp Car Crash Conference*, San Diego, CA. 1983. 399-406.

Cheng, Z., Rizer, A. L., Pellettiere, J. A., & Aharonson-Daniel, L. Modelling and simulation of OOP occupant-airbag interaction. *SAE Trans. 2003-01-0510*. Warrendale, PA: Society of Automotive Engineers. 2003.

Cheynel, N., Serre, T., Arnoux, P. J., Ortega-Deballon, P., Benoit, L., & Brunet, C. Comparison of the biomechanical behavior of the liver during frontal and lateral deceleration. *The Journal of Trauma*, 67(1), 2009, 40-44.

Chiles, J. T., Mintzer, R. A., Hoffer, P. B., & Gottschalk, A. Splenic mobility and its effect on estimates of splenic mass. *Radiology*, 114(2), 1975, 407-410.

Christe, A., Ross, S., Oesterhelweg, L., Spendlove, D., Bolliger, S., Vock, P., & Thali, M. J. Abdominal trauma--sensitivity and specificity of postmortem noncontrast imaging findings compared with autopsy findings. *The Journal of Trauma*, 66(5), 2009, 1302-1307.

Chung, J., Cavanaugh, J. M., King, A. I., Koh, S. -., & Deng, Y. C. Thoracic injury mechanisms and biomechanical responses in lateral velocity pulse impacts. *43rd Stapp Car Crash Conference*, San Diego, CA. 1999.

Coben, L. E. The risk and benefits of airbag systems: Are they needlessly killing and injuring motorists?. *SAE Trans. 970492*. Warrendale, PA: Society of Automotive Engineers. 1997.

Copes, W. S., Champion, H. R., Sacco, W. J., Lawnick, M. M., Gann, D. S., Gennarelli, T. A., MacKenzie, E., & Schwaitzberg, S. Progress in characterizing anatomic injury. *The Journal of Trauma*, 30(10), 1990, 1200-1207.

Crandall, J. R., Bass, C. R., & Duma, S. M. Evaluation of 5th percentile female hybrid III thoracic biofidelity during out-of-position tests with a driver airbag. *SAE Trans. 980636*. Warrendale, PA: Society of Automotive Engineers. 1998.

Cummings, P., McKnight, B., Rivara, F. P., & Grossman, D. C. Association of driver air bags with driver fatality: A matched cohort study. *BMJ (Clinical Research Ed.)*, 324(7346), 2002, 1119-1122.

Dalmotas, D., German, A., & Tylko, S. The crash and field performance of side-mounted airbag systems. *17th International Technical Conference on the Enhanced Safety of Vehicles*, Amsterdam. 2001.

Dalmotas, D. J., German, A., Hendrick, B. E., & Hurley, R. M. Airbag deployments: The canadian experience. *The Journal of Trauma*, 38(4), 1995, 476-481.

Dargaud, R., & Bourdillon, T. Simulation of lateral impact with mobile deformable barrier. *SAE 860051*. Warrendale, PA: Society of Automotive Engineers. 1986.

Davies, B. N., & Withrington, P. G. The actions of drugs on the smooth muscle of the capsule and blood vessels of the spleen. *Pharmacological Reviews*, 25(3), 1973, 373-413.

Davies, D. A., Fecteau, A., Himidan, S., Mikrogianakis, A., & Wales, P. W. What's the incidence of delayed splenic bleeding in children after blunt trauma? an institutional experience and review of the literature. *The Journal of Trauma*, 67(3), 2009, 573-577.

Davies, P. J., Carter, F. J., & Cuschieri, A. Mathematical modelling for keyhole surgery simulations: A biomechanical model for spleen tissue. *IMA J Appl Math*, 67(1), 2002, 41-67.

de Lange, R., van Rooij, L., Mooi, H., & Wismans, J. Objective biofidelity rating of a numerical human occupant model in frontal to lateral impact. *Stapp Car Crash Journal*, 49, 2005, 457-479.

Deng, Y. C. Design considerations for occupant protection in side impact - a modeling approach. *32nd Stapp Car Crash Conference*, Atlanta, Georgia. 1988. 71-79.

Deng, Y. C. The importance of the test method in determining the effects of door padding in side impact. *33rd Stapp Car Crash Conference,* Washington, DC. 1989. 79-85.

Deng, Y. C., & Tzeng, B. Side impact countermeasure study using a hybrid modeling technique. *SAE Trans. 962413*. Warrendale, PA: Society of Automotive Engineers. 1996.

Deng, Y. C., Wang, J. T., Peng, J. H., & Kulkarni, S. An analytical study of side airbag designs for TTI reduction in a large size car. *SAE Trans. 982322*. Warrendale, PA: Society of Automotive Engineers. 1998.

Deng, Y. C., Kong, W., & Ho, H. Development of a finite element human thorax model for impact injury studies. *SAE Trans. 1999-01-0715*. Warrendale, PA: Society of Automotive Engineers. 1999.

Deodhar, H. A., Marshall, R. J., & Barnes, J. N. Increased risk of sepsis after splenectomy. *BMJ (Clinical Research Ed.),* 307(6916), 1993, 1408-1409.

Digges, K., Noureddine, A., Eskandarian, A., & Bedewi, N. E. Effect of occupant position and air bag inflation parameters on driver injury measures. *SAE Trans. 980637*. Warrendale, PA: Society of Automotive Engineers. 1998.

Dinas, A., & Fildes, B. N. Observations of seating position of front seat occupants relative to the side of the vehicle. *Annual Proceedings of the Association for the Advancement of Automotive Medicine,* 46, 2002, 27-43.

Dischinger, P. C., Cushing, B. M., & Kerns, T. J. Injury patterns associated with direction of impact: Drivers admitted to trauma centers. *The Journal of Trauma,* 35(3), 1993, 454-459.

Dissanaike, S., & Frezza, E. E. Laparoscopic splenectomy in blunt trauma. *JSLS : Journal of the Society of Laparoendoscopic Surgeons / Society of Laparoendoscopic Surgeons,* 10(4), 2006, 499-503.

Donaldson, W. F.,3rd, Hanks, S. E., Nassr, A., Vogt, M. T., & Lee, J. Y. Cervical spine injuries associated with the incorrect use of airbags in motor vehicle collisions. *Spine,* 33(6), 2008, 631-634.

Douglas, C. A., Fildes, B. N., Gibson, T. J., Bostrom, O., & Pintar, F. A. Modeling the seat belt to shoulder-complex interaction in far-side crashes. *20th International Technical Conference on the Enhanced Safety of Vehicles,* Lyon, France. 2007.

Drake, R. L., Vogl, W., & Mitchell, A. W. M. (2005). *Gray's anatomy for students* (1st ed.). Philadelphia: Churchill Livingstone.

Duma, S. M., Crandall, J. R., Hurwitz, S. R., & Pilkey, W. D. Small female upper extremity interaction with a deploying side air bag. *42nd Stapp Car Crash Conference,* Tempe, AZ. 1998. 47-63.

Duma, S. M., Boggess, B. M., Crandall, J. R., Hurwitz, S. R., Seki, K., & Aoki, T. Upper extremity interaction with a deploying side airbag: A characterization of elbow joint loading. *Accident; Analysis and Prevention,* 35(3), 2003a, 417-425.

Duma, S. M., Crandall, J. R., Rudd, R. W., & Kent, R. W. Small female head and neck interaction with a deploying side airbag. *Accident; Analysis and Prevention,* 35(5), 2003b, 811-816.

Durbin, D. R., Kallan, M. J., Elliott, M., Cornejo, R. A., Arbogast, K. B., & Winston, F. K. Risk of injury to restrained children from passenger air bags. *Traffic Injury Prevention,* 4(1), 2003, 58-63.

El-Alfy, M. S., & El-Sayed, M. H. Overwhelming postsplenectomy infection: Is quality of patient knowledge enough for prevention? *The Hematology Journal,* 5(1), 2004, 77-80.

Eppinger, R. H., Augustyn, K., & Robbins, D. H. Development of a promising universal thoracic trauma prediction methodology. *22nd Stapp Car Crash Conference,* Ann Arbor, MI. 1978. 221-268.

Eppinger, R. H., Marcus, J. H., & Morgan, R. M. Development of dummy and injury index for NHTSA's thoracic side impact protection research program. *SAE 840885*. Warrendale, PA: Society of Automotive Engineers. 1984.

Eppinger, R. H. On the development of a deformation measurement system and its application toward developing mechanically based injury indices. *33rd Stapp Car Crash Conference,* Washington, DC. 1989. 21-28.

EuroNCAP. Side impact testing protocol. Brussels, Belgium: European New Car Assessment Program. 2004a.

EuroNCAP. Assessment protocol and biomechanical limits. Brussels, Belgium: European New Car Assessment Program. 2004b.

Farke, A. A. Frontal sinuses and head-butting in goats: A finite element analysis. *The Journal of Experimental Biology,* 211(Pt 19), 2008, 3085-3094.

Fazekas, J. G., Kosa, F., Jobba, G., & Meszaros, E. Compression strength of the human spleen under the action of blunt force. [Beitrage zur Druckfistigkeit der menschlichen Milz bei stumpfen Krasseinwirkungen] *Archiv Fur Kriminologie,* 149(5), 1972, 158-174.

Fijalkowski, R. J., Yoganandan, N., Zhang, J., & Pintar, F. A. A finite element model of region-specific response for mild diffuse brain injury. *Stapp Car Crash Journal*, 53, 2009, 193-213.

Federal Motor Vehicle Safety Standard no. 214; Side Impact Protection, 49 CFR 571.214 (1998).

Forbes, P. A., Cronin, D. S., & Deng, Y. C. Multi-scale human body model to predict side impact thoracic trauma. *International Journal of Crashworthiness*, 11(3), 2006, 203-216.

Foret-Bruno, J. Y., Hartemann, F., Thomas, C., Tarriere, C., Loyat, B., Stcherbatcheff, G., Got, C., & Patel, A. Occupant velocity change in side impact method of calculation - application to a sample of real-world crashes. *24th Stapp Car Crash Conference,* Troy, MI. 1980. 329-373.

Funk, J. R., Cormier, J. M., & Gabler, H. C. Effect of delta-V errors in NASS on frontal crash risk calculations. *52nd Annual AAAM Conference*, 52, 2008, 155-164.

Furusu, K., Watanabe, I., Kato, C., Miki, K., & Hasegawa, J. Fundamental study of side impact analysis using the finite element model of the human thorax. *JSAE Review*, 22(2), 2001, 195-199.

Geraghty, E. M., Boone, J. M., McGahan, J. P., & Jain, K. Normal organ volume assessment from abdominal CT. *Abdominal Imaging,* 29(4), 2004, 482-490.

Gilchrist, M. D., O'Donoghue, D., & Horgan, T. J. A two-dimensional analysis of the biomechanics of frontal and occipital head impact injuries. *International Journal of Crashworthiness,* 6(2), 2001, 253-262.

Glass, J. M., & Gilbert, J. M. Splenectomy in a general hospital. *Journal of the Royal Society of Medicine*, 89(4), 1996, 199-201.

Graham, J. D., Goldie, S. J., Segui-Gomez, M., Thompson, K. M., Nelson, T., Glass, R., Simpson, A., & Woerner, L. G. Reducing risks to children in vehicles with passenger airbags. *Pediatrics,* 102(1), 1998, e3.

Gray, H. (1918). In Lewis W. H. (Ed.), *The anatomy of the human body* (20th ed.). Philadelphia: Lea & Febiger.

Guyton, A. C., & Hall, J. E. (2006). *Medical physiology* (11th ed.). Philadelphia: Saunders.

Hackney, J. R., Monk, M. W., Hollowell, W. T., Sullivan, L. K., & Willke, D. T. Results of the national highway traffic safety administration's thoracic side impact protection

research program. *SAE 840886*. Warrendale, PA: Society of Automotive Engineers. 1984.

Haland, Y., & Pipkorn, B. A parametric study of a side airbag system to meet deflection based criteria. *Journal of Biomechanical Engineering,* 118(3), 1996, 412-419.

Hallman, J. J., Yoganandan, N., & Pintar, F. A. Torso side airbag out-of-position evaluation using stationary and dynamic occupants. *Biomedical Sciences Instrumentation,* 44, 2008, 123-128.

Hallman, J. J., Brasel, K. J., Yoganandan, N., & Pintar, F. A. Splenic trauma as an adverse effect of torso-protecting side airbags: Biomechanical and case evidence. *Annals of Advances in Automotive Medicine,* 53, 2009a, 13-24.

Hallman, J. J., Yoganandan, N. A., & Pintar, F. A. Characterization of torso side airbag aggressivity. *Biomedical Sciences Instrumentation,* 45, 2009b, 101-106.

Hallman, J. J., Yoganandan, N., & Pintar, F. A. Thoracic injury metrics with side airbag: Stationary and dynamic occupants. *Traffic Injury Prevention,* 11(4), 2010, 433-442.

Happee, R., Ridella, S., Nayef, A., Morsink, P., de Lange, R., Bours, R., & van Hoof, J. Mathematical human body models representing a mid size male and a small female for frontal, lateral, and rearward impact loading. *2000 International IRCOBI Conference,* Montpellier, France. 2000. 67-89.

Harbrecht, B. G., Zenati, M. S., Ochoa, J. B., Puyana, J. C., Alarcon, L. H., & Peitzman, A. B. Evaluation of a 15-year experience with splenic injuries in a state trauma system. *Surgery,* 141(2), 2007, 229-238.

Harbrecht, B. G., Franklin, G. A., Miller, F. B., & Richardson, J. D. Is splenectomy after trauma an endangered species? *The American Surgeon,* 74(5), 2008, 410-412.

Hardy, W. N., Schneider, L. W., Reed, M. P., & Ricci, L. L. Biomechanical investigation of airbag-induced upper-extreminty injuries. *41st Stapp Car Crash Conference,* Lake Buena Vista, FL. 1997. 131-149.

Hartemann, F., Thomas, C., Foret-Bruno, J. Y., Henry, C., Fayon, A., & Tarriere, C. Description of lateral impacts. *6th International Technical Conference on the Enhanced Safety of Vehicles,* Washington, DC. 1976a. 541-562.

Hartemann, F., Thomas, C., Foret-Bruno, J. Y., Henry, C., Fayon, A., & Tarriere, C. Occupant protection in lateral impacts. *20th Stapp Car Crash Conference,* Dearborn, Michigan. 1976b. 191-219.

Hartemann, F., Foret-Bruno, J. Y., Thomas, C., Tarriere, C., Got, C., & Patel, A. Influence of mass ratio and structural compatibility on severity of injuries sustained

by the near side occupants in car-to-car side collisions. *23rd Stapp Car Crash Conference,* San Diego, California. 1979. 235-259.

Hartnett, K. L., Winchell, R. J., & Clark, D. E. Management of adult splenic injury: A 20-year perspective. *The American Surgeon,* 69(7), 2003, 608-611.

Hayashi, S., Yasuki, T., Yamamae, Y., & Takahira, Y. A study of side airbag effectiveness in reducing chest injury in car to car side impacts using a human FE model. *2006 International IRCOBI Conference,* Madrid, Spain. 2006. 397-400.

Hayashi, S., Yasuki, T., & Kitagawa, Y. Occupant kinematics and estimated effectiveness of side airbags in pole side impacts using a human FE model with internal organs. *Stapp Car Crash Journal,* 52, 2008, 363-377.

Hinch, J., Hollowell, W. T., Kanianthra, J., Evans, W. D., Klein, T., Longthorne, A., Ratchford, S., Morris, J., & Subramanian, R. Airbag technology in light passenger vehicles. Washington, DC: National Highway Traffic Safety Administration. 2001.

Hitchcock, R. J., & Nash, C. E. Protection of children and adults in crashes of cars with automatic restraints. *8th International Technical Conference on the Enhanced Safety of Vehicles,* Wolfsburg, Germany. 1980. 317-325.

Hobbs, C. A. Dispelling the misconceptions about side impact protection. *SAE Trans. 950879*. Warrendale, PA: Society of Automotive Engineers. 1995.

Horn, P., Sotonyi, P., & Repa, I. (2005). Cross-sectional CT and MR anatomy atlas of the domestic pig. University of Kaposvar, Lang Publishing and Holding Company.

Horsch, J. D., & Culver, C. C. A study of driver interactions with an inflating air cushion. *23rd Stapp Car Crash Conference,* San Diego, California. 1979.

Horsch, J. D., Lau, I. V., Andrzejak, D. V., Viano, D. C., Melvin, J. W., Pearson, J., Cok, D., & Miller, G. Assessment of air bag deployment loads. *34th Stapp Car Crash Conference,* Orlanda, Florida. 1990. 267-288.

Huang, Y., King, A. I., & Cavanaugh, J. M. A MADYMO model of near-side human occupants in side impacts. *Journal of Biomechanical Engineering,* 116(2), 1994, 228-235.

Iazzetti, G., & Rigutti, E. (2005). In Giunti Editorial Group (Ed.), *Atlas of anatomy* Taj.

Idelchik, I. E. (1986). In Martynenko O. G., Fried E. (Eds.), *Handbook of hydraulic resistance* (G. R. Malyavskaya Trans.). (2nd ed.). United States: Hemisphere.

Igarashi, T., Ehama, M., & Sunabashiri, Y. Development of side impact air bag system for head chest protection. *The 16th International Technical Conference on the*

Enhanced Safety of Vehicles Proceedings, Windsor, Ontario, Canada. 1998. 1708-1712.

IIHS. Recommended procedures for evaluating occupant injury risk from deploying side airbags. Arlington, VA: Insurance Institute for Highway Safety. 2003.

IIHS. Side impact crashworthiness evaluation: Crash test protocol. Arlington, VA: Insurance Institute for Highway Safety. 2008.

IIHS. (2010). *Vehicles equipped with side airbags.* Retrieved 2/11, 2010, from http://www.iihs.org/ratings/side_airbags/side_airbags.aspx

Irwin, A. L., Walilko, T. J., Cavanaugh, J. M., Zhu, Y., & King, A. I. Displacement responses of the shoulder and thorax in lateral sled impacts. *37th Stapp Car Crash Conference,* San Antonio, Texas. 1993. 165-173.

ISO. Road vehicles -- anthropomorphic side impact dummy -- lateral impact response requirements to assess the biofidelity of the dummy. *ISO/TR 9790*. Geneva, Switzerland: International Organization for Standardization. 1999.

Iwamoto, M., Kisanuki, Y., Watanabe, I., Furusu, K., Miki, K., & Hasegawa, J. Development of a finite element model of the total human model for safety (THUMS) and application to injury reconstruction. *2002 International IRCOBI Conference,* Munich, Germany. 2002. 31-42.

Jacquemoud, C., Bruyere-Garnier, K., & Coret, M. Methodology to determine failure characteristics of planar soft tissues using a dynamic tensile test. *Journal of Biomechanics*, 40(2), 2007, 468-475.

Johnson, N., Hampton, C., & Gabler, H. C. Evaluation of the accuracy of side impact crash test reconstructions. *Biomedical Sciences Instrumentation,* 45, 2009, 250-255.

Jonsson, A., Clemedson, C. J., Sundqvist, A. B., & Arvebo, E. Dynamic factors influencing the production of lung injury in rabbits subjected to blunt chest wall impact. *Aviation, Space, and Environmental Medicine,* 50(4), 1979, 325-337.

Jost, R., & Nurick, G. N. Finite element simulation of biomechanical response of the human body subjected to lateral impact. *International Journal of Crashworthiness,* 6(1), 2001, 123-134.

Kahane, C. J. An evaulation of side impact protection: FMVSS 214 TTI(d) improvements and side airbags. *DOT HS 810 748*. Washington, DC: National Highway Traffic Safety Administration. 2007.

Kallieris, D., Mattern, R., Schmidt, G., & Eppinger, R. H. Quantification of side impact responses and injuries. *25th Stapp Car Crash Conference,* San Francisco, CA. 1981. 329-366.

Kawamata, S., Ozawa, J., Hashimoto, M., Kurose, T., & Shinohara, H. Structure of the rat subcutaneous connective tissue in relation to its sliding mechanism. *Archives of Histology and Cytology,* 66(3), 2003, 273-279.

Kendall, J. L., Faragher, J., Hewitt, G. J., Burcham, G., & Haukoos, J. S. Emergency department ultrasound is not a sensitive detector of solid organ injury. *The Western Journal of Emergency Medicine,* 10(1), 2009, 1-5.

Kent, R., Crandall, J., Butcher, J., & Morris, R. Sled system requirements for the analysis of side impact thoraic injury criteria and occupant protection. *SAE Trans. 2001-0-0721*. Warrendale, PA: Society of Automotive Engineers. 2001.

Kent, R., Bass, C. R., Woods, W., Sherwood, C., Madeley, N. J., Salzar, R., & Kitagawa, Y. Muscle tetanus and loading condition effects on the elastic and viscous characteristics of the thorax. *Traffic Injury Prevention,* 4(4), 2003, 297-314.

Kent, R., Viano, D. C., & Crandall, J. The field performance of frontal air bags: A review of the literature. *Traffic Injury Prevention,* 6(1), 2005, 1-23.

Kent, R. W., Crandall, J. R., Bolton, J., Prasad, P., Nusholtz, G., & Mertz, H. The influence of superficial soft tissues and restraint condition on thoracic skeletal injury prediction. *Stapp Car Crash Journal,* 45, 2001, 183-204.

Kent, R. W. Frontal thoracic response to dynamic loading: The role of superficial tissues, viscera and the rib cage. *International Journal of Crashworthiness,* 13(3), 2008, 289-300.

Khadilkar, A. V., & Pauls, L. S. Assessment of injury protection performance of side impact airbags for out-of-position and other than 50th percentile adult male occupants. *The 16th International Technical Conference on the Enhanced Safety of Vehicles,* Windsor, Ontario, Canada. 1998. 1858-1867.

Khaewpong, N., Eppinger, R. H., & Morgan, R. M. Analytical trauma research using the chestband. *13th International Technical Conference on the Enhanced Safety of Vehicles,* Paris, France. 1991. 907-915.

Kim, Y. S., Park, S. H., Ahn, S. D., Lee, J. E., Choi, E. K., Lee, S. W., Shin, S. S., Yoon, S. M., & Kim, J. H. Differences in abdominal organ movement between supine and prone positions measured using four-dimensional computed tomography. *Radiotherapy and Oncology : Journal of the European Society for Therapeutic Radiology and Oncology,* 85(3), 2007, 424-428.

Kimpara, H., Lee, J. B., Yang, K. H., King, A. I., Iwamoto, M., Watanabe, I., & Miki, K. Development of a three-dimensional finite element chest model for the 5(th) percentile female. *Stapp Car Crash Journal,* 49, 2005, 251-269.

Kincaid, P. (1986). *The rule of the road: An international guide to history and practice.* USA: Greenwood Press.

Kirk, A., & Morris, A. Side airbag deployments in the UK - initial case reviews. *18th International Technical Conference on the Enhanced Safety of Vehicles,* Nagoya, Japan. 2003.

Kiss, M. Z., Varghese, T., & Hall, T. J. Viscoelastic characterization of in vitro canine tissue. *Physics in Medicine and Biology,* 49(18), 2004, 4207-4218.

Kiuchi, T., Ogata, K., Warner, C. Y., & Gordon, J. J. Air bag system for side impact occupant protection. *The 13th International Technical Conference on the Enhanced Safety of Vehicles,* Paris, France. 1991. 533-541.

Kleinberger, M., & Summers, L. Mechanisms of injuries for adults and children resulting from airbag interaction. *Annual Proceedings of the Association for the Advancement of Automotive Medicine,* 41, 1997, 405-420.

Kleinberger, M., Yoganandan, N., & Kumaresan, S. Review: Biomechanics of child occupant protection. *Journal of Crash Prevention and Injury Control,* 2(1), 2000, 63-73.

Kotsanas, D., Al-Souffi, M. H., Waxman, B. P., King, R. W., Polkinghorne, K. R., & Woolley, I. J. Adherence to guidelines for prevention of postsplenectomy sepsis. age and sex are risk factors: A five-year retrospective review. *ANZ Journal of Surgery,* 76(7), 2006, 542-547.

Kucharova, M., Doubal, S., Klemera, P., Rejchrt, P., & Navratil, M. Viscoelasticity of biological materials - measurement and practical impact on biomedicine. *Physiological Research / Academia Scientiarum Bohemoslovaca,* 56 Suppl 1, 2007, S33-7.

Kuijpers, A. H., Claessens, M. H., & Sauren, A. A. The influence of different boundary conditions on the response of the head to impact: A two-dimensional finite element study. *Journal of Neurotrauma,* 12(4), 1995, 715-724.

Kuppa, S., Eppinger, R. H., McKoy, F., Nguyen, T., Pintar, F. A., & Yoganandan, N. Development of side impact thoracic injury criteria and their application to the modified ES-2 dummy with rib extensions (ES-2re). *Stapp Car Crash Journal,* 47, 2003, 189-210.

Kuppa, S. M., & Eppinger, R. H. Development of an improved thoracic injury criterion. *42nd Stapp Car Crash Conference,* Tempe, AZ. 1998.

Lafon, Y., Smith, F. W., & Beillas, P. Combination of a model-deformation method and a positional MRI to quantify the effects of posture on the anatomical structures of the trunk. *Journal of Biomechanics,* In Press, Corrected Proof, 2010

Lancaster, G. I., DeFrance, J. H., & Borruso, J. J. Air-bag-associated rupture of the right atrium. *The New England Journal of Medicine,* 328(5), 1993, 358.

Langwieder, K., Hummel, T. A., & Anselm, D. The effect of airbags on injuries and accident costs. *16th International Technical Conference on the Enhanced Safety of Vehicles,* Windsor, Ontario, Canada. 1998. 338-358.

Lau, I. V., & Viano, D. C. The viscous criterion - bases and applications of an injury severity index for soft tissues. *30th Stapp Car Crash Conference,* San Diego, CA. 1986. 123-142.

Lau, I. V., Capp, J. P., & Obermeyer, J. A. A comparison of frontal and side impact: Crash dynamics, countermeasures, and subsystem tests. *35th Stapp Car Crash Conference,* San Diego, California. 1991. 109-124.

Lau, I. V., Horsch, J. D., Viano, D. C., & Andrzejak, D. V. Mechanism of injury from air bag deployment loads. *Accident; Analysis and Prevention,* 25(1), 1993, 29-45.

Lau, V. K., & Viano, D. C. Influence of impact velocity on the severity of nonpenetrating hepatic injury. *The Journal of Trauma,* 21(2), 1981, 115-123.

Lee, J. B., & Yang, K. H. Development of a finite element model of the human abdomen. *Stapp Car Crash Journal,* 45, 2001, 79-100.

Leppaniemi, A., Haapiainen, R., Standertskjold-Nordenstam, C. G., Taavitsainen, M., & Hastbacka, J. Delayed presentation of blunt splenic injury. *American Journal of Surgery,* 155(6), 1988, 745-749.

Liu, P., Li, P., He, W., & Zhao, L. Q. Liver and spleen volume variations in patients with hepatic fibrosis. *World Journal of Gastroenterology : WJG,* 15(26), 2009, 3298-3302.

Lizee, E., Robin, S., Song, E., Bertholon, N., Le Coz, J. Y., Besnault, B., & Lavaste, F. Development of a 3D finite element model of the human body. *42nd Stapp Car Crash Conference,* Tempe, Arizona. 1998.

Lobdell, T. E., Kroell, C. K., Schneider, D. C., Hering, W. E., & Nahum, A. M. (1973). Impact response of the human thorax. *Human impact response: Measurement and simulation* (pp. 201-245). New York: Plenum Press.

Louden, A. E. Side airbag out-of-position testing of recent model year vehicles. *20th International Technical Conference on the Enhanced Safety of Vehicles,* Lyon, France. 2007.

Lundell, B., Edvardsson, M., Johansson, L., Korner, J., & Pilhall, S. SIPSBAG - the seat-mounted side impact airbag system. *SAE Trans. 950878*. Warrendale, PA: Society of Automotive Engineers. 1995.

Madoff, D. C., Denys, A., Wallace, M. J., Murthy, R., Gupta, S., Pillsbury, E. P., Ahrar, K., Bessoud, B., & Hicks, M. E. Splenic arterial interventions: Anatomy, indications, technical considerations, and potential complications. *Radiographics : A Review Publication of the Radiological Society of North America, Inc,* 25 Suppl 1, 2005, S191-211.

Mahangare, M., Trepess, D., Blundell, M., Freisinger, M., Hoffmann, J., & Smith, S. J. A methodology for the simulation of out-of-position driver airbag deployment. *International Journal of Crashworthiness,* 11(6), 2006, 511-517.

Malczyk, A., & Adomeit, H. -. The airbag folding pattern as a means for injury reduction of out-of-position occupants. *39th Stapp Car Crash Conference,* San Diego, CA. 1995. 19-35.

Maltese, M. R., Eppinger, R. H., Rhule, H. H., Donnelly, B. R., Pintar, F. A., & Yoganandan, N. Response corridors of human surrogates in lateral impacts. *Stapp Car Crash Journal,* 46, 2002, 321-351.

Mao, Y., & Appel, H. Influence of air bag folding pattern on OOP-injury potential. *SAE Trans. 2001-01-0164*. Warrendale, PA: Society of Automotive Engineers. 2001.

Marcus, J. H., Morgan, R. M., Eppinger, R. H., Kallieris, D., Mattern, R., & Schmidt, G. Human response to and injury from lateral impact. *27th Stapp Car Crash Conference,* San Diego, CA. 1983. 419-432.

Marine, M. C., & Werner, S. M. Delta-V analysis from crash test data for vehicles with post-impact yaw motion. *SAE Trans. 980219*. Warrendale, PA: Society of Automotive Engineers. 1998.

Marklund, P. O., & Nilsson, L. Simulation of airbag inflation processes using a coupled fluid structure approach. *Computational Mechanics,* 29(5), 2002, 289-297.

McCartt, A. T., & Kyrychenko, S. Y. Efficacy of side airbags in reducing driver deaths in driver-side car and SUV collisions. *Traffic Injury Prevention,* 8(2), 2007, 162-170.

McCullagh, P., & Nelder, J. A. (1990). *Generalized linear models*. New York: Chapman & Hall.

McElhaney, J. H., Stalnaker, R. L., Roberts, V. L., & Snyder, R. G. Door crashworthiness criteria. *15th Stapp Car Crash Conference,* San Diego, CA. 1971. 489-517.

McGwin, G.,Jr, Metzger, J., Porterfield, J. R., Moran, S. G., & Rue, L. W.,3rd. Association between side air bags and risk of injury in motor vehicle collisions with near-side impact. *The Journal of Trauma,* 55(3), 2003, 430-434.

McGwin, G.,Jr, Metzger, J., & Rue, L. W.,3rd. The influence of side airbags on the risk of head and thoracic injury after motor vehicle collisions. *The Journal of Trauma,* 56(3), 2004, 512-516.

McGwin, G.,Jr, Modjarrad, K., Duma, S., & Rue, L. W.,3rd. Association between upper extremity injuries and side airbag availability. *The Journal of Trauma,* 64(5), 2008, 1297-1301.

McKay, M. P. The national highway traffic safety administration and special crash investigations. *Annals of Emergency Medicine,* 41(4), 2003, 576-578.

McLellan, B. A., Rizoli, S. B., Brenneman, F. D., Boulanger, B. R., Sharkey, P. W., & Szalai, J. P. Injury pattern and severity in lateral motor vehicle collisions: A canadian experience. *The Journal of Trauma,* 41(4), 1996, 708-713.

Melvin, J. W., Stalnaker, R. L., Roberts, V. L., & Trollope, M. L. Impact injury mechanismsin abdominal organs. *17th Stapp Car Crash Conference,* Oklahoma City, OK. 1973. 115-126.

Melvin, J. W., Robbins, D. H., & Stalnaker, R. L. Side impact response and injury. *Sixth International Technical Conference on the Enhanced Safety of Vehicles,* London. 1976. 681-689.

Melvin, J. W., O'Day, J., Campbell, K. L., Robbins, D. H., & Huelke, D. F. Side impacts: A comparison of laboratory experiments and NCSS crashes. *SAE 800176*. Warrendale, PA: Society of Automotive Engineers. 1980.

Melvin, J. W., Horsch, J. D., McCleary, J. D., Wideman, L. C., Jensen, J. L., & Wolanin, M. J. Assessment of airbag deployment loads with the small female hybrid III dummy. *37th Stapp Car Crash Conference,* San Antonio, TX. 1993.

Mertz, H. J., Driscoll, G. D., Lenox, J. B., Nyquist, G. W., & Weber, D. A. Responses of animals exposed to deployment of various passenger inflatable restraint system concepts for a variety of collision severities and animal positions. *9th International Technical Conference on the Enhanced Safety of Vehicles,* Koyoto, Japan. 1982. 352-368.

Mertz, H. J. Restraint performance of the 1973-76 GM air cushion restraint system. *SAE 880400*. Warrendale, PA: Society of Automotive Engineers. 1988.

Miller, M. A. The biomechanical response of the lower abdomen to belt restraint loading. *The Journal of Trauma,* 29(11), 1989, 1571-1584.

Miller, P. M.,Jr., & Gu, H. Sled testing procedure for side impact airbag development. *SAE Trans. 970570*. Warrendale, PA: Society of Automotive Engineers. 1997.

Mizuno, K., Iwata, K., Deguchi, T., Ikami, T., & Kubota, M. Development of a three-year-old child FE model. *Traffic Injury Prevention,* 6(4), 2005, 361-371.

Mohr, M., Abrams, E., Engel, C., Long, W. B., & Bottlang, M. Geometry of human ribs pertinent to orthopedic chest-wall reconstruction. *Journal of Biomechanics,* 40(6), 2007, 1310-1317.

Monk, M. W., Morgan, R. M., & Sullivan, L. K. Side impact sled and padding development. *24th Stapp Car Crash Conference,* Troy, Michigan. 1980. 257-326.

Morgan, R. M., & Waters, H. P. Comparison of two promising side impact dummies. *8th International Technical Conference on the Experimental Safety of Vehicles,* Wolfsburg, Germany. 1980. 472-482.

Morgan, R. M., Marcus, J. H., & Eppinger, R. H. Correlation of side impact dummy / cadaver tests. *25th Stapp Car Crash Conference,* San Francisco, CA. 1981. 301-326.

Morgan, R. M., Marcus, J. H., & Eppinger, R. H. Side impact —the biofidelity of NHTSA's proposed ATD and efficacy of TTI. *30th Stapp Car Crash Conference,* San Diego, CA. 1986. 27-40.

Morgan, R. M., Eppinger, R. H., Haffner, M. P., Yoganandan, N., Pintar, F. A., Sances, A., Crandall, J. R., Pilkey, W. D., Klopp, G. S., Kallieris, D., Miltner, E., Mattern, R., Kuppa, S. M., & Sharpless, C. L. Thoracic trauma assessment formulations for restrained drivers in simulated frontal impacts. *38th Stapp Car Crash Conference,* Ft. Lauderdale, Florida. 1994. 15-34.

Morris, J. B. Airbags for small cars. *SAE Trans. 851200*. Warrendale, PA: Society of Automotive Engineers. 1985.

Morris, A., Welsh, R., Thomas, P., & Kirk, A. Head and chest injury outcomes in struck-side crashes. *2005 International IRCOBI Conference,* Prague, Czech Republic. 2005. 73-83.

Morris, C. R., Zuby, D. S., & Lund, A. K. Measuring airbag injury risk to out-of-position occupants. *The 16th International Technical Conference on the Enhanced Safety of Vehicles Proceedings,* Windsor, Ontario, Canada. 1998. 1036-1043.

Morris, R. A., Crandall, J. R., & Pilkey, W. D. Multibody modelling of a side impact test apparatus. *International Journal of Crashworthiness,* 4(1), 1999, 17-29.

Moss, A. A., Friedman, M. A., & Brito, A. C. Determination of liver, kidney, and spleen volumes by computed tomography: An experimental study in dogs. *Journal of Computer Assisted Tomography,* 5(1), 1981, 12-14.

Murakami, D., Kobayashi, S., Torigaki, T., & Kent, R. Finite element analysis of hard and soft tissue contributions to thoracic response: Sensitivity analysis of fluctuations in boundary conditions. *Stapp Car Crash Journal,* 50, 2006, 169-189.

Mustard, R. A.,Jr, Hanna, S. S., Blair, G., Harrison, A. W., Taylor, G. A., Miller, H. A., & Maggisano, R. Blunt splenic trauma: Diagnosis and management. *Canadian Journal of Surgery.Journal Canadien De Chirurgie,* 27(4), 1984, 330-333.

Nasseri, S., Bilston, L. E., & Phan-Tien, N. Viscoelastic properties of pig kidney in shear, experimenteal results and modelling. *Rheologica Acta,* 41, 2002, 180-192.

Naumann, R. B., Dellinger, A. M., Zaloshnja, E., Lawrence, B. A., & Miller, T. R. Incidence and total lifetime costs of motor vehicle-related fatal and nonfatal injury by road user type, united states, 2005. *Traffic Injury Prevention,* 11(4), 2010, 353-360.

Nava, A., Mazza, E., Furrer, M., Villiger, P., & Reinhart, W. H. In vivo mechanical characterization of human liver. *Medical Image Analysis,* 12(2), 2008, 203-216.

Naylor, R., Coln, D., & Shires, G. T. Morbidity and mortality from injuries to the spleen. *The Journal of Trauma,* 14(9), 1974, 773-778.

Neathery, R. F., & Lobdell, T. E. Mechanical simulation of human thorax under impact. *17th Stapp Car Crash Conference,* Oklahoma City, Oklahoma. 1973. 451-466.

Netter, F. H. (2006). *Atlas of human anatomy* (4th ed.). Philadelphia: Saunders.

Newgard, C. D., & Lewis, R. J. Effects of child age and body size on serious injury from passenger air-bag presence in motor vehicle crashes. *Pediatrics,* 115(6), 2005, 1579-1585.

NHTSA. Actions to reduce the adverse effects of airbags: Depowering. final regulatory evaluation. Washington, DC: National Highway Traffic Safety Administration. 1997.

NHTSA. National automotive sampling system analytical user's manual. Washington, DC: National Highway Traffic Safety Administration. 1999.

NHTSA. Effectiveness of occupant protection systems and their use: Report to congress. *DOT HS 809 442*. Washington, DC: National Highway Traffic Safety Administration. 2001.

NHTSA. Counts of airbag related fatalities and seriously injured persons. *AB0708*. Washington, DC: National Highway Traffic Safety Administration. 2008a.

NHTSA. Laboratory test procedure for new car assessment program side impact moving deformable barrier testing. Washington, DC: National Highway Traffic Safety Administration. 2008b.

Niehoff, P., & Gabler, H. C. The accuracy of WinSmash delta-V estimates: The influence of vehicle type, stiffness, and impact mode. *50th Annual AAAM Conference,* 50, 2006, 73-89.

Nirula, R., Talmor, D., & Brasel, K. Predicting significant torso trauma. *The Journal of Trauma,* 59(1), 2005, 132-135.

Nirula, R., & Pintar, F. A. Identification of vehicle components associated with severe thoracic injury in motor vehicle crashes: A CIREN and NASS analysis. *Accident; Analysis and Prevention,* 40(1), 2008, 137-141.

Nusholtz, G. S., Melvin, J. W., Mueller, G., MacKenzie, J. R., & Burney, R. Thoracoabdominal response and injury. *24th Stapp Car Crash Conference,* Troy, Michigan. 1980. 189-228.

Nusholtz, G. W., Melvin, J. W., & Lux, P. The influence of impact energy and direction on thoracic response. *27th Stapp Car Crash Conference,* San Diego, California. 1983. 69-94.

Olson, C. M., Cummings, P., & Rivara, F. P. Association of first- and second-generation air bags with front occupant death in car crashes: A matched cohort study. *American Journal of Epidemiology,* 164(2), 2006, 161-169.

Olsson, J. A., Skotte, L. G., & Svensson, S. E. Air bag system for side impact protection. *The 12th International Technical Conference on the Enhanced Safety of Vehicles,* Goteborg, Sweden. 1989. 976-983.

O'Sullivan, S. T., Reardon, C. M., O'Donnell, J. A., Kirwan, W. O., & Brady, M. P. "How safe is splenectomy?". *Irish Journal of Medical Science,* 163(8), 1994, 374-378.

Page, Y., Thomas, P., Herve, V., & Kirk, A. The effectiveness of side airbags in preventing thoracic injuries in europe. *2nd International Expert Symposium on Accident Research,* Hannover, Germany. 2006.

Parithivel, V. S., Sajja, S. B., Basu, A., Schein, M., & Gerst, P. H. Delayed presentation of splenic injury: Still a common syndrome. *International Surgery,* 87(2), 2002, 120-124.

Park, W., & Hong, S. A study on the modelling technique for the passenger out-of-position simulation. *SAE Trans. 2005-01-1298*. Warrendale, PA: Society of Automotive Engineers. 2005.

Petit, P., Trosseille, X., Baudrit, P., & Gopal, M. Finite element simulation study of a frontal driver airbag deployment for out-of-position situations. *Stapp Car Crash Journal,* 47, 2003, 211-241.

Pintar, F. A., Yoganandan, N., Sances, A., & Eppinger, R. H. Instrumentation of human surrogates for side impact. *40th Stapp Car Crash Conference,* Albuquerque, NM. 1996. 29-42.

Pintar, F. A., Yoganandan, N., Hines, M. H., Maltese, M. R., McFadden, J., Saul, R., Eppinger, R. H., Khaewpong, N., & Kleinberger, M. Chestband analysis of human tolerance to side impact. *41st Stapp Car Crash Conference,* Lake Buena Vista, FL. 1997. 63-74.

Pintar, F. A., Yoganandan, N., Maltese, M. R., Samaha, R. R., & Eppinger, R. H. Three-year-old child out-of-position side airbag studies. *43rd Stapp Car Crash Conference,* San Diego, CA. 1999. 25-38.

Pintar, F. A., Maiman, D. J., & Yoganandan, N. Injury patterns in side pole crashes. *51st Annual AAAM Conference,* 51, 2007, 419-433.

Pipkorn, B., & Haland, Y. A side airbag system to meet chest injury measures: Evaluation by mathematical simulations. *International Journal of Crashworthiness,* 1(2), 1996, 145-161.

Plank, G. R., & Eppinger, R. H. An improved finite element model of the human thorax. *13th International Technical Conference on the Enhanced Safety of Vehicles,* Paris, France. 1991. 902-907.

Plank, G. R., Kleinberger, M., & Eppinger, R. H. Analytical investigation of driver thoracic response to out-of-position airbag deployment. *42nd Stapp Car Crash Conference,* Tempe, AZ. 1998.

Pottakkat, B., Kashyap, R., Kumar, A., Sikora, S. S., Saxena, R., & Kapoor, V. K. Redefining the role of splenectomy in patients with idiopathic splenomegaly. *ANZ Journal of Surgery,* 76(8), 2006, 679-682.

Power, E. D., Duma, S. M., Stitzel, J. D., Herring, I. P., West, R. L., Bass, C. R., Crowley, J. S., & Brozoski, F. T. Computer modeling of airbag-induced ocular injury in pilots wearing night vision goggles. *Aviation, Space, and Environmental Medicine,* 73(10), 2002, 1000-1006.

Prasad, A. K., Samaha, R. R., & Louden, A. E. Evaluation of injury risk from side impact air bags. *17th International Technical Conference on the Enhanced Safety of Vehicles,* Amsterdam. 2001.

Putukian, M., O'Connor, F. G., Stricker, P., McGrew, C., Hosey, R. G., Gordon, S. M., Kinderknecht, J., Kriss, V., & Landry, G. Mononucleosis and athletic participation: An evidence-based subject review. *Clinical Journal of Sport Medicine : Official Journal of the Canadian Academy of Sport Medicine,* 18(4), 2008, 309-315.

Pyttel, T., Floss, A., Thibaud, C., & Goertz, C. Realistic simulation models for airbags and humans-new possibilities and limits of FE simulation. *International Journal of Crashworthiness,* 12(5), 2007, 481-492.

Quinones-Hinojosa, A., Jun, P., Manley, G. T., Knudson, M. M., & Gupta, N. Airbag deployment and improperly restrained children: A lethal combination. *The Journal of Trauma,* 59(3), 2005, 729-733.

Reiff, D. A., McGwin, G.,Jr, & Rue, L. W.,3rd. Splenic injury in side impact motor vehicle collisions: Effect of occupant restraints. *The Journal of Trauma,* 51(2), 2001, 340-345.

Rietzel, E., Rosenthal, S. J., Gierga, D. P., Willet, C. G., & Chen, G. T. Moving targets: Detection and tracking of internal organ motion for treatment planning and patient set-up. *Radiotherapy and Oncology : Journal of the European Society for Therapeutic Radiology and Oncology,* 73 Suppl 2, 2004, S68-72.

Robbins, D. H., Melvin, J. W., & Stalnaker, R. L. The prediction of thoracic impact injuries. *20th Stapp Car Crash Conference,* Dearborn, MI. 1976. 699-729.

Robbins, D. H., & Lehman, R. J. Predition of thoracic injuries as a function of occupant kinematics. *Seventh International Technical Conference on the Experimental Safety of Vehicles,* Paris, France. 1979. 374-383.

Roberts, J. C., Merkle, A. C., Biermann, P. J., Ward, E. E., Carkhuff, B. G., Cain, R. P., & O'Connor, J. V. Computational and experimental models of the human torso for non-penetrating ballistic impact. *Journal of Biomechanics,* 40(1), 2007, 125-136.

Roberts, V. L., & Compton, C. P. The relationship between delta v and injury. *37th Stapp Car Crash Conference,* San Antonio, TX. 1993. 35-41.

Robertson, F., Leander, P., & Ekberg, O. Radiology of the spleen. *European Radiology,* 11(1), 2001, 80-95.

Roselt, T., Langwieder, K., Hummel, T. A., & Koester, H. J. Injury patterns of front seat occupants in frontal car collisions with airbags. *2002 International IRCOBI Conference,* Munich. 2002.

Rosen, J., Brown, J. D., De, S., Sinanan, M., & Hannaford, B. Biomechanical properties of abdominal organs in vivo and postmortem under compression loads. *Journal of Biomechanical Engineering*, 130(2), 2008, 021020.

Rouhana, S. W., Lau, I. V., & Ridella, S. A. Influence of velocity and forced compression on the severity of abdominal injury in blunt, nonpenetrating lateral impact. *The Journal of Trauma*, 25(6), 1985, 490-500.

Rouhana, S. W., & Kroell, C. K. The effect of door topography on abdominal injury in lateral impact. *33rd Stapp Car Crash Conference,* Washington, DC. 1989. 143-151.

Rouhana, S. W. (1993). Biomechanics of abdominal trauma. In A. M. Nahum, & J. W. Melvin (Eds.), *Accidental injury: Biomechanics and prevention* (pp. 391-428). New York: Springer-Verlag.

Roychoudhury, R., Sun, D., Hamid, M., & Hanson, C. 5th percentile driver out of position computer simulation. *SAE Trans. 2000-01-1006*. Warrendale, PA: Society of Automotive Engineers. 2000.

Ruan, J., El-Jawahri, R., Chai, L., Barbat, S., & Prasad, P. Prediction and analysis of human thoracic impact responses and injuries in cadaver impacts using a full human body finite element model. *Stapp Car Crash Journal*, 47, 2003, 299-321.

Ruan, J. S., El-Jawahri, R., Barbat, S., & Prasad, P. Biomechanical analysis of human abdominal impact responses and injuries through finite element simulations of a full human body model. *Stapp Car Crash Journal*, 49, 2005, 343-366.

Ruan, J. S., El-Jawahri, R., Rouhana, S. W., Barbat, S., & Prasad, P. Analysis and evaluation of the biofidelity of the human body finite element model in lateral impact simulations according to ISO-TR9790 procedures. *Stapp Car Crash Journal*, 50, 2006, 491-507.

Rubin, A. (2003). *Sports injuries and emergencies: A quick response manual*. USA: McGraw-Hill.

Ruff, C., Jost, T., & Eichberger, A. Simulation of an airbag deployment in out-of-position situations. *Vehicle System Dynamics*, 45(10), 2007, 953-967.

Ruffolo, D. C. Delayed splenic rupture: Understanding the threat. *Journal of Trauma Nursing : The Official Journal of the Society of Trauma Nurses*, 9(2), 2002, 34-40.

Rutkow, I. M. Rupture of the spleen in infectious mononucleosis: A critical review. *Archives of Surgery (Chicago, Ill.: 1960)*, 113(6), 1978, 718-720.

Ryb, G. E., Dischinger, P. C., Kufera, J. A., & Burch, C. A. Delta V, principal direction of force, and restraint use contributions to motor vehicle crash mortality. *The Journal of Trauma,* 63(5), 2007, 1000-1005.

Samaha, R. R., & Elliott, D. S. NHTSA side impact research: Motivation for upgraded test procedures. *18th International Technical Conference on the Enhanced Safety of Vehicles*, Nagoya, Japan. 2003.

Saraf, H., Ramesh, K. T., Lennon, A. M., Merkle, A. C., & Roberts, J. C. Mechanical properties of soft human tissues under dynamic loading. *Journal of Biomechanics,* 40(9), 2007a, 1960-1967.

Saraf, H., Ramesh, K. T., Lennon, A. M., Merkle, A. C., & Roberts, J. C. Measurement of the dynamic bulk and shear response of soft human tissues. *Experimental Mechanics*, 47(3), 2007b, 439-449.

Scally, J. T., McCullough, C. A., Brown, L. J., & Eppinger, R. Development of the crash injury research and engineering network. *International Journal of Trauma Nursing,* 5(4), 1999, 136-138.

Schmitt, K. U., & Snedeker, J. G. Analysis of the biomechanical response of kidneys under blunt impact. *Traffic Injury Prevention,* 7(2), 2006, 171-181.

Schneider, L. W., Robbins, D. H., Pflueg, M. A., & Snyder, R. G. (1985). *Anthropometry of motor vehicle occupants*. Washington, DC: National Highway Traffic Safety Administration.

Schroeder, G., Kallieris, D., Tschaeschke, U., Scheunert, D., Schuetz, J., & Zobel, R. Are side airbags dangerous in certain seating positions? *1998 International IRCOBI Conference,* Goeteborg, Sweden. 1998. 447-483.

Seki, S., & Iwamoto, H. Disruptive forces for swine heart, liver, and spleen: Their breaking stresses. *The Journal of Trauma,* 45(6), 1998, 1079-1083.

Shackford, S. R. (2002). In Thal E. R., Weigelt J. A. and Carrico C. J. (Eds.), *Operative trauma management* (2nd ed.). New York: McGraw-Hill.

Shah, M., Muquit, S., & Azam, B. Infective splenic rupture presenting with symptoms of a pulmonary embolism. *Emergency Medicine Journal : EMJ,* 25(12), 2008, 855-856.

Shatney, C. H. Complications of splenectomy. *Acta Anaesthesiologica Belgica,* 38(4), 1987, 333-339.

Shaw, J. M., Herriott, R. G., McFadden, J. D., Donnelly, B. R., & Bolte, J. H.,4th. Oblique and lateral impact response of the PMHS thorax. *Stapp Car Crash Journal,* 50, 2006, 147-167.

Shen, W., Niu, Y., & Stuhmiller, J. H. Biomechanically based criteria for rib fractures induced by high-speed impact. *The Journal of Trauma*, 58(3), 2005, 538-545.

Shen, W., Niu, Y., Mattrey, R. F., Fournier, A., Corbeil, J., Kono, Y., & Stuhmiller, J. H. Development and validation of subject-specific finite element models for blunt trauma study. *Journal of Biomechanical Engineering*, 130(2), 2008, 021022.

Siegel, J. H., Mason-Gonzalez, S., Dischinger, P., Cushing, B., Read, K., Robinson, R., Smialek, J., Heatfield, B., Hill, W., & Bents, F. Safety belt restraints and compartment intrusions in frontal and lateral motor vehicle crashes: Mechanisms of injuries, complications, and acute care costs. *The Journal of Trauma*, 34(5), 1993, 736-58; discussion 758-9.

Sieveka, E., Crandall, J. R., Duma, S. M., & Pilkey, W. Development and application of a side airbag computer model using the CVS/ATB multi-body dynamics program. *16th International Technical Conference on the Enhanced Safety of Vehicles*, Windsor, Ontario, Canada. 1998. 1925-1935.

Sieveka, E. M., Kent, R. W., & Crandall, J. R. Comparison of seat belt force-limiting methods using the MADYMO multi-body/finite element program. *Annual Proceedings of the Association for the Advancement of Automotive Medicine*, 45, 2001, 11-21.

Skandalakis, P. N., Colborn, G. L., Skandalakis, L. J., Richardson, D. D., Mitchell, W. E.,Jr, & Skandalakis, J. E. The surgical anatomy of the spleen. *The Surgical Clinics of North America*, 73(4), 1993, 747-768.

Smith, G. R. Airbag update- recent crash case histories. *SAE 770155*. Warrendale, PA: Society of Automotive Engineers. 1977.

Smith, M. J., Kaleto, H. A., Nowak, T. J., & Gotwals, D. G. Advancements in equipment and testing methodologies for airbag systems in response to changes to federal safety requirements. *SAE Trans. 2003-01-0497*. Warrendale, PA: Society of Automotive Engineers. 2003.

Snedeker, J. G., Barbezat, M., Niederer, P., Schmidlin, F. R., & Farshad, M. Strain energy density as a rupture criterion for the kidney: Impact tests on porcine organs, finite element simulation, and a baseline comparison between human and porcine tissues. *Journal of Biomechanics*, 38(5), 2005a, 993-1001.

Snedeker, J. G., Niederer, P., Schmidlin, F. R., Farshad, M., Demetropoulos, C. K., Lee, J. B., & Yang, K. H. Strain-rate dependent material properties of the porcine and human kidney capsule. *Journal of Biomechanics*, 38(5), 2005b, 1011-1021.

Snedeker, J. G., Barnstuble, B. B., Iaizzo, P. A., Farshad, M., Niederer, P., & Schmidlin, F. R. A comprehensive renal injury concept based on a validated finite element model of the human abdomen. *The Journal of Trauma,* 62(5), 2007, 1240-1249.

Song, E., Trosseille, X., & Baudrit, P. Evaluation of thoracic deflection as an injury criterion for side impact using a finite elements thorax model. *Stapp Car Crash Journal,* 53, 2009, 155-191.

Spark, N. T. (2003, Jul). 46.2 gs: The story of john paul stapp, the fastest man on earth. *Wings and Airpower, 33*

Spitzer, V., Ackerman, M. J., Scherzinger, A. L., & Whitlock, D. The visible human male: A technical report. *Journal of the American Medical Informatics Association : JAMIA,* 3(2), 1996, 118-130.

Stalnaker, R. L., Tarriere, C., Fayon, A., Walfisch, G., Balthazard, M., Masset, J., Got, C., & Patel, A. Modification of part 572 dummy for lateral impact according to biomechanical data. *23rd Stapp Car Crash Conference,* San Diego, CA. 1979. 843-859.

Stalnaker, R. L., Roberts, V. L., & McElhaney, J. H. Side impact tolerance to blunt trauma. *17th Stapp Car Crash Conference,* Oklahoma City, OK. 1973. 377-408.

Stapp, J. P. Human tolerance to deceleration; summary of 166 runs. *The Journal of Aviation Medicine,* 22(1), 1951, 42-45.

States, J. D., & States, D. J. Pathology and pathogenesis of injuries caused by lateral impact accidents. *12th Stapp Car Crash Conference,* Detroit, Michigan. 1968. 72-93.

Stingl, J., Baca, V., Cech, P., Kovanda, J., Kovandova, H., Mandys, V., Rejmontova, J., & Sosna, B. Morphology and some biomechanical properties of human liver and spleen. *Surgical and Radiologic Anatomy : SRA,* 24(5), 2002, 285-289.

Stitzel, J. D., Cormier, J. M., Barretta, J. T., Kennedy, E. A., Smith, E. P., Rath, A. L., Duma, S. M., & Matsuoka, F. Defining regional variation in the material properties of human rib cortical bone and its effect on fracture prediction. *Stapp Car Crash Journal,* 47, 2003, 243-265.

Stitzel, J. D., Gayzik, F. S., Hoth, J. J., Mercier, J., Gage, H. D., Morton, K. A., Duma, S. M., & Payne, R. M. Development of a finite element-based injury metric for pulmonary contusion part I: Model development and validation. *Stapp Car Crash Journal,* 49, 2005, 271-289.

Sundaram, S. H., & Feng, C. C. Finite element analysis in the human thorax. *Journal of Biomechanics,* 10(8), 1977, 505-516.

Tablin, F., Chamberlain, J. K., & Weis, L. (2002). The microanatomy of the mammalian spleen. In A. J. Bowdler (Ed.), *The complete spleen* (2nd ed., pp. 11-21). USA: Humana Press.

Talantikite, Y., Bouquet, R., Ramet, M., Guillemot, H., Robin, S., & Voiglio, E. Human thorax behavior for side impact: Influence of impact masses and velocities. *16th International Technical Conference on the Enhanced Safety of Vehicles,* Windsor, Ontario, Canada. 1998. 1542-1549.

Tamura, A., Omori, K., Miki, K., Lee, J. B., Yang, K. H., & King, A. I. Mechanical characterization of porcine abdominal organs. *Stapp Car Crash Journal,* 46, 2002, 55-69.

Tanavde, A. S., Gudipaty, K., & Vaidyaraman, S. Simulation of seat integrated side airbag deployment. *SAE Trans. 970127*. Warrendale, PA: Society of Automotive Engineers. 1997.

Tannous, R. E., Campbell, J. Q., Takhounts, E. G., & Eppinger, R. H. A 2-D finite element model representing the human thorax. *31st International Workshop on Injury Biomechanics Research,* San Diego, CA. 2003. 145-156.

Tarriere, C., Walfisch, G., Fayon, A., Rosey, J. P., Got, C., Patel, A., & Delmas, A. Synthesis of human tolerances obtained from lateral impact simulations. *Seventh International Technical Conference on the Experimental Safety of Vehicles,* Paris, France. 1979. 359-373.

Tencer, A. F., Kaufman, R., Huber, P., & Mock, C. The role of door orientation on occupant injury in a nearside impact: A CIREN, MADYMO modeling and experimental study. *Traffic Injury Prevention,* 6(4), 2005a, 372-378.

Tencer, A. F., Kaufman, R., Mack, C., & Mock, C. Factors affecting pelvic and thoracic forces in near-side impact crashes: A study of US-NCAP, NASS, and CIREN data. *Accident; Analysis and Prevention,* 37(2), 2005b, 287-293.

Tinkoff, G., Esposito, T. J., Reed, J., Kilgo, P., Fildes, J., Pasquale, M., & Meredith, J. W. American association for the surgery of trauma organ injury scale I: Spleen, liver, and kidney, validation based on the national trauma data bank. *Journal of the American College of Surgeons,* 207(5), 2008, 646-655.

Tomaszewski, P. K., Verdonschot, N., Bulstra, S. K., & Verkerke, G. J. A comparative finite-element analysis of bone failure and load transfer of osseointegrated prostheses fixations. *Annals of Biomedical Engineering*, 38(7), 2010, 2418-2427.

Tong, P., & Fung, Y. C. (1993). Biomechanics of injury and healing. In Y. C. Fung (Ed.), *Biomechanics: Mechanical properties of living tissues* (2nd ed., pp. 237-263). USA: Springer.

Trollope, M. L., Stalnaker, R. L., McElhaney, J. H., & Frey, C. F. The mechanism of injury in blunt abdominal trauma. *The Journal of Trauma,* 13(11), 1973, 962-970.

Trosseille, X., Baudrit, P., Leport, T., & Vallancien, G. Rib cage strain pattern as a function of chest loading configuration. *Stapp Car Crash Journal,* 52, 2008, 205-231.

Trosseille, X., Baudrit, P., Leport, T., Petitjean, A., Potier, P., & Vallancien, G. The effect of angle on the chest injury outcome in side loading. *Stapp Car Crash Journal,* 53, 2009, 403-419.

Tulikoura, I., Lassus, J., Konttinen, Y. T., Juutilainen, T., & Santavirta, S. A safe surgical technique for the partial resection of the ruptured spleen. A clinical report. *Injury,* 30(10), 1999, 693-697.

Tylko, S., & Dalmotas, D. Assessment of injury risk to children from side airbags. *44th Stapp Car Crash Conference,* Atlanta, GA. 2000.

Tylko, S., & Dalmotas, D. Static out-of-position test methodologies: Identifying a realistic worst case for small stature female drivers. *17th International Technical Conference on the Enhanced Safety of Vehicles,* Amsterdam, Netherlands. 2001.

Vaidyaraman, S., Khandelwal, H., Lee, C., Xu, J., & Nayef, A. State-of-the-art side airbag modeling and its application in occupant safety in lateral collisions. *SAE Trans. 980915*. Warrendale, PA: Society of Automotive Engineers. 1998.

Valtorta, D., & Mazza, E. Dynamic measurement of soft tissue viscoelastic properties with a torsional resonator device. *Medical Image Analysis,* 9(5), 2005, 481-490.

Vasef, M., & Platz, C. E. (2002). The pathology of the spleen. In A. J. Bowdler (Ed.), *The complete spleen* (2nd ed., pp. 72-106). USA: Humana Press.

Viano, D. C. Evaluation of biomechanical response and potential injury from thoracic impact. *Aviation, Space, and Environmental Medicine,* 49(1 Pt. 2), 1978, 125-135.

Viano, D. C. Evaluation of the benefit of energy-absorbing material in side impact protection: Part I. *31st Stapp Car Crash Conference,* New Orleans. 1987a. 185-203.

Viano, D. C. Evaluation of the benefit of energy-absorbing material in side impact protection: Part II. *31st Stapp Car Crash Conference,* New Orleans. 1987b. 205-224.

Viano, D. C. Biomechanical responses and injuries in blunt lateral impact. *33rd Stapp Car Crash Conference,* Washington, DC. 1989. 113-142.

Viano, D. C., Lau, I. V., Andrzejak, D. V., & Asbury, C. Biomechanics of injury in lateral impacts. *Accident; Analysis and Prevention,* 21(6), 1989a, 535-551.

Viano, D. C., Lau, I. V., Asbury, C., King, A. I., & Begeman, P. Biomechanics of the human chest, abdomen, and pelvis in lateral impact. *Accident; Analysis and Prevention,* 21(6), 1989b, 553-574.

Viano, D. C. Comparison of arm up and down in side impacts with BioSID and different armrests. *Journal of Biomechanical Engineering,* 116(3), 1994, 270-277.

Viscardi, F., Vergara, C., Antiga, L., Merelli, S., Veneziani, A., Puppini, G., Faggian, G., Mazzucco, A., & Luciani, G. B. Comparative finite element model analysis of ascending aortic flow in bicuspid and tricuspid aortic valve. *Artificial Organs,* , 2010

Waghorn, D. J. Overwhelming infection in asplenic patients: Current best practice preventive measures are not being followed. *Journal of Clinical Pathology,* 54(3), 2001, 214-218.

Wang, J. T. Analytical studies of injury criteria for the thorax. *Journal of Biomechanical Engineering,* 111(2), 1989, 128-135.

Wang, J. T. Are tank pressure curves sufficient to discriminate airbag inflators?. *SAE 910808*. Warrendale, PA: Society of Automotive Engineers. 1991.

Warner, C. Y., Strother, C. E., James, M. B., Struble, D. E., & Egbert, T. P. Crash protection in near-side impact~Advantages of a supplemental inflatable restraint. *SAE Trans. 890602*. Warrendale, PA: Society of Automotive Engineers. 1989.

Watson, B., Cronin, D. S., & Campbell, B. Study of vehicle dynamics and occupant response in side impact crash tests. *21st International Technical Conference on the Enhanced Safety of Vehicles,* Stuttgart, Germany. 2009.

Weber, K. Child restraint and airbag interaction: Problem and progress. *SAE 933094*. Warrendale, PA: Society of Automotive Engineers. 1993.

Weber, P. R., Cassatta, S. J., Sochor, M. R., Faust, D. P., Fakry, S., Watts, D., Mock, C., & Wang, S. C. Lateral air bag performance in CIREN field studies. *SAE Trans. 2004-01-0331*. Warrendale, PA: Society of Automotive Engineers. 2004.

Wismans, J., Happee, R., & van Dommelen, J. A. W. Computational human body models. *IUTAM Prodeedings on Impact Biomechanics: From Fundamental Insights to Applications,* Dublin, Ireland. 2005. 417-429.

Wooldridge, B. F. Traumatic rupture of the spleen. A review. *Missouri Medicine,* 66(10), 1969, 804-806.

Yamada, H. (1970). *Strength of biological materials*. Huntington, New York: Williams & Wilkins.

Yoganandan, N., Pintar, F. A., Kumaresan, S., Sances, A., & Haffner, M. P. Response of human lower thorax to impact. *40th AAAM Conference,* Vancouver, British Columbia. 1996. 33-43.

Yoganandan, N., Pintar, F. A., Kumaresan, S., Haffiner, M., & Kuppa, S. Impact biomechanics of the human thorax-abdomen complex. *International Journal of Crashworthiness,* 2(2), 1997, 219.

Yoganandan, N., & Pintar, F. A. Biomechanics of human thoracic ribs. *Journal of Biomechanical Engineering,* 120(1), 1998, 100-104.

Yoganandan, N., Pintar, F. A., Gennarelli, T. A., & Maltese, M. R. Patterns of abdominal injuries in frontal and side impacts. *Annual Proceedings of the Association for the Advancement of Automotive Medicine,* 44, 2000, 17-36.

Yoganandan, N., Pintar, F. A., & Maltese, M. R. Biomechanics of abdominal injuries. *Critical Reviews in Biomedical Engineering,* 29(2), 2001, 173-246.

Yoganandan, N., & Pintar, F. A. Deflection, acceleration, and force corridors for small females in side impacts. *Traffic Injury Prevention,* 6(4), 2005, 379-386.

Yoganandan, N., Pintar, F. A., & Gennarelli, T. A. Field data on head injuries in side airbag vehicles in lateral impact. *Annual Proceedings of the Association for the Advancement of Automotive Medicine,* 49, 2005, 171-184.

Yoganandan, N., Pintar, F. A., Gennarelli, T. A., Martin, P. G., & Ridella, S. A. Chest injuries and injury mechanisms in oblique lateral impacts. *2007 International IRCOBI Conference,* Maastricht, The Netherlands. 2007a. 311-324.

Yoganandan, N., Pintar, F. A., Stemper, B. D., Gennarelli, T. A., & Weigelt, J. A. Biomechanics of side impact: Injury criteria, aging occupants, and airbag technology. *Journal of Biomechanics,* 40(2), 2007b, 227-243.

Yoganandan, N., Pintar, F. A., Zhang, J., & Gennarelli, T. A. Lateral impact injuries with side airbag deployments--a descriptive study. *Accident; Analysis and Prevention,* 39(1), 2007c, 22-27.

Yoganandan, N., & Pintar, F. A. Deflections from two types of human surrogates in oblique side impacts. *Annals of Advances in Automotive Medicine,* 52, 2008, 301-313.

Yoganandan, N., Pintar, F. A., Gennarelli, T. A., Martin, P. G., & Ridella, S. A. Chest deflections and injuries in oblique lateral impacts. *Traffic Injury Prevention,* 9(2), 2008, 162-167.

Zaborowski, A. B. Human tolerance to lateral impact with lap belt only. *8th Stapp Car Crash Conference*, Detroit, Michigan. 1964.

Zaouk, A. K., Eigen, A. M., & Digges, K. H. Occupant injury patterns in side crashes. *SAE Trans. 2001-01-0723*. Warrendale, PA: Society of Automotive Engineers. 2001.

Zissin, R., Gutman, M., Even-Sapir, E., & Gayer, G. Anatomic and pathologic computed tomographic findings following splenectomy. *Seminars in Ultrasound, CT, and MR*, 28(1), 2007, 67-78.

Zou, H., & Schmiedeler, J. P. Predicting brain injury under impact with a strain measure from analytical models. *International Journal of Crashworthiness*, 13(3), 2008, 337-348.

APPENDIX A

Table A.1. Post mortem human subject testing sponsored by the National Highway Traffic Safety Administration and documented in the NHTSA Biomechanics Test Database.

Test #	Test Site [a]	Test Device	ΔV (m/s)	B.C.	Skeletal Injury [b]	Visceral Injury [c]
83E106	UMTRI	Pendulum	2.82	Flat Rigid	-	-
83E108	UMTRI	Pendulum	2.82	Flat Rigid	-	-
83E085	UMTRI	Pendulum	3.49	Flat Rigid	-	-
76T062	UMTRI	Pendulum	4.25	Flat Rigid	L:7fx	heart lac.
76T065	UMTRI	Pendulum	4.25	Flat Rigid	-	pericardium cont.
77T074	UMTRI	Pendulum	4.25	Flat Rigid	R:4	-
77T071	UMTRI	Pendulum	4.34	Flat Rigid	-	pericardium cont.
H-83-008	Heidelberg	Sled	4.47	Padded Door	-	-
H-83-030	Heidelberg	Sled	5.01	Padded Door	-	-
SIC21-DOT	WSU	Pendulum	5.10	Flat Rigid	L:4-5,7-10;R:flail	liver lac.; diaphragm lac.
SIC31.DOT	WSU	Pendulum	5.10	Flat Rigid	L:flail;R:4-8	-
SIC26-DOT	WSU	Pendulum	5.32	Flat Rigid	-	-
SIC45.DOT	WSU	Pendulum	5.72	Flat Rigid	L:6;R:4-5,7-10	-
76T003	UMTRI	Sled	6.04	Flat Rigid	L4	-
77T077	UMTRI	Pendulum	6.08	Flat Rigid	R:4-6	heart cont.; lung cont.
77T080	UMTRI	Pendulum	6.08	Flat Rigid	L:5-9;R:5-6	heart cont.
SC105	MCW	Sled	6.17	Padded Wall	-	-
H-80-011	Heidelberg	Sled	6.26	Flat Rigid	L:6	-
H-80-014	Heidelberg	Sled	6.26	Flat Rigid	L:2,5,6	-
SC106	MCW	Sled	6.39	Padded Wall	L:7-8	-
SC121	MCW	Sled	6.39	Flat Rigid	L:2-7	-

Test #	Test Site [a]	Test Device	ΔV (m/s)	B.C.	Skeletal Injury [b]	Visceral Injury [c]
SC124	MCW	Sled	6.39	Flat Rigid	-	-
H82015	Heidelberg	Sled	6.44	Flat Rigid	L:7,8	-
H82018	Heidelberg	Sled	6.44	Flat Rigid	L:2-8,10,11	pleura lac.
H82019	Heidelberg	Sled	6.44	Flat Rigid	L:2-8	pleura lac.
SC101	MCW	Sled	6.50	Flat Rigid	L2-7;R:4	-
H81015	Heidelberg	Sled	6.53	Padded Door	-	-
SC103	MCW	Sled	6.61	Flat Rigid	L:2-8	-
SC120	MCW	Sled	6.61	Flat Rigid	-	-
SIC07	WSU	Sled	6.66	Flat Rigid	L:1-7;R:1,2,5	-
SAC101	MCW	Sled	6.67	Side airbag	-	-
SAC105	MCW	Sled	6.67	Side airbag	R:5-6	-
SC135	MCW	Sled	6.67	Flat Rigid	L:2-8	-
SC136	MCW	Sled	6.67	Padded Wall	L:6-9	-
SC137	MCW	Sled	6.67	Flat Rigid	L:1-4	-
SC138	MCW	Sled	6.67	Padded Wall	L:2-7	-
SC140	MCW	Sled	6.67	Pelvic Offset	-	-
SC141	MCW	Sled	6.67	Thoracic Offset	L:1-9	-
SC20A101	MCW	Sled	6.67	Oblique Rigid	L:3-7,9,10	-
SC20A102	MCW	Sled	6.67	Oblique Rigid	L:2-9	pleura lac.
SC30A101	MCW	Sled	6.67	Oblique Rigid	L:1,4,5,8	-
SC30A102	MCW	Sled	6.67	Oblique Rigid	L:flail;R:5	-
SC30A103	MCW	Sled	6.67	Oblique Rigid	-	-
SIC08	WSU	Sled	6.67	Flat Rigid	Bilat.: 24fx	spleen lac.; liver lac.
SC115	MCW	Sled	6.69	Padded Wall	L:2-9	-
SC119	MCW	Sled	6.69	Padded Wall	L:2-9	-
SC122	MCW	Sled	6.69	Padded Wall	L:4	-

Test #	Test Site [a]	Test Device	ΔV (m/s)	B.C.	Skeletal Injury [b]	Visceral Injury [c]
484	WSU	Sled	6.71	Padded Wall	L:2-7	-
490	WSU	Sled	6.71	Flat Rigid	L:1-9;R:1	-
76T029	UMTRI	Sled	6.71	Padded Door	L:4fx	-
H-80-017	Heidelberg	Sled	6.71	Flat Rigid	L:3-8	-
H81021	Heidelberg	Sled	6.71	Padded Door	-	-
SIC05	WSU	Sled	6.71	Flat Rigid	L:1-6;R:1-7	-
SC123	MCW	Sled	6.72	Padded Wall	L:2-7	-
SC102	MCW	Sled	6.80	Flat Rigid	-	-
SIC13-DOT	WSU	Pendulum	6.80	Flat Rigid	L:4-8;R:7-8	-
SC111	MCW	Sled	6.81	Pelvic Offset	L:3-10	L pneumo.
SC117	MCW	Sled	6.81	Pelvic Offset	L:4-5;R:8	-
SC118	MCW	Sled	6.81	Pelvic Offset	L:4-7	-
SC126	MCW	Sled	6.86	Abdominal Offset	L:4-6,8-9	L kidney lacs.
H-80-013	Heidelberg	Sled	6.93	Flat Rigid	L:3-9	-
SAC102	MCW	Sled	6.94	Flat Rigid	L:2-5;R:8-9	-
SAC103	MCW	Sled	6.94	Side airbag	-	-
SAC104	MCW	Sled	6.94	Side airbag	L:3-6	-
SC131	MCW	Sled	6.94	Flat Rigid	L:4-9,11	-
SC139	MCW	Sled	6.94	Pelvic Offset	L:1-6;R:5	pleura lac.
SC142	MCW	Sled	6.94	Thoracic Offset	L:4,7-10	-
SC143	MCW	Sled	6.94	Pelvic Offset	L:4	-
SC144	MCW	Sled	6.94	Pelvic Offset	L:2-3,5-6,8:R:3-5	-
SC129	MCW	Sled	6.98	Abdominal Offset	L:3-6,8-9	-
SC128	MCW	Sled	7.06	Thoracic Offset	L:8-9	-
SC110	MCW	Sled	7.11	Pelvic Offset	L:2-9	L pneumo.

Test #	Test Site [a]	Test Device	ΔV (m/s)	B.C.	Skeletal Injury [b]	Visceral Injury [c]
SC125	MCW	Sled	7.14	Abdominal Offset	L:2-5,7-9	liver lac.
SC130	MCW	Sled	7.14	Thoracic Offset	L:4-10	L kidney lacs.; L lung lac.
SC127	MCW	Sled	7.22	Thoracic Offset	L:1-9	-
H-83-010	Heidelberg	Sled	7.51	Padded Wall	-	-
H-83-031	Heidelberg	Sled	7.51	Padded Door	L:2-9	-
488	WSU	Sled	7.60	Flat Rigid	L:1-7	-
83E107	UMTRI	Pendulum	7.91	Flat Rigid	L:2-5	-
SC112	MCW	Sled	8.00	Pelvic Offset	L:2-9;R:5-6	-
SIC13	WSU	Sled	8.33	Padded Wall	L:11fx;R:7fx	-
82E007	UMTRI	Pendulum	8.41	Padded Pendulum	R:3,5,7	aortic cont.
82E027	UMTRI	Pendulum	8.49	Padded Pendulum	L:flail	-
82E048	UMTRI	Pendulum	8.49	Padded Pendulum	L:3,7,8	-
82E066	UMTRI	Pendulum	8.49	Padded Pendulum	R:flail	-
83E086	UMTRI	Pendulum	8.49	Flat Rigid	L:3-6;R:3-6,8	L lung lac.
H-80-020	Heidelberg	Sled	8.49	Padded Wall	L:7,8.12;R:5,6	spleen lac.; liver lac.; L kidney cont.
SIC16-DOT	WSU	Pendulum	8.50	Flat Rigid	L:3,5,6;R:3-5	-
H-80-018	Heidelberg	Sled	8.63	Padded Wall	-	-
H82016	Heidelberg	Sled	8.67	Flat Rigid	L:3-10	-
H82020	Heidelberg	Sled	8.67	Flat Rigid	L:flail,R:>2fx	spleen lacs.; liver lacs.
SIC03-DOT	WSU	Pendulum	8.70	Flat Rigid	L:flail;R:7-10	-
76T010	UMTRI	Sled	8.76	Flat Rigid	L1-8; R1-5	-
76T034	UMTRI	Sled	8.76	Padded Door	L: flail	-
SC107	MCW	Sled	8.86	Padded Wall	L:3,9;R:7	-

Test #	Test Site [a]	Test Device	ΔV (m/s)	B.C.	Skeletal Injury [b]	Visceral Injury [c]
SC133	MCW	Sled	8.89	Padded Wall	L:3-10;R:4-6	-
SIC10	WSU	Sled	8.89	Padded Wall	L:3fx;R:2fx	-
SIC11	WSU	Sled	8.89	Padded Wall	L:2fx;R:1fx	-
SIC12	WSU	Sled	8.89	Padded Wall	L:15fx;R:10fx	-
SIC15	WSU	Sled	8.89	Padded Wall	-	-
SIC16	WSU	Sled	8.89	Padded Wall	L:19fx;R:7fx	-
SIC17	WSU	Sled	8.89	Padded Wall	L:2fx	-
SIC01	WSU	Sled	8.90	Pelvic Offset	L:2-10;R:2-10	liver lac.
487	WSU	Sled	8.94	Padded Wall	L:4-6	-
487	WSU	Sled	8.94	Padded Wall	L:4-6	-
489	WSU	Sled	8.94	Padded Wall	L:4-8;R:7-8	-
76T011	UMTRI	Sled	8.94	Flat Rigid	L flail; R2-6	spleen lacs.; liver lac.
76T039	UMTRI	Sled	8.94	Padded Door	L&R: 9fx	heart cont.
77T089	UMTRI	Sled	8.94	Flat Rigid	L:2-8; R:1-2	aortic lac.; lung lac.
77T092	UMTRI	Sled	8.94	Flat Rigid	L:flail	heart cont.; L pneumo.
77T095	UMTRI	Sled	8.94	Padded Wall	L:2-9;R:1,2,4	L lung lac.
77T098	UMTRI	Sled	8.94	Padded Wall	L:flail;R:2fx	L pneumo.
H-80-021	Heidelberg	Sled	8.94	Padded Door	-	-
H-81-004	Heidelberg	Sled	8.94	Flat Rigid	L:flail;R:1-7	spleen lacs.;
H81006	Heidelberg	Sled	8.94	Flat Rigid	L:1-8	-
H81011	Heidelberg	Sled	8.94	Padded Door	-	-
H81012	Heidelberg	Sled	8.94	Padded Door	L:2-5	-
H82008	Heidelberg	Sled	8.94	Padded Wall	L:flail;R:3,5,10	liver lacs.
H82014	Heidelberg	Sled	8.94	Flat Rigid	L:1-12	L kidney lacs.; stomach lac.
H82021	Heidelberg	Sled	8.94	Padded Wall	L:flail;R:3,8-10	pleura lac.
H82022	Heidelberg	Sled	8.94	Padded Wall	L:flail;R:>2fx	spleen lac.

Test #	Test Site [a]	Test Device	ΔV (m/s)	B.C.	Skeletal Injury [b]	Visceral Injury [c]
H-83-011	Heidelberg	Sled	8.94	Padded Wall	-	-
H-83-012	Heidelberg	Sled	8.94	Padded Wall	-	-
H-83-020	Heidelberg	Sled	8.94	Padded Wall	-	-
H-84-008	Heidelberg	Sled	8.94	Padded Wall	L:flail	-
LSI32P16	VRTC	Sled	8.94	Padded Wall	L:7fx;R:11fx	spleen lac.
LSI32P15	VRTC	Sled	8.96	Padded Wall	L:9fx;R:6fx	-
98LSI32R17	VRTC	Sled	8.97	Flat Rigid	Bilat.: 11fx	L lung lac.
LSI32R13	VRTC	Sled	8.98	Flat Rigid	L:6fx;R:6fx	pleura lac.
LSI32P12	VRTC	Sled	8.98	Padded Wall	L:4fx,R:5fx	liver lac.
SC108	MCW	Sled	9.00	Flat Rigid	L:4-6	-
SC114	MCW	Sled	9.00	Padded Wall	L:4-10;R:4-8	-
LSI32P11	VRTC	Sled	9.01	Padded Wall	L:4fx;R:3fx	-
LSI32R10	VRTC	Sled	9.01	Flat Rigid	L:8fx	spleen lac.; liver lac.
LSI32R09	VRTC	Sled	9.02	Flat Rigid	L:6fx,R:5fx	-
SC132	MCW	Sled	9.06	Padded Wall	L:2-6,7-8	-
SIC02	WSU	Sled	9.08	Pelvic Offset	L:1-11;R:1-9	spleen lac.
SIC04	WSU	Sled	9.08	Flat Rigid	L:1-10;R:1,4,8	spleen lac.
SIC06	WSU	Sled	9.08	Flat Rigid	L:1-7;R:1,5	-
SC134	MCW	Sled	9.08	Padded Wall	L:1-6	-
SC116	MCW	Sled	9.11	Padded Wall	L:1-6;R:4	-
93LSI32R01	VRTC	Sled	9.14	Flat Rigid	Bilat.	spleen lacs.
94LSI32R05	VRTC	Sled	9.14	Flat Rigid	Bilat.: 12fx	liver lac.
94LSI32P03	VRTC	Sled	9.17	Flat Rigid	Bilat.: 19fx	spleen lac.; liver lac.
LSI32P14	VRTC	Sled	9.17	Padded Wall	L:7fx;R:5fx	spleen lac.; liver lac.
SC109	MCW	Sled	9.17	Flat Rigid	L:2-3,5-6;R:2	L pneumo.
93LSI32R02	VRTC	Sled	9.19	Flat Rigid	Bilat.	spleen lac.; liver lac.

Test #	Test Site [a]	Test Device	ΔV (m/s)	B.C.	Skeletal Injury [b]	Visceral Injury [c]
94LSI32P04	VRTC	Sled	9.19	Padded Wall	Bilat.	spleen lac.
95LSI32P06	VRTC	Sled	9.19	Flat Rigid	Bilat.: 13fx	spleen lac.; liver lac.
LSI32R08	VRTC	Sled	9.19	Flat Rigid	Bilat.:24fx	spleen lac.; liver lac.
H-80-023	Heidelberg	Sled	9.39	Padded Door	L:1-9,R:1-5	spleen lacs.
H-80-024	Heidelberg	Sled	9.39	Flat Rigid	-	-
H-81-002	Heidelberg	Sled	9.39	Flat Rigid	L:flail,R:2-6	spleen lacs.
SIC09	WSU	Sled	9.44	Padded Wall	Bilat.: 34fx	-
SIC14	WSU	Sled	9.44	Padded Wall	L:12fx;R:6fx	-
SC113	MCW	Sled	9.60	Pelvic Offset	L:flail;R:1-4	L lung lac.
H-83-016	Heidelberg	Sled	9.84	Padded Door	L:2-6;R:2-5	-
SIC27.DOT	WSU	Pendulum	9.88	Flat Rigid	-	-
H-83-021	Heidelberg	Sled	10.01	Padded Door	L:2-11,R:3-6	-
SIC35.DOT	WSU	Pendulum	10.10	Flat Rigid	R:flail	liver lac.
SIC03	WSU	Sled	10.46	Pelvic Offset	L:1-8;R:1-7	lung lac.
SIC39.DOT	WSU	Pendulum	10.73	Flat Rigid	L:flail;R:2-5	spleen lacs.; R kidney lac.; L&R lung cont.
8426 FAT	Heidelberg	Car Body	11.13	Unmodified	L:3-7	-
8427 FAT	Heidelberg	Car Body	11.13	Unmodified	L:4-7	-
8431 FAT	Heidelberg	Car Body	11.13	Unmodified	L:9fx;R:6fx	-
76T042	UMTRI	Sled	11.18	Padded Door	L:flail; R:2fx	-
H81016	Heidelberg	Sled	11.18	Flat Rigid	L:flail	spleen lac.; liver lac.
H82009	Heidelberg	Sled	11.18	Flat Rigid	L:1-12	L kidney cont.; L lung lac.
H82012	Heidelberg	Sled	11.18	Flat Rigid	L:2-10	spleen lac.; L kidney lacs.; L lung lac.
H84004	Heidelberg	Car Body	11.18	Unmodified	L:flail	-
76T009	UMTRI	Sled	11.53	Flat Rigid	L:flail;R:>2fx	L kidney lac.
8506 FAT	Heidelberg	Car Body	12.29	Unmodified	L:1-10;R:1	-
8415 FAT	Heidelberg	Car Body	12.38	Unmodified	Bilat.:4fx	L kidney lac.

Test #	Test Site [a]	Test Device	ΔV (m/s)	B.C.	Skeletal Injury [b]	Visceral Injury [c]
8433 FAT	Heidelberg	Car Body	12.38	Unmodified	L:3-8	-
8412 FAT	Heidelberg	Car Body	12.52	Unmodified	Bilat.:8fx	-
8413 FAT	Heidelberg	Car Body	12.52	Unmodified	Bilat.:8fx	-
H84007	Heidelberg	Car Body	12.52	Unmodified	L:flail	-
H84009	Heidelberg	Car Body	12.52	Unmodified	L:flail	-
8503 FAT	Heidelberg	Car Body	12.70	Unmodified	L:1-10;R:1,4-9	spleen lac.
S06	WSU	Sled	12.92	Padded Door	L:flail	spleen lac.
S07	WSU	Sled	13.19	Padded Door	L:flail	-
H82004	Heidelberg	Car Body	13.86	Unmodified	L:flail	-
H82005	Heidelberg	Car Body	13.86	Unmodified	L:flail	-
H82007	Heidelberg	Car Body	13.86	Unmodified	L:flail	-
H82011	Heidelberg	Car Body	13.86	Unmodified	-	L pneumo.
H83001	Heidelberg	Car Body	13.86	Unmodified	L:flail	-
H83004	Heidelberg	Car Body	13.86	Unmodified	L:flail	-
H83005	Heidelberg	Car Body	13.86	Unmodified	L:flail	liver lacs.
H83027	Heidelberg	Car Body	13.86	Unmodified	L:4fx	-
H83028	Heidelberg	Car Body	13.86	Unmodified	L:flail	-
H84002	Heidelberg	Car Body	13.86	Unmodified	L:flail	-
8509 FAT	Heidelberg	Car Body	13.99	Unmodified	L:1-5;R:1,4-8	liver lac.
8513 FAT	Heidelberg	Car Body	13.99	Unmodified	L:4	-
8430 FAT	Heidelberg	Car Body	14.13	Unmodified	-	-
S05	WSU	Sled	16.14	Padded Door	Bilat.	spleen lac., pleura lac.
H83014	Heidelberg	Car Body	16.68	Unmodified	L:flail	spleen lac.; L kidney lacs.
H83017	Heidelberg	Car Body	16.68	Unmodified	L:flail	spleen lac.; liver lac.
H83019	Heidelberg	Car Body	16.68	Unmodified	L:flail	liver lac.
8517 FAT	Heidelberg	Car Body	16.76	Unmodified	L:1-11	-

Test #	Test Site [a]	Test Device	ΔV (m/s)	B.C.	Skeletal Injury [b]	Visceral Injury [c]
8518 FAT	Heidelberg	Car Body	16.76	Unmodified	-	-
BMD001	ONSER	Vehicle	17.78	Unmodified	L:flail;R:>2fx	spleen lac.; L kidney lac.
BMD002	ONSER	Vehicle	17.78	Unmodified	L:<3fx	spleen lac.; L kidney lac.
BMD003	ONSER	Vehicle	17.89	Reinforced Door	L:flail;R:<2fx	spleen lac.; L kidney lac.

a. Heidelberg = University of Heidelberg, MCW = Medical College of Wisconsin, ONSER = French National Organization for Road Safety, UMTRI = University of Michigan Transportation Research Institute, VRTC = NHTSA Vehicle Research and Test Center, WSU = Wayne State University
b. L/R = left/right aspect; bilat. = bilateral; flail = flail chest; #fx = # of fractures
c. L/R = left/right aspect; lac. = laceration; cont. = contusion; pneumo. = pneumothorax;